Development of an Active Anti-Whiplash Automotive Seat

to Reduce Whiplash Injuries Following a Rear-End Collision

by

Daniel Mang

B.Sc., Boston University, 2007
M.Sc., University of British Columbia, 2010

A DISSERTATION SUBMITTED IN PARTIAL FULFILMENT OF THE REQUIREMENTS FOR THE DEGREE OF

DOCTOR OF PHILOSOPHY

in

THE FACULTY OF GRADUATE AND POSTDOCTORAL STUDIES

(Kinesiology)

THE UNIVERSITY OF BRITISH COLUMBIA

(Vancouver)

October 2019

The following individuals certify that they have read, and recommend to the Faculty of Graduate and Postdoctoral Studies for acceptance, the dissertation entitled:

Development of an Active Anti-Whiplash Automotive Seat to Reduce Whiplash Injuries Following a Rear-End Collision

submitted by Daniel Mang in partial fulfilment of the requirements for

the degree of Doctor of Philosophy

in Kinesiology

Examining Committee:

Dr. Jean-Sébastien Blouin, Kinesiology
Co-supervisor

Dr. Gunter P. Siegmund, Kinesiology
Co-supervisor

Dr. Douglas P. Romilly, Mechanical Engineering
Supervisory Committee Member

Dr. Anita Vasavada, Chemical Engineering and Bioengineering (Washington State University)
External Examiner

Dr. Bonita Sawatzky, Orthopaedics
University Examiner

Dr. Guy Faulkner, Kinesiology
University Examiner

Abstract

Whiplash injuries remain the most common injury associated with motor vehicle crashes despite the introduction of anti-whiplash seats. The overall goal of the experiments presented in this dissertation was to design, build and test a novel Experimental anti-whiplash automotive seat to prevent whiplash injuries following low-speed, rear-end collisions. The key safety features of the Experimental seat included the dynamic control of seat hinge rotation and seatback cushion deformation. These safety features were deployed before and during the collision with the aim to reduce occupant kinematic and kinetic responses and to better minimize the relative motion between the head and the upper torso. Four experiments were conducted to better understand the performance of current anti-whiplash seats during low to moderate collision severities (Experiment 1) and to evaluate the performance of the Experimental seat (Experiments 2–4). In Experiment 1, the performance of four existing anti-whiplash seats were compared in their abilities to reduce anthropomorphic test device (ATD) responses during a series of low to moderate collision speed changes (Δv=2–14 km/h). Good-rated seats, according to the Research Council for Automobile Repairs/International Insurance Whiplash Prevention Group (RCAR/IIWPG), attenuated only four peak ATD responses compared to poor-rated seats. The next three experiments tested the two safety mechanisms of the Experimental seat: seat hinge rotation only (Experiment 2), seatback cushion deformation only (Experiment 3) and the co-activation of both safety mechanisms (Experiment 4). In comparison to a Control seat, actively controlling seat hinge rotation decreased most ATD responses and neck injury criteria by 23–85% while modulating seatback deformation attenuated most occupant responses and all neck injury criteria by 15–82%. In Experiment 4, the Experimental seat combining both safety mechanisms was compared to four existing anti-whiplash seats and yielded decreases in ATD responses of 25–99% and in neck injury criteria of 9–73% for collision speeds of 4 km/h or greater. The results of these experiments demonstrated that the Experimental anti-whiplash seat with the dynamic control of seat hinge rotation and seatback cushion deformation could potentially be an effective solution to reduce the risk of whiplash injuries and improve occupant safety.

Lay Summary

Whiplash injuries are the most common injury associated with low-speed, rear-end collisions. The goal of the experiments presented in this dissertation was to develop an Experimental anti-whiplash seat that controlled seat hinge and seatback cushion properties to reduce the accelerations experienced by an occupant and to better support an occupant's head and neck during a whiplash perturbation. Compared to other anti-whiplash seats, the Experimental seat reduced occupant responses during rear-end collisions less than 12 km/h. The co-activation of the seat hinge rotation and the seatback cushion deformation on the Experimental seat reduced the occupant responses from a 12 km/h collision to the equivalent of a 4 km/h collision on other existing anti-whiplash seats. Thus, the Experimental anti-whiplash seat with the dynamic control of seat hinge rotation and seatback cushion deformation could potentially be an effective solution to further reduce the risk of whiplash injuries and improve occupant safety in vehicles.

Preface

The four experiments presented in this dissertation were conducted at MEA Forensic Engineers & Scientists in Richmond, British Columbia. The four experiments were written up as separate studies to assist with future publication (Chapters 2 through 5). Each chapter contains complete Introduction, Methods, Results and Discussion sections relevant to each experiment. Since all experiments were conducted using a 50^{th} percentile male BioRID II anthropomorphic test device (ATD) and most experiments were conducted on the novel Experimental anti-whiplash seat (Chapters 3 through 5), there was inevitably some repetition within the Methods section of these experiments, in particular the Anthropomorphic Test Device and Instrumentation, Test Procedures and Data Analysis subsections.

A version of Chapter 2 has been provisionally accepted for publication as Mang, D.W.H., Siegmund, G. P., & Blouin, J. S. A Comparison of Anti-Whiplash Seats During Low/Moderate Speed, Rear-End Collisions. All authors contributed to the concept and design of the experiment, data interpretation, and editing of the manuscript. I was solely responsible for the data collection, data analysis, and writing of the manuscript.

Chapters 3, 4 and 5 are in preparation for publication with the following authors: Mang, D.W.H., Siegmund, G. P., and Blouin, J. S. All authors contributed to the concept and design of the experiment, data interpretation, and editing of the manuscript. I was solely responsible for the data collection, data analysis, and writing of the manuscript.

Table of Contents

List of Tables

List of Figures

Acronyms and Abbreviations

α	Significance level
AIS	Abbreviated injury scale
AOJ	Atlanto-occiptal joint
$a_{resultant\text{-}T1}$	Forward resultant acceleration of T1
ATD	Anthropomorphic test device
$a_{X\text{-}head}$	Linear forward acceleration of the head
$a_{X\text{-}sled}$	Linear forward acceleration of the whiplash sled
$a_{X\text{-}T1}$	Linear forward acceleration of the T1 vertebra
BioRID	Biofidelic rear impact dummy
COV	Coefficient of variation
DAQ	Data acquisition
$d_{backset}$	Horizontal backset of the head restraint relative to the head
df	Degrees of freedom
d_{height}	Vertical height of the head restraint relative to the head
$d_{penetration\text{-}pelvis}$	Occupant penetration of the pelvis into the seatback
$D_{rebound}$	Forward rebound of the head relative to the head restraint
EXP	Experimental seat
EXP90	Experimental condition with $d_{backset}$ = 86.2 mm and d_{height} = -24.6 mm
FSR	Force sensitive resistor
F_X	Upper neck shear force
F_Z	Upper neck axial force
GM	General Motor
GMHR	General Motor High Retention seat
ICBC	Insurance Corporation of British Columbia
IIHS	Insurance Institute for Highway Safety
IIWPG	International Insurance Whiplash Prevention Group
IRED	Infrared light emitting diode
M_Y	Upper neck flexion/extension bending moment
n	Number of trials
NHTSA	National Highway Traffic Safety Administration
NIC	Neck Injury Criterion
N_{ij}	Normalized Neck Injury Criterion

N_{km}	Neck Protection Criterion
p	Significance level
RCAR	Research Council for Automobile Repairs
RPM	Revolutions per minute
R_X	Retraction
SAHR	Saab's Active Head Restraint
SD	Standard deviation
T1	First thoracic vertebrae
$t_{deformation\text{-}forward}$	Onset of seatback motor rotation to control deformation
$t_{deformation\text{-}onset}$	Onset of rearward seatback motor rotation to control deformation
$t_{forward\text{-}onset}$	Onset of forward seat hinge rotation
$t_{rearward\text{-}onset}$	Onset of rearward seat hinge rotation
$t_{rotation\text{-}onset}$	Onset of seat hinge rotation
WAD	Whiplash-associate disorders
WHIPS	Volvo's Whiplash Injury Prevention seat
WIL	Toyota's Whiplash Injury Lessening seat
Δt	Collision pulse duration
$\Delta t_{head\text{-}contact}$	Head-to-head-restraint contact time
Δv	Collision speed change
$\theta_{deformation\text{-}peak}$	Peak angle of rearward seatback motor rotation to control deformation
$\theta_{deformation\text{-}peak}$	Peak angle of forward seatback motor rotation to control deformation
$\theta_{forward\text{-}peak}$	Peak angle of forward seat hinge rotation
θ_{head}	Head extension angle
$\theta_{rearward\text{-}peak}$	Peak angle of rearward seat hinge rotation
$\theta_{seat\text{-}hinge}$	Seat hinge rotation angle
χ^2	Chi-squared value
$\omega_{deformation\text{-}forward}$	Initial angular velocity of forward seatback motor rotation to control deformation
$\omega_{deformation\text{-}int}$	Initial angular velocity of rearward seatback motor rotation to control deformation
$\omega_{rearward\text{-}int}$	Initial angular velocity of rearward seat hinge rotation
$\omega_{Y\text{-}head}$	Angular velocity of the head
$\omega_{Y\text{-}T1}$	Angular velocity of the T1 vertebra

Acknowledgements

Undertaking this Doctor of Philosophy (PhD) degree has been a truly memorable and life-changing experience for me and it would not have been possible without the support and guidance I received from many people

Firstly, I would like to express my sincerest gratitude to my co-supervisors, Drs. Jean-Sébastien Blouin and Gunter Siegmund, for their continued patience, guidance and support throughout the duration of my PhD. I have been extremely lucky to have supervisors who cared so much about my work and were always available to answer my questions no matter how trivial they might be. Thank you to Jean-Sébastien and Gunter for your wealth of knowledge in the field of whiplash injuries and constant guidance to help better my technical writing skills. It has been a long journey, but without your constant feedback, words of encouragement and faith in me as a researcher this PhD would not have been achievable.

Many thanks to Dr. Douglas Romilly for being a part of my PhD committee and for introducing me to the AUT021 Network Center for Excellence. Thank you for your encouragement, support and time to discuss my research.

To Mr. Jeff Nickel and Mr. Mircea Oala-Florescu of MEA Forensic Engineers and Scientists, who work endlessly behind the scenes to ensure that all the students have what they need no matter how crazy the idea might be. Thank you both for your willingness to always lend a helping hand with big smiles. Your guidance and assistance in the design and fabrication of the

anti-whiplash seat and seat support structures utilized throughout this dissertation were greatly appreciated.

Completing this work would have been all the more difficult were it not for the support of my friends, fellow graduate students and colleagues in the Sensorimotor Physiology Laboratory. I am indebted to them for their patience, moral support and years of friendship. Also, many thanks to the numerous undergraduate students who helped in the design, fabrication and programming of the anti-whiplash automotive seat: Devin Luu, Roein Manafi, Alex Jew and Geoffery Hohert.

I would like to say a heartfelt thank you to my family for providing me with support and encouragement to pursue my dreams. This accomplishment was only possible because of the many opportunities you provided me.

And finally, to my loving wife Betty, thank you for your patience, emotional support and encouragement throughout my entire PhD. You were always there to keep me grounded during the high points and always found the right words to support me during the low points. I am eternally grateful to you for taking care of Oliver these past months and making it possible for me to complete what I started.

Dedication

To Oliver, never stop seeking knowledge and exploring the world.

Chapter 1. Introduction

1.1 Literature Review

1.1.1 Epidemiology

Whiplash injuries are the most common type of injuries associated with motor vehicle collisions. Rear-end vehicle-to-vehicle collisions pose the greatest risk of whiplash injury (38%) when compared to other collision directions such as frontal (15.7%) and side (10.8%) impacts (ICBC, 2006, ICBC, 2007, Jakobsson et al., 2000). For rear-end collisions, whiplash injury is commonly defined as any injury to a person's neck resulting when the head is suddenly accelerated backwards into extension and then forwards into flexion. Whiplash injuries account for approximately 70% of all injury claims made to the Insurance Corporation of British Columbia (ICBC) (ICBC, 2000). In 2000, ICBC paid out over $500 million—50% of all injury payouts—for whiplash injuries and whiplash-associated disorders (WAD). Half of the money was spent on medical treatments for occupants and the other half covered the lost wages and diminished earning capacity of drivers and occupants injured (ICBC, 2000). In 2006, the estimated cost of whiplash injuries and WAD (excluding litigation costs) increased to approximately $850 million (ICBC, 2007).

The annual incidence of whiplash injuries in the western world ranges from 28 to 834 per 100,000 inhabitants (Cassidy et al., 2000, Holm et al., 2008, Otremski et al., 1989). Females are 1.2 to 3 times more likely to suffer from whiplash injuries after a rear-end automotive collision

as compared to males (Mordaka and Gentle, 2003, Harder et al., 1998, Versteegen et al., 2000). Females between the ages 20 to 24 present the highest incidence rate of reported whiplash injuries with 965 cases per 100,000 people annually (Quinlan et al., 2004). The greater susceptibility of younger females is hypothesized to be related to the sex differences in anatomical, physiological, behavioral and sociological parameters (Mordaka and Gentle, 2003) as well as the influence of seat properties on neck biomechanics and occupant dynamics (Viano, 2003c).

The type of injury and recovery times following whiplash collisions vary greatly and depend on factors such as impact severity, seat position, seat stiffness, and initial posture of the occupant (Suissa et al., 2001, Viano, 2003b). The most common symptoms following whiplash injuries are neck pain (88-100% of patients) and headaches (54-66% of patients) (Todman, 2007). Other symptoms of whiplash injuries include dizziness, auditory symptoms (tinnitus – perceived ringing noise in the ears), paresthesias in the upper extremities, and back pain (Mordaka and Gentle, 2003, Evans, 1992, Sterner and Gerdle, 2004, Spitzer et al., 1995). The recovery time from whiplash injuries depends on the initial whiplash injury severity, but 26% of occupants recover within the first week and the median recovery time is approximately 32 days (Suissa et al., 2001). However, 12% of occupants do not fully recover within six months (Suissa et al., 2001) and 5 to 8% of patients do not return to work within a year following the collision (Buitenhuis et al., 2009, Evans et al., 2001). Between 14 and 42% of injured occupants develop chronic neck pain and approximately 10% are left with permanent severe pain and

disability (Barnsley et al., 1994). Due to the persistence of chronic symptoms of WAD, these injuries are a serious economic and social burden to society. Therefore, it is important to reduce the incidence rate and the risk of whiplash injuries during rear-end collisions.

1.1.2 Biomechanics of Whiplash Injury

The biomechanics of human occupants during a low-speed, rear-end collision are variable and depend on the magnitude and shape of the acceleration pulse, seatback properties (i.e. seat hinge stiffness, seatback cushion compliance and seatback angle) and an occupant's anthropometry and initial posture. To help understand the whiplash motions, the movements of the torso, head and neck can be divided into two phases: the retraction phase and the rebound phases (Pearson et al., 2004, Brault et al., 2000, Vasavada et al., 2007). The retraction phase is defined from onset of head movement to peak linear rearward excursion of the head relative to the torso; whereas, the rebound phase is defined from peak head retraction to peak forward excursion of the head relative to the torso. During the retraction phase, forces are applied by the seatback to the torso as the seat is accelerated forward by the vehicle-to-vehicle impact. The torso is accelerated forward by the seat earlier than the head, which causes the head to lag behind (Luan et al., 2000, McConnell et al., 1995) and forces the cervical spine into a non-physiological "S"-shaped curve, in which the lower cervical vertebrae are in extension and the upper cervical vertebrae are in flexion. This shearing motion between the top and bottom of the cervical spine stretches portions of the cervical facet joint capsular ligament (Luan et al., 2000, Pearson et al., 2004) and other ligaments in the neck.

After peak head retraction, the head is accelerated forward relative to the torso due to the internally generated forces of the neck (McConnell et al., 1995) and rebound from the head restraint. The head is accelerated forward and overtakes the torso before being actively decelerated by the neck muscles and other passive structures of the neck (McConnell et al., 1995). After the head reaches maximum forward excursion with respect to the torso, the occupant's head and torso return back to their pre-perturbation position.

1.1.3 Injury Mechanisms of Whiplash

The etiology of whiplash injury remains uncertain, but there have been many proposed injury mechanisms. Some possible anatomical sites of injury in the neck include the neck muscles, spinal ligaments, intervertebral discs, vertebral arteries, dorsal root ganglia and the facet joints. Dorsal root ganglia damage and cervical facet joint disruption are two possible whiplash injury mechanisms that have been most thoroughly examined through animal and human occupant experiments, as well as clinical studies. The dorsal root ganglia are located along the vertebral column and consist of a collection of cell bodies from afferent nerve fibers that encode touch, stretch, temperature, pain, etc., from the skin, muscle, joint and other tissues. Injury to the cervical dorsal root ganglia, particularly in the lower cervical region, could explain most of the symptoms that are typically associated with neck injury sustained in rear-end collisions (Bostrom et al., 1996, Svensson et al., 1993, Svensson et al., 2000). Svensson et al. (1993) proposed that the sudden cervical extension-flexion motion would cause pressure gradients in the spinal canal that apply injurious stresses and strains to the dorsal root ganglia.

Fluids inside the spinal canals are virtually incompressible and fluid transportation must occur during the flexion and extension movements to relieve pressure within the cervical spinal canal (Aldman, 1986, Ortengren et al., 1996, Svensson et al., 1993). This injury mechanism is supported by histopathological studies of anaesthetized pigs exposed to swift extension-flexion motion of the cervical spine that produced nerve cell damage within the dorsal root ganglia (Ortengren et al., 1996, Svensson et al., 1993).

Another possible source of pain in whiplash injury is the cervical facet joint. Barnsley et al. (1994) performed clinical studies that identified the cervical facet joints as the source of neck pain in 40 – 68% of patients with chronic whiplash injuries following a rear-end collisions (Barnsley et al., 1995). The facet joint injury mechanism has further been support through animal studies (Macnab, 1971), cadaver experiments (Luan et al., 2000, Winkelstein and Myers, 2000) and human volunteer studies (Kaneoka et al., 1999). There are three possible causes of injury to the cervical facet joint: joint injury, synovial fold injury or joint capsule injury.

Joint injuries can occur when the sudden flexion and extension of the neck causes rotations of the cervical vertebral bodies about abnormally-located instantaneous axes of rotation (Kaneoka et al., 1999). As a result, the articular processes of the facet joints do not glide normally over one another, but instead the inferior articular processes of one vertebra are forced into the superior articular processes of the subjacent vertebra (Bogduk and Yoganandan, 2001, Kaneoka et al., 1999). At low impact speeds these abnormal rotations will cause no major injury, but at higher speeds (> 10 km/h) the facet joint may be injured.

Another possible source of cervical facet joint pain is injury to the synovial fold located between the two articulating facet joints (Kaneoka et al., 1999). Inami et al. (2001) used immunohistochemistry and immunostaining to show the presence of free nerve fibers, including nociceptive fibers, in human cervical synovial folds. It has been hypothesized that facet joint rotation during low-speed, rear-end collision could impinge on the synovial folds to cause cervical facet joint pain (Kaneoka et al., 1999).

The cervical facet capsule and its role in whiplash injury have been studied in both animals (Winkelstein and Santos, 2008) and human cadaver neck segments (Siegmund et al., 2008b, Winkelstein et al., 2000). In rat experiments, allodynia has been produced by applying tension across the joint capsule (Winkelstein and Santos, 2008). Cadaveric studies of whiplash injury have also shown that capsular ligament strains during the whiplash motion are largest in the lower cervical spine (C6/C7: 39.9%, C5/C6: 38.5%, C4/C5: 26.5%, C3/C4: 29.9%, C2/C3: 16.7%; Pearson et al., 2004). Due to the direct attachment of the cervical multifidus muscles onto the capsular ligaments of C4/5, C5/6 and C6/7 (Anderson et al., 2005), the early activation of the multifidus muscles during a rear-end impact could further increase the capsular ligaments strain induced by the intervertebral kinematics (Anderson et al., 2005, Siegmund et al., 2008a, Winkelstein et al., 2000). Failure testing of the joint capsules has quantified the maximum capsular strain at subcatastrophic (35 – 64.6% strain) and catastrophic (94 – 103.6% strain) failure (Siegmund et al., 2001, Winkelstein et al., 2000). A head-turned posture has been shown to increase capsular strain significantly, by as much as twice the strain in the neutral

head position, on the side towards which the head is turned (Siegmund et al., 2008b). These observations suggest that, in some individuals, cervical facet joint pain may be caused by subcatastrophic failure due to excessive capsular strains, which is significantly increased if the occupant's head is turned.

1.1.4 Anti-Whiplash Automotive Seats and Existing Safety Features

The automotive seat is not only designed for comfort but is also the primary safety device for occupants in a rear-end collision. To motivate manufacturers to design seats and head restraints that reduce the risk of whiplash injury in low/moderate-speed rear-end collisions, the Insurance Institute for Highway Safety (IIHS) publishes ratings of seats and head restraints using a two-part protocol developed by the Research Council for Automobile Repairs/International Insurance Whiplash Prevention Group (RCAR/IIWPG) (Insurance Institute of Highway Safety, 2004, Insurance Institute of Highway Safety, 2008a). First, a static test evaluates head restraint height (distance between the top of the head and the top of the head restraint) and backset (distance between the back of the head and the front of the head restraint) relative to the head of a median-sized male occupant. If the top of the head restraint is no more than 8 cm below the top of the head and the backset is no more than 9 cm (i.e., rated acceptable or good), the seat undergoes a dynamic test that simulates a rear-end collision with a peak acceleration of 10 g and a speed change of 16 km/h over 91 ms. The dynamic test is graded using a combination of peak upper neck forces (shear and axial), time-to-head-restraint contact, and peak forward acceleration of the T1 vertebra of a BioRID II anthropometric test device (ATD). Seats and head

restraints are rated as good, acceptable, marginal or poor depending on the combined rating of both the static and dynamic test results. In a comparison between RCAR/IIWPG ratings and real-world insurance claims, occupant neck injury rates were only 11 – 15% lower in seats rated good compared to seats rated poor (Farmer et al., 2008, Trempel et al., 2016). This meager benefit suggests that there remains considerable room for improving automotive seats and perhaps the rating system to better protect occupants from whiplash injuries.

Currently, anti-whiplash seats attempt to mitigate the risk of whiplash injuries during rear-end collisions by reducing the relative accelerations and displacements between the head and torso. Reducing these relative accelerations and displacements reduces the forces and strains that develop in the tissues of the neck. The magnitude of these accelerations and displacements are modulated by the occupant's interaction with the seatback, and can vary with seatback stiffness (Viano, 2003b, Viano, 2003d). Stiffer seatbacks are less likely to deform and thus provide better occupant retention but result in higher forces applied to the occupant. Yielding seatbacks attenuate forces applied to the occupants but increase the likelihood of the seatback collapse and occupant ejection from the seat. In the late 1990's, General Motors (GM) introduced the "high retention" seat design that embodied the beneficial characteristics of both a yielding and a rigid seat design. The GM High Retention seat (GMHR) utilized a stiffer outer seatback frame with a yielding seatback center. The two components work together as the yielding seatback center section absorbs energy and more gradually decelerates the torso

during the collision, while the stiffer seatback frame enhances occupant retention and prevents large seatback deflections.

Volvo's Whiplash Injury Prevention seat (WHIPS) is another implementation of an anti-whiplash device that reduces occupant accelerations during a collision. The WHIPS seat also utilizes a yielding seatback center, but includes an energy-absorbing recliner mechanism that controls the motion of the seatback relative to the seat pan (Jakobsson et al., 2000, Lundell et al., 1998a). The recliner mechanism initially translates the seatback horizontally rearward with respect to the seat pan to improve an occupant's head, neck, and torso alignment as well as to absorb some of the energy generated by the collision. The mechanism then rotates the seatback rearward to further reduce the accelerations and the occupant's subsequent forward rebound (Lundell et al., 1998a). Since the WHIPS system is passive, the degree of rearward translation, rearward rotation, and overlap of the two motions depends on parameters such as occupant mass, seating posture and crash severity.

Minimizing the displacement of the head relative to the upper torso also contributes to reducing the risk of whiplash injury. Proper head restraint positioning is critical to reducing neck extension and head-to-head-restraint responses during collisions to mitigate whiplash injury (Viano, 2002). Active head restraints (e.g., Saab's Active Head Restraint, or SAHR) have been developed to improve head-to-head-restraint alignment during collisions. The SAHR is a passive device that reduces the need for an occupant to manually adjust the head restraint to the correct position. As with the WHIPS and GMHR, the SAHR seat utilizes a stiff outer seatback

frame with a yielding seatback center. The main difference in the SAHR seat is the addition of a metal back plate located within the seatback that is connected to the head restraint. As an occupant's torso penetrates the seatback, the torso triggers the back plate and linkage mechanism to move the head restraint upwards and forwards to the back of an occupant's head. The SAHR is designed to move the head restraint early in the collision to support the head/neck complex through most of the whiplash motion. Decreasing the backset between the head and head restraint will result in a reduction in the rearward translation of the head relative to the torso.

1.1.5 Effectiveness of Current Anti-Whiplash Devices

Epidemiological studies of current anti-whiplash devices have shown the benefits of both the WHIPS and SAHR in reducing whiplash injury following rear-end collisions (Farmer et al., 2003, Ivancic, 2011, Viano and Olsen, 2001). In a 2003 study, Farmer and colleagues analyzed real-life insurance claims in the United States occurring between January 1st, 1999 and June 30th, 2001 and observed that WHIPS and SAHR decreased the neck injury rates by 49% and 43%, respectively (Farmer et al., 2003). In another study conducted by Volvo, self-reported injury data from 2521 occupants in Volvo cars of model year 1999 (1858 occupants in WHIPS vs. 663 occupants in conventional seats) indicated a neck injury risk reduction between 21 and 47% depending on impact severity and symptom duration (Jakobsson et al., 2008). Similarly, Saab Automobiles conducted a questionnaire and phone-interview study of 177 insurance claims (92 occupants in SAHR vs. 85 occupants with standard head restraints) from September 28th, 1998

through April 4th, 2000 (Viano and Olsen, 2001). This study indicated a potential for SAHR to decrease the number of injured occupants by 20% (incident rate: SAHR: 41% vs. standard head restraint: 53%) and to reduce whiplash injuries leading to medium- and long-term symptoms in occupants by 75% (incident rate: SAHR: 4% vs. standard head restraint: 18%). Current anti-whiplash devices (e.g. Volvo's WHIPS and Saab's SAHR) have not eliminated the risk of whiplash injury, but they have decreased the risk of whiplash injury during rear-end collisions (Farmer et al., 2003, Jakobsson et al., 2008, Viano and Olsen, 2001). Thus, additional research addressing whiplash injury mechanisms may lead to the design of novel and efficient injury prevention devices that further reduce the risk of whiplash injury following a rear-end collision.

1.2 **Overall Research Objective and Goals**

The overall objective of the experiments presented in this dissertation was to develop a novel anti-whiplash seat that dynamically modified the seat hinge and seatback cushion properties to attenuate the occupant response during low-speed, rear-end collisions (see **Appendix A** for details on the anti-whiplash seat design). The main safety features of the Experimental anti-whiplash seat were the active control of seat hinge rotation and seatback cushion deformation to decrease the accelerations experienced by the occupant and to reduce the relative motion between the occupant's head and torso. This dissertation was divided into four experiments with the goal of answering the following questions:

Experiment 1: How do current anti-whiplash seats perform during low-speed, rear-end collisions?

Experiment 2: Can active control of seat hinge rotation attenuate ATD responses during low-speed, rear-end collisions?

Experiment 3: Can active control of seatback cushion deformation attenuate ATD responses during low-speed, rear-end collisions?

Experiment 4: Can co-activation of the seat hinge rotation and seatback cushion deformation further attenuate ATD responses compared to current anti-whiplash seats during low-speed, rear-end collisions?

These experiments were designed to test the different safety features of our Experimental anti-whiplash seat. To minimize potential sources of variability in the experimental design, the following procedures were chosen despite restricting the potential generalizability of the results. First, a 50th percentile male BioRID II anthropomorphic test device (ATD; Humanetics Innovative Solutions, Farmington Hills, MI, USA) was selected as a surrogate to human occupants. Even though females are more at risk of developing symptoms following rear-end collisions (Mordaka and Gentle, 2003, Harder et al., 1998, Versteegen et al., 2000), a female ATD is currently in development and only the 50th percentile male BioRID II ATD was validated at the time of performing these experiments. Second, only front passenger seats were used for all experiments. Passenger seats share similar designs and structures to driver seats, but are typically used less in vehicles (average vehicle occupancy rate = 1.67; McGuckin and Fucci, 2018). Third, neither a steering wheel nor a seatbelt were used in the experiments to better isolate the influence of the seat properties on the occupant responses. Due to the low

collision severities used in our experiments, most peak occupant responses are expected to occur during the retraction phase of whiplash motion (Siegmund et al., 2005a) when the occupant is translating rearward into the seatback away from the steering wheel and stationary seatbelt. Hence, these experimental decisions allowed a specific investigation of the role of anti-whiplash seats on the occupant responses following rear-end collisions but require careful consideration prior to further development of a seat that better protects all occupants.

Chapter 2. A Comparison of Anti-Whiplash Seats During Low/Moderate Speed, Rear-End Collisions

2.1 Introduction

Whiplash injuries are the most common type of injuries associated with motor vehicle crashes, and rear-end collisions pose the greatest risk of whiplash injury (Jakobsson et al., 2000, National Highway Traffic Safety Administration, 2014). To motivate manufacturers to design seats and head restraints that reduce the risk of whiplash injury in low/moderate-speed rear-end collisions, the Insurance Institute for Highway Safety (IIHS) publishes ratings of seats and head restraints using a two-part protocol developed by the Research Council for Automobile Repairs/International Insurance Whiplash Prevention Group (RCAR/IIWPG) (Insurance Institute of Highway Safety, 2008b, Insurance Institute of Highway Safety, 2008a). First, a static test evaluates head restraint height (distance between the top of the head and the top of the head restraint) and backset (distance between the back of the head and the front of the head restraint) relative to the head of a median-sized male occupant. If the top of the head restraint is no more than 8 cm below the top of the head and the backset is no more than 9 cm, the seat undergoes a dynamic test that simulates a rear-end collision with a peak acceleration of 10 g and a speed change of 16 km/h over 91 ms. The dynamic test is graded using a combination of peak upper neck forces (shear and axial), head-to-head restraint contact time, and peak forward acceleration of the T1 vertebra of a BioRID II anthropometric test device (ATD). Seats and head restraints are rated as good, acceptable, marginal or poor depending on the

combined rating of both the static and dynamic test results. In a comparison between RCAR/IIWPG ratings and real-world insurance claims, occupant neck injury rates were only 11 – 15% lower in seats rated good compared to seats rated poor (Farmer et al., 2008, Trempel et al., 2016). This meager benefit suggests that there remains considerable room for improving both automotive seats and the rating system to better protect occupants from whiplash injuries.

Some manufacturers have developed seats specifically focused on reducing the risk of whiplash injury. Current anti-whiplash seats, such as General Motors' High Retention seat (GMHR), Volvo's Whiplash Injury Prevention seat (WHIPS) and Saab's Active Head Restraint seat (SAHR), attempt to reduce whiplash injury risk by reducing key occupant kinematics such as the relative motion between the head and upper torso. According to the IIHS (Insurance Institute of Highway Safety, 2004), the GMHR was rated poor, whereas both the WHIPS and SAHR were rated good. The GMHR is designed with a rigid perimeter seat frame and a compliant seatback suspension to allow the occupant to "pocket" into the seatback and increase occupant retention (Viano, 2003a, Viano and Parenteau, 2015). The WHIPS and SAHR seats are equipped with dynamic anti-whiplash devices that rely on occupant loading of the seatback to deform a recliner mechanism that controls seatback translation and rotation (WHIPS) (Jakobsson et al., 2008, Jakobsson et al., 2000) or to move the head restraint upward and forward (SAHR) (Viano and Olsen, 2001). Epidemiological studies have shown that these dynamic anti-whiplash seats reduce the risk of whiplash injury by 20 to 75% when compared to previous versions of the

same seat without the anti-whiplash mechanism and dependent on how injury is defined. Although most studies converging on a reduction in the risk of whiplash injury of about 40 to 50% (Viano and Olsen, 2001, Jakobsson et al., 2008, Kullgren and Krafft, 2010, Farmer et al., 2003, Kullgren et al., 2007), these injury reduction rates suggest that many people still do not benefit from current dynamic anti-whiplash seats.

One possible reason for the incomplete effectiveness of anti-whiplash seats is that they have been tested at the RCAR/IIWPG dynamic test pulse (10 g, 16 km/h, Δt = 91 ms). This pulse is more severe than the speed change reported to cause many whiplash injuries, some of which are reported following collisions with speed changes as low as 6 to 8 km/h (Bartsch et al., 2008, Krafft et al., 2005). The RCAR/IIWPG test pulse represents a generic collision pulse that is a necessary compromise for a safety standard, but nevertheless eliminates a wide range of actual collision pulses in terms of pulse shape, duration and severity (Cappon et al., 2001, Langwieder and Hell, 2002, Linder et al., 2003, Linder et al., 2001). Moreover, seats optimized for a single pulse (e.g. the RCAR/IIWPG test pulse) may perform sub-optimally under other conditions inducing whiplash injuries. The goal of this study was to evaluate the performance of some anti-whiplash seats across a range of speed changes below 16 km/h to gain a better understanding of how occupant kinematic and kinetic parameters vary with collision severity. We hypothesized that both the WHIPS and SAHR anti-whiplash seats (rated good by RCAR/IIWPG) would cause lower occupant kinematic and kinetic responses in comparison to the GMHR seat (rated poor RCAR/IIWPG) across a range of collision severities.

2.2 Methods

2.2.1 Anthropomorphic Test Device and Instrumentation

A BioRID II ATD (Humanetics, Plymouth, MI, USA) was instrumented to measure the kinematic and kinetic responses of the head, neck and torso during controlled laboratory rear-end impacts. Linear accelerations were measured using two uni-axial accelerometers (7264C; ±500 g, Endevco, San Juan Capistrano, CA, USA) mounted at both the head center of mass and T1 vertebra. Uni-axial angular velocity sensors were also mounted to the head (ARS-1500; ±26.2 rad/s, DTS, Seal Beach, CA, USA) and to the T1 vertebra (ARS-04E; ±100 rad/s, ATA Sensors, Albuquerque, NM, USA) to measure angular kinematics in the sagittal plane (i.e. flexion and extension of the head and T1). A six-axis load cell (Model 4949a, Robert A. Denton, Inc., Rochester Hills, MI, USA) was installed to measure upper neck forces and moments. A motion capture system (Optotrak Certus, Northern Digital, Waterloo, ON, Canada) was used to track infrared light emitting diode (IRED) markers affixed to the ATD's head, C1 and T1 vertebrae to measure head and neck displacements. Head restraint contact was detected with a force sensitive resistor (FSR, Model 406; Interlink Electronics, Camarillo, CA, USA) attached to the front of the head restraint. Horizontal sled acceleration was measured with a uni-axial accelerometer (2220-100; ±100 g, Silicon Design Inc., Issaquah, WA, USA).

2.2.2 Test Procedures

The BioRID II ATD was clad in two layers of lycra and seated on a feedback-controlled linear sled (Kollmorgen IC55-100A7, Waltham, MA, USA) fitted with one of four different front

passenger seats: A) 2005 Volvo S40 WHIPS, B) 2004 Volvo S60 WHIPS, C) 2005 Saab 9.3 SAHR, and D) 2004 Pontiac Grand Am GMHR (**Figure 2.1**). On each seat, the unbelted ATD was exposed to a series of seven whiplash-like perturbations at increasing speed changes (Δv = 2, 4, 6, 8, 10, 12 and 14 km/h) with a pulse duration (Δt) of 141 ms (**Figure 2.2**). The sled was accelerated forward from a stationary position for the 2, 4 and 6 km/h tests, and from a constant rearward speed of 6 km/h for the higher speed changes (8, 10, 12 and 14 km/h). Pilot tests comparing ATD responses of an 8 km/h collision starting from a stationary position to an 8 km/h collision starting from a 6 km/h rearward velocity showed between 0.2% and 10.1% differences (mean = 4.7%) in the peak ATD responses and neck injury criteria (**Figure 2.3**). Four additional repeated trials were collected at the 8 km/h collision speed change for all seats, as well as at the 4 and 12 km/h speed changes only on the GMHR seat (for a total of 5 trials in each experimental condition) to assess the repeatability and reliability of BioRID II ATD occupant responses. A total of 52 trials were collected: 11 trials were collected for the SAHR, S40 WHIPS and S60 WHIPS seats and 19 trials were collected for the GMHR seat.

Seat geometry was measured before and after each collision to ensure no permanent deformation had occurred. We also verified that no damage occurred to the deformable elements in the WHIPS seat and that the SAHR mechanism had returned to its original position following each test. Additional Optotrak markers were placed on the seats and linear sled to determine seatback and head restraint position as well as to create a global experimental

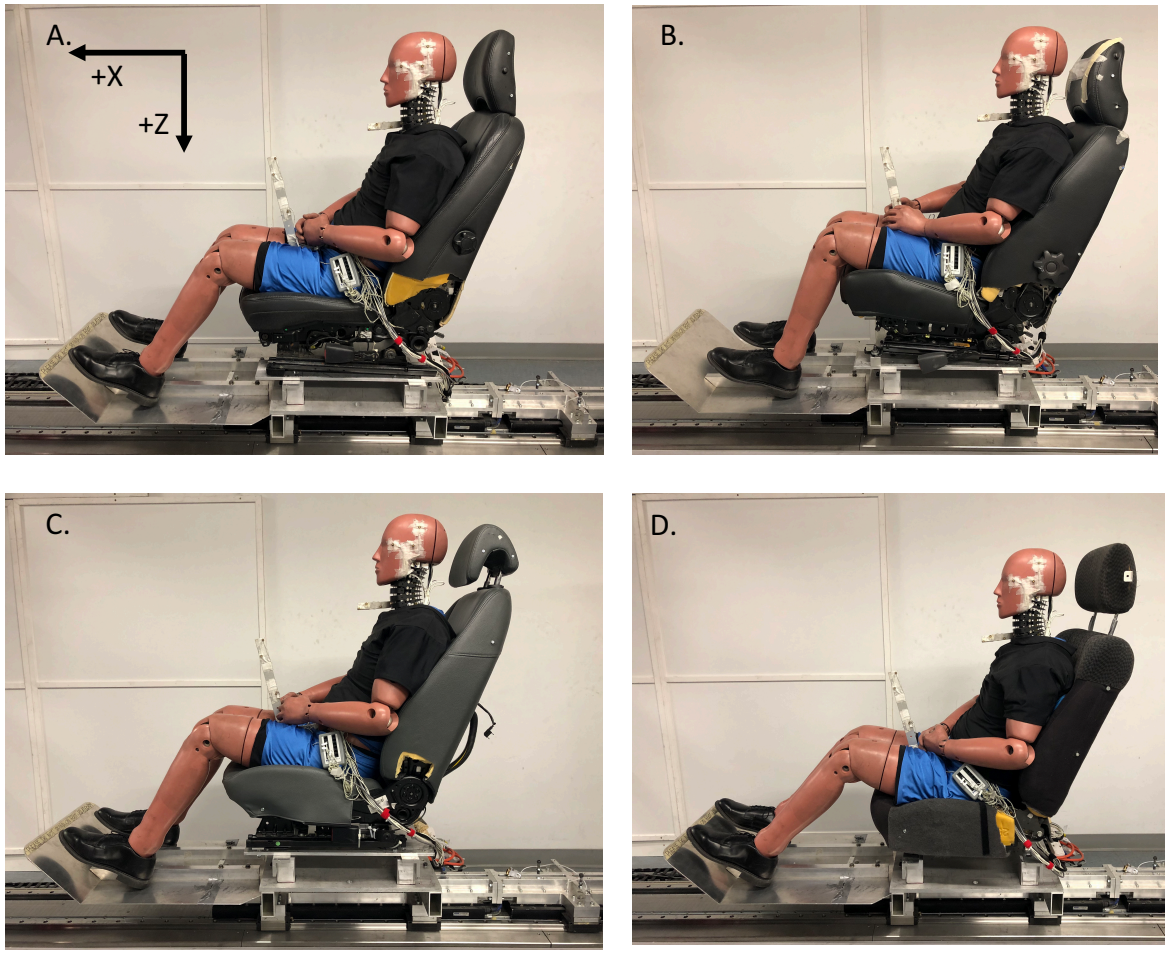

Figure 2.1. Photographs of the experimental set-up with the BioRID II ATD on the four test seats in the laboratory reference frame (X, Z). A.) 2005 Volvo S40 WHIPS, B.) 2004 Volvo S60 WHIPS, C.) 2005 Saab 9.3 SAHR and D.) 2004 Pontiac Grand Am GMHR.

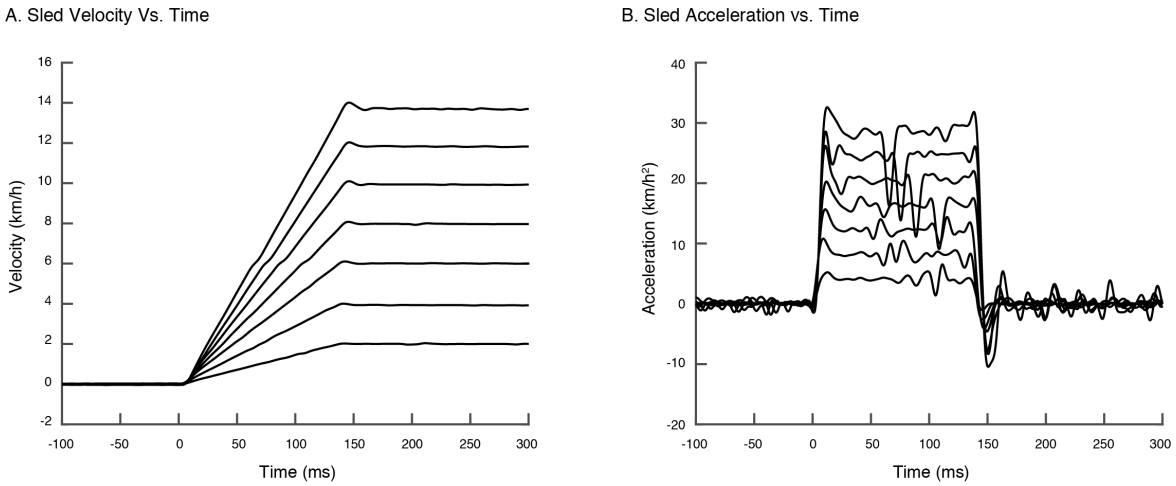

Figure 2.2. Exemplar sled A.) velocity and B.) acceleration pulses for increasing collision speeds (Δv = 2, 4, 6, 8, 10, 12 and 14 km/h with a pulse duration (Δt) of 141 ms). Collision onset occurred at time = 0 ms.

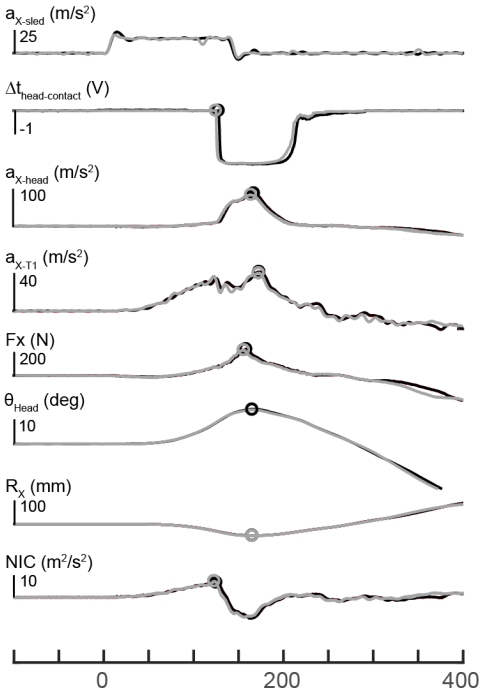

Figure 2.3. ATD occupant responses comparing an 8km/h collision severity from a stationary position (grey line) and from a 6km/h constant rearward speed (black line) on the Pontiac Grand Am GMHR seat. Hollow circles represent peak responses for a given variable.

reference frame (+X forward, +Y right, and +Z down). The initial position of the ATD was adjusted to a pre-defined posture that was constant within each seat and as similar as possible between seats. This pre-defined posture was confirmed using the 3D positions measured by the Optotrak at the beginning of all trials. Initial seatback angles were set to 27 deg rearward of vertical (Siegmund et al., 2005a) and the height of the head restraint was adjusted according to the RCAR/IIWPG seat/head restraint evaluation protocol (Insurance Institute of Highway Safety, 2008b). For all seats, the top of the head restraint was less than 6 cm lower than the top of the ATD head (positive values indicate that the top of head was higher than the top of the head restraint) and would receive good ratings for head restraint height (**Table 2.1**). The backset distance for each head restraint was defined as the average distance between the back of the ATD head and the front face of the head restraint over the 100 ms immediately preceding the onset of forward sled acceleration. Backset distances less than 7 cm were considered good, between 7 and 9 cm were considered acceptable, between 9 and 11 cm were considered marginal, and greater than 11 cm were considered poor according to the RCAR/IIWPG rating (**Table 2.1**).

Table 2.1. Mean (standard deviation) of head restraint backset and height determined by Optotrak prior to the onset of each collision.

Seat	n	Backset (cm)	Height (cm)
Volvo S40 WHIPS	11	4.66 (0.51)	0.42 (0.52)
Volvo S60 WHIPS	11	3.74 (1.5)	5.41 (0.52)
Saab 9.3 SAHR	11	7.86 (0.77)	3.38 (0.36)
Pontiac Grand Am GMHR	19	9.52 (0.70)	2.50 (0.29)

Notes: n denotes the number of trials for each seat used for the calculations. Backset: distance between the back of the head to the front face of the head restraint. Height: distance between the top of the head to the top of the head restraint (positive values indicated the top of the ATD head is higher than the head restraint).

2.2.3 Data Analysis

All accelerometer, load cell and angular velocity transducer signals were simultaneously sampled at 2000 Hz using a National Instruments Data Acquisition (DAQ) PXI system (PXI-4495 & PXI-6289, National Instruments Corporation, Austin, Texas, USA) and a custom-written LabVIEW virtual instrument (National Instruments Corporation, Austin, Texas, USA). Optotrak data were acquired at 200 Hz per frame and the onset of collection was triggered by the DAQ system to synchronize the data. All data channels conformed to SAE J211 (Channel class 180 for the ATD sensors and Channel Class 60 for the sled accelerometer) (SAE, 1995). Subsequent data analysis was performed using Matlab (R2017A, Mathworks, Newton, MA, USA).

To compare the BioRID II ATD responses between the different seats and different collision pulses, peak kinematic and kinetic responses were extracted for each trial. Accelerometer data were reported in local head and T1 reference frames and were corrected to remove the earth's gravitation field using the head and T1 orientations determined from Optotrak data. Peak linear forward acceleration of the sled ($a_{X\text{-}sled}$), head ($a_{X\text{-}head}$) and T1 vertebra ($a_{X\text{-}T1}$) were extracted directly from the transformed accelerometer data. Peak rotational velocities of the head ($\omega_{Y\text{-}head}$) and T1 ($\omega_{Y\text{-}T1}$) in the sagittal plane were determined from the angular velocity sensors. Peak upper neck shear (F_X) and axial (F_Z) forces and the flexion/extension bending moment (M_Y) were determined from the upper neck load cell and reported in the ATD reference frame as the forces/moments applied by the neck to the head. Initial head angle was defined as the average angle over the 250 ms preceding the onset of forward sled acceleration and peak head extension angle (θ_{head}) was defined as the maximum rearward rotation of the head into extension relative to initial head angle. Peak retraction (R_x) was defined as the maximum horizontal rearward displacement in the laboratory reference frame between the atlanto-occipital joint (AOJ) pin and T1 vertebrae with rearward displacements defined as negative values. Head-to-head restraint contact time ($\Delta t_{head\text{-}contact}$) was extracted from the onset of the FSR data attached to the head restraint with the onset of forward sled acceleration defined as t = 0 ms. Onset of sled acceleration and head restraint contact were determined when the accelerometer and FSR signals, respectively, reached 1.5 times the peak background noise level measured over 2 seconds prior to the onset of the collision pulse and confirmed visually.

Three neck injury criteria (NIC, N_{ij}, and N_{km}) were computed from the accelerometer and load cell data. The Neck Injury Criterion (NIC) was calculated from the relative horizontal acceleration and velocity in the global reference frame between the head center of mass and the T1 joint (Equation 2.1) (Bostrom et al., 1996). The Normalized Neck Injury Criterion (N_{ij}) was calculated from the axial load (F_Z) and the flexion/extension bending moment (M_Y) measured from the upper neck load cell (Equation 2.2; critical F_{int} and M_{int} intercept values used for normalization: $F_{int\text{-}tension}$ = 6806 N, $F_{int\text{-}compression}$ = -6160 N, $M_{int\text{-}flexion}$ = 310 N, and $M_{int\text{-}extension}$ = -135 N; Eppinger et al., 1999, Eppinger et al., 2000). The Neck Protection Criterion (N_{km}) was calculated from the sagittal shear force (F_X) and the flexion/extension bending moment (M_Y) measured from the upper neck load cell (Equation 2.3; critical F_{int} and M_{int} intercept values used for normalization: $F_{int\text{-}shear\text{-}positive}$ = 845 N, $F_{int\text{-}shear\text{-}negative}$ = 845 N, $M_{int\text{-}extension}$ = 47.5 Nm, and $M_{int\text{-}flexion}$ = 88.1 Nm; Schmitt et al., 2001, Schmitt et al., 2002). Peak values of the three neck injury criteria were then extracted for analysis and compared to proposed injury thresholds (NIC: 15 m^2/s^2, Eichberger et al., 1998; N_{ij} and N_{km} : a normalized value of one, Schmitt et al., 2001, Schmitt et al., 2002, Eppinger et al., 1999). These injury thresholds correspond to different human tolerance levels for the causation of whiplash-related injuries – NIC: long-term whiplash-associated disorders (WAD) levels 1-3 (Bostrom et al., 2000, Bostrom et al., 1996), N_{ij}: 22% risk of abbreviated injury scale (AIS) level 3 (i.e., fracture; Eppinger et al., 1999, Eppinger et al., 2000), and N_{km}: AIS level 1 injury causation (i.e., minor injury; Schmitt et al., 2001, Schmitt et al., 2002).

$$\mathrm{NIC(t)} = a_{rel}(t) \cdot L + (v_{rel}(t))^2 \quad \ldots \quad \text{Equation 2.1}$$

$$\mathrm{N_{ij}(t)} = \frac{\mathrm{F_z(t)}}{\mathrm{F_{int}}} + \frac{\mathrm{M_{yOC}(t)}}{\mathrm{M_{int}}} \quad \ldots \quad \text{Equation 2.2}$$

$$\mathrm{N_{km}(t)} = \frac{|\mathrm{F_x(t)}|}{\mathrm{F_{int}}} + \frac{|\mathrm{M_{yOC}(t)}|}{\mathrm{M_{int}}} \quad \ldots \quad \text{Equation 2.3}$$

The repeatability of the BioRID II ATD was assessed using the Coefficient of Variation (COV), which was calculated as the standard deviation divided by the mean and expressed as a percent (Davidsson, 1999, Moorhouse et al., 2012, Rhule et al., 2005, Siegmund et al., 2005b). The National Highway Traffic Safety Administration (NHTSA) defines a COV of 5% or less as good, a COV of 10% or less as acceptable and a COV greater than 10% as poor (Rhule et al., 2005). To quantify the repeatability, we calculated the COV for the peak occupant responses from five repeated trials at three different collision severities (Δv = 4, 8 and 12 km/h) on the GMHR seat and at the 8 km/h collision severity for the SAHR and WHIPS seats. For the GMHR seat, most of the COVs were below 5%, except for the shear and axial neck forces (7.9% and 5.8% respectively), both of which were lower than values reported by other researchers (Davidsson, 1999, Moorhouse et al., 2012) (**Table 2.2**). For the SAHR and WHIPS seats, the COVs of the upper neck loads (F_X and F_Z) were greater than 10%, but consistent with earlier work (Davidsson, 1999). Detailed COV data for all seats and variables are presented in the **Appendix E: Tables E2.1** and **E2.2**.

To compare BioRID II ATD responses between seats, 99th percentile predictive intervals were created around the peak responses using the maximum variability observed for the GMHR

seat at 4, 8 and 12 km/h (Horslen et al., 2015). The maximum COV values were multiplied by 2.58 to estimate 99% predictive limits and applied to the respective peak responses for all collision severities. ATD responses observed on the other seats that fell outside these point-wise 99% predictive corridors were judged to be statistically different from the responses of the ATD in the GMHR seat. Averaged peak responses were used for test conditions with repeated trials (GMHR: Δv = 4, 8, and 12 km/h trials; SAHR & WHIPS: 8 km/h trials).

Table 2.2. Coefficients of Variation (COV) for some peak ATD responses compared to previous literature.

Parameter	Davidsson (1999) BioRID I (n = 5)		Moorhouse et al. (2012) BIORID II (n = 3)		Current study, GMHR BioRID II (n = 5)	
	Mean (SD)	COV (%)	Mean	COV (%)	Mean (SD)	COV (%)
ΔV	17 km/h		17 km/h		12 km/h	
$a_{X\text{-sled}}$ (m/s^2)	104 (1.1)	1.0	-	-	28.6 (0.1)	0.4
$a_{X\text{-head}}$ (m/s^2)	283 (13.0)	4.6	96.4	<u>8.8</u>	130.4 (1.4)	1.1
$a_{X\text{-T1}}$ (m/s^2)	116 (4.0)	3.4	23.9	<u>7.5</u>	51.3 (0.5)	1.0
F_X (N)	455 (45.9)	**10.1**	-	<u>9.0</u>	220.9 (17.5)	<u>7.9</u>
F_Z (N)	2900 (817.0)	**28.1**	820.3	<u>6.8</u>	684.7 (39.5)	<u>5.8</u>
M_Y (Nm)	-	-	-	<u>7.9</u>	14.0(0.6)	4.2
NIC (m^2/s^2)	-	-	-	-	11.0 (0.3)	3.1

<u>Notes:</u> The <u>underlined</u> COV values indicate a COV rating of acceptable (5% ≤ COV < 10%), the **bolded** COV values indicate a COV rating of poor (COV > 10%), and all other values are rated good (COV < 5%). Full list of COV values for all experimental parameters is given in **Appendix E: Tables E2.1** and **E2.2**.

2.3 **Results**

Positively graded responses with increasing speed change were observed in most kinematic and kinetic variables (**Figures 2.4** and **2.5,** see also **Figures E2.1 – E2.4** in the **Appendix E**). For all four seats, peak forward accelerations of the head ($a_{X\text{-}head}$) and torso ($a_{X\text{-}T1}$), peak angular head velocity (ω_{head}), and the three neck injury criteria (NIC, N_{ij}, and N_{km}) increased with collision severity (**Figure 2.5A-C, Figure 2.5G, and Figure 2.5I-L**). Peak head extension remained relatively constant across all speed changes for the four seats (**Figure 2.5H**).

The ATD kinematic and kinetic responses were generally similar for the three good seats, but the good seats were only clearly different from the GMHR seat for four variables: peak upper neck forces (F_X and F_Z) and moments (M_Y) as well as peak rearward head retraction (R_X). Peak upper neck shear forces (F_X) and retraction (R_X) increased with increasing speed change for the GMHR seat, but generally decreased (or remained constant) for the WHIPS and SAHR seats (F_X: 25 to 79% and R_X: 30 to 55% of the poor rated seat responses for $\Delta v > 6$ km/h) (**Figure 2.5E** & **I**). At and above 8 km/h ($\Delta v \geq 8$ km/h), the WHIPS and SAHR seats decreased, or eliminated, the peak positive shear forces ($+F_X$) and extension bending moments ($+M_Y$) ((F_X: -1 to 55% and M_Y: 31 to 70% of poor rated seat responses) but increased the peak negative shear forces ($-F_X$) and flexion bending moments ($-M_Y$) (**Figure 2.4**, **2.5D** & **2.5E,** see also **Figures E2.1 – E2.4** in the **Appendix E**).

All three neck injury criteria (NIC, N_{ij} and N_{km}) increased with speed change for all four seats (**Figure 2.5J-L**). Neither NIC nor N_{ij} exceeded their respective proposed injury thresholds, but N_{km} exceeded the injury threshold value of 1 in the 14 km/h performed on the SAHR seat (**Figure 2.5L**).

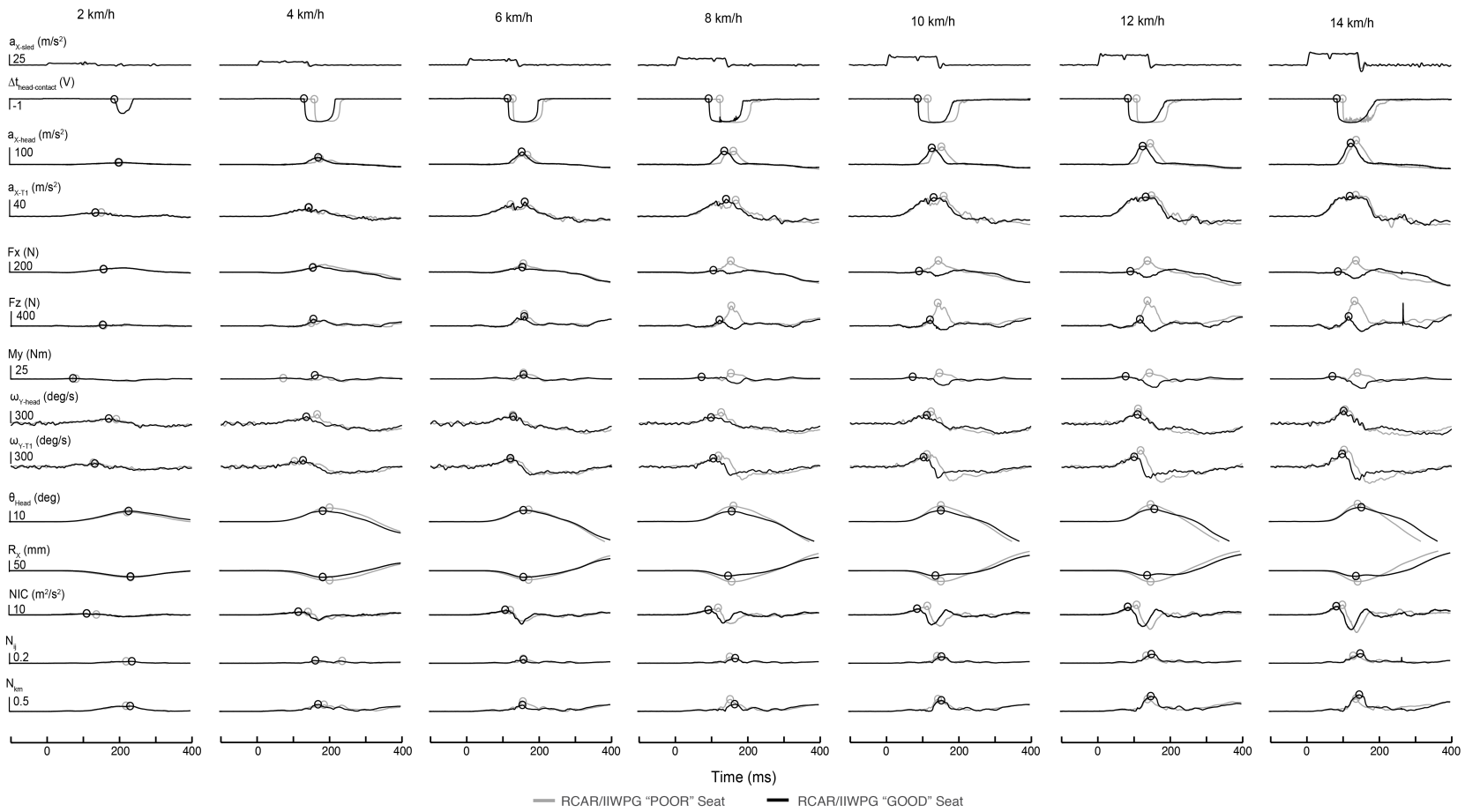

Figure 2.4. Exemplar data comparing a RCAR/IIWPG good rated (Volvo S40 WHIPS; black line) and a RCAR/IIWPG poor rated (Pontiac Grand Am GMHR; grey line) seat for the BioRID II ATD. Each column represents occupant responses for a good and poor seat while exposed to various collision severities (Δv = 2, 4, 6, 8, 10, 12 and 14 km/h with a collision pulse duration (Δt) of 141 ms). Hollow circles represent the onset of head-to-head-restraint contact and peak responses of each ATD response parameter for each trial. Similar plots for all seats are given in the **Appendix E: Figures E2.1 – E2.4**.

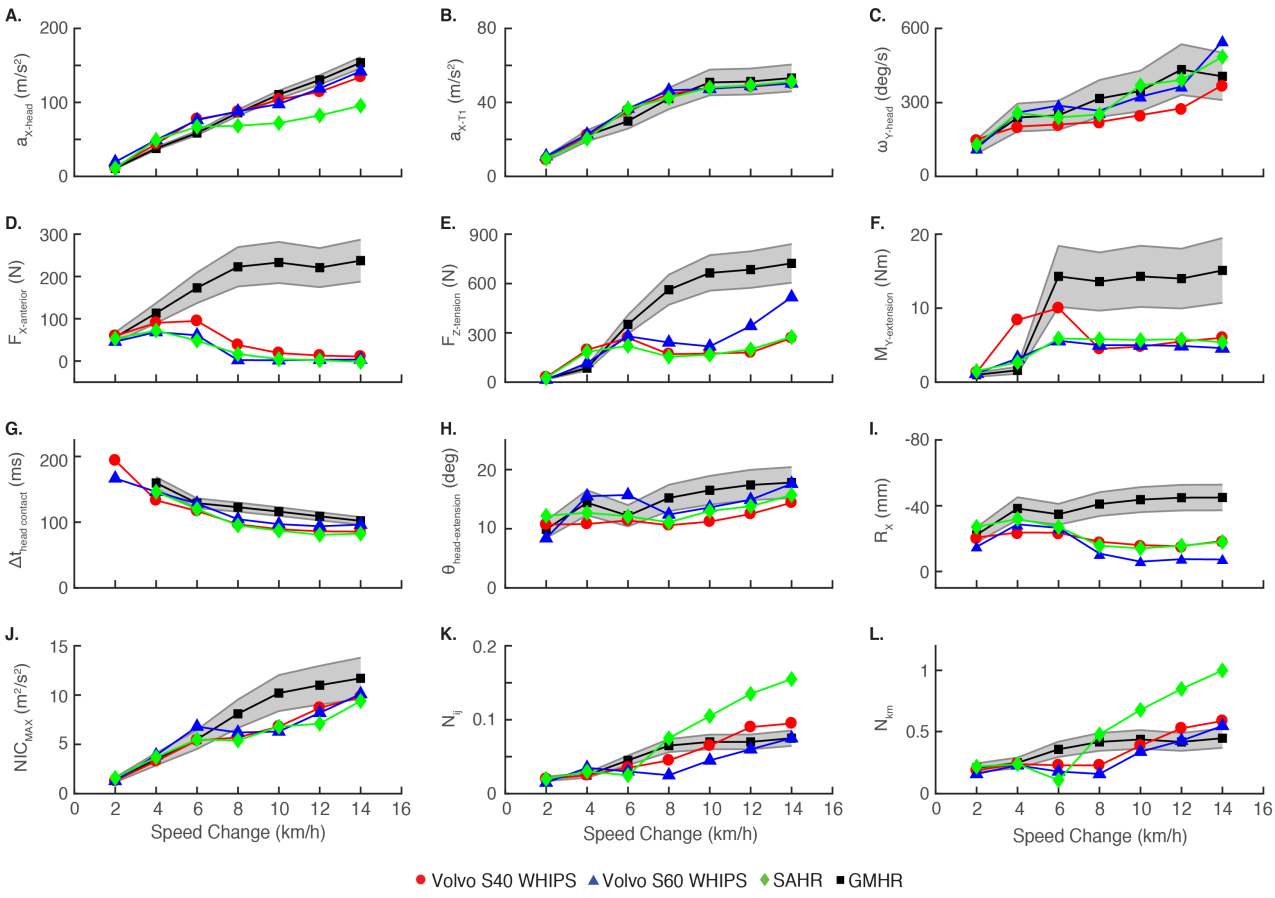

Figure 2.5. Experimental results of peak kinematic and kinetic responses for the BioRID II ATD seated on the WHIPS, SAHR and GMHR seats. For all the graphs, red circles represent the Volvo S40 WHIPS seat, blue triangles represent the Volvo S60 WHIPS seat, green diamonds represent the SAHR seat, and black squares represent the GMHR seat. Grey corridors represent 99% predictive interval for ATD responses on the poor rated GMHR seat. Y-axis values for panel I have been inverted for visual purposes to show increasing responses from bottom to top.

2.4 **Discussion**

The goal of this study was to evaluate the performance of anti-whiplash seats across a range of speed changes. This goal was motivated in part by the marginal reductions in whiplash injury risk between seats rated good and poor by the IIHS using the RCAR/IIWPG test method (Insurance Institute of Highway Safety, 2008b). Moreover, we sought to examine the changes in ATD kinematic and kinetic responses for speed changes below the 16 km/h level prescribed by the RCAR/IIWPG test to gain a better understanding of why anti-whiplash seats have not generated a greater reduction in whiplash injury risk.

Although the exact injury mechanisms causing whiplash injury remains unclear, the ability of the WHIPS and SAHR seats to attenuate the peak ATD upper neck loads and moments, and head retraction suggested that these responses may be associated with a higher risk of whiplash injuries (Viano and Olsen, 2001, Jakobsson et al., 2008, Kullgren and Krafft, 2010, Farmer et al., 2003, Kullgren et al., 2007). For these variables (F_X, F_Z, M_Y and R_X), the three good rated seats generated lower responses with increasing speed change in comparison to the GMHR seat where the responses continued to increase with speed change. The poor rated seat did not attenuate these four ATD responses suggesting it was unable to support the head and neck complex and, thus, increased both the relative head/torso motion and resulted in additional stresses/strains applied to neck structures. A shift in peak shear forces (F_X) and neck bending moment (M_Y) from positive shear forces ($+F_X$) and extension moments ($+M_Y$) to negative shear forces ($-F_X$) and extension moments ($-M_Y$) was also observed in the good rated

seats at speed changes greater than 6 km/h ($\Delta v > 6$ km/h). These results, in combination with earlier head contact times ($\Delta t_{head\text{-}contact}$) and decreased retraction (R_X), suggested that the WHIPS and SAHR seats supported the head and neck complex earlier into a forward flexed position instead of the rearward extended position observed in the GMHR seat. This adaptation of the forward flexion position during the whiplash motion may explain why good rated seats performed better than poor rated seats at reducing the neck injury rate by 11% to 15% (Farmer et al., 2008, Trempel et al., 2016*)*. However, the ability of the WHIPS and SAHR seat to only attenuate four peak ATD responses (F_X, F_Z, M_Y and R_X) in comparison to the GMHR seat may explain why real-world epidemiological studies have observed a limited reduction in the risk of whiplash injury of about 40 to 50% (Jakobsson et al., 2008, Kullgren and Krafft, 2010, Viano and Olsen, 2001). Anti-whiplash seats are designed to attenuate the kinematic or kinetic responses thought to be responsible for whiplash injury but because the injury mechanisms underlying whiplash remain unclear, reducing occupant accelerations (head and torso) and/or minimizing the movement of the head relative to the upper torso, although potential targets, may not completely protect occupants against whiplash injuries (Siegmund et al., 2009). Future work is needed to identify the biomechanical factors leading to whiplash injuries to help the development of anti-whiplash automotive seats.

Across the four seats and seven speed changes tested, NIC did not exceed the proposed threshold of 15 m^2/s^2 (Eichberger et al., 1998) and N_{ij} remained well below the injury thresholds of one (Schmitt et al., 2001, Schmitt et al., 2002, Eppinger et al., 1999). N_{km} was the only neck

injury to exceed the proposed injury threshold of one, which corresponds to an AIS level 1 injury (i.e. minor injury) following the 14 km/h speed change with the SAHR seat (Schmitt et al., 2001, Schmitt et al., 2002). N_{km} attempts to capture the combination of shear forces and neck flexion/extension bending moment related to the formation of the S-shape curve of the spine, where the head lags the torso in the retraction phase (Schmitt et al., 2001, Schmitt et al., 2002). Peak N_{km} value occurred 146 ms after the collision onset, while the head was in contact with the head restraint. The neck was in the posterior shear and flexion quadrant of the N_{km} load space, indicating that the neck was applying a posteriorly-directed shear force and a flexor moment to the head at the AOJ. During this time, the ATD initiated the rebound phase of the whiplash collision and the head was lifting off from the head restraint. Given the real-world success of the SAHR seat at reducing the risk of whiplash injury (Farmer et al., 2003, Viano and Olsen, 2001), the supra-threshold N_{km} values observed during the flexion and posterior shear quadrant suggest they may not play a dominant role in the etiology of whiplash injuries. However, a better understanding of the biomechanical factors leading to whiplash injuries is required to better interpret current neck injury criteria and related head/neck kinematic and kinetic responses or to help develop a criterion more specific and sensitive to whiplash injuries.

The collision severities used in this study were less severe than the IIWPG standard (16 km/h, Δt = 91 ms) but provided a graded range of collision velocities applicable to some real-world collisions that cause whiplash injury (Krafft et al., 2005, Kullgren et al., 2007). Although the collision pulse duration (Δt = 141 ms) was longer than the RCAR/IIWPG pulse (Δt = 91 ms)

due to sled limitations at the highest speed change, it was similar to the 135 ms observed in prior vehicle-to-vehicle rear-end crashes (Brault et al., 2000, Brault et al., 1998, Siegmund et al., 2000). Another limitation of the present study was that we did not maintain proper automotive floor geometry relative to the seat base. The Volvo WHIPS and Saab SAHR seats contained electrical motors under the seat pan to adjust fore/aft position and seat pan angle. To mount these seats, we elevated the seat base to allow for clearance under the seat pan. However, the relative geometry between the BioRID II ATD's head, torso and pelvis were replicated between the different seats to ensure that the ATD was in a similar initial position and confirmed using IRED marker positions (**Figure 2.1**). Despite the resulting differences in ATD lower limb positions, T1 accelerations were similar across all tested seats (see **Appendix E: Table E2.1** and **Table E2.2**), which suggests that lower limb/foot position had little influence on peak head and torso kinematic and kinetic responses.

2.5 **Conclusion**

Compared to the poor-rated GMHR seat, the good-rated WHIPS and SAHR seats only attenuated four ATD responses across the range of collision severities tested. Differences in peak upper neck forces, moments and peak head rearward retraction were observed between seats rated good and poor at speed changes greater than 6 km/h. The RCAR/IIWPG head restraint evaluation protocol and seat rating system captures improvements in some kinematic/kinetic parameters related to the risk of whiplash injury, but the similar responses observed for other kinematic/kinetic parameters between good and poor seats may explain

why even good seats have not achieved consistent reductions of more than about 50% in whiplash injuries (Jakobsson et al., 2008, Kullgren and Krafft, 2010, Viano and Olsen, 2001). Further research is required to develop anti-whiplash seat devices that reduce occupant responses and injuries across a wider range of collision severities and other collision conditions.

Chapter 3. Effects of Seat Hinge Rotation on ATD Responses

3.1 Introduction

Automotive seats are the primary safety devices for whiplash injury prevention during rear-end collisions. Modern automotive seatbacks are designed to address two primary safety functions: 1) reduce the forces applied by the seat to the occupant, and 2) prevent occupant ejection out of the seat (Viano, 2003b, Viano, 2003d, Viano, 2008). Yielding and compliant seatbacks offer better energy-absorbing properties decreasing the accelerations applied to the occupant over time and minimize head movements relative to the torso (Viano, 2003d). If a seatback is too compliant, however, large rearward deflection of the seatback can occur when the occupant loads the seat during a high-speed, rear-end collision. This loading can lead to the seat collapsing and the occupant sliding rearward under the seatbelt into the rear of the cabin, possibly being ejected from the vehicle. If, on the other hand, the seatback is too rigid, the forces applied by the seat to the occupant during lower speed, rear-end collisions will be high. Thus, automotive seat designs must balance the structural stiffness to perform well during both low- and high-speed, rear-end crashes.

There are currently several automotive seats designed to reduce or prevent whiplash injuries. These seats include the General Motor's High Retention seat (GMHR), Volvo's Whiplash Injury Prevention seat (WHIPS), Saab's Self-Aligning Head Restraint (SAHR), and Toyota's Whiplash Injury Lessening seat (WIL) (Jakobsson et al., 2000, Viano, 2008, Viano and

Olsen, 2001, Wiklund and Larsson, 1997, Sekizuka, 1998). Epidemiological studies have shown that the WHIPS and SAHR reduce whiplash injury risk by 20% to 50% following rear-end collisions (Farmer et al., 2003, Ivancic, 2011, Viano and Olsen, 2001, Jakobsson et al., 2008, Kullgren and Krafft, 2010). A comparison of four anti-whiplash seats (see **Chapter 2**) showed that even the seats rated good by the Research Council for Automobile Repairs/International Insurance Whiplash Prevention Group (RCAR/IIWPG) consistently attenuated only four peak occupant responses (i.e., peak upper neck shear and axial forces, flexion/extension bending moment and head retraction). This inability to attenuate all of the occupant responses may explain why the good-rated anti-whiplash seats have yet to reduce the risk of whiplash injury by more than 50% (Farmer et al., 2003, Ivancic, 2011, Jakobsson et al., 2008, Viano and Olsen, 2001). Thus, an additional scope remains to improve anti-whiplash seats to address those occupants who continue to be injured with the currently available anti-whiplash seats.

We developed a novel anti-whiplash seat that actively rotates the seat hinge during a rear-end collision to change the apparent structural stiffness of the seat hinge with the goal of reducing the kinematics and kinetics experienced by an occupant and thus reduce the risk of whiplash injury (see **Appendix A**). The seat rotates forward before the crash to decrease the head-to-head-restraint distance (i.e., backset) and start applying a forward force to the occupant before the collision occurs (see **Appendix B**). The seatback then actively rotates rearward as the occupant loads the seat in order to attenuate the acceleration experienced by the occupant. The seatback then stops and does not rebound forward, further attenuating the

acceleration and speed change experienced by the occupant. Preliminary testing to determine an effective seat hinge rotation profile was conducted at only one speed change (Δv) of 12 km/h with a collision pulse duration (Δt) of 208 ms. The primary goal of the present study was to compare the kinematic and kinetic responses of a BioRID II anthropomorphic test device (ATD) seated on the anti-whiplash seat with the seat hinge rotation profile (Experimental seat) and on an unmodified automotive seat (Control seat) during a range of low-speed, rear-end perturbations with speed changes of 2 to 12 km/h. A secondary goal of the study was to quantify the repeatability of the seat and ATD responses. In comparison to an unmodified Control seat, we hypothesized that the Experimental anti-whiplash seat would reduce most of the peak ATD responses across all tested collision severities.

3.2 Methods

3.2.1 Experimental Anti-Whiplash Seat

The Experimental anti-whiplash seat design consisted of a modified 2004 GMHR seat and two motors to control the seat hinge (**Figure 3.1**). The seat pan and head restraint of the GMHR seat remained unmodified in this design. The seatback consisted of a rigid aluminum outer frame and an GMHR upper seatback rigidly mounted within this outer frame. Two large rotational servomotors (AKM52K, Kollmorgen, Waltham, MA, USA) connected to helical right-angle gearheads (VTR014-035, 35:1 gear ratio, Thomson Linear, Radford, VA, USA) were mounted on either side of the outer frame at the seat hinge location and were geared to rotate

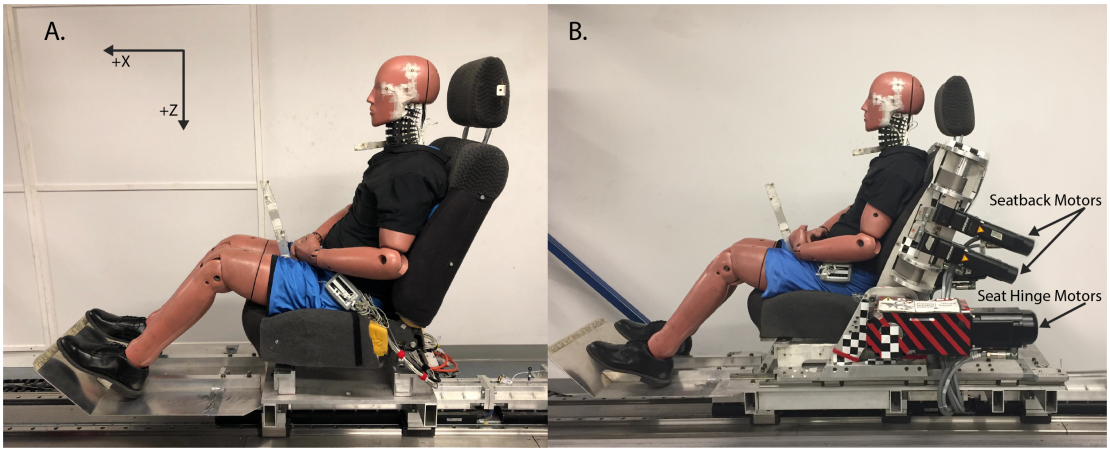

Figure 3.1. Photographs of the experimental set-up with the BioRID II ATD on A.) the Control seat and B.) the novel anti-whiplash automotive seat and global reference frame (X, Z). The seat hinge and seatback motors on the left side of the anti-whiplash seat are labelled. Additional seat hinge and seatback motors are located on the right side of the seat (not labelled). The seatback motors are not used in this current study.

in unison (one in a positive direction and the other in a negative direction) to control the rotation of the seat hinge through predefined rotation profiles (**Figure 3.1**). Through a series of preliminary experiments (see **Appendix B**), we explored different seat hinge rotation profiles to find a profile that effectively reduced ATD responses at a single speed change (Δv = 12 km/h). The chosen dynamic seat hinge rotation profile (**Figure 3.2**, grey line) was programmed to rotate the seatback forward beginning 90 ms ($t_{forward\text{-}onset}$) before the collision onset to a peak pre-perturbation angle ($\theta_{forward\text{-}peak}$) of -5.6 deg and to then rotate the seatback rearward to a peak rearward angle ($\theta_{rearward\text{-}peak}$) of 5.7 deg at an initial angular velocity ($\omega_{rearward\text{-}int}$) of 3.8 deg/s beginning 90 ms ($t_{rearward\text{-}onset}$) after collision onset. The observed output seat hinge rotation (**Figure 3.2**, red line) resulted in a pre-perturbation $\theta_{forward\text{-}peak}$ of -3.6 deg occurring at a

$t_{forward\text{-}onset}$ of -90 ms followed by rearward seat hinge rotation to a $\theta_{forward\text{-}peak}$ of 3.6 deg occurring at a $t_{rearward\text{-}onset}$ of 40 ms.

Both seat hinge motors were controlled by separate digital servo drives (Servostar 600, Kollmorgen, Waltham, MA, USA) connected to an universal motion interface and a motion controller (NI UMI 7774 & NI PXI 7350, National Instruments Corporation, Austin, Texas, USA). A custom LabVIEW program (National Instruments Corporation, Austin, Texas, USA) was created to send commands, monitor the status of and record encoder data directly from the motors.

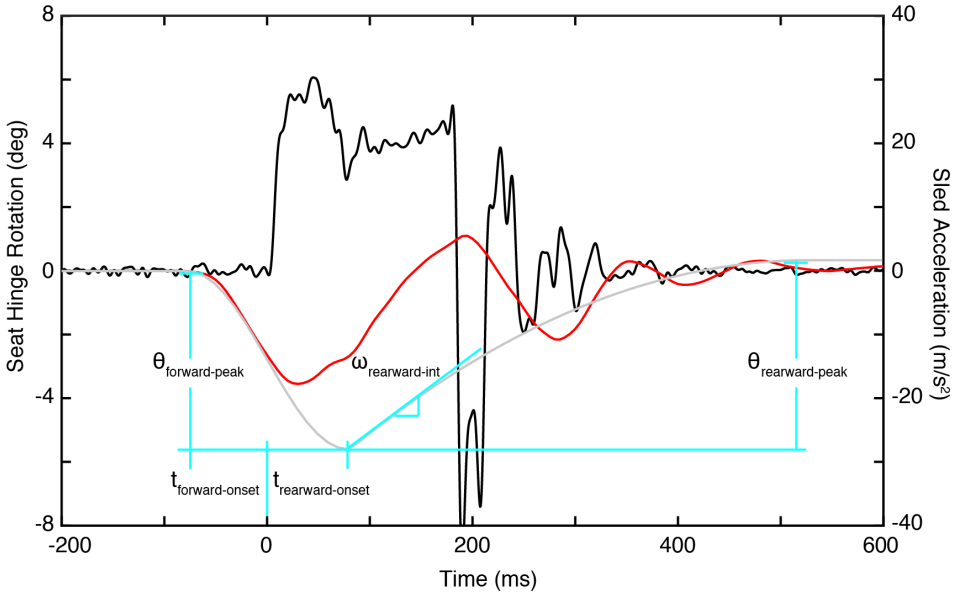

Figure 3.2. The programed input seat hinge rotation profile (grey line) and the observed output seat hinge rotation (red line) of the anti-whiplash seat during a 12 km/h perturbation (black line, right axis). The cyan lines illustrated measurements of each seat hinge rotation parameter used to define the input rotation profile (onset delay of pre-perturbation forward rotation: $t_{forward\text{-}onset}$, peak pre-perturbation forward rotation angle: $\theta_{forward\text{-}peak}$, peak rearward rotational angle: $\theta_{rearward\text{-}peak}$, initial rearward angular velocity: $\omega_{rearward\text{-}int}$, and onset delay of rotation: $t_{rearward\text{-}onset}$).

3.2.2 Anthropomorphic Test Device and Instrumentation

A BioRID II ATD (Humanetics, Plymouth, MI, USA) was instrumented to measure head, torso (T1), and pelvis kinematics and kinetics (**Figure 3.1**). A six-axis load cell (Forces: F_X, F_Y, F_Z; and Moments: M_X, M_Y, M_Z; Model 4949a, Robert A. Denton, Inc., Rochester Hills, MI, USA) was mounted at the atlanto-occipital joint (AOJ) to measure upper neck forces and moments. Linear forward accelerations of the head and T1 were measured using two uni-axial accelerometers (7264C sensors; ±500 g, Endevco, San Juan Capistrano, CA, USA) mounted at both the head center of mass and to the T1 vertebra. A uni-axial angular rate sensor was mounted at the head center of mass (ARS-1500; ±26.2 rad/s, DTS, Seal Beach, CA, USA) to measure angular kinematics in the sagittal plane (i.e., flexion and extension).

A motion capture system (Optotrak Certus, Northern Digital, Waterloo, ON, Canada) was used to track infrared light emitting diode (IRED) markers affixed to the head, AOJ, T1 and pelvis of the ATD to measure displacements. Additional IRED markers were mounted to the seat to record displacements and rotations of the seatback and to create a global reference frame (+X forward, +Y right, and +Z down, **Figure 3.1**). Horizontal sled acceleration was measured with a uni-axial accelerometer (2220-100; ±100 g, Silicon Design Inc., Issaquah, WA, USA) mounted directly to the base of the linear sled frame. Head restraint contact was detected with a force sensitive resistor (FSR, Model 406, Interlink Electronics, Camarillo, CA, USA) attached to the front of the head restraint.

All accelerometer, load cell and angular rate transducer signals were simultaneously sampled at 10 kHz using a National Instruments Data Acquisition (DAQ) PXI system (PXI-4495 & PXI-6289, National Instruments Corporation, Austin, Texas, USA) and a custom-written LabVIEW virtual instrument. Optotrak data were acquired at 200 Hz and collection was triggered by the DAQ system to synchronize the data. Subsequent data and statistical analyses were performed using Matlab (Mathworks, Natick, MA, USA). All data channels were digitally filtered in Matlab and conformed to the SAE J211 (Channel class 180 for the ATD sensors and Channel Class 60 for the sled accelerometer) (SAE, 1995).

3.2.3 Test Procedures

The BioRID II ATD was dressed in two layers of lycra and was seated on either an unmodified GMHR seat (Control seat) or the anti-whiplash seat (Experimental seat) mounted on a 10 m long, feedback-controlled linear sled (Kollmorgen IC55-100A7, Waltham, MA, USA; **Figure 3.1)**. For both seats, the initial seatback angle was set to 27 deg rearward from vertical (Siegmund et al., 2005a). To ensure the repeatability of the experiments, the initial position of the ATD was adjusted to a pre-defined posture that was constant within each seat and as similar as possible between seats. This pre-defined posture was confirmed using the 3D positions measured by Optotrak at the beginning of all trials. The seatbelt was removed from the seat to prevent interactions that could affect head, neck and torso kinematics.

For both the Control and Experimental seats, the ATD was exposed to five rear-end perturbations of increasing speed changes (Δv = 2, 4, 6, and 8 km/h with a Δt of 148 ms, and 12 km/h with a Δt of 185 ms) (**Figure 3.3)**. Due to limitations in the force-generating ability of the linear motors, a longer pulse duration was needed for the 12 km/h speed change. All of the pulses used here have a longer duration than the RCAR/IIWPG pulse (Δt = 91 ms) (Insurance Institute of Highway Safety, 2008b). The sled was accelerated forward from a stationary position for the 2, 4 and 6 km/h speed changes and from a constant rearward speed of 6 km/h for the 8 and 12 km/h speed changes. A comparison of the ATD responses for an 8 km/h collision starting from a stationary position to an 8 km/h collision starting from a 6km/h rearward velocity showed less than 10% differences in most of the occupant responses and neck injury criteria (mean: 2.50% ± 2.53%; range: 0.5% – 9.2%; see **Chapter 2**). To assess the repeatability of the ATD's responses, four additional repeated trials were collected at the 8 and 12 km/h collision speed changes for both the Control and Experimental seats (for a total of 5 trials for each seat at both speed changes).

The horizontal position ($d_{backset}$) and vertical position (d_{height}) of the head relative to the head restraint is known to affect the occupant response and the risk of whiplash injury (Nygren et al., 1985, Siegmund et al., 1999, Stemper et al., 2006). For the ATD postures used here, the head-to-head-restraint geometry was different for the Experimental seat ($d_{backset}$ = 57.5 mm and d_{height}= -2.3 mm prior to any forward rotation of the seat hinge) and Control seat ($d_{backset}$ = 95.9 mm and d_{height} = -29.9 mm). This difference arose because we wanted the Experimental

anti-whiplash seat to be rated as good according to the RCAR/IIWPG criteria. An extra experimental condition (EXP90), where the Experimental seat's backset and head restraint height were 86.2 mm and -24.6 mm respectively, was added to determine whether the observed differences in ATD responses between the Experimental and Control seats were caused by these head restraint geometry differences rather than the active seat hinge control. This extra condition was run only once at a 12 km/h speed change.

A total of 27 trials were collected, 13 trials for the Control seat and 13 trials for the Experimental seat, and one trial for the EXP90 condition. For test conditions with five repeated trials (i.e., the Δv = 8 and 12 km/h trials), the average of the peak responses across the five trials was used for analysis.

3.2.4 Data Analysis

Peak horizontal, forward, sled accelerations ($a_{X\text{-}sled}$) were extracted directly from the accelerometer mounted to the sled. Head and torso accelerometer data were reported in local ATD head and T1 reference frames and were corrected to remove the earth's gravity using the head and T1 orientations determined from the Optotrak data. Peak linear forward accelerations of the head ($a_{X\text{-}head}$) and T1 vertebra ($a_{X\text{-}T1}$) were extracted directly from the corrected accelerometer data, and peak rotational velocities of the head ($\omega_{Y\text{-}head}$) in the sagittal plane were extracted directly from the angular rate sensor. Peak upper neck shear (F_X) and axial (F_Z) forces and the flexion/extension bending moment (M_Y) were determined from the upper neck load cell and reported in the ATD reference frame as the forces/moments applied by the neck

to the head. Initial head angle was defined as the average angle between -300 ms and -200 ms preceding the onset of $a_{X\text{-}sled}$, and peak head extension angle (θ_{head}) was defined as the maximum rotation of the head into extension relative to the initial head angle. A foreperiod between -300 ms and -200 ms before the onset of forward $a_{X\text{-}sled}$ was used to define initial values because the pre-perturbation forward rotation of the seat hinge could start as early as 170 ms before collision onset (see **Appendix D**). Peak retraction (R_x) was defined as the maximum horizontal displacement in the global reference frame of the AOJ with respect to the T1 vertebrae with rearward displacements defined as negative values.

The shapes of the back of the ATD's head and front of the head restraint were digitized relative to existing Optotrak IRED markers. These shapes were then used to calculate the initial head restraint backset and vertical position for each trial. The initial backset ($d_{backset}$) and height (d_{height}) of the head restraint were defined as the average head-to-head-restraint horizontal and vertical distances between -300 ms and -200 ms before the onset of forward $a_{X\text{-}sled}$. Negative values indicated that the top of the head restraint was lower than the top of the ATD head. The same head and head restraint shapes were used to calculate the peak forward rebound ($d_{rebound}$), which was defined as the maximum forward head-to-head-restraint distance. Time-to-head-restraint contact ($\Delta t_{head\text{-}contact}$) was extracted from the time of force onset in the FSR attached to the head restraint (onset of forward sled acceleration defined as t = 0 ms). Onsets of sled acceleration and head restraint contact were determined when the accelerometer and FSR signals, respectively, reached 1.5 times the peak background noise level present

between -300 ms to -200 ms before the onset of the collision perturbation and were confirmed visually. The sled accelerometer ($a_{X\text{-}sled}$) and head contact FSR signals had high signal-to-noise ratios after filtering according to SAE J211 Channel class 180 and did not require further manual corrections of the onsets.

Three neck injury criteria (NIC_{max}, N_{ij}, and N_{km}) were computed from the accelerometer and load cell data. The Neck Injury Criterion (NIC_{max}) was calculated from the relative horizontal acceleration and velocity in the global reference frame between the head center of mass and the T1 joint (Equation 3.1; Bostrom et al., 1996). The Normalized Neck Injury Criterion (N_{ij}) was calculated from the axial load (F_Z) and the flexion/extension bending moment (M_Y) measured from the upper neck load cell (Equation 3.2; critical F_{int} and M_{int} intercept values used for normalization: $F_{int\text{-}tension}$ = 6806 N, $F_{int\text{-}compression}$ = -6160 N, $M_{int\text{-}flexion}$ = 310 N, and $M_{int\text{-}extension}$ = -135 N; Eppinger et al., 1999, Eppinger et al., 2000). The Neck Protection Criterion (N_{km}) was calculated from the sagittal shear force (F_X) and the flexion/extension bending moment (M_Y) measured from the upper neck load cell (Equation 3; critical F_{int} and M_{int} intercept values used for normalization: $F_{int\text{-}shear\text{-}positive}$ = 845 N, $F_{int\text{-}shear\text{-}negative}$ = 845 N, $M_{int\text{-}extension}$ = 47.5 Nm, and $M_{int\text{-}flexion}$ = 88.1 Nm; Schmitt et al., 2001, Schmitt et al., 2002). Peak values of the three neck injury criteria were then extracted for analysis and compared to proposed injury thresholds (NIC: 15 m^2/s^2, Eichberger et al., 1998; N_{ij} and N_{km} : a normalized value of one, Schmitt et al., 2001, Schmitt et al., 2002, Eppinger et al., 1999). These injury thresholds correspond to different human tolerance levels for the causation of whiplash-related injuries – NIC: long-term whiplash-

associated disorders (WAD) levels 1-3 (Bostrom et al., 2000, Bostrom et al., 1996), N_{ij}: 22% risk of abbreviated injury scale (AIS) level 3 (i.e., fracture; Eppinger et al., 1999, Eppinger et al., 2000), and N_{km}: AIS level 1 injury causation (i.e., minor injury; Schmitt et al., 2001, Schmitt et al., 2002).

$$NIC_{max}(t) = \text{maximum}_{\text{first 150 ms}}(a_{rel}(t) \cdot L + (v_{rel}(t))^2) \quad \ldots \quad \text{Equation 3.1}$$

$$N_{ij}(t) = \frac{F_z(t)}{F_{int}} + \frac{M_{yOC}(t)}{M_{int}} \quad \ldots \quad \text{Equation 3.2}$$

$$N_{km}(t) = \frac{|F_x(t)|}{F_{int}} + \frac{|M_{yOC}(t)|}{M_{int}} \quad \ldots \quad \text{Equation 3.3}$$

The repeatability of the ATD on the Control and Experimental seats was assessed for the 8 and 12 km/h speed changes using the coefficient of variation (COV), which was calculated as the standard deviation (SD) divided by the mean and expressed as a percentage. The National Highway Traffic Safety Administration (NHTSA) defines a COV of 5% or less as excellent, a COV of 10% or less as acceptable and a COV greater than 10% as poor (Rhule et al., 2005). If most of the COV values for a given seat (Control or Experimental) were rated as excellent or acceptable, then the ATD responses on the given seat were considered repeatable. Because COV is dependent on the mean and SD values of the responses, the expected decreases in mean responses (which form the denominator in the COV calculation) for the Experimental seat may generate larger COV values. A comparison of the SD values between the GMHR and the Experimental seats would provide an alternate assessment of variability and would help to

determine whether the larger COV values for the Experimental seat were likely due to the lower mean responses or due to the greater inherent variability (i.e., SD) in the ATD responses. The SD values for all kinematic and kinetic responses as well as neck injury criteria observed at both the 8 and 12 km/h collision speeds were used in this assessment of variability. The COV and SD values were assumed to be independent observations and were analyzed with a paired Student's t-test after a Kolmogorov-Smirnov test determined the COV and SD values were normally distributed. All tests were performed using predefined functions (`kstest` and `ttest`) in Matlab (R2017A, Mathworks, Natick, MA, USA) at a significance level $\alpha = 0.05$.

To compare ATD responses between the Control and Experimental seats, 99th percentile predictive intervals were created around the peak responses on each seats using their respective maximum variability (COV value) observed from repeated trials at either the 8 or 12 km/h collision severity (Horslen et al., 2015). The maximum COV value from either the 8 or 12 km/h collision severity was selected to represent the largest observed variance within each response. This COV value was multiplied by 2.58 (z-score for two-tailed 99th percentile) to estimate the 99th percentile predictive limits. Since the COV values were defined as the maximum variances (i.e., SD values) divide by the mean of the peak ATD responses, these predictive limits were represented as a percentage and were then applied to their respective peak responses to create predictive intervals at each collision severity (2 – 12 km/h). Any ATD responses where the 99th percentile predictive intervals from the Control and Experimental seats did not overlap were assumed to be statistically different. The 99th percentile predictive

limits were selected to account for the numerous comparisons between Control and Experimental seats for the ATD responses at each collision severity and to provide a conservative estimate of statistical significance.

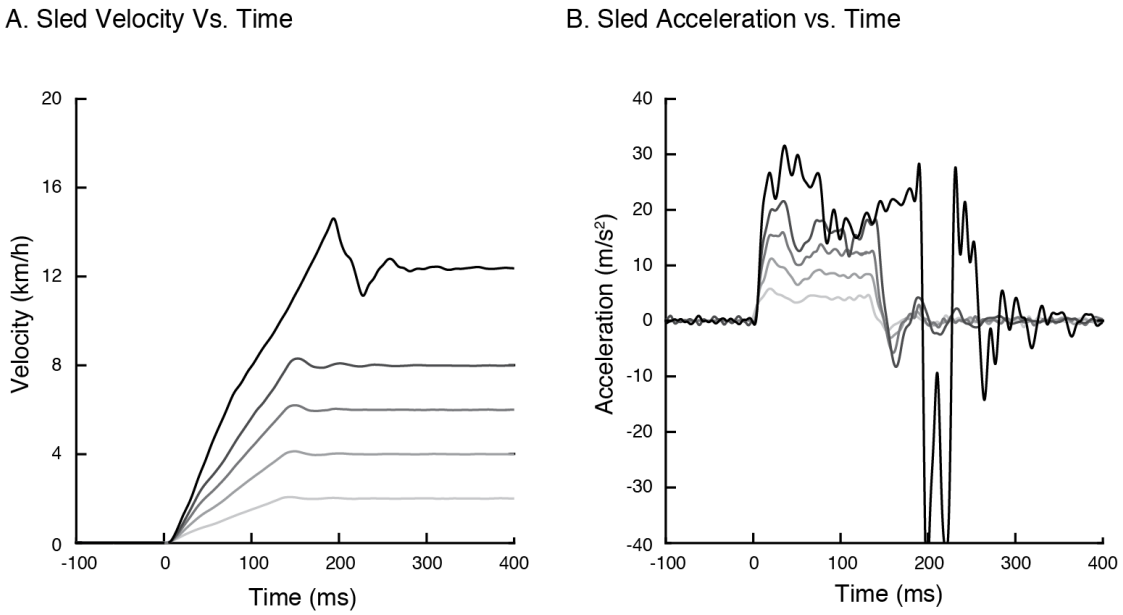

Figure 3.3. Exemplar sled A) velocity and B) acceleration profiles for increasing collision speeds (Δv = 2, 4, 6, and 8 km/h with a pulse duration (Δt) of 148 ms, and Δv = 12 km/h with a Δt of 185 ms; lightest to darkest). Collision onset occurred at time = 0 ms.

3.3 **Results**

Both the Control and Experimental seats generated graded kinematic and kinetic responses to increasing collision severities (**Figure 3.4** & **3.5**, **Table 3.1**). In comparison to the Control seat, active seat hinge rotation in the Experimental seat decreased the ATD's kinematics and kinetics ($a_{X\text{-}head}$, $a_{X\text{-}T1}$, $\omega_{Y\text{-}head}$, F_X, F_Z, M_Y, θ_{head}, R_X and $d_{rebound}$) and neck injury criteria (NIC_{max}, N_{km}, and N_{ij}) for speed changes of 4 km/h and higher (**Figure 3.5**). With the exception of $\Delta t_{head\text{-}contact}$ (all collision severities) and N_{ij} (only 4km/h severity), there was no overlap between the 99th percentile predictive intervals of the ATD response in the Control and Experimental seats. Peak forward head ($a_{X\text{-}head}$) and torso ($a_{X\text{-}T1}$) accelerations decreased by 50 – 69% and 24 – 38% respectively, while peak angular velocity of the head ($\omega_{Y\text{-}head}$) decreased by 52 – 66% (**Figure 3.5A – 3.5C**). The Experimental seat also decreased upper neck forces and moments compared to the Control seat (F_X: 43 – 57% reduction, F_Z: 54 – 74% reduction, and M_Y: 53 – 76% reduction) (**Figure 3.5D – 3.5F**). The Experimental seat also reduced head displacements relative to the torso: head angle (θ_{head}) decreased by 44 – 73% and peak retraction (R_X) decreased by 43 – 75% (**Figure 3.5H** & **3.5I**).

At the 2 km/h speed change, most ATD responses ($a_{X\text{-}T1}$, $\omega_{Y\text{-}head}$, F_X, θ_{head}, R_X and $\Delta t_{head\text{-}contact}$) and neck injury criteria (NIC_{max} and N_{km}) in the Experimental seat decreased from the Control seat by between 10 to 65%. Some of the ATD responses, however, were larger in the Experimental seat compared to the Control seat: $a_{X\text{-}head}$ increased by 24%, F_Z increased by 95%, M_Y increased by 433%, and N_{ij} increased by 4% (**Table 3.1**). Based on the comparison between

99th percentile predictive intervals, a statistically significant difference was observed between Control and Experimental seats only for F_Z, M_Y, $\theta_{head,}$ and R_X at the 2 km/h collision severity (**Figure 3.5**).

None of the neck injury criteria (NIC_{max}, N_{ij}, nor N_{km}) exceeded their respective proposed injury thresholds for either the Control or Experimental seat. The Experimental seat decreased the magnitude of all three neck injury criteria (NIC_{max}: 44 – 85% reduction, N_{ij}: 23 – 66% reduction, and N_{km}: 41 – 59% reduction) (**Figure 3.5J – 3.5L**).

The repeatability of the BioRID II ATD responses for both the Control and Experimental seats were assessed using COV values from repeated trials at both the 8 and 12 km/h speed changes (**Table 3.2**). The COV values for the Control seat were excellent or acceptable at both speed changes for all parameters except for head restraint height (d_{height}, COV = 22.2% and 11.3% at 8 and 12 km/h respectively). The Experimental seat also exhibited excellent or acceptable repeatability, except for head restraint height (COV = 60.4 and 75% at 8 and 12 km/h respectively), NIC_{max} (COV = 19.6% and 10.7% at 8 and 12 km/h respectively) and N_{ij} (COV = 13.3% at 12 km/h). The COV values on the Experimental seat were significantly higher than those on the Control seat for the 8 and 12 km/h speed changes (paired t-test; 8 km/h: $t(15) = -3.03$, $p = 0.020$, and 12 km/h: $t(15) = -3.20$, $p = 0.008$). The SD values of the Experimental and GMHR seats were not significantly different (paired t-test; 8 km/h: $t(15) = -0.73$, $p = 0.56$, and 12 km/h: $t(15) = 0.60$, $p = 0.53$). The larger COV values on the Experimental seat with similar SD

values to the GMHR seat suggested that the COV values considered poor (> 10%) were more likely due to decreased mean responses than due to increased variability in the ATD responses.

Prior to the collision, the initial (preset) head restraint backset ($d_{backset}$) and head restraint height (d_{height}) were smaller on the Experimental seat compared to the Control seat (**Figure 3.6** and **Table 3.1**). The average initial backset of the Experimental seat (57.5 ± 10.5 mm) was 43% less than the average initial backset of the Control seat (95.9 ± 2.8 mm) across all collision severities. The pre-perturbation forward seat hinge rotation of the Experimental seat, which began 90 ms before the collision, moved the head restraint closer to the ATD's head and decreased the backset to 13.9 ± 6.5 mm (73% decrease from the initial Experimental seat backset) prior to the onset of the collision (t = 0 ms) (**Figure 3.6**). Across all collision severities, the average initial head restraint height (d_{height}) for the Experimental seat was -2.29 ± 3.5 mm, which placed the top of the head restraint closer to, but still below, the top of the head than for the Control seat (d_{height} = -29.8 ± 8.6 mm) (**Table 3.1**). Peak forward rebound ($d_{rebound}$) increased with collision severity for both the Experimental and Control seats (**Table 3.1**). The forward rebound for the Experimental seat was on average 48% lower than for the Control seat at the equivalent collision severity (range: 32 – 66%).

A comparison of the ATD responses in the EXP90 condition (the active seat hinge rotation with head restraint geometry similar to that of the Control seat) to the Control and Experimental seats showed that the active seat hinge was responsible for most of the ATD response changes observed between the Control and Experimental seats (**Table 3.3**, **Figure**

3.7). Aside from the time-to-head-restraint contact, the active seat hinge response generated an average of 85% (range: 67 to 110%) of the difference in ATD responses between the Control and Experimental seats.

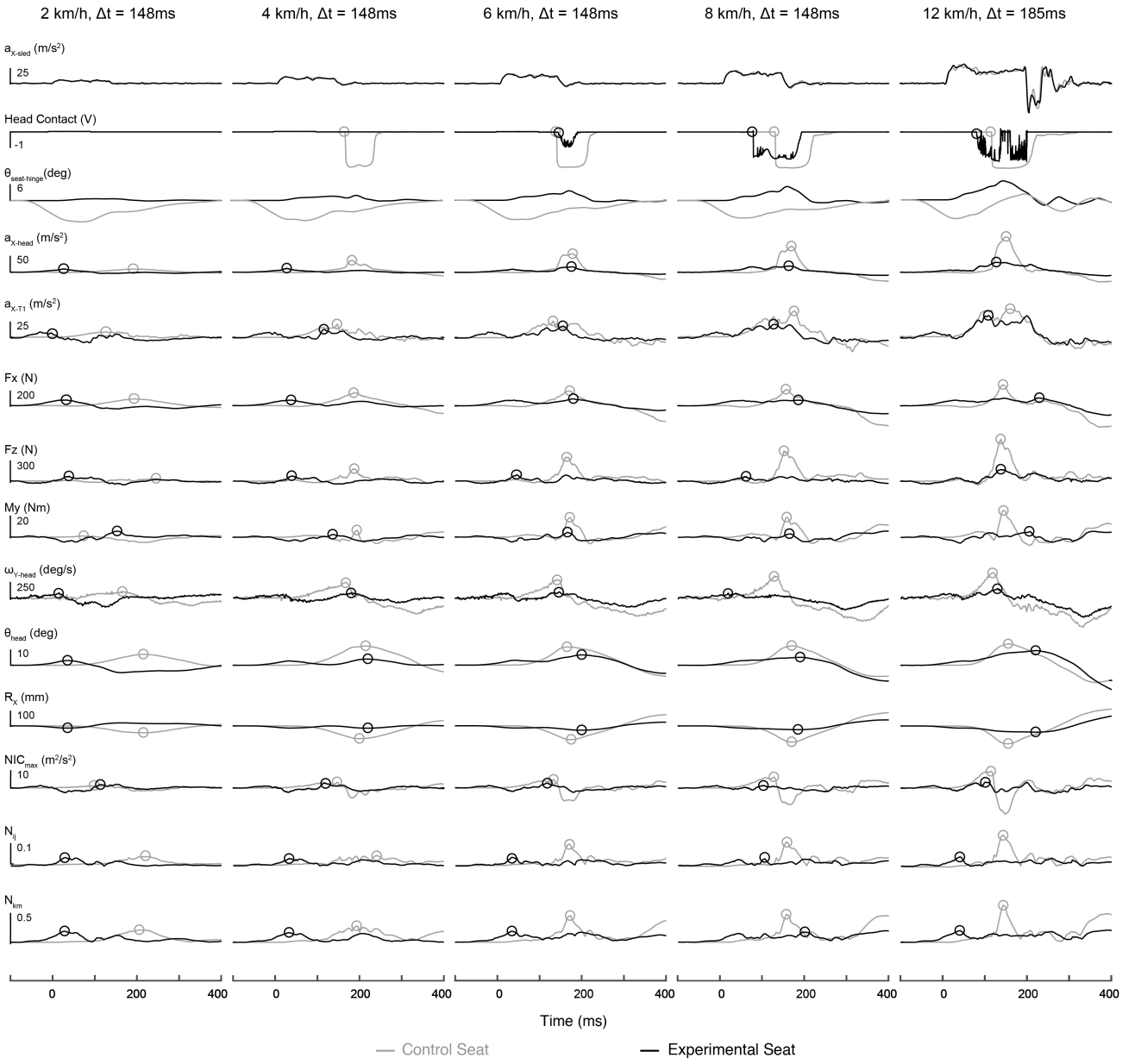

Figure 3.4. Exemplar data comparing an unmodified Control seat (Pontiac Grand Am GMHR) and the Experimental seat with dynamic seat hinge rotation ($\theta_{seat\text{-}hinge}$) for the BioRID II ATD. Each column represents occupant responses for a Control and Experimental seat while exposed to various collision severities (Δv = 2, 4, 6, and 8 km/h with a collision pulse duration (Δt) of 148 ms and 12 km/h with Δt = 185 ms). Hollow circles represent the onset of head-to-head-restraint contact and peak responses of each ATD response parameter for each trial.

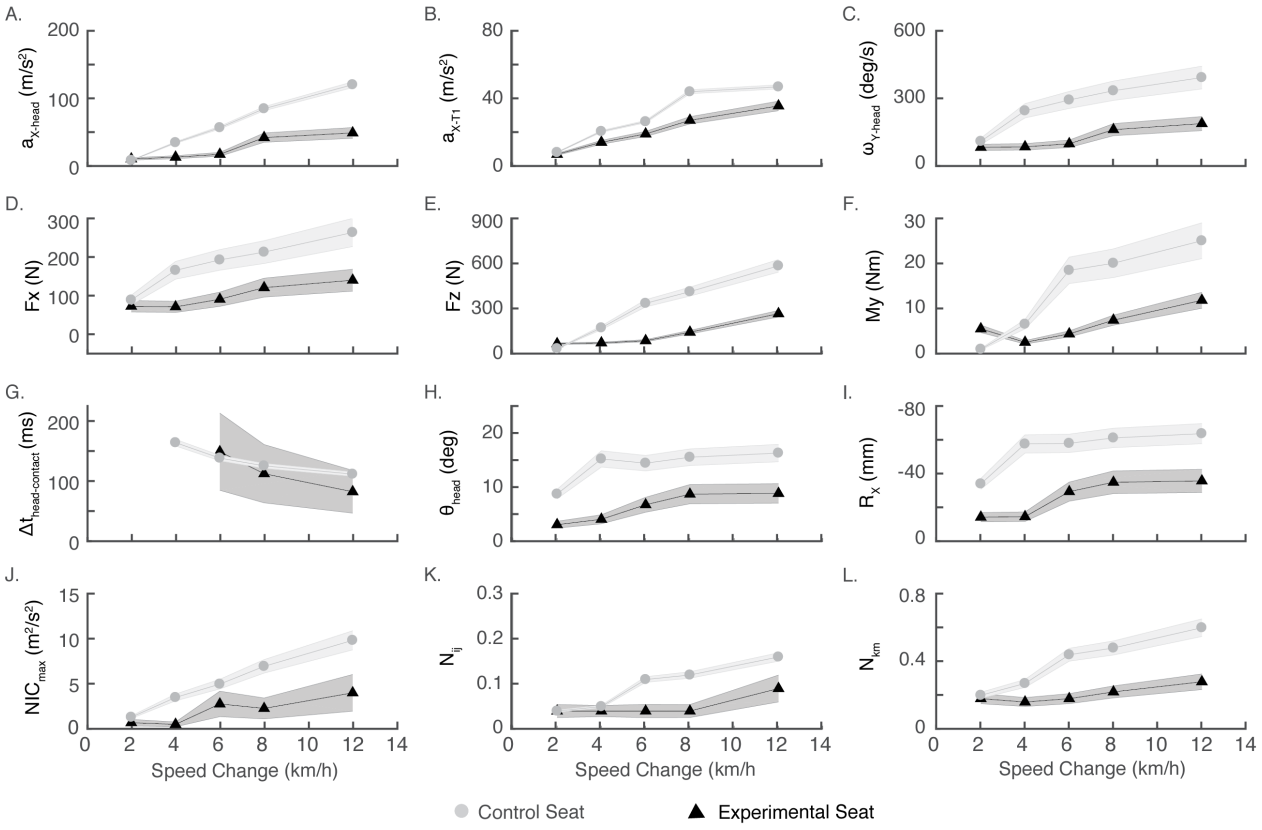

Figure 3.5. Experimental results of peak kinematic and kinetic responses for the BioRID II ATD seated on the Control and Experimental anti-whiplash seats. For all the graphs, grey circles represent the Control seat and black triangles represent the Experimental seat with the seat hinge rotation. The faded grey bars represent the 99th percentile predictive corridors for the Control and Experimental seats. Y-axis values for panels 5C and 5I have been inverted for visual purposes to show increasing responses from bottom to top.

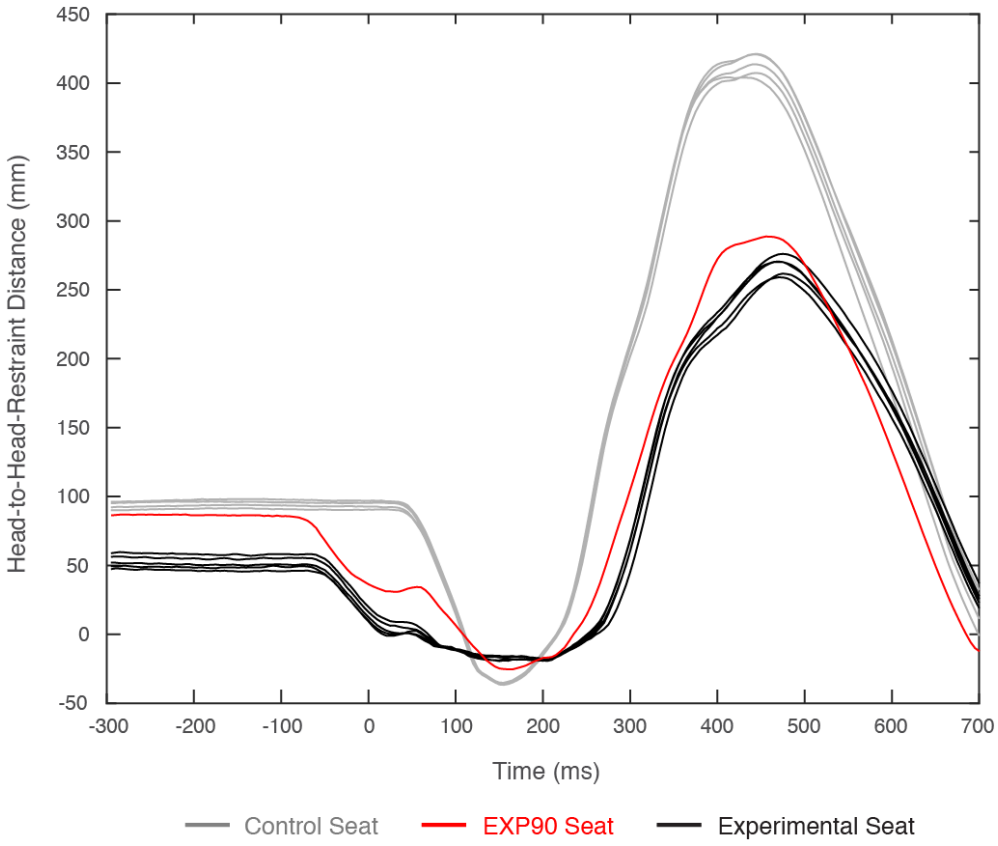

Figure 3.6. Exemplar horizontal head-to-head-restraint distance in the X-axis measured from the back of the BioRID II ATD head to the front face of the head restraint. Five repeated trials of the ATD seated on the Control GMHR seat (grey) and on the Experimental seat with dynamic seat hinge rotation (black) as well as single trial of the EXP90 condition (red) at a collision severity of 12 km/h (Δt = 185 ms). Collision onset occurred at time = 0 ms and a head-to-head restraint distance ≤ 0 mm indicated that the head was in contact with the head restraint.

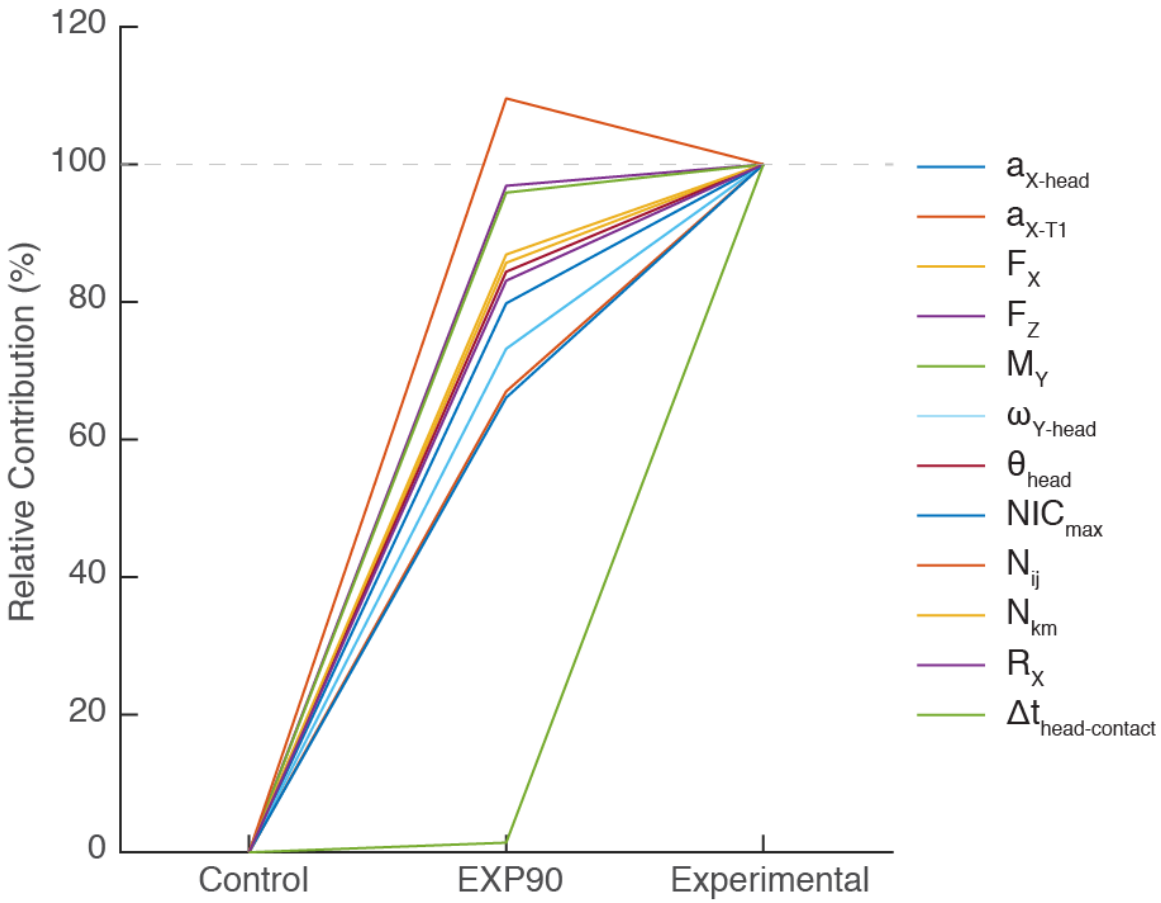

Figure 3.7. The relative contributions of the active seatback response and head restraint geometry to the improved response of the Experimental seat compared to the Control seat. Thirteen ATD response parameters are shown here for the Control seat (set to 0%), the Experimental seat (set to 100%) and the extra condition (EXP90) of the Experimental seat with a head restraint geometry similar to the Control seat (intermediate percentage values). Most of the improvements observed between the Control and Experimental seats comes from adding the active seat hinge response (difference between Control and EXP90 data in this graph) rather than from the change in head restraint geometry (difference between EXP90 and Experimental seat data in this graph).

Table 3.1. Peak Responses for Control and Experimental (EXP) seats for each collision severity. Underlined results highlight case where the Experimental trials had larger responses than the Control trials.

Δv (km/h)	2 km/h, Δt = 148 ms		4 km/h, Δt = 148 ms		6 km/h, Δt = 148 ms		8 km/h, Δt = 148 ms		12 km/h, Δt = 185 ms	
Trial	Control	EXP	Control	EXP	Control	EXP	Control	EXP	Control	EXP
$d_{backset}$ (mm)	90.4	49.1	91.0	45.8	90.2	48.7	94.7	69.2	95.1	51.5
d_{height} (mm)	-31.0	2.7	-32.3	-6.4	-42.3	-4.7	-20.0	-1.7	-23.7	-1.4
$a_{X\text{-}sled}$ (m/s^2)	5.8	5.7	11.2	10.9	15.9	15.8	22.8	21.7	31.6	30.2
$\Delta t_{head\ contact}$ (ms)	-	-	164.5	-	138.8	149.4	129.5	112.8	112.1	92.8
$a_{X\text{-}head}$ (m/s^2)	<u>8.7</u>	<u>10.8</u>	35	13.4	57.1	17.6	85.2	42.4	120.7	49.3
$a_{X\text{-}T1}$ (m/s^2)	8.2	7.1	20.6	14.2	26.4	191.1	44.1	27.2	47.0	35.7
F_X (N)	89.5	73.4	166.4	71.7	193.3	91.4	213.5	121.5	264.4	140.7
F_Z (N)	<u>34.5</u>	<u>67.4</u>	173.5	72.9	336.5	87.6	414.4	144.3	586.1	267.3
M_Y (Nm)	<u>1.0</u>	<u>5.5</u>	6.6	2.6	18.5	4.4	20.1	7.5	25.1	11.9
$\omega_{Y\text{-}head}$ (deg/s)	110.6	84.0	246.3	86.2	294.4	99.8	335.3	162.4	393.8	189.4
θ_{head} (deg)	8.8	3.1	15.3	4.1	14.5	6.8	15.6	8.7	16.4	8.9
$d_{rebound}$ (mm)	119.6	81.3	175.5	65.0	269.0	88.0	336.1	185.8	413.4	267.5
R_X (mm)	-34.1	-14.4	-57.7	-14.7	-58.1	-29.5	-61.3	-35.1	-63.8	-35.8
NIC_{max} (m^2/s^2)	1.3	0.7	3.5	0.5	5.0	2.8	7.0	2.3	9.8	4.0
N_{ij}	0.0	0.0	0.0	0.0	0.1	0.0	0.1	0.0	0.2	0.1
N_{km}	0.2	0.2	0.3	0.2	0.4	0.2	0.5	0.2	0.6	0.3

Table 3.2. Mean (standard deviation) and Coefficient of Variation (COV) from five repeated whiplash-like perturbation (n = 5) on the Control and Experimental seats at collision severities of Δv = 8 km/h with Δt = 148 ms and Δv = 12 km/h with Δt = 185 ms.

Δv (km/h)	8 km/h, Δ = 148 ms				12 km/h, Δ = 185 ms			
Trial	Control		Experimental		Control		Experimental	
Parameter	Mean (SD)	COV (%)	Mean (SD)	COV (%)	Mean (SD)	COV (%)	Mean (SD)	COV (%)
Initial $d_{backset}$ (mm)	94.7 (2.2)	<u>5.9</u>	69.3 (4.1)	<u>5.9</u>	95.1 (2.6)	2.8	51.5 (4.8)	<u>9.3</u>
Initial d_{height} (mm)	-23.8 (5.3)	**22.2**	5.3 (3.2)	**60.4**	-25.0 (2.8)	**11.3**	-1.6 (1.2)	**75.0**
$a_{X\text{-}sled}$ (m/s^2)	22.8 (1.1)	4.7	21.7 (1.1)	4.6	31.6 (0.4)	1.2	30.2 (0.4)	1.4
$\Delta t_{head\ contact}$ (ms)	125.9 (1.1)	0.8	112.8 (1.1)	0.8	112.1 (1.4)	1.3	82.8 (6.0)	<u>7.3</u>
$a_{X\text{-}head}$ (m/s^2)	85.2 (1.0)	1.1	42.4 (2.1)	5.0	120.7 (1.7)	1.4	49.3 (3.1)	<u>6.3</u>
$a_{X\text{-}T1}$ (m/s^2)	44.1 (0.4)	1.0	27.2 (0.8)	3.1	47.0 (0.3)	0.7	35.7 (1.0)	2.8
F_X (N)	213.5 (3.8)	1.8	121.5 (9.5)	<u>7.8</u>	264.4 (14.1)	<u>5.4</u>	140.7 (5.7)	4.0
F_Z (N)	414.4 (9.3)	2.2	144.3 (4.5)	3.1	586.1 (16.2)	2.8	267.3 (4.4)	1.7
M_Y (Nm)	20.1 (1.2)	<u>6.1</u>	7.5 (0.4)	4.8	25.1 (0.1)	0.2	11.9 (0.7)	<u>5.8</u>
$\omega_{Y\text{-}head}$(deg/s)	335.3 (16.7)	5.0	162.4 (10.4)	<u>6.4</u>	393.8 (7.4)	1.9	189.4 (11.5)	<u>6.1</u>
θ_{head} (deg)	15.6 (0.3)	2.1	8.7 (0.7)	<u>7.9</u>	16.4 (0.6)	3.8	8.9 (0.4)	4.0
R_X (mm)	-61.3 (1.1)	1.7	-35.1 (2.6)	<u>7.4</u>	-63.8 (2.3)	3.6	-35.8 (1.3)	3.6
$d_{rebound}$ (mm)	335.1 (10.4)	3.5	185.8 (6.5)	3.5	413.4 (7.7)	1.9	267.5 (7.0)	2.6
NIC_{max} (m^2/s^2)	7.0 (0.3)	4.2	2.3 (0.4)	**19.6**	9.8 (0.3)	2.6	4.0 (0.4)	**10.7**
N_{ij}	0.12 (0.00)	2.3	0.04 (0.00)	3.1	0.16 (0.00)	1.5	0.09 (0.01)	**13.3**
N_{km}	0.48 (0.02)	3.4	0.22 (0.01)	5.0	0.60 (0.02)	2.9	0.28 (0.02)	<u>6.3</u>

<u>Notes:</u> The <u>underlined</u> COV values indicate a COV rating of acceptable (5% ≤ COV < 10%), the **bolded** COV values indicate a COV rating of poor (COV > 10%), and all other values are rated good (COV < 5%).

Table 3.3. Peak ATD responses and normalized percentages (Norm %) for the extra EXP90 condition relative to the Control and Experimental (EXP) seats at a speed change of 12 km/h. Normalize percentages show where the EXP90 response falls within the interval between the Control (0%) and Experimental (100%) seats. The normalized percentages for the ATD responses (bottom 13 parameters in this table) are shown graphically in **Figure 3.7**.

Trial	Control		EXP90		EXP	
Parameter	Peak	Norm %	Peak	Norm %	Peak	Norm %
Initial $d_{backset}$ (mm)	95.1	0	86.2	19.8	51.5	100
Initial d_{height} (mm)	-25.0	0	-24.6	1.7	-1.6	100
$a_{X\text{-}sled}$ (m/s^2)	31.6	0	-31.0	40.4	30.2	100
$\Delta t_{head\ contact}$ (ms)	112.1	0	111.7	1.4	82.8	100
$a_{X\text{-}head}$ (m/s^2)	120.7	0	63.8	79.8	49.3	100
$a_{X\text{-}T1}$ (m/s^2)	47.0	0	39.4	67.0	35.7	100
F_X (N)	264.4	0	158.5	85.7	140.7	100
F_Z (N)	586.1	0	277.2	96.9	267.3	100
M_Y (Nm)	25.1	0	12.4	95.9	11.9	100
$\omega_{Y\text{-}head}$(deg/s)	393.8	0	244.2	73.2	189.4	100
θ_{head} (deg)	16.4	0	10.1	84.4	8.9	100
$d_{rebound}$ (mm)	413.4	0	288.6	96.1	267.5	100
R_X (mm)	-63.8	0	-40.5	83.1	-35.8	100
NIC_{max} (m^2/s^2)	9.8	0	6.0	66.1	4.0	100
N_{ij}	0.16	0	0.08	109.6	0.09	100
N_{km}	0.60	0	0.32	86.9	0.28	100

3.4 **Discussion**

The results of this study showed that actively controlling seat hinge rotation before and during a collision pulse consistently and significantly reduced the peak amplitude of the ATD's responses during rear-end impacts for speed changes between 4 and 12 km/h. In comparison to the Control seat, the Experimental seat reduced peak ATD kinematics (linear accelerations, angular velocities, displacements and head angles) by 24 – 75%, peak ATD kinetics (forces and moments) by 43 – 76%, and neck injury criteria (NIC_{max}, N_{ij}, N_{km}) by 23 – 85% for speed changes from 4 to 12 km/h. For the 2 km/h speed change, only 5 out of 12 peak ATD responses (F_Z, M_Y, $\theta_{head,}$ R_X, and NIC_{max}) were significantly different, with peak F_Z and M_Y larger on the Experimental seat than on the Control seat. This equivocal outcome at a speed change of 2 km/h was judged to be inconsequential because field data have not shown whiplash injuries at this speed change (Krafft, 2002, Krafft et al., 2005). For all other speed changes tested here (4 – 12 km/h), with the exception of $\Delta t_{head\text{-}contact}$ (all collision severities) and N_{ij} (only 4 km/h severity), peak ATD responses for the Experimental seat were significantly lower than for the Control seat.

The observed dynamics of the seat hinge rotation (**Figure 3.2**, red line) consisted of two phases: a pre-perturbation forward rotation ($\theta_{forward\text{-}peak}$ = -3.6 deg, $t_{forward\text{-}onset}$ = -90 ms) and a within-perturbation rearward rotation ($\theta_{rearward\text{-}peak}$ = 3.7 deg, $t_{rearward\text{-}onset}$ = 40 ms). During the pilot tests used to develop the seat hinge profile used here (see **Appendix B**), the pre-perturbation forward rotation was the primary contributor to the overall reduction of ATD

responses. At the 12 km/h speed change used for the pilot tests, the ATD responses for the Experimental seat were 11 to 53% lower than the Control seat when only the pre-perturbation forward-rotation profile was used. When only the rearward-rotation profile was used, the ATD responses for the Experimental seat varied from 19% higher to 10% lower than for the Control seat. The combination of the two rotation phases was similar to the pre-perturbation forward-rotation-only profile and generated reductions in the ATD responses between 23 – 48%. One possible explanation for the larger effect of the forward rotation may be an increase in the effective stiffness of the seat hinge to improve its ability to resist the rearward seatback rotation created by the ATD's inertia as the sled is accelerated forward. Actively increasing the effective seat hinge stiffness during the pre-perturbation forward rotation followed by actively decreasing the effective seat hinge stiffness during the within-perturbation rearward rotation appeared to generate three effects: i) a prolonged collision pulse, ii) longer head-to-head-restraint interaction at higher speed changes, and iii) a reduced forward rebound. All three effects appeared to contribute to attenuating the peak kinematics and kinetics experienced by the ATD, particularly at higher speed changes.

The Experimental anti-whiplash seat was designed to be rated good ($d_{backset} < 70$ mm and $d_{height} > -60$ mm) according to the RCAR/IIWPG seat/head restraint criteria. The effect of the differences in backset and head restraint height between the poor-rated Control seat and the good-rated Experimental seat were isolated from the effect of the active seat hinge rotation profile by adding the EXP90 condition in which the head restraint backset and height of the

Experimental seat better matched that present on the Control seat. Even with an initial $d_{backset}$ and d_{height} similar to the Control seat, the Experimental seat reduced peak ATD kinematics and kinetics by an average of 85% compared to the Control seat. These data suggested that the differences in initial $d_{backset}$ and d_{height} was a relatively small confounding factor in the reduction of kinematic and kinetic responses observed with the Experimental seat.

Even though both the Control seat and EXP90 condition had similar initial head restraint geometries, the pre-perturbation forward rotation of the seat hinge in the EXP90 condition brought the head restraint closer to the back of the head by the time the collision pulse began (**Figure 3.6**). Computational simulations of rear-end collisions have shown that peak NIC_{max} values decrease by approximately 5 m^2/s^2 for every 30 mm decrease in backset and injury risk decreases by 10% for every 25 mm decrease in backset (Eriksson, 2005). The pre-perturbation forward seat hinge rotation decreased the head-to-head-restraint distance in the EXP90 condition from 86.2 mm to 36.3 mm at collision onset (t = 0 ms) (**Figure 3.6**). Thus, the observed 49.9 mm decrease in the EXP90 seat's head-to-head-restraint distance prior to impact may have reduced peak NIC_{max} by approximately 8 m^2/s^2 and the risk of whiplash injuries by 20%. In comparison to the Control seat, the total difference in head-to-head-restraint distance at the onset of the collision pulse for the EXP90 condition was 58.8 mm (95.1 mm for the Control seat and 36.3 mm for the EXP90 condition at the onset of the collision pulse). NIC_{max} was reduced by 3.8 m^2/s^2 (Control: NIC_{max} = 9.8 $m^{2/}s^2$ and EXP90: NIC_{max} = 6.0 $m^{2/}s^2$), which was less than half of the reduction predicted (Eriksson, 2005) for a 58.8 mm reduction in head-to-

head-restraint distance. This discrepancy in the predicted vs observed reductions may be due to the smaller NIC_{max} values resulting from the lower collision severities used in the present study (Δv = 2 – 12 km/h, $a_{X\text{-}sled}$ = 5.7 – 31.6 m/s^2) compared to the computational study (Δv = 12 – 33 km/h, $a_{X\text{-}sled}$ = 76.5 – 212.9 m/s^2). Regardless, the pre-perturbation forward seat hinge rotation reduces the head-to-head-restraint distance prior to the collision onset to decrease ATD responses and can, potentially, reduce the risk of whiplash injuries by 20%.

In comparison to current anti-whiplash seats, the motion of the Experimental seat combines features from both the SAHR and WHIPS seats. The SAHR anti-whiplash system uses the occupant's penetration into the seatback cushion to activate a mechanism that moves the head restraint upwards and forwards towards the back of the occupant's head (Viano and Olsen, 2001). In contrast, the WHIPS system uses a deformable element in the seat hinge to control rearward translation and rotation of the seatback (Jakobsson et al., 2008, Jakobsson et al., 2000). The pre-perturbation forward rotation of the Experimental seat moves the head restraint closer to the head, similar to the SAHR mechanism. The subsequent rearward rotation of the seatback reduces the effective rearward stiffness of the Experimental seat and reduces forward rebound, which is not unlike the net effect of the yielding element in the WHIPS system. In contrast to these two prior designs, however, the Experimental seat is active rather than reactive and begins responding to the crash before the crash actually occurs. These active (and therefore programmable) features potentially allow the seat hinge behavior to adapt to

occupant characteristics and predictive estimates of the collision severity—two areas that require further research.

The net effect that the predictive anti-whiplash seat would have on the real-world risk of whiplash injury remains unknown. However, the SAHR and WHIPS seats, which were previously shown to attenuate only four ATD responses in comparison to the Control seat used here (see **Chapter 2**), have been shown to reduce the risk of whiplash injuries by 20 – 75% (Farmer et al., 2003, Ivancic, 2011, Jakobsson et al., 2008, Viano and Olsen, 2001). The results from the present study show reductions in all measured ATD kinematic and kinetic responses and suggests that the Experimental seat could further reduce the risk of whiplash injuries. A direct comparison the magnitude of these kinematic and kinetic reductions between the anti-whiplash seat and SAHR and WHIPS seats will be performed in a subsequent study (see **Chapter 5**).

The Experimental and Control seats generated ATD responses that had mostly excellent (COV ≤ 5%) and acceptable (5% < COV ≤ 10%) repeatability at 8 and 12 km/h speed changes (the two speed changes at which the repeatability of the seat and ATD was evaluated). Only two ATD response parameters (NIC_{max} and N_{ij}) had COV values that were rated poor (COV > 10%). Despite these similarities, post-hoc comparisons of the COV values showed that they were signficantly higher for the Experimental seat than for the Control seat (paired t-tests, $p = 0.020$ and $p = 0.008$ for the 8 and 12 km/h speed changes, respectively). A similar comparison of the SD values, however, showed no signficant differences between the Experimental and

Control seats (paired t-tests, p = 0.56 and p = 0.53 for the 8 and 12 km/h speed changes, respectively). Based on this follow-up analysis, the larger COV values for the Experimental seat were likely due to lower mean values (which form the denominator in the COV calculation) than due to greater inherent variability in the ATD responses. Thus we believe that the Control and Experimental seats have sufficient repeatability to justify the comparisons made in this study.

The speed changes used in this study were lower than the 16 km/h speed change and longer than the 91 ms collision pulse duration used to rate seat performance by the RCAR/IIWPG (Insurance Institute of Highway Safety, 2008b, Insurance Institute of Highway Safety, 2008a). Nevertheless, the pulses used here provide a graded range of speed changes that represent some real-world collisions that cause whiplash injury (Bartsch et al., 2008, Krafft et al., 2005). The weight of the Experimental seat, especially the seat hinge motors and drives, limited the peak accelerations that was achievable with the test sled. These large seat hinge motors were selected to allow for testing a wide range of seat hinge rotation parameters and to explore different seat hinge rotation profiles. A collision pulse duration of Δt = 148 ms was selected for collision speeds up to 8 km/h because it was achievable and not dissimilar to the 135 ms duration observed in prior vehicle-to-vehicle rear-end crashes (Brault et al., 2000, Brault et al., 1998, Siegmund et al., 2000, Siegmund et al., 1997). However, a collision pulse duration of Δt = 185 ms was needed to reach a 12 km/h collision speed. This longer duration is longer than those of many modern vehicles (Linder et al., 2003, Linder et al., 2001, Stigson et al., 2006), but shorter than those observed in some older vehicles with bumper isolators (Siegmund

et al., 1994). Nevertheless, further work is needed to explore the ATD responses on the Experimental anti-whiplash seat at higher speed changes and shorter collisions pulses.

The BioRID ATD used for this study represented a 50th percentile male, and further work is needed to evaluate the Experimental seat for male and female occupants of different heights and weights. Although the BioRID ATD was designed to mimic the motion of human occupants, including their active muscle response, further work is needed to evaluate whether the pre-perturbation forward rotation of the seat hinge alters the neck muscle response in humans and whether the BioRID ATD remains a valid surrogate for human occupants under these pre-crash conditions. Further work is also needed on how to affordably and efficiently implement an active seat that behaves like the large, heavy and expensive prototype seat used for this study. Despite these limitations, the results of this study provided a better understanding of how to actively control seat hinge rotation to minimize ATD responses during a rear-end collision.

3.5 **Conclusion**

In this study, we investigated whether a novel anti-whiplash seat that actively controls seat hinge rotation could reduce peak ATD responses during a series of low-speed, rear-end collisions of varying severity (Δv = 2, 4, 6, 8 and 12 km/h). The results showed that in comparison to a Control seat modifying the seat hinge rotation could reduce all ATD responses by 24% - 76% ($a_{X\text{-}head}$, $a_{X\text{-}T1}$, $\omega_{Y\text{-}head}$, F_X, F_Z, M_Y, θ_{head}, R_X, and $d_{rebound}$) and neck injury criteria (NIC_{max}, N_{km}, and N_{ij}) by 23 – 85% for speed changes greater than 4 km/h. Based on these

results, active rotation of the seat hinge is a repeatable method of decreasing head-to-head-restraint distance, reducing peak ATD responses, and thus could potentially reduce the risk of whiplash injury following low-speed, rear-end collisions.

Chapter 4. Effects of Seatback Cushion Deformation on ATD Responses

4.1 Introduction

The design of the automotive seat is a key parameter in preventing whiplash injuries following rear-end, vehicle-to-vehicle collisions (Hofinger et al., 1999, Jakobsson et al., 2008, Stemper et al., 2006, Viano, 2003d, Viano, 2008, Svensson et al., 1996). Seatback cushion properties are not only designed for comfort, but more importantly determine the energy absorption and occupant retention during a collision (Viano, 2003a, Viano and Parenteau, 2015, Hofinger et al., 1999). Most current automotive seatbacks are comprised of an outer frame with a compliant spring center that is wrapped in cushioning foam and a seat cover. Hofinger et al. (1999) tested different types of foam (soft and hard) on a custom-designed rigid seat to determine the influence of seatback cushioning on anthropomorphic test device (ATD) responses at speed changes (Δv) of 9.6 and 14.2 km/h. The seatback was divided into upper and lower halves to study the effects of different soft and hard foam combinations. The softer foam across the entire seatback delayed the onset of torso acceleration, increased occupant penetration into the seatback and increased peak linear torso and pelvis acceleration magnitudes. In contrast, the harder foam minimized occupant penetration into the seatback and distributed the pressure more evenly over the ATD's back to decrease peak linear torso and pelvis acceleration magnitudes. Hofinger et al. (1999) suggested that the combination of stiffer foam at the pelvis and softer foam at the torso best reduced occupant acceleration by initiating

earlier torso and pelvis rotation and decreasing the backset, whereas the combination of stiffer foam at the torso and softer foam at the pelvis increased head accelerations. Thus, careful dynamic modifications of seatback cushion properties during the collision may represent a viable option to reduce ATD responses and, consequently, the risk of whiplash injuries.

Modification of the seatback cushion, however, may also alter pre-impact seat geometry such as the horizontal distance between the back of the ATD head and the front face of the head restraint (backset; $d_{backset}$) as well as the vertical distance been the top of the head and the top of the head restraint (head restraint height; d_{height}). Increasing backset and head restraint height has been shown to increase the risk of whiplash injuries following rear-end collisions (Nygren et al., 1985, Siegmund et al., 1999, Stemper et al., 2006, Eriksson, 2005). Specifically, the risk of neck injury was found to be lowest when the backset was zero and the top of the head restraint was level with the top of the occupant's head (Eriksson, 2005). Eriksson also found that changes to backset had a larger effect on the risk of neck injury than head restraint height: for every 25 mm decrease in backset, the risk of neck injury decreased by 10%. Thus, any difference in pre-impact seat geometry (backset and head restraint height) caused by the dynamic modification in seatback cushion properties may influence and potentially confound the reduction peak ATD responses during rear-end collisions.

We developed an Experimental anti-whiplash seat to control seatback deformation using motor-driven seatbelt straps that translate a suspended seatback support frame with fixed foam properties (**Appendix A**). The seatback deformation profile is induced by releasing the

motor-driven seatbelt straps prior to the collision, increasing the ATD penetration into the seatback during the collision. Preliminary experiments to determine the seatback deformation profile allowing the ATD to pocket into the seatback were only conducted at one collision speed (Δv: 12 km/h, Δt: 195 ms; see **Appendix C**). The primary goal of the present study was to compare the kinematic and kinetic responses of a BioRID II ATD seated on the Experimental anti-whiplash seat with the dynamic modulation of the seatback cushion (Experimental seat) to the ATD responses seated on an unmodified automotive seat (Control seat) during a range of low-speed, rear-end perturbations (speed changes of 2 to 12 km/h). A secondary goal of the study was to quantify the repeatability of the seat and ATD responses. In comparison to the Control seat, we hypothesized that the Experimental anti-whiplash seat would reduce most of the peak ATD responses across all tested collision severities.

4.2 Methods

4.2.1 Experimental Anti-Whiplash Seat

The Experimental anti-whiplash seat design consisted of a modified General Motor's High Retention seat (GMHR) and three motors mounted to a modified seat frame to control seatback cushion deformation (**Figure 4.1**). The seat pan and head restraint of the GMHR seat remained unmodified in this design. The seatback was replaced by a rigid aluminum outer frame with four straps made of 47 mm seatbelt webbing spanning between the sides of the

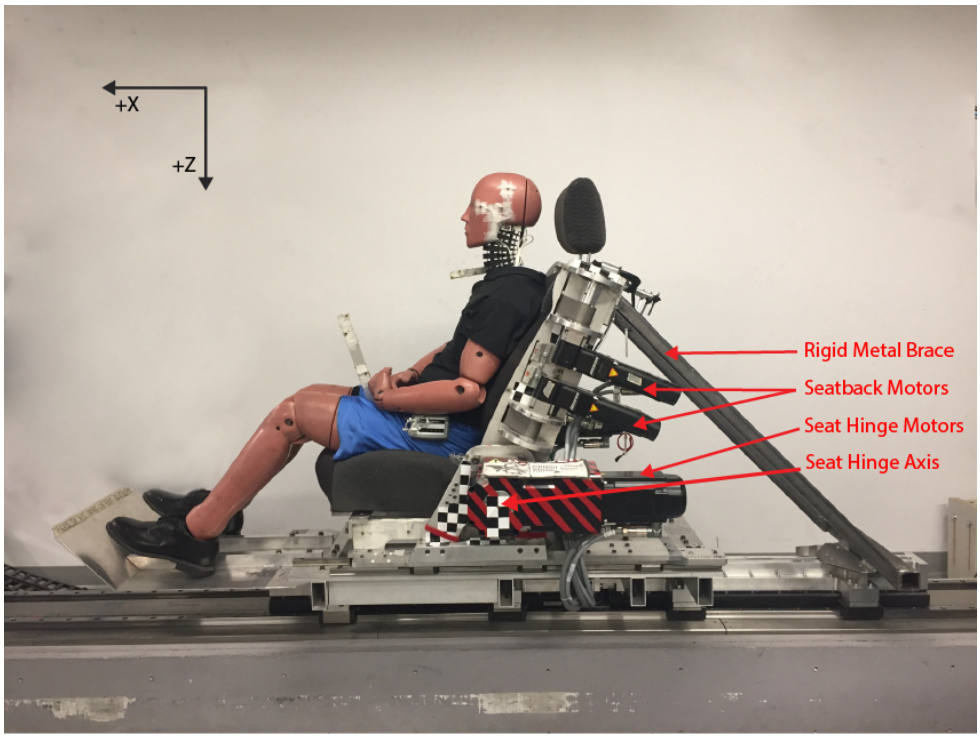

Figure 4.1. Photograph of the experimental set-up with the BioRID II ATD on the Experimental anti-whiplash automotive seat and rigid metal braces to prevent seat hinge rotation. The global laboratory reference frame is illustrated with positive X-axis forward and positive Z-axis downwards. The seat hinge and seatback motors on the left side of the Experimental seat are labelled. Additional seat hinge and seatback motors are located on the right side of the seat (not labelled). The seat hinge motors are not used in this current study.

outer frame at the upper, middle and lower back locations (upper: 1 strap, middle: 2 straps and lower: 1 strap). The seatback cushion from the GMHR seatback was suspended on the front surface of the four straps. Seatback cushion deformations were controlled by modulating the amount of webbing using three rotational servomotors (AKM24D, Kollmorgen, Waltham, MA, USA) connected to helical right-angle gearheads (VTR006-008, 8:1 gear ratio, Thomson Linear, Radford, VA, USA) mounted staggered to both sides of the rigid seatback. The three motors

were placed at the top, middle and bottom of the seatback and attached to the 4 seatbelt straps (with the middle motor connected to the 2 middle straps) that spanned across the perimeter frame to separately control the seatback deformation at the upper-torso, mid-torso and lower pelvis regions (**Figure 4.2**). Tightening the webbing would pull the suspended GMHR seatback cushion towards the front of the seat (+X direction) and increase the stiffness of the seatback; whereas loosening the webbing would allow the seatback cushion to translate towards the rear of the seat (-X direction) and allow for deeper occupant penetration into the seatback during rear-end collisions. Slack was introduced into all the webbing straps to set the initial seatback angle to 27 deg rearward from vertical (Siegmund et al., 2005a). To isolate the effects of seatback cushion deformation, seat hinge rotation was prevented by installing rigid metal braces between the seat outer frame and the sled.

Through a series of iterative experiments (see **Appendix C**), different seatback motor parameters were varied and tested to create a seatback motor rotation profile that reduced ATD responses during a 12 km/h speed change (**Figure 4.3**). The seatback rotation profile was characterized by an input rotation to the two lower motors with a peak angle ($\theta_{deformation\text{-}peak}$) of 168 deg and an initial angular velocity of ($\omega_{deformation\text{-}int}$) 980 deg/s. The rotational input to the two lower motors introduced slack in the webbing and ultimately linear rearward translation of the ATD with respect to the seatback. The upper-torso motor was locked in a stationary position, effectively creating a hinge point at the upper back and pocketing of the pelvis into the seat during the collisions. The onset of the seatback deformation profile occurred 200 ms

prior to the collision ($t_{deformation\text{-}onset}$ = -200 ms). A motion capture system (Optotrak Certus, Northern Digital, Waterloo, ON, Canada) was used to estimate the deformation of the seatback cushion during low-speed, rear-end collisions. Maximum rearward penetration of the T1 vertebra ($d_{penetration\text{-}T1}$) and pelvis ($d_{penetration\text{-}pelvis}$) were used to describe the seatback cushion deformation and were defined as the horizontal displacement (along the global X-axis, **Figure 4.1**) between the infrared light emitting diode(IRED) markers mounted to the seatback frame and the T1 vertebra and pelvis, respectively **(Figure 4.3**). The initial position of the ATD at rest was set as zero ($d_{penetration\text{-}T1}$ = 0 mm and $d_{penetration\text{-}pelvis}$ = 0 mm) and rearward displacements into the seatback were defined as negative values. For a 12 km/h collision, the programmed seatback rotation profile allowed maximum occupant penetration into the seatback of 84 mm at T1 and 97 mm at the pelvis (**Figure 4.3,** see **Appendix C**).

All three seatback motors were controlled independently by separate digital servo drives (Servostar 600, Kollmorgen, Waltham, MA, USA) connected to a universal motion interface and a motion controller (NI UMI 7774 and NI PXI 7350, National Instruments Corporation, Austin, Texas, USA). A custom LabVIEW program (National Instruments Corporation, Austin, Texas, USA) was created to send commands to, monitor the status of and record encoder data from the three motors.

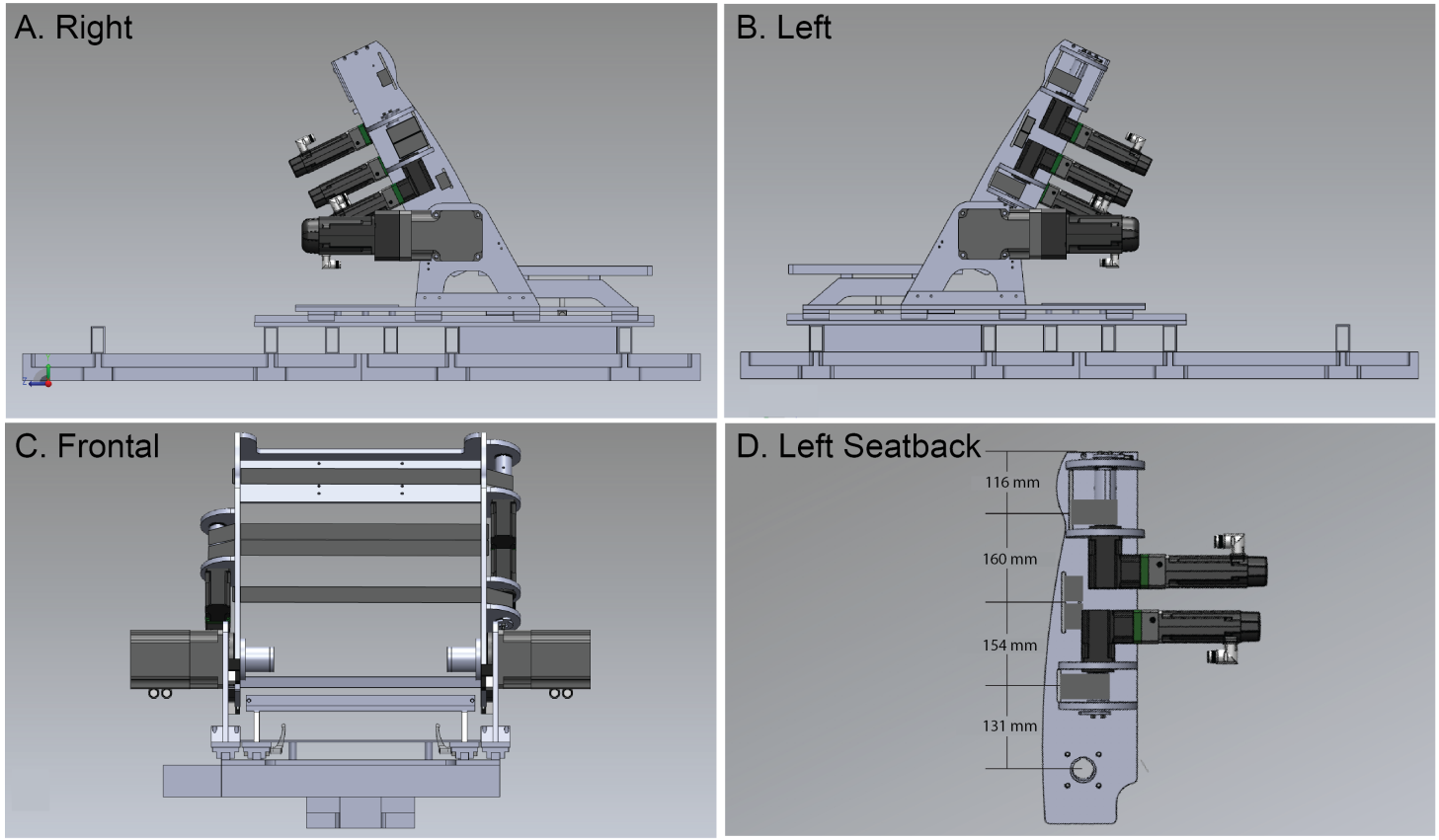

Figure 4.2. Computer-aided design (CAD) drawings of Experimental seat with three seatback motors placed at the top, middle and bottom of the seatback, and the 4 seatbelt straps that spanned across the perimeter frame to separately control the seatback deformation at the upper-torso, mid-torso and lower pelvis regions. The middle motor was connected to the 2 middle straps. Panel A., B. & C. show the right, left and frontal views, respectively. The distances between the center of the seatbelts and the seat hinge are illustrated in Panel D.

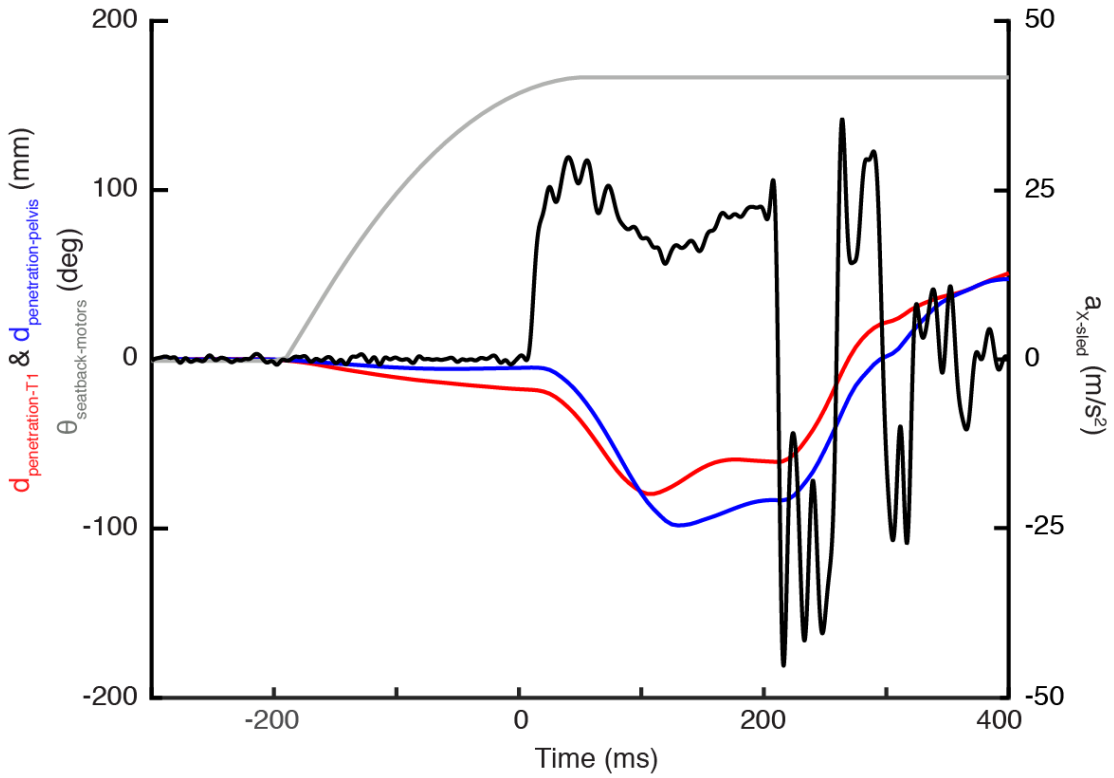

Figure 4.3. Estimated horizontal seatback cushion deformation using displacement of the T1 vertebra and pelvis ($d_{penetration\text{-}T1}$, red plot & $d_{penetration\text{-}pelvis}$, blue plot) in response to the seatback motor rotation profile ($\theta_{seatback\text{-}motor}$, grey plot) with $\theta_{deformation\text{-}peak}$ = 168 deg, $\omega_{deformation\text{-}int}$ = 980 deg/s, and $t_{deformation\text{-}onset}$ = -200 ms during a 12 km/h collision pulse with a collision pulse duration of 194 ms ($a_{X\text{-}sled}$, black plot).

4.2.2 Anthropomorphic Test Device and Instrumentation

A BioRID II ATD (Humanetics, Plymouth, MI, USA) was instrumented to measure head, chest (T1), and pelvis kinematics and kinetics (**Figure 4.1**). A six-axis load cell (Forces: F_X, F_Y, F_Z; and Moments: M_X, M_Y, M_Z; Model 4949a, Robert A. Denton, Inc., Rochester Hills, MI, USA) was mounted at the atlanto-occipital joint (AOJ) to measure upper neck forces and moments. Linear forward accelerations of the head and T1 were measured using two uni-axial

accelerometers (7264C sensors; ±500 g, Endevco, San Juan Capistrano, CA, USA) mounted at both the head center of mass and the T1 vertebra. A uni-axial angular rate sensor was also mounted at the head center of mass (ARS-1500; ±26.2 rad/s, DTS, Seal Beach, CA, USA) to measure angular kinematics about the sagittal plane (i.e. flexion and extension of the neck).

A motion capture system (Optotrak Certus, Northern Digital, Waterloo, ON, Canada) was used to track IRED markers affixed to the head, AOJ, T1, and pelvis of the ATD to measure head, T1 and pelvis displacements. Additional IRED markers were mounted to the Experimental anti-whiplash seat to record displacements and rotations of the seatback as well as to create a global experimental reference frame (+X forward, +Y right, and +Z down). Horizontal sled acceleration was measured with a uni-axial accelerometer (2220-100; ±100 g, Silicon Design Inc., Issaquah, WA, USA) mounted directly to the base of the linear sled frame. Head restraint contact was detected with a force sensitive resistor (FSR; Model 406, Interlink Electronics, Camarillo, CA, USA) attached to the front of the head restraint.

All accelerometer, load cell and angular rate sensor signals were simultaneously sampled at 10 kHz using a National Instruments Data Acquisition (DAQ) PXI system (PXI-4495 & PXI-6289, National Instruments Corporation, Austin, Texas, USA) and a custom-written LabVIEW virtual instrument (National Instruments Corporation, Austin, Texas, USA). Optotrak data were acquired at 200 Hz and collection was triggered by the DAQ system to synchronize the data. Subsequent data and statistical analyses were performed using Matlab (R2017A, Mathworks, Natick, MA, USA). All data were digitally filtered in Matlab and conformed to the SAE J211

(Channel class 180 for the ATD sensors and Channel Class 60 for the sled accelerometer; SAE, 1995).

4.2.3 Test Procedures

The ATD was dressed in two layers of lycra and was seated on either the Control or Experimental seats mounted on a 10 m long, feedback-controlled linear sled (Kollmorgen IC55-100A7, Waltham, MA, USA), as illustrated in **Figure 4.1**. To ensure the repeatability of the experiments, the initial position of the ATD was measured by Optotrak and adjusted to a pre-defined posture that was constant within each seat and as similar between Control and Experimental seats. The seatbelt was removed from the seats to prevent interactions that could affect ATD head, neck and torso kinematics. Initial pre-impact seatback angle was set to 27 deg rearward from vertical (Siegmund et al., 2005a) and the vertical placement of the head restraint was adjusted to the midpoint between the lowest and highest vertical position according to the Research Council for Automobile Repairs/International Insurance Whiplash Prevention Group (RCAR/IIWPG) seat/head restraint evaluation protocol (Insurance Institute of Highway Safety, 2008b).

The kinematic and kinetic responses of the ATD seated on the Experimental seat with the seatback deformation profile were first compared to the ATD responses seat on the Control seat. For each seat, the ATD was exposed to a series of five rear-end whiplash-like perturbations at increasing speed changes (Δv = 2, 4, 6, and 8 km/h with a Δt of 148 ms and 12

km/h with a Δt of 194 ms) (**Figure 4.4**). Due to limitations in the force-generating ability of the linear motors, a longer pulse duration was needed for the 12 km/h speed change. All of the pulses had a longer duration than the RCAR/IIWPG pulse (Δt = 91 ms) (Insurance Institute of Highway Safety, 2008b). The sled was accelerated forward from a stationary position for the 2, 4 and 6 km/h speed changes and from a constant rearward speed of 6 km/h for the higher speed changes (8 and 12 km/h). Preliminary results comparing occupant responses of an 8 km/h collision starting from a stationary position to an 8 km/h collision starting from a 6 km/h rearward velocity showed less than 10% differences (mean: 2.50% ± 2.53%; range: 0.5% – 9.2%) in most of the occupant responses and neck injury criterions between the two collision perturbations (see **Chapter 2**). To assess the repeatability of the ATD responses, four additional repeated trials were collected at the 8 and 12 km/h collision speed changes for both the Control and Experimental seats (for a total of 5 trials for each seat at these two speed changes).

The Experimental anti-whiplash seat was designed to receive a good-rating ($d_{backset}$ < 70 mm and d_{height} > -60 mm) whereas the Control GMHR seat received a poor-rating due to the backset being greater than 90 mm (Insurance Institute of Highway Safety, 2004). Consequently, the static pre-impact position of the head restraint on the Control seat ($d_{backset}$ = 94.4 ± 2.6 mm, d_{height} = -24.2 ± 2.6 mm) was different from the Experimental seat ($d_{backset}$ = 52.0 ± 7.3 mm, d_{height} = 2.5 ± 7.1 mm). To determine whether differences in pre-impact backset potentially confounded the results, the kinematic and kinetic responses of the ATD observed on the Control and Experimental seats were compared to a No Motion condition on the Experimental

Seat. For the No Motion condition, the seatback motors did not unspool and remained at their pre-impact position during the 12 km/h collision. The pre-impact backset and height geometry of the head restraint ($d_{backset}$ = 60.2 ± 5.8 mm, d_{height} = -0.23 ± 9.6 mm) of the No Motion condition matched more closely to the Control seat than on the Experimental seat. Five trials of the No Motion condition were collected at the 12 km/h collision speed change (Δt = 194 ms).

A total of 31 trials were collected, 13 trials for the Control seat, 5 for the No Motion condition and 13 for the Experimental seat. Averaged peak responses were used for test conditions with repeated trials in subsequent analysis (Control and Experimental seats: Δv = 8 and 12 km/h trials, and No Motion condition: Δv = 12 km/h trials).

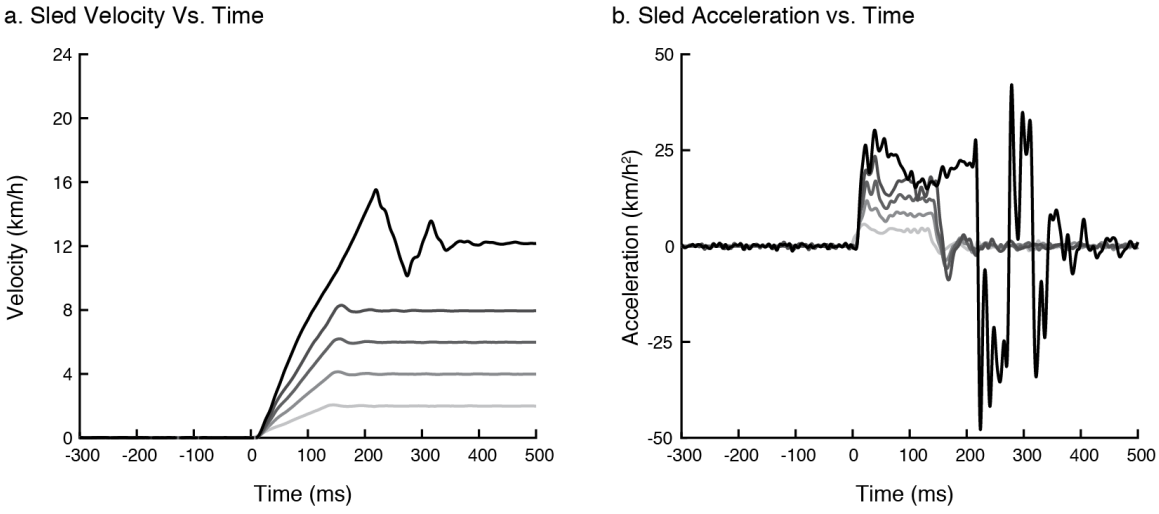

Figure 4.4. Exemplar sled a) velocity and b) acceleration pulses for increasing collision speeds (Δv = 2, 4, 6, and 8 km/h with a pulse duration (Δt) of 148 ms, and Δv = 12 km/h with a Δt of 194 ms; lightest to darkest). Collision onset occurred at time = 0 ms.

4.2.4 Data Analysis

Head and torso accelerometer data were reported in local head and T1 reference frames and were corrected to remove the earth's gravity using the head and T1 orientations determined from Optotrak data. Peak linear forward acceleration of the head ($a_{X\text{-}head}$) and T1 vertebra ($a_{X\text{-}T1}$) were extracted directly from the transformed accelerometer data. Peak horizontal sled acceleration ($a_{X\text{-}sled}$) was extracted directly from the accelerometer mounted to the sled and peak rotational velocity of the head ($\omega_{Y\text{-}Head}$) in the sagittal plane was determined from the angular rate sensor. Peak upper neck shear (F_X) and axial (F_Z) forces and the flexion/extension bending moment (M_Y) were determined from the upper neck load cell and reported in the ATD reference frame as the forces/moments applied by the neck to the head. Initial head angle was defined as the average angle between -300 ms and -200 ms preceding the onset of sled acceleration ($a_{X\text{-}sled}$) and peak head extension angle (θ_{head}) was defined as the maximum rotation of the head into extension relative to initial head angle. A foreperiod between -300 ms and -200 ms immediately before the onset of forward $a_{X\text{-}sled}$ was used to define initial values to account for any possible interactions of the early onset of seatback cushion deformation ($t_{penetration\text{-}onset}$ = -200 ms) on ATD kinematic and kinetic responses. Peak retraction (R_x) was defined as the maximum horizontal displacement in the laboratory reference frame of the AOJ with respect to the T1 vertebra with rearward displacements defined as negative values. The back and top of the ATD head as well as front face and top of the head restraint were digitized relative to existing Optotrak IRED markers. These digitized

points were used to determine, in the laboratory reference frame, the head-to-head-restraint distance ($d_{backset}$) and the height of the head restraint (d_{height}; negative values indicate that the top of the head restraint was lower than the top of the ATD head). Initial pre-impact $d_{backset}$ and d_{height} were defined as the average head-to-head-restraint horizontal and vertical distances between -300 ms and -200 ms before the onset of forward $a_{X\text{-}sled}$. Peak forward rebound distance ($d_{rebound}$) was defined as the maximum forward head-to-head-restraint distance. Maximum rearward penetration of the torso and pelvis into the seatback ($d_{penetration\text{-}T1}$ and $d_{penetration\text{-}pelvis}$) were defined as the maximum horizontal displacement in the laboratory reference frame between the seatback frame and T1 vertebra or pelvis markers, respectively (rearward displacements defined as negative values). Time-to-head-restraint contact ($\Delta t_{head\text{-}contact}$) was extracted from the time of force onset in the FSR attached to the head restraint with respect to the onset of forward sled acceleration (t = 0 ms). Onsets of sled acceleration and head restraint contact were determined when the accelerometer and FSR signals reached 1.5 times the peak background noise level between -300 ms to -200 ms before the onset of the collision and were confirmed visually.

Three neck injury criteria (NIC_{max}, N_{ij}, and N_{km}) were computed from the accelerometer and load cell data. The Neck Injury Criterion (NIC_{max}) was calculated from the relative horizontal acceleration (corrected for gravity) and velocity in the global reference frame between the head center of mass and the T1 joint (Equation 4.1; Bostrom et al., 1996). The Normalized Neck Injury Criterion (N_{ij}) was calculated from the axial load (F_Z) and the

flexion/extension bending moment (M_Y) measured from the upper neck load cell (Equation 4.2; critical F_{int} and M_{int} intercept values used for normalization: $F_{int\text{-}tension}$ = 6806 N, $F_{int\text{-}compression}$ = -6160 N, $M_{int\text{-}flexion}$ = 310 N, and $M_{int\text{-}extension}$ = -135 N; Eppinger et al., 1999, Eppinger et al., 2000). The Neck Protection Criterion (N_{km}) was calculated from the sagittal shear force (F_X) and the flexion/extension bending moment (M_Y) measured from the upper neck load cell (Equation 4.3; critical F_{int} and M_{int} intercept values used for normalization: $F_{int\text{-}shear\text{-}anterior}$ = 845 N, $F_{int\text{-}shear\text{-}posterior}$ = 845 N, $M_{int\text{-}extension}$ = 47.5 Nm, and $M_{int\text{-}flexion}$ = 88.1 Nm; Schmitt et al., 2001, Schmitt et al., 2002). Peak values of the three neck injury criteria were then extracted for analysis and compared to proposed injury thresholds (NIC: 15 m^2/s^2, Eichberger et al., 1998; N_{ij} and N_{km} : a normalized value of one, Schmitt et al., 2001, Schmitt et al., 2002, Eppinger et al., 1999). These injury thresholds correspond to different human tolerance levels for the causation of whiplash-related injuries – NIC: long-term whiplash-associated disorders (WAD) levels 1-3 (Bostrom et al., 2000, Bostrom et al., 1996), N_{ij}: 22% risk of abbreviated injury scale (AIS) level 3 (i.e., fracture; Eppinger et al., 1999, Eppinger et al., 2000), and N_{km}: AIS level 1 injury causation (i.e., minor injury; Schmitt et al., 2001, Schmitt et al., 2002).

$$NIC_{max}(t) = \text{maximum}_{\text{first 150 ms}}(a_{rel}(t) \cdot L + (v_{rel}(t))^2) \quad \ldots \quad \text{Equation 4.1}$$

$$N_{ij}(t) = \frac{F_z(t)}{F_{int}} + \frac{M_{yOC}(t)}{M_{int}} \quad \ldots \quad \text{Equation 4.2}$$

$$N_{km}(t) = \frac{|F_x(t)|}{F_{int}} + \frac{|M_{yOC}(t)|}{M_{int}} \quad \ldots \quad \text{Equation 4.3}$$

The repeatability of the BioRID II ATD on the Control and Experimental seats were assessed using the Coefficient of Variation (COV), which was calculated as the standard deviation (SD) divided by the mean and expressed as a percentage. The National Highway Traffic Safety Administration (NHTSA) defines a COV of 5% or less as excellent, a COV of 10% or less as acceptable and a COV greater than 10% as poor (Rhule et al., 2005). To quantify the repeatability of the ATD, the COV for all of the peak responses were calculated from the five repeated trials at the 8 and 12 km/h collision severities on the Control and Experimental seats. Because COV is dependent on the mean and SD values of the responses, the expected decreases in mean responses (which form the denominator in the COV calculation) for the Experimental seat may generate larger COV values. A comparison of the SD values between the GMHR and the Experimental seats would provide an alternate assessment of variability and would help to determine whether the larger COV values for the Experimental seat were likely due to the lower mean responses or due to the greater inherent variability (i.e., standard deviation) in the ATD responses. The SD values for all kinematic and kinetic responses as well as neck criteria observed at both the 8 and 12 km/h collision speeds were used in this assessment of variability. The COV and SD values were assumed to be independent observations. A Kolmogorov-Smirnov test determined that the COV values of the Control and Experimental seats at the 8 km/h collision severity were normally distributed and a paired Student's t-test was performed. For all other COV (12 km/h) and SD (8 and 12 km/h) values of the Control and Experimental seats, the Kolmogorov-Smirnov test determined the data were not normally

distributed and Wilcoxon Signed-Rank tests were performed. All tests were performed using predefined functions (`kstest`, `ttest`, and `signrank`) in Matlab (R2017A, Mathworks, Natick, MA, USA) at a significance level $\alpha = 0.05$.

First, to compare the ATD responses between the Control and Experimental seats across the different speed changes, 99th percentile predictive intervals were created around the peak responses for each seat using their respective maximum variability (COV value) observed from repeated trials at either the 8 or 12 km/h collision severity (Horslen et al., 2015). The maximum COV values from either the 8 or 12 km/h collision severity were selected to represent the largest observed variance within each response and were multiplied by 2.58 (z-score for two-tailed 99th percentile) to estimate 99th percentile predictive limits. Since the COV values were defined as the maximum variances (i.e. standard deviation) divide by the mean of the peak ATD responses, these predictive limits were represented as a percentage and were then applied to their respective peak responses to create predictive intervals at each collision severity (2 – 12 km/h). Any ATD responses where the 99th percentile predictive intervals from the Control and Experimental seats did not overlap were assumed to be statistically different. The 99th percentile predictive limits were used in this study to account for numerous comparisons between Control and Experimental seats for each ATD responses at each collision severity and to provide a conservative estimate of statistical significance.

Because backset and head restraint height varied between the Control and Experimental seats, a No Motion condition was also collected on the Experimental seat to isolate the

contribution of seatback deformation. The effects of the Control seat, No Motion condition (no seatback deformation), and Experimental seat (with seatback deformation) on the ATD responses during a 12 km/h collision severity were compared by conducting one-way analysis of variance (ANOVA) tests for each peak ATD responses. Post-hoc comparisons were performed using the Tukey's Honest Significant Difference (HSD) test. All statistical tests were performed using predefined functions (`anova1` and `multcompare`) in Matlab at a significance level $\alpha = 0.05$. To determine the additional contribution of seatback deformation from those associated with pre-impact seat geometry (and other seat-related factors such as the rigid brace preventing seat hinge rotation), the differences in each peak kinematic and kinetic ATD responses between the Control seat and No Motion condition were divided by the differences observed between the Control and Experimental seats and expressed this ratio as a percentage. A score of 0% indicates that the No Motion yielded ATD responses identical to the Control seat and a 100% score that the No Motion yielded ATD responses identical Experimental seat. Thus, a lower percentage score revealed the relative contribution (100% - percentage score) of seatback cushion deformation compared to the pre-impact seat geometry (and other seat-related factors) on the overall reduction of ATD responses.

4.3 **Results**

The repeatability of the ATD responses for both the Control and Experimental seats were assessed using COV and SD values from the repeated trials at both the 8 and 12 km/h collision speed changes (**Table 4.1**). With the exception of initial head restraint height (d_{height}, 8 km/h: 20.4% and 12 km/h: 11.6%), the COV values for the Control seat were acceptable or better (less than 10%) for both collision severities. The Experimental seat on the anti-whiplash seat, however, exhibited poor peak COV values (greater than 10%) in all the neck injury criteria (NIC: 45.9%; N_{ij}: 22.2% and N_{km}: 23.3%) and in most ATD responses ($d_{backset}$: 14.1%, d_{height}: 280.3%, F_X: 26.0%, F_Z: 16.9%, M_Y: 25.2%, $\omega_{Y\text{-}head}$: 15.1%, θ_{head}: 32.4%, $d_{rebound}$: 20.6%, R_X: 20.6% and $\Delta t_{head\text{-}contact}$: 19.9%). The COV values on the Experimental seat were significantly higher than those on the Control seat for the 8 and 12 km/h speed changes (paired t-test; 8 km/h: $t(17) = 5.01$, $p = 0.001$, and Wilcoxon Signed-Rank Test; 12 km/h: $Z = 3.72$, $p = 0.0002$). The SD values of the Experimental and Control seats were not significantly different for the 8 km/h (Wilcoxon Signed-Rank Test; $Z = 1.02$, $p = 0.31$), but were significantly different for the 12 km/h (Wilcoxon Signed-Rank Test; $Z = 2.94$, $p = 0.0033$). The similarities of the SD values between the Control and the Experimental seats at the 8 km/h suggested that the larger COV values for the Experimental seat were more likely due to the lower mean responses than to the inherent variability in the ATD responses.

Graded kinematic and kinetic responses to increasing collision severities were observed for both Control and Experimental seats (**Figure 4.5, 4.6** & **4.7**, **Table 4.2**). In comparison to the

Control seat, the Experimental seat reduced most ATD kinematic and kinetic responses ($a_{X\text{-head}}$, $\omega_{Y\text{-head}}$, F_X, F_z, $\theta_{head,}$ R_X and $\Delta t_{head\text{-}contact}$) as well as neck injury criteria (NIC, N_{km}, and N_{ij}) by 15 – 82% of peak Control responses at collision speeds of 4 km/h or higher. With the exception of $a_{X\text{-}sled}$ and $a_{X\text{-}T1}$ (all collision severities), M_Y (2 – 6 km/h collision speeds), and Nij (2 & 4 km/h severities), there were no overlap between the 99th percentile predictive intervals of the Control and Experimental seat responses and were considered significantly different between the two seats. At the 2 km/h collision severity, most ATD responses ($\omega_{Y\text{-head}}$, F_X, $\theta_{head,}$ R_X and $\Delta t_{head\text{-}contact}$) and neck injury criteria (NIC, N_{ij}, and N_{km}) decreased from Control seat between 17 to 58%. However, the addition of a dynamic seatback cushion deformation increased $a_{X\text{-head}}$ (+26%), F_Z (+163%), and M_Y (+281%) ATD responses in comparison to the Control seat (**Table 4.2**)

In comparison to the Control seat, peak head linear acceleration ($a_{X\text{-head}}$) decreased by 38 – 51%, while peak angular velocity of the head ($\omega_{Y\text{-head}}$) decreased by 59 – 81% (**Figure 4.7B** & **4.7F**). Upper neck shear and axial forces and the flexion/extension bending moment (M_Y) also decreased from Control trials (F_X: 56 – 67%, F_Z: 36 – 72%, and M_Y: 29 – 77%, respectively) (**Figure 4.7G** – **4.7I**). No head-to-head-restraint contact ($\Delta t_{head\text{-}contact}$) occurred at the 2 km/h collision severity, but at collision severities greater than 2 km/h the Experimental seat decreased $\Delta t_{head\text{-}contact}$ by 50 to 82 ms representing a decrease of 45 to 53% (**Figure 4.7J**). Kinematic responses of the head relative to the torso were decreased as measured by head angle (θ_{head}: 56 – 79%) and peak retraction (R_X: 37 – 71%) (**Figure 4.7K** & **4.7L**).

None of the neck injury criteria (NIC_{max}, N_{ij}, nor N_{km}) exceeded their respective proposed injury thresholds during the experiments. The Experimental seat also attenuated all three neck injury criteria for whiplash injuries – Neck Injury Criterion (NIC_{max}: 58 – 69%), Normalized Neck Injury Criterion (N_{ij}: 15 – 81%), and Neck Protection Criterion (N_{km}: 41 – 64%) (**Figure 4.7M – 4.7O**).

Maximum rearward penetration of the ATD torso and pelvis ($d_{penetration\text{-}T1}$ & $d_{penetration\text{-}pelvis}$, respectively) also exhibited a graded response to increasing collision speed changes (**Table 4.2**). The early onset of seatback cushion deformation ($t_{penetration\text{-}onset}$ = -200 ms) prior to the onset of the whiplash perturbation (t = 0 ms) decreased the backset ($d_{backset}$) and increased the peak rearward occupant penetration ($d_{penetration\text{-}T1}$ & $d_{penetration\text{-}pelvis}$) into the seatback from the Control seat (**Figure 4.6**). The addition of the pre-perturbation forward seatback cushion deformation at -200 ms before the collision allowed deeper 'pocketing' into the seatback and decreased the backset to 13.9 ± 6.5 mm (74% decrease from resting Experimental seat $d_{backset}$) prior to the onset of the whiplash collision (**Figure 4.6**). Across the different collision severities, peak forward rebound ($d_{rebound}$) values in the Experimental seat were 51 – 75% lower than in the Control seat, while the penetration of the ATD into the seatback increased at the T1 ($d_{penetration\text{-}T1}$: 18 – 26%) and pelvis ($d_{penetration\text{-}pelvis}$: 75 – 1100%) (**Figure 4.7D** & **4.7E**).

The averaged pre-impact head restraint geometry of the Control seat ($d_{backset}$ = 94.3 ± 2.2 mm, d_{height} = -23.8 ± 4.0 mm) were larger than the Experimental seat ($d_{backset}$ = 53.8 ± 6.0 mm and d_{height} = 6.3 ± 6.5 mm) and the No Motion condition ($d_{backset}$ = 60.7 ± 6.0 mm and d_{height} = -

8.7 ± 4.4 mm). The one-way ANOVAs (**Table 4.3;** $F_{(2,12)}$ = 8.43 – 553.10, p ≤ 0.0052) and post-hoc comparisons revealed that the ATD responses observed on the Control seat were different than those observed in the No Motion condition and all but one response ($a_{X\text{-}T1}$, p = 0.0685) on the Experimental seat. Between the No Motion condition and the Experimental seat most responses were different with the exception for five of the eighteen responses ($d_{backset}$, $a_{X\text{-}sled}$, $a_{X\text{-}T1}$, M_Y, and N_{km}: p = 0.0765 – 0.6646). These results suggest that seatback deformation provides a unique benefit over pre-impact head restraint geometry. The percentage scores computed to determine the additional contribution of seatback deformation from those associated with pre-impact seat geometry revealed that across all ATD responses, the No Motion condition reduced ATD responses by 66.7% from the Control seat (normalized % = 14.1% - 163.7%). This analysis suggests that approximately 33.3% of the total reduction in ATD responses observed between the Control and the Experimental seats are due to the added seatback cushion deformation.

Table 4.1. Mean (standard deviation) and Coefficient of Variation (COV: %) from five repeated whiplash-like perturbation (n = 5) on the Control and Experimental anti-whiplash seats at collision severities of Δv = 8 km/h with Δt = 148 ms and Δv = 12 km/h with Δt = 194 ms.

Δv (km/h)	8 km/h, Δ = 148 ms				12 km/h, Δ = 194 ms					
Trial	Control		Experimental		Control		No Motion		Experimental	
Parameter	Mean (SD)	COV	Mean (SD)	COV	Mean (SD)	COV	Mean (SD)	COV	Mean (SD)	COV
$d_{backset}$ (mm)	94.2 (1.9)	2.0	55.7 (4.4)	7.9	94.4 (2.6)	2.8	60.7 (6.0)	10.0	52.0 (7.3)	**14.1**
d_{height} (mm)	-23.4 (4.8)	**20.4**	-10.0 (3.0)	**30.2**	-24.2 (2.8)	**11.6**	-8.7 (4.4)	**50.8**	2.5 (7.1)	**280.3**
$a_{X\text{-}sled}$ (m/s^2)	22.8 (1.1)	4.7	22.2 (0.3)	1.5	31.6 (0.4)	1.2	30.3 (0.4)	1.3	30.7 (0.5)	1.7
$d_{penetration\text{-}T1}$ (mm)	-58.1 (2.2)	3.8	-68.4 (1.8)	2.6	-67.8 (1.0)	1.5	-74.3 (2.7)	3.7	-78.5 (1.7)	2.2
$d_{penetration\text{-}pelvis}$ (mm)	-38.9 (1.1)	2.9	-83.8 (2.7)	3.2	-55.8 (2.2)	2.2	-62.0 (3.4)	5.5	-99.6 (3.8)	3.8
$\Delta t_{head\text{-}contact}$ (ms)	127.2 (1.1)	0.9	60.1 (5.8)	9.6	112.4 (2.6)	2.3	87.0 (4.9)	5.6	51.4 (10.2)	**19.9**
$a_{X\text{-}head}$ (m/s^2)	85.2 (1.0)	1.1	41.5 (1.9)	4.6	120.7 (1.7)	1.4	75.4 (2.2)	3.0	60.7 (4.6)	7.5
$a_{X\text{-}T1}$ (m/s^2)	45.0 (0.7)	1.6	27.2 (0.8)	3.1	48.5 (0.4)	0.9	46.1 (1.2)	2.5	47.1 (1.0)	2.1
F_X (N)	213.5 (3.8)	1.8	71.6 (10.9)	7.8	264.4 (14.1)	5.4	172.0 (15.0)	8.7	87.8 (22.8)	**26.0**
F_Z (N)	414.4 (9.3)	2.2	118.2 (9.8)	8.3	586.1 (16.2)	2.8	307.3 (37.9)	**12.4**	134.7 (21.6)	**16.0**
M_Y (Nm)	20.1 (1.2)	6.0	4.6 (1.2)	**25.2**	25.1 (0.1)	0.2	4.6 (1.5)	**33.0**	5.9 (1.2)	**19.7**
$\omega_{Y\text{-}head}$ (deg/s)	335.3 (16.7)	5.0	62.2 (9.4)	**15.1**	393.8 (7.4)	1.9	230.5 (19.5)	8.5	147.8 (11.9)	8.1
θ_{head} (deg)	15.7 (0.4)	2.3	3.8 (1.0)	**26.1**	16.5 (0.6)	3.9	12.1 (1.1)	9.3	5.3 (1.7)	**32.4**
$d_{rebound}$ (mm)	336.1 (10.4)	3.1	83.6 (5.9)	7.1	413.5 (7.7)	1.9	320.9 (15.2)	4.7	126.0 (17.1)	**13.6**
R_X (mm)	-61.8 (1.1)	1.8	-26.8 (3.7)	**13.7**	-64.2 (2.4)	3.7	-54.0 (4.4)	8.1	-32.6 (6.7)	**20.6**
NIC_{max} (m^2/s^2)	6.9 (0.2)	3.1	1.9 (0.4)	**22.7**	9.7 (0.1)	1.4	7.8 (0.5)	5.9	2.0 (0.9)	**45.9**
N_{ij}	0.12 (0.003)	2.3	0.02 (0.003)	**12.9**	0.16 (0.002)	1.5	0.06 (0.011)	**19.1**	0.027 (0.006)	**22.2**
N_{km}	0.48 (0.02)	3.7	0.17 (0.03)	**17.3**	0.60 (0.02)	2.9	0.26 (0.03)	**13.0**	0.23 (0.05)	**23.3**

Notes: The underlined COV values indicate a COV rating of acceptable (5% ≤ COV < 10%), the **bolded** COV values indicate a COV rating of poor (COV > 10%), and all other values are rated good (COV < 5%).

Table 4.2. Peak responses for Control and Experimental anti-whiplash (EXP) seats for each collision severity.

Δv (km/h)	2km/h, Δt = 148ms		4km/h, Δt = 148ms		6km/h, Δt = 148ms		8km/h, Δt = 148ms		12km/h, Δt = 194ms	
Condition	Control	EXP	Control	EXP	Control	EXP	Control	EXP	Control	EXP
$d_{backset}$ (mm)	90.5	58.1	91.1	50.2	90.2	54.6	94.2	55.7	94.4	52.0
d_{height} (mm)	-31.0	8.8	-32.3	-3.6	-42.3	-3.1	-23.4	-10.0	-24.2	2.5
$a_{X\text{-}sled}$ (m/s^2)	5.8	5.6	11.2	11.3	15.9	16.0	22.8	22.2	31.6	30.7
$d_{penetration\text{-}T1}$ (mm)	-18.4	-43.9	-37.0	-46.5	-41.7	-51.4	-58.1	-68.4	-67.8	-78.5
$d_{penetration\text{-}pelvis}$ (mm)	-0.05	-27.6	-4.2	-50.9	-14.0	-62.3	-38.9	-83.8	-55.8	-99.6
$\Delta t_{head\text{-}contact}$ (ms)	0.0	0.0	164.5	81.2	138.8	72.0	127.2	60.1	112.4	61.5
$a_{X\text{-}head}$ (m/s^2)	8.7	12.7	35	21.6	57.1	34.4	85.2	41.5	120.7	66.0
$a_{X\text{-}T1}$ (m/s^2)	8.2	9.4	20.6	17.6	26.4	27.8	45.0	27.2	48.5	47.8
F_X (N)	89.5	53.8	166.4	55.3	193.3	85.7	213.5	71.6	264.4	115.5
F_Z (N)	34.5	53.9	173.5	111.6	336.5	137.4	414.4	118.2	586.1	166.7
M_Y (Nm)	1.0	4.0	6.6	8.8	18.5	13.2	20.1	4.6	25.1	6.1
$\omega_{Y\text{-}head}$ (deg/s)	110.6	42.4	246.3	50.6	294.4	60.6	335.3	62.2	393.8	163.6
θ_{head} (deg)	8.8	4.0	15.3	3.4	14.5	3.1	15.7	3.8	16.5	7.3
$d_{rebound}$ (mm)	119.6	58.4	175.5	75.0	260.0	98.0	336.1	83.6	413.5	126.0
R_X (mm)	-34.1	-18.7	-57.7	-16.8	-58.1	-24.0	-61.8	-26.8	-64.2	-40.2
NIC_{max} (m^2/s^2)	1.3	0.6	3.5	2.3	5.0	2.1	6.9	1.9	9.7	3.0
N_{ij}	0.0	0.0	0.0	0.0	0.1	0.0	0.12	0.02	0.16	0.03
N_{km}	0.2	0.2	0.3	0.2	0.4	0.2	0.48	0.17	0.60	0.30

Table 4.3. One-way ANOVA results and normalized percentage value to determine the effects of seat geometry (i.e. backset and head restraint height) on the reduction of ATD responses in Control, No Motion and Experimental conditions during a Δv = 12 km/h speed change. Five repeated trials of the ATD seated on the Control (CTRL: unmodified GMHR seat, $d_{backset}$ = 94.4 mm), No Motion (Experimental seat with no seatback cushion deformation, $d_{backset}$ = 60.7 mm) and Experimental (EXP: Experimental seat with seatback cushion deformation, $d_{backset}$ = 52.0 mm) conditions. Normalized percentage values were determined by normalizing the differences in ATD responses between CTRL – No Motion with the difference between Control – EXP (100%). See **Table 4.1** for means and standard deviations for each variable. Blank cells represent p-values < 0.0000. **Bolded** values denote a non-significant difference between the indicated conditions.

	ANOVA		Post Hoc Tukey's HSD			Normalized %
Parameter	F(2,12)	p-value	CTRL – No Motion	CTRL - EXP	No Motion - EXP	No Motion
$d_{backset}$ (mm)	77.42				**0.0765**	79.4
d_{height} (mm)	34.66		0.0012		0.0115	57.9
$a_{X\text{-}sled}$ (m/s^2)	12.93	0.0010	0.0012	0.0055	**0.6646**	122.4
$d_{penetration\text{-}T1}$ (mm)	37.08		0.0006		0.0142	60.5
$d_{penetration\text{-}pelvis}$ (mm)	306.81		0.0189			14.1
$\Delta t_{head\text{-}contact}$ (ms)	108.09		0.0001			41.6
$a_{X\text{-}head}$ (m/s^2)	510.57					75.5
$a_{X\text{-}T1}$ (m/s^2)	8.43	0.0052	0.0041	**0.0685**	**0.2890**	163.7
F_X (N)	123.75					52.3
F_Z (N)	358.98					61.8
M_Y (Nm)	549.87				**0.1810**	106.9
$\omega_{Y\text{-}head}$(deg/s)	407.46					66.4
θ_{head} (deg)	103.13		0.0004			38.7
$d_{rebound}$ (mm)	553.10					32.2
R_X (mm)	56.30		0.0153			32.1
NIC_{max} (m^2/s^2)	228.00		0.0009			24.1
N_{ij}	462.34				0.0001	78.6
N_{km}	145.87				**0.5462**	93.0

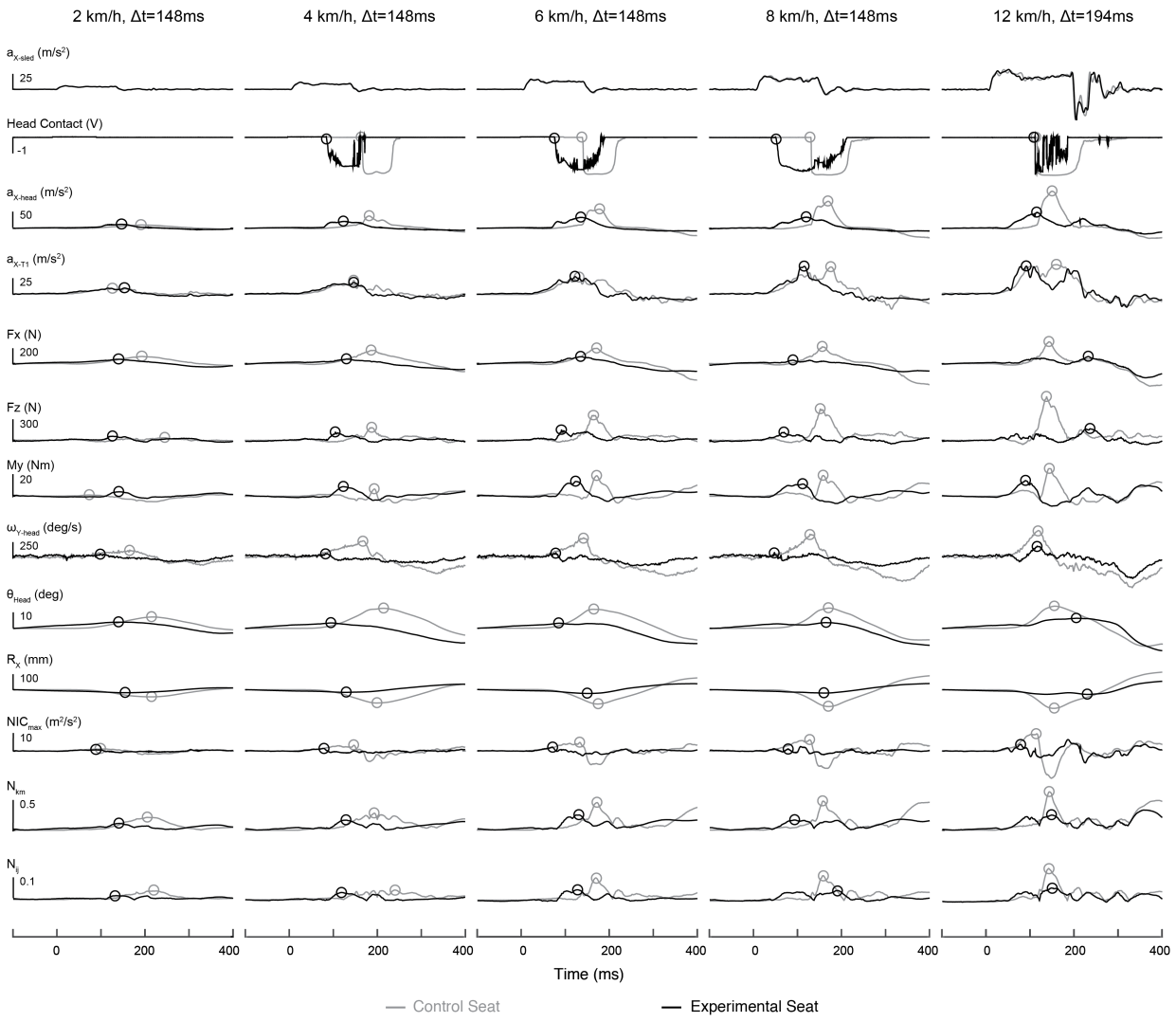

Figure 4.5. Data comparing the BioRID II ATD response seated on either the Control seat (grey lines) or the Experimental seat with the seatback cushion deformation profile (black lines) while exposed to various collision severities (Δv = 2, 4, 6, and 8kmh with a collision pulse duration (Δt) of 148 ms and Δv = 12 km/h with a Δt = 194 ms). Hollow circles represent the onset of head-to-head-restraint contact and peak responses of each ATD response parameter for each trial.

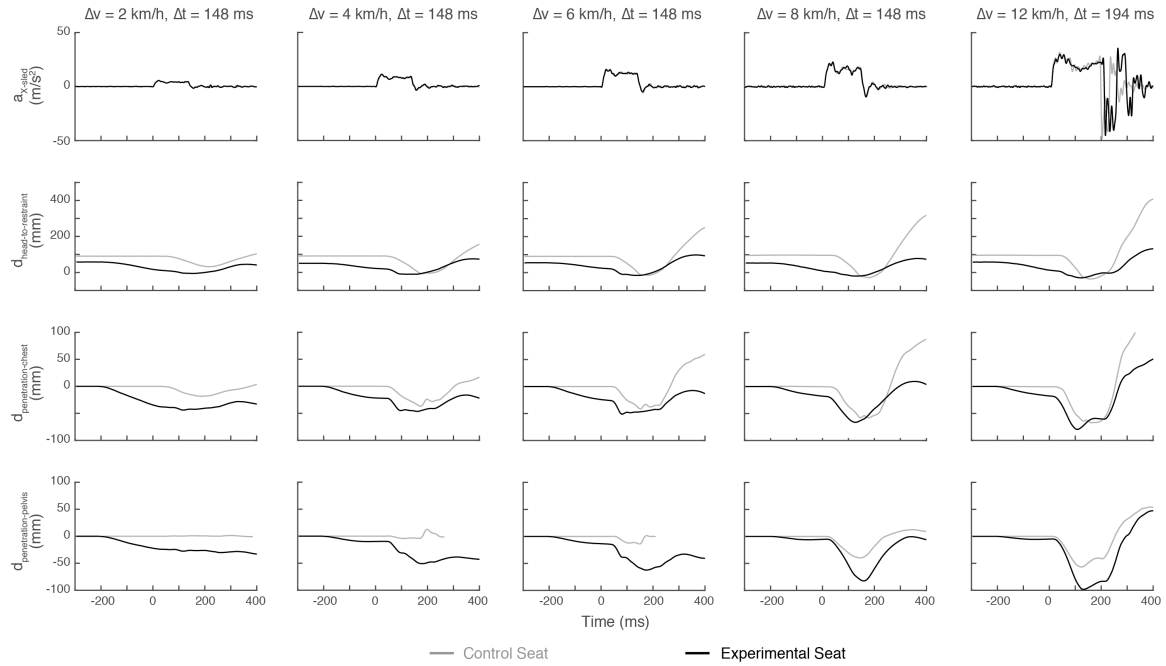

Figure 4.6. BioRID II ATD and seatback interaction data comparing the Control seat (grey lines) and the Experimental anti-whiplash seat with seatback deformation profile (black lines) while exposed to various collision severities (Δv = 2, 4, 6, and 8kmh with a collision pulse duration (Δt) of 148 ms and Δv = 12 km/h with a Δt = 194 ms). From top to bottom (+X-direction represents towards the front of the seat): Horizontal sled acceleration ($a_{X\text{-}sled}$), head-to-head restraint backset distance ($d_{backset}$ = 0 mm represents head contact with head restraint), and rearward penetration of the ATD's T1 ($d_{penetration\text{-}T1}$) and pelvis ($d_{penetration\text{-}pelvis}$) into the seatback.

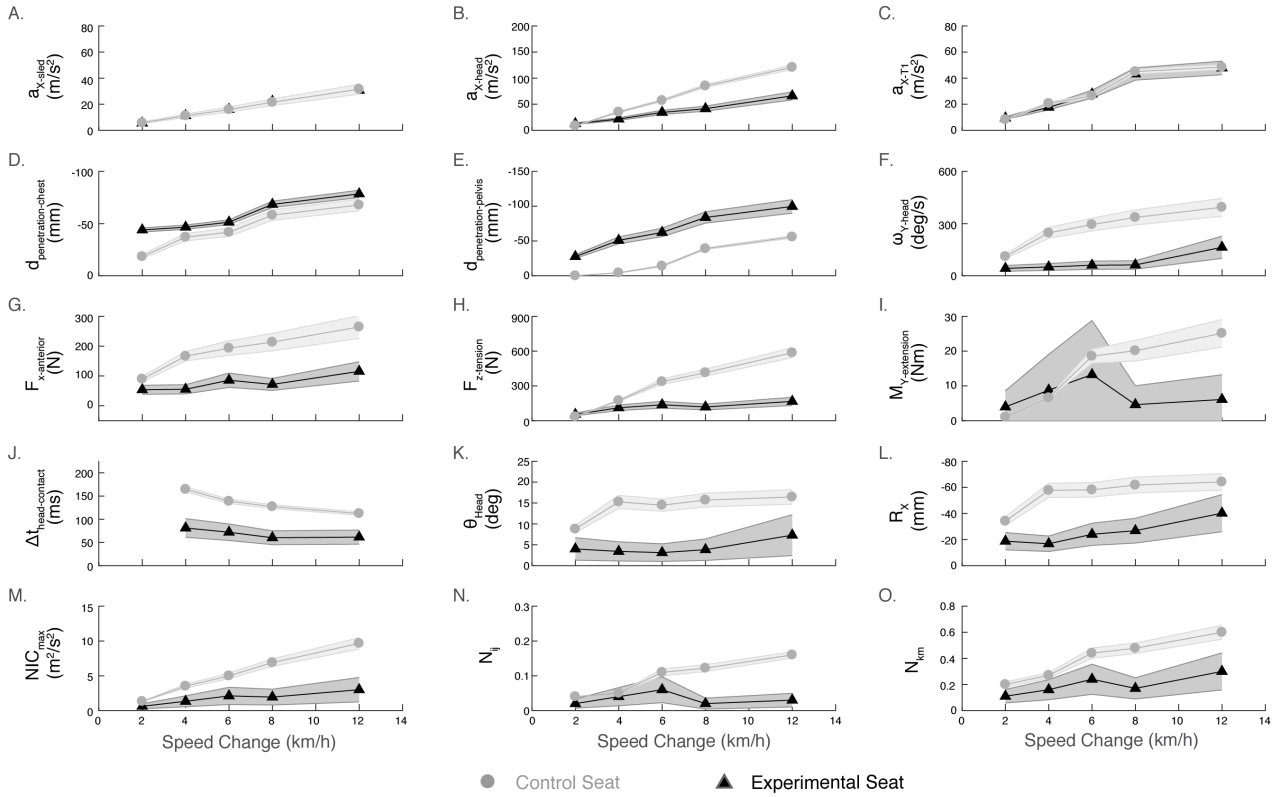

Figure 4.7. Experimental results of peak kinematic and kinetic responses for the BioRID II ATD seated on Control and Experimental seats. For all the graphs, grey circles represent the control seat and black triangles represent the Experimental seat with the seatback deformation profiles. The shaded bands represent the 99th percentile predictive intervals for the Control and Experimental seats. Y-axis values for panels D, E and L have been inverted for visual purposes to show increasing responses from bottom to top.

4.4 **Discussion**

The goal of this study was to compare the performance of the Experimental anti-whiplash seat that dynamically modified seatback cushion deformation to a standard unmodified GMHR Control seat during a series of low-speed, rear-end collisions (Δv = 2, 4, 6, 8 and 12 km/h). In comparison to the Control seat, the Experimental seat significantly reduced most ATD responses ($a_{X\text{-head}}$, $\omega_{Y\text{-head}}$, F_X, F_Z, My, $\theta_{head,}$ R_X and $\Delta t_{head\text{-}contact}$) by 37 – 82% and neck injury criteria (NIC_{max}, N_{km}, and N_{ij}) by 15 – 81% at collision speeds 4 km/h or higher. At the lower collision severities (Δv < 4 km/h), the Experimental seat was less effective at reducing most ATD responses (increased $a_{X\text{-head}}$ and F_Z responses but decreased all other ATD responses by 17 – 58%). Linear acceleration of T1 was not significantly different between Control and Experimental seats across all collision severities. The results from this study suggest that the dynamic deformation of the seatback cushion to reduce the apparent stiffness of the seatback may be a novel safety mechanism to reducing the risk of whiplash injuries following low-speed, rear-end collisions.

In comparison to the Control seat, the Experimental seat with the seatback deformation mechanism increased both the maximum $d_{penetration\text{-}T1}$ by -16.4 ± 6.9 mm and $d_{penetration\text{-}pelvis}$ by -52.7 ± 18.4 mm to allow deeper penetration, or “pocketing”, of the ATD into the seatback. Prior to the onset of the collision (i.e. at t = 0 ms), the seatback deformation further decreased the pre-impact backset by 74% to 13.9 ± 6.5 mm. During an impact, the Experimental seat decreased the head-to-head restraint contact times, peak head accelerations, upper neck

forces and moments, and neck injury criteria as well as head movement relative to the torso (θ_{head} and R_X). Head restraint geometry, however, also differed between seats and could have influenced peak ATD responses. Based on additional analyses using the No Motion condition (without seatback deformation), the effect of seatback cushion deformation alone was estimated to account for potentially 33% of the reduction observed between Control and Experimental seats (67% due to head restraint geometry and the different seats). In comparison to the No Motion Condition, the Experimental seat yielded a significant decrease in 11 of 15 peak ATD responses and in 2 of 3 neck injury criteria despite observing a similar acceleration at T1. Hence, the added decreases in peak head accelerations, upper neck forces and moments, and neck injury criteria may be a result of the deeper pocketing of the occupant into the rigid seatback due to the unspooling of the straps attached to the middle and lower seatback motors. The motion of the seatback cushion deformation allowed for more time to gradually propagate the acceleration and forces from the sled to the occupant.

Peak linear forward acceleration at T1 ($a_{X\text{-}T1}$) was the only ATD response that was not reduced by the Experimental seat at the higher speed changes. Many anti-whiplash devices (e.g., Volvo Whiplash Injury Prevention Seat – WHIPS, Saab's Active Head Restraint – SAHR, and the GMHR) and the neck injury criteria (NIC_{max}) have been designed with the reduction of T1 acceleration as one of the key components (Bostrom et al., 1996, Jakobsson et al., 2008, Viano, 2003d, Viano and Olsen, 2001, Viano and Parenteau, 2015). One possible explanation as to why $a_{X\text{-}T1}$ was not reduced by the Experimental seat was because of the rigid support frame installed

to prevent seat hinge rotation. On the Control seat, the seat hinge is naturally allowed to deflect rearward to potentially reduce $a_{X\text{-}T1}$. No seat hinge rotation was allowed on the Experimental seat causing earlier time of peak $a_{X\text{-}T1}$ responses at similar peak amplitude to sled acceleration (**Figure 4.4**). Further research is required to understand why the lack of a reduction in the horizontal acceleration of T1 ($a_{X\text{-}T1}$), a variable that is currently used as a test metric in evaluating the performance of anti-whiplash seats, was the only variable not attenuated by the seatback-deformation mechanism.

The results from the present and previous studies (Viano, 2003a, Viano and Parenteau, 2015, Hofinger et al., 1999) suggested that increased occupant penetration into the seatback by either using softer seatback cushion properties or dynamically deforming the seatback reduced backset distance and other ATD responses. Hofinger et al. (1999) used different types of foam mounted on a stiff seatback and a pre-impact $d_{backset}$ of 100 mm to determine the influence of seatback cushioning. They suggested that the combination of stiffer foam at the pelvis and softer foam at the torso best reduced occupant acceleration by initiating earlier torso and pelvis rotation and decreasing the backset. When Hofinger et al. (1999) tested the combination of stiffer foam at the torso and softer foam at the pelvis, they observed large backset and higher head accelerations. The seatback cushion deformation profile was akin to having a soft foam at both the torso and the pelvis to delay the onset of torso acceleration, increase occupant penetration into the seatback and decrease backset. One key difference between these two experiments was that Hofinger et al. (1999) used a rigid solid seatback panel to

support the different foam combination while the Experimental anti-whiplash seat utilized a perimeter frame with a compliant center. The rigid perimeter seat frame and the compliant seatback suspension of the Experimental seat was designed to create softer seatback cushion properties and increase occupant retention during a collision (Viano, 2003a, Viano and Parenteau, 2015). The two components work in unison as the yielding center section of the seatback absorbs energy and gradually decelerates the torso during the collision, while the stiffer seatback frame enhances occupant retention and prevents seatback deflection. Regardless of the seatback deformation mechanism (i.e. foam, springs or motors), these results suggested that a soft, yielding seat center that allows for decreased backset and deep penetration ($d_{penetration}$: 80 – 100 mm) of an occupant's torso and pelvis into the seatback could potentially reduce the risk of whiplash injury following low-speed, rear-end collisions.

The repeatability of the ATD responses on the Control seat was mostly acceptable or good (COV < 10%) with only head restraint height (d_{height}) receiving a poor rating at both the 8 km/m (COV = 20.4%) and the 12 km/h (COV = 11.6). For the Experimental seat, the COVs were typically larger, with 5 good, 5 acceptable and 8 poor parameters (a total of 18 parameters) at the 8 km/h level, and 4 good, 2 acceptable, and 12 poor parameters at the 12 km/h level. A key reason for the higher COV values in the Experimental seat is the lower mean responses observed in this seat (Rhule et al., 2005). By comparing the variability of the SD values, the similarities between the Control and Experimental SD values for the 8 km/h collision speed suggested that the COV values considered poor (> 10%) were more likely due to decreased

mean responses than due to increased variability in the ATD responses. The larger SD values in the ATD responses on the Experimental seat at the 12 km/h speed change compared to the Control seat may be due to the additional dynamics and degrees of freedom introduced by the active seatback deformation. Regardless, the increased SD values in the Experimental seat remained smaller than previously observed SD (see **Table 2.2** in **Chapter 2**; Davidsson, 1999, Moorhouse et al., 2012)**.** In addition, the mean responses close to zero, as observed in pre-impact head restraint height (d_{height}: Control = -30.4 mm and Experimental = -1.1 mm), generated a large COV above the acceptable range (> 10%) with a small SD value. Thus, COV values from the Experimental seat have to be interpreted cautiously due to the reduced mean responses by the addition of the seatback deformation mechanism. The additional assessment of the SD values has shown that the ATD seated on both the Control and Experimental seats have sufficient repeatability to justify the comparisons made in this study.

The speed changes used in this study were lower than the 16 km/h speed change and longer than the 91 ms collision pulse duration used by RCAR/IIWPG (Insurance Institute of Highway Safety, 2008b, Insurance Institute of Highway Safety, 2008a). Nevertheless, the pulses used here provided a graded range of speed changes that represent some real-world collisions that cause whiplash injury (Bartsch et al., 2008, Krafft et al., 2005). The weight of the Experimental seat with the seatback motors and rigid frame (total weight = 204 kg) limited the peak accelerations that could be achieved by the test sled. These seatback motors were selected to allow for testing a wide range of seatback motor parameters and explore different

seatback cushion deformation profiles. A collision pulse duration of Δt = 148 ms was selected for collision speeds up to 8 km/h because it was achievable and not dissimilar to the 135 ms observed in prior vehicle-to-vehicle rear-end crashes (Brault et al., 2000, Brault et al., 1998, Siegmund et al., 2000, Siegmund et al., 1997). However, a collision pulse duration of Δt = 194 ms was needed to reach a 12 km/h collision speed. This longer duration is longer than those of many modern vehicles (Linder et al., 2003, Linder et al., 2001, Stigson et al., 2006) but shorter than those observed in some older vehicles with bumper isolators (Siegmund et al., 1994). Nevertheless, the results of this study provided a better understanding of how to dynamically control seatback cushion deformation to minimize ATD responses during a rear-end collision. Future work should aim to refine the methods for deforming the seatback and to conduct tests at higher speed changes and shorter pulse durations.

Another possible limitation of this study was the structural differences between the Control and Experimental seats. A rigid metal brace was attached to the back of the Experimental seat to prevent the seat hinge from influencing ATD kinematic and kinetic responses; whereas, the Control seat was an unmodified GMHR seat that was allowed to rotate freely about the seat hinge. In the Experimental seat, the onsets of ATD responses were earlier than those seen on the Control seat as the rigid seat reduced the ability of the seat hinge to absorb and delay the transfer of acceleration from the seat to the ATD. Finally, the seats were not instrumented to determine the different forces applied by the seat to an occupant on either the Control or Experimental seats. Thus, further work is needed to better understand

the pressure distribution and interactions between an occupant's back and the seatback to develop a seat that better reduces the forces applied to the occupant.

4.5 **Conclusion**

This study highlights the potential importance of a dynamic seatback cushion deformation safety mechanism to reduce the risk of whiplash injuries during rear-end impacts. Approximately 67% of the observed reduction in ATD responses between the Control and Experimental seats was determined to be due to the differences in pre-impact head restraint geometry. The remaining 33% of the observed reductions in ATD responses could be attributed to the addition of a dynamic seatback deformation on the Experimental seat. The Experimental anti-whiplash seat with the seatback cushion deformation profile increased occupant penetration into the seatback to decrease backset and help maintain pre-impact alignment of the head, neck and torso. Further development of the Experimental anti-whiplash seat could, potentially, yield a new device that can reduce the risk of whiplash injuries following low-speed, rear-end collision.

Chapter 5. Combined Effect of Seat Hinge Rotation and Seatback Cushion Deformation on ATD Responses

5.1 Introduction

Whiplash injuries are the most common type of injuries during rear-end collision with an annual incident rate in the western world ranging from 28 to 834 per 100,000 inhabitants (Cassidy et al., 2000, Holm et al., 2008, Jakobsson et al., 2000, National Highway Traffic Safety Administration, 2014, Otremski et al., 1989). Whiplash injuries are classified as a soft tissue injury to the cervical spine most commonly resulting from a sudden acceleration of the head relative to the torso, but the exact injury mechanism remains uncertain (Kaneoka et al., 1999, McConnell et al., 1995, Svensson et al., 2000). In vehicles, the automotive seat and head restraint are the primary safety devices for protecting against whiplash injuries during low-speed, rear-end collisions. Current anti-whiplash seats, such as General Motors' High Retention seat (GMHR), Volvo's Whiplash Injury Prevention seat (WHIPS) and Saab's Active Head Restraint seat (SAHR), attempt to reduce the risk of whiplash injuries by reducing head and torso acceleration of the occupant and/or by minimizing the relative motion between the head and upper torso (Lundell et al., 1998a, Lundell et al., 1998b). Epidemiological studies have estimated that these anti-whiplash seats have reduced the risk of whiplash injury by about 50% (Jakobsson et al., 2008, Kullgren and Krafft, 2010, Viano and Olsen, 2001). Further research and development are required to understand why current anti-whiplash seats are only partially effective in preventing whiplash injuries.

According to the Research Council for Automobile Repairs/International Insurance Whiplash Prevention Group (RCAR/IIWPG) seat and head restraint rating protocol, anti-whiplash seats can be rated as good (e.g. WHIPS and SAHR) or poor (e.g. GMHR) in their abilities to reduce the risk of whiplash injury in low-/moderate-speed, rear-end collisions (Insurance Institute of Highway Safety, 2008b, Insurance Institute of Highway Safety, 2008a). Based on real-world insurance claims, good-rated seats appear to better lower occupant neck injury risk by 11 to 15% compared to poor-rated seats (Farmer et al., 2008, Trempel et al., 2016). The apparent minor real-world benefits of good-rated seats prompted a previous study to compare the performance of good-rated (2005 Volvo S40 WHIPS, 2004 Volvo S60 WHIPS, 2005 Saab 9.3 SAHR) and poor-rated (2004 Pontiac Grand Am GMHR) anti-whiplash front passenger seats during low-speed, rear-end collisions (speed changes: Δv = 2 to 14 km/h, collision pulse duration: Δt = 141ms; see **Chapter 2**). The good-rated seats only attenuated four key occupant responses (peak upper neck shear and axial forces, flexion/extension moment and rearward head retraction) in comparison to the poor-rated seat at speed changes greater than 6 km/h. The lack of attenuation in other peak occupant kinematic and kinetic responses suggests that current anti-whiplash seats could be improved to better protect occupants from whiplash injuries during low-speed, rear-end collisions. An Experimental anti-whiplash seat that actively rotates the seat hinge (see **Chapter 3**) and modulates the compliance of the seatback cushion (see **Chapter 4**) during a rear-end collision to change the apparent structural stiffness of the seat hinge and seatback cushion was developed to address this need. When activated in isolation, seat hinge rotation and seatback cushion deformation reduced peak occupant

responses for collision speed changes greater than 4 km/h compared to a control seat by 15 – 85%; however, the performance of the anti-whiplash seat when both seat hinge and seatback deformation are co-activated and its performance relative to existing anti-whiplash seats remain unknown.

The primary goal of this study was to compare the performance of the Experimental anti-whiplash seat with the co-activation of the seat hinge rotation and seatback cushion deformation to existing anti-whiplash seats (WHIPS, SAHR, and GMHR) in attenuating the kinematic and kinetic responses of a BioRID II anthropomorphic test device (ATD) exposed to low-speed, rear-end perturbations (speed changes of 2 to 12 km/h). The seat hinge and seatback deformation profiles identified in **Chapters 3** and **4** were combined and the relative timing between each profile was determined from preliminary experiments performed at a single speed change (Δv = 12 km/h; see **Appendix D**). We hypothesized that the Experimental anti-whiplash seat would attenuate most peak ATD responses and neck injury criteria across all tested collision severities in comparison to the existing anti-whiplash seats. A secondary goal of the experiments was to quantify the repeatability of the ATD responses evoked on the anti-whiplash seat.

5.2 Methods

5.2.1 Experimental Anti-Whiplash Seat

The Experimental anti-whiplash seat design consisted of a modified GMHR and five motors to control seat hinge rotation and seatback cushion deformation (**Figure 5.1**). All 5

motors (2 seat hinge and 3 seatback) were controlled by separate digital servo drives (Servostar 600, Kollmorgen, Waltham, MA, USA) connected to two universal motion interfaces and a motion controller (NI UMI 7774 and NI PXI 7350, National Instruments Corporation, Austin, Texas, USA). A custom LabVIEW program (National Instruments Corporation, Austin, Texas, USA) was created to send commands to, monitor the status of, and record encoder data directly from the motors.

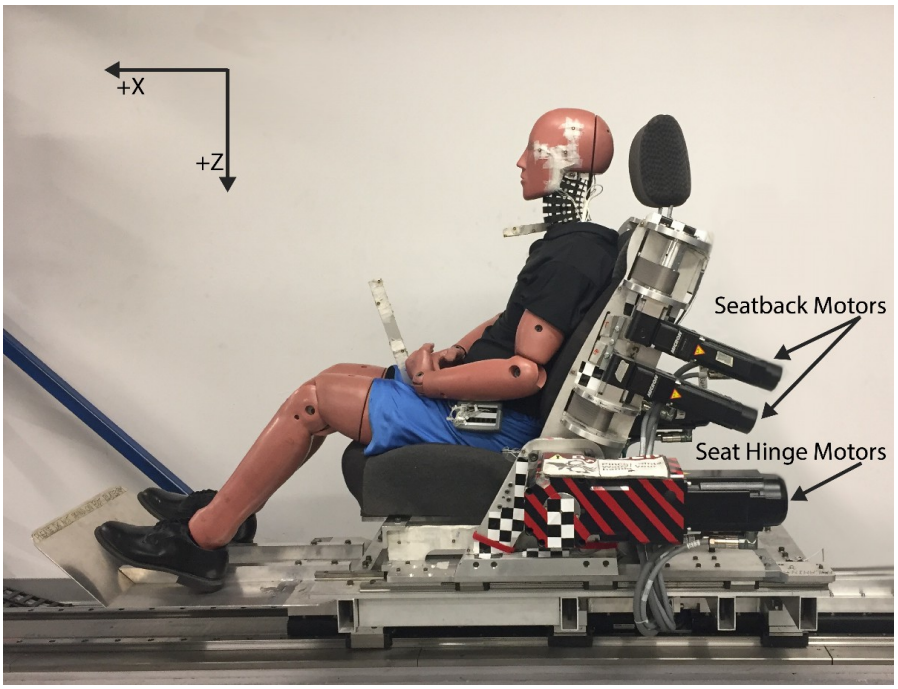

Figure 5.1. Photograph of the experimental set-up with the BioRID II ATD on the Experimental anti-whiplash automotive seat and laboratory reference frame (X, Z). The seat hinge and seatback motors on the left side of the anti-whiplash seat are labelled. Additional seat hinge and seatback motors are located on the right side of the seat (not labelled). (**Figure 5.1** is a repeat of **Figure 3.1B**.)

The seat pan and head restraint used in the Experimental anti-whiplash seat were from a GMHR seat and remained unmodified. The seatback consisted of a rigid aluminum outer frame with a yielding seatback center (i.e., a modified GMHR upper seatback cushion suspended within the outer aluminum frame). Two large rotational servomotors (AKM52K, Kollmorgen, Waltham, MA, USA) connected to helical right-angle gearheads (VTR014-035, 35:1 gear ratio, Thomson Linear, Radford, VA, USA) were mounted on either side of the outer frame at the seat hinge location and were geared to rotate in unison (one in a positive direction and the other in a negative direction) to control the rotation of the seat hinge through predefined rotation profiles. Seatback cushion deformations were controlled by three rotational servomotors (AKM24D, Kollmorgen, Waltham, MA, USA) connected to helical right-angle gearheads (VTR006-008, 8:1 gear ratio, Thomson Linear, Radford, VA, USA) staggered on either side of the rigid outer frame. The three motors were placed at the top, middle and bottom of the seatback and attached to four 47mm-wide seatbelt straps (with the middle motor connecting to the 2 middle straps) that spanned horizontally across the rigid outer frame (see **Figure 4.2**).

The GMHR upper seatback cushion was suspended from these straps and the rotation of each motor separately controlled the seatback cushion deformation at the upper-torso, mid-torso and pelvis regions. Tightening the seatbelt straps served to limit the seatback cushion's rearward deformation and increase the apparent stiffness of the seatback; whereas, loosening the straps allowed the seatback cushion to deform further rearward and allow for deeper

occupant penetration into the seatback. The initial tension in all the straps were set to generate an initial seatback angle of 27 deg rearward from vertical (Siegmund et al., 2005a).

Through a series of preliminary experiments performed at a 12 km/h speed change (see **Appendix D**), a combined seat hinge rotation and seatback cushion deformation profile was identified that effectively reduced the ATD responses. The dynamic seat hinge rotation profile (**Figure 5.2A**, grey line) was programmed to rotate the seatback forward commencing at 90 ms ($t_{forward\text{-}onset}$) before the collision onset by 5.6 deg ($\theta_{forward\text{-}peak}$) at an angular velocity of -33.4 deg/s ($\omega_{forward\text{-}int)}$ and to then rotate the seatback rearward by 5.7 deg ($\theta_{rearward\text{-}peak}$) at an angular velocity ($\omega_{rearward\text{-}int}$) of 24.0 deg/s beginning 70 ms ($t_{rearward\text{-}onset}$) after collision onset. The observed output seat hinge rotation (**Figure 5.2A**, red line) resulted in a forward rotation of 4.6 deg followed by a rearward rotation of 3.8 deg. The seatback motor deformation profile was programmed to unspool the webbing from the two lower seatback motors beginning 200 ms ($t_{deformation\text{-}onset}$) before the collision onset to a peak angle ($\theta_{rearward\text{-}peak}$) of 168 deg and an initial angular velocity ($\omega_{deformation\text{-}int}$) of 980 deg/s. The upper-torso motor was maintained in a stationary position, effectively creating a hinge point at the upper back and increased the pocketing of the pelvis into the seat during the collision.

A motion capture system (Optotrak Certus, Northern Digital, Waterloo, ON, Canada) was used to estimate the deformation of the seatback cushion during the perturbation because slack in the straps induced by the two lower seatback motors did not correspond with the physical penetration of the occupant. Maximum rearward penetration of the T1 vertebra

($d_{penetration\text{-}T1}$) and pelvis ($d_{penetration\text{-}pelvis}$) were used to describe the seatback cushion deformation and were defined as the horizontal displacement (along the global X-axis) between the infrared light emitting diode(IRED) markers mounted to the seatback frame and the T1 vertebra and pelvis, respectively **(Figure 5.2**). The initial position of the ATD at rest was set to zero ($d_{penetration\text{-}T1}$ = 0 mm and $d_{penetration\text{-}pelvis}$ = 0 mm) and rearward displacements into the seatback were defined as negative values. For a 12 km/h collision, the programmed seatback rotation profile allowed maximum occupant penetration into the seatback of 62 mm at T1 and 94 mm at the pelvis (**Figure 5.2B**, green and blue lines, respectively).

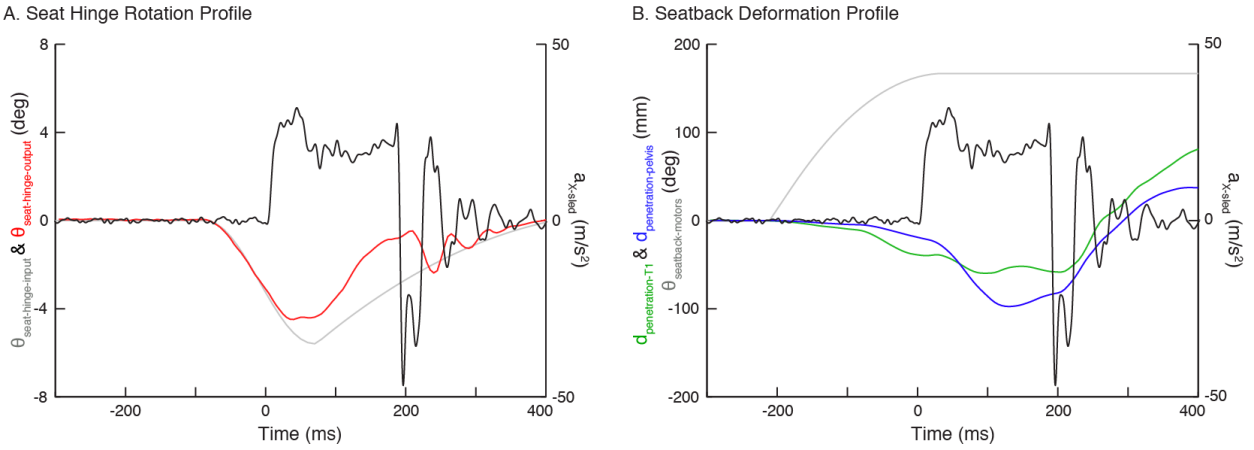

Figure 5.2. Programmed inputs and resulting outputs for A.) seat hinge rotation and B.) seatback cushion deformation profiles during a 12 km/h collision (Δt = 187 ms; black line). Grey lines represent input A. rotation ($\theta_{seat\text{-}hinge}$) and B. deformation ($\theta_{seatback\text{-}motors}$) profiles to seat hinge and seatback motors, respectively. Theses programmed input seat hinge rotation and seatback deformation profiles were used across all collision speeds. Seat hinge rotation ($\theta_{seat\text{-}hinge\text{-}output}$: red line) as well as rearward penetration of ATD T1 ($d_{penetration\text{-}T1}$: green line) and pelvis ($d_{penetration\text{-}pelvis}$: blue line) into the seatback indicate resulting outputs to their respective input profiles.

5.2.2 Anthropomorphic Test Device and Instrumentation

A BioRID II ATD (Humanetics, Plymouth, MI, USA) was instrumented to measure head, torso (T1), and pelvis kinematics and kinetics (**Figure 5.1**). A six-axis load cell (Forces: F_X, F_Y, F_Z; and Moments: M_X, M_Y, M_Z; Model 4949a, Robert A. Denton, Inc., Rochester Hills, MI, USA) was mounted at the atlanto-occipital joint (AOJ) to measure upper neck forces and moments. Linear forward accelerations of the head and T1 were measured using two uni-axial accelerometers (7264C sensors; ±500g, Endevco, San Juan Capistrano, CA, USA) mounted at the head center of mass and the T1 vertebra. A uni-axial angular rate sensor (ARS-1500; ±26.2 rad/s, DTS, Seal Beach, CA, USA) was also mounted at the head center of mass to measure angular kinematics in the sagittal plane (i.e., flexion and extension).

The Optotrak system was used to track IRED markers affixed to the head, AOJ, T1, and pelvis of the ATD to measure their displacements. Additional IRED markers were mounted to the seat to record displacements and rotations of the seatback and to create a global reference frame (+X forward, +Y right, and +Z down, **Figure 5.1**). Horizontal sled acceleration was measured with a uni-axial accelerometer (2220-100; ±100g, Silicon Design Inc., Issaquah, WA, USA) mounted directly to the base of the linear sled frame. Head restraint contact was detected with a force sensitive resistor (FSR; Model 406, Interlink Electronics, Camarillo, CA, USA) attached to the front of the head restraint.

All accelerometer, load cell and angular rate sensor signals were simultaneously sampled at 10kHz using a National Instruments Data Acquisition (DAQ) PXI system (PXI-4495 &

PXI-6289, National Instruments Corporation, Austin, Texas, USA) and a custom-written LabVIEW virtual instrument. Optotrak data were acquired at 200 Hz and collection was triggered by the DAQ system to synchronize the data. Subsequent data and statistical analyses were performed using Matlab (R2017A, Mathworks, Natick, MA, USA). All data channels were digitally filtered in Matlab and conformed to the SAE J211 (Channel Class 180 for the ATD sensors and Channel Class 60 for the sled accelerometer) (SAE, 1995).

5.2.3 Test Procedures

The BioRID II ATD was clad in two layers of lycra and seated on the Experimental anti-whiplash seat (**Figure 5.1**) or one of four different, unmodified front passenger seats: A) 2005 Volvo S40 WHIPS, B) 2004 Volvo S60 WHIPS, C) 2005 Saab 9.3 SAHR, and D) 2004 Pontiac Grand Am GMHR (**Figure 5.3**). The seats were mounted on a 10 m long, feedback-controlled linear sled (Kollmorgen IC55-100A7, Waltham, MA, USA). For all seats, the initial seatback angle was set to 27 deg rearward from vertical (Siegmund et al., 2005a). To maximize the repeatability of the experiments, the initial position of the ATD was adjusted to a pre-defined posture that was constant within each seat and as similar as possible between seats. This pre-defined posture was confirmed using the 3D positions measured by Optotrak at the beginning of each trial. Seat geometry was measured before and after each collision to ensure no permanent deformation had occurred. After each test, the deformable elements in the WHIPS seat were verified to have not been damaged and the SAHR mechanism was verified to have returned to its original

position. The seatbelt was removed from the seat to prevent interactions that could affect head, neck and torso kinematics.

For all conditions, the ATD was exposed to five rear-end perturbations of increasing speed changes (Δv = 2, 4, 6, and 8 km/h with a Δt of 147 ms, and 12 km/h with a Δt of 187 ms) (**Figure 5.3)**. Due to limitations in the force-generating ability of the linear motors, a longer pulse duration was needed for the 12 km/h speed change. All of the pulses used here have a longer duration than the RCAR/IIWPG pulse (Δt = 91 ms) (Insurance Institute of Highway Safety, 2008b). The sled was accelerated forward from a stationary position for the 2, 4 and 6 km/h speed changes and from a constant rearward speed of 6 km/h for the 8 and 12 km/h speed changes. A comparison of the ATD responses for an 8 km/h collision starting from a stationary position to an 8 km/h collision starting from a 6km/h rearward velocity showed less than 10% differences in most of the occupant responses and neck injury criteria (see **Chapter 2**). To assess the repeatability of the ATD responses, four additional repeated trials were collected at the 8 and 12 km/h collision speed changes for both the GMHR and Experimental seats (for a total of 5 trials for each seat at both speed changes).

For all seats the horizontal position ($d_{backset}$) and vertical position (d_{height}) of the head relative to the head restraint before the collision onset were adjusted (SAHR, GMHR and Experimental seats: midrange of its vertical adjustment positions and most rearward horizontal position; WHIPS: fixed head restraints) and rated according to the RCAR/IIWPG seat and head restraint evaluation protocol as good, acceptable, marginal or poor (**Table 5.1**) (Insurance

Institute of Highway Safety, 2008b, Insurance Institute of Highway Safety, 2008a). Both WHIPS seats had good-rated head-to-head-restraint geometry (S40 WHIPS: $d_{backset}$ = 42.8 mm and d_{height} = -2.3 mm, and S60 WHIPS: $d_{backset}$ = 69.2 mm and d_{height} = -42.2 mm) and the SAHR's seat ($d_{backset}$ = 89.8 mm and d_{height} = -44.7 mm) had an acceptable-rated geometry. The GMHR seat had a marginal-rated head-to-head-restraint geometry ($d_{backset}$ = 93.5 mm and d_{height} = -26.9 mm) that would receive an overall RCAR/IIWPG rating of poor. The anti-whiplash seat was rated as good according to the RCAR/IIWPG criteria with a pre-impact $d_{backset}$ = 50.4 mm and d_{height} = 1.5 mm. Differences in pre-impact $d_{backset}$ and d_{height} are known to affect the occupant responses and the risk of whiplash injuries (Eriksson, 2005, Nygren et al., 1985, Siegmund et al., 1999, Stemper et al., 2006), and have been shown to potentially confound the reduction in ATD responses observed on the anti-whiplash seat (see **Chapter 4**). Thus, the comparison of the Experimental anti-whiplash seat to other good-rated seats with similar head-to-head-restraint geometry (i.e., WHIPS S40 and S60) will be used to determine whether the observed differences in ATD responses between seats are caused by differences in head restraint geometry or by the active control of seat hinge rotation and seatback deformation.

A total of 41 trials were collected: 13 trials each for the Experimental and GMHR seats, and 5 trials each for the SAHR and two WHIPS seats. Only the results of the 13 trials on the GMHR seat have been previously reported as the Control condition in **Chapters 3** and **4**. The trials on the existing anti-whiplash seats (WHIPS, SAHR, and GMHR seats) were similar to the trials reported in **Chapter 2**, but utilized different collision pulse durations for the same speed

changes (**Chapter 2**: Δv = 2 – 14 km/h with a Δt of 141 ms, and current study: Δv = 2 – 8 km/h with a Δt of 147 ms and Δv = 12 km/h with a Δt of 187 ms). For test conditions with five repeated trials (i.e., the Δv = 8 and 12 km/h trials on the GMHR and Experimental seat), the average of the peak responses across the five trials was used for analysis.

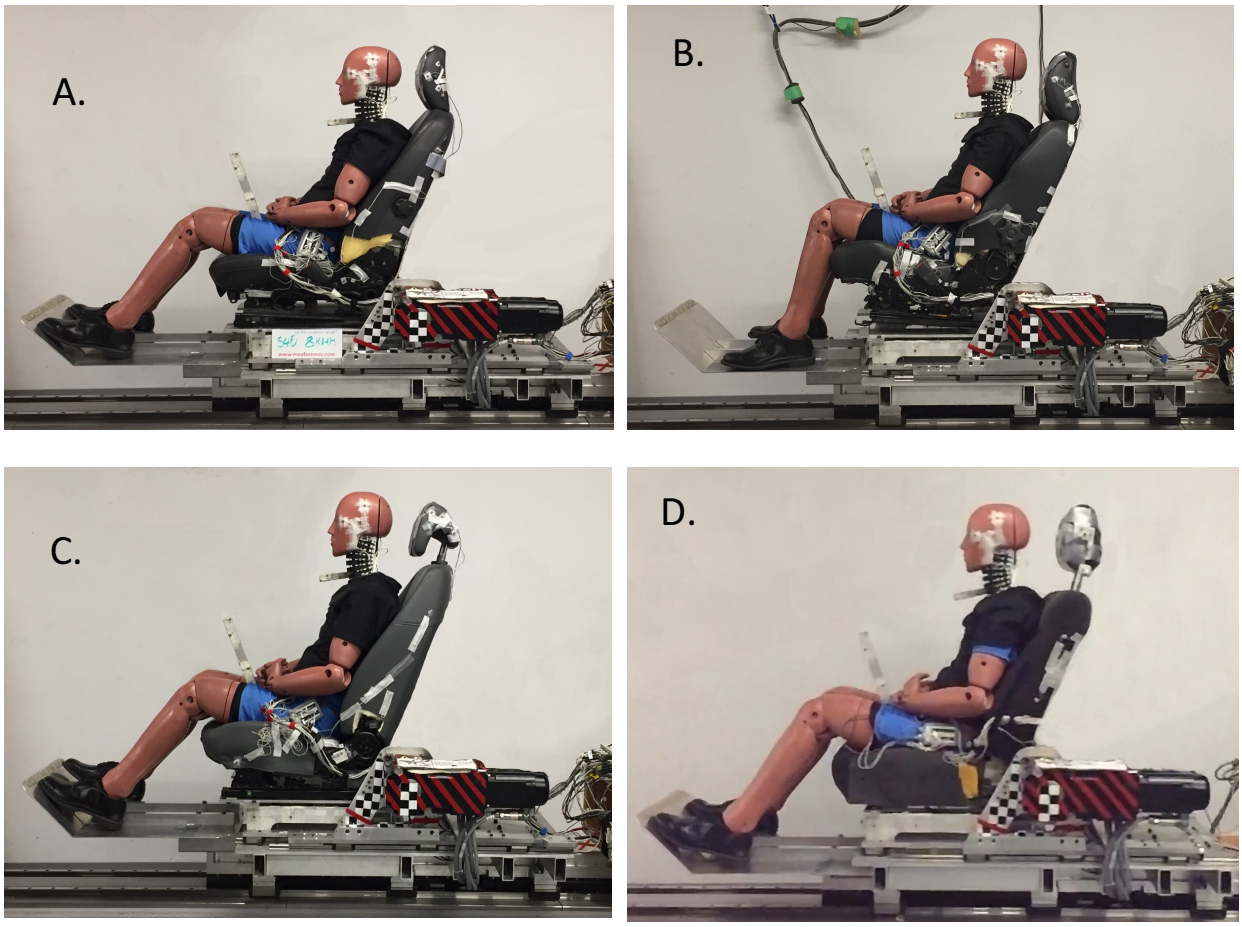

Figure 5.3. Photographs of the experimental set-up with the BioRID II ATD on the four existing anti-whiplash seats: A.) 2005 Volvo S40 WHIPS, B.) 2004 Volvo S60 WHIPS, C.) 2005 Saab 9.3 SAHR and D.) 2004 Pontiac Grand Am GMHR

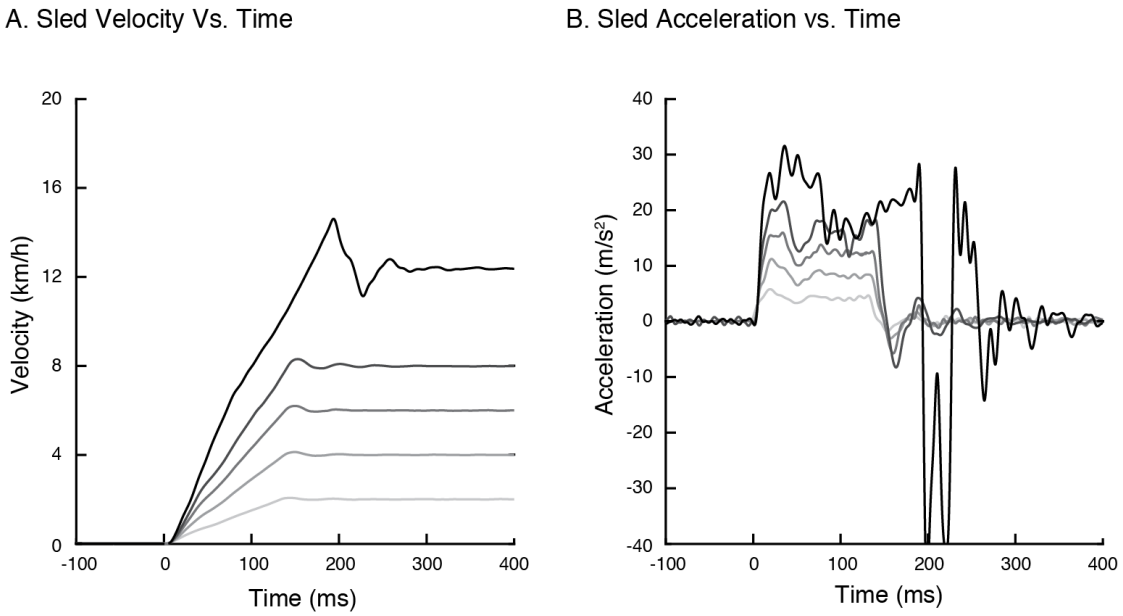

Figure 5.4. Exemplar sled A.) velocity and B.) acceleration pulses for increasing collision speeds (Δv of 2, 4, 6, and 8 km/h with a pulse duration (Δt) of 147 ms, and Δv of 12 km/h with a Δt of 187 ms; lightest to darkest). Collision onset occurred at time = 0 ms. This figure is a repeat of **Figure 3.3**.

Table 5.1. Mean (standard deviation) of head restraint backset ($d_{backset}$) and height (d_{height}) as well as resulting RCAR/IIWPG static seat geometry rating.

Seat	n	$d_{backset}$ (mm)	d_{height} (mm)	RCAR/IIWPG Rating
Volvo S40 WHIPS	4	42.8 (8.4)	-2.3 (5.1)	Good
Volvo S60 WHIPS	4	69.2 (13.0)	-42.2 (4.8)	Good
Saab 9.3 SAHR	3	89.8 (6.0)	-44.7 (3.6)	Acceptable
Pontiac Grand Am GMHR	13	93.5 (2.5)	-26.9 (6.4)	Marginal/Poor
Experimental Anti-Whiplash Seat	13	50.4 (3.1)	1.5 (4.1)	Good

Notes: n denotes the number of trials for each seat used to determine mean and standard deviation backset and height values. Trials with missing Optotrak IRED markers were excluded from these calculations. Backset: distance between the back of the head to the front face of the head restraint. Height: distance between the top of the head to the top of the head restraint (negative values indicated the top of the head restraint was lower than the ATD head).

5.2.4 Data Analysis

Peak horizontal, forward, sled accelerations ($a_{X\text{-}sled}$) were extracted directly from the accelerometer mounted to the sled. Head and torso linear accelerations were reported in local ATD head and T1 reference frames and were corrected to remove the earth's gravity using the head and T1 orientations determined from the Optotrak data. Peak linear forward accelerations of the head ($a_{X\text{-}head}$) and T1 vertebra ($a_{X\text{-}T1}$) were extracted directly from the gravity-corrected accelerometer data, and peak rotational velocities of the head ($\omega_{Y\text{-}head}$) in the sagittal plane were extracted directly from the angular rate sensor. Peak upper neck shear (F_X) and axial (F_Z) forces and the flexion/extension bending moment (M_Y) were determined from the upper neck load cell and reported in the ATD reference frame as the forces/moments applied by the neck to the head. Initial head angle was defined as the average angle between -300 ms and -200 ms preceding the onset of $a_{X\text{-}sled}$, and peak head extension angle (θ_{head}) was defined as the maximum rotation of the head into extension relative to the initial head angle. A foreperiod between -300 ms and -200 ms before the onset of forward $a_{X\text{-}sled}$ was used to define initial values because the pre-perturbation deformation of the seatback was initiated 200 ms before collision onset ($t_{deformation-onset}$ = -200 ms). Peak retraction (R_x) was defined as the maximum horizontal displacement in the global reference frame of the AOJ with respect to the T1 vertebrae, with rearward displacements defined as negative values.

The shape of the back of the ATD's head and front of the head restraint was digitized relative to Optotrak IRED markers. These shapes were then used to calculate the initial head

restraint backset (the back of ATD's head to the front face of the head restraint) and vertical position (the top of ATD head to the top of the head restraint) for each trial. The initial backset ($d_{backset}$) and height (d_{height}) of the head restraint were defined as the average head-to-head-restraint horizontal and vertical distances between -300 ms and -200 ms before the onset of forward $a_{X\text{-}sled}$. Negative values for the height of the head restraint indicated that the top of the head restraint was lower than the top of the ATD head. The same head and head restraint shapes were used to calculate the peak forward rebound ($d_{rebound}$), which was defined as the maximum forward head-to-head-restraint distance. Time-to-head-restraint contact ($\Delta t_{head\text{-}contact}$) was extracted from the time of force onset in the FSR attached to the head restraint (onset of forward sled acceleration defined as t = 0 ms). Onsets of sled acceleration and head restraint contact were determined when the accelerometer and FSR signals, respectively, reached 1.5 times the peak background noise level present between -300 ms to -200 ms before the onset of the collision perturbation and were confirmed visually. The sled accelerometer ($a_{X\text{-}sled}$) and head contact FSR signals had high signal-to-noise ratios after filtering according to SAE J211 Channel class 180 and did not require further manual corrections of the onsets.

Three neck injury criteria (NIC_{max}, N_{ij}, and N_{km}) were computed from the accelerometer and load cell data. The Neck Injury Criterion (NIC_{max}) was calculated from the relative horizontal acceleration (corrected for gravity) and velocity in the global reference frame between the head center of mass and the T1 joint (Equation 5.1; Bostrom et al., 1996). The Normalized Neck Injury Criterion (N_{ij}) was calculated from the axial load (F_Z) and the

flexion/extension bending moment (M_Y) measured from the upper neck load cell (Equation 5.2; critical F_{int} and M_{int} intercept values used for normalization: $F_{int\text{-}tension}$ = 6806 N, $F_{int\text{-}compression}$ = -6160 N, $M_{int\text{-}flexion}$ = 310 N, and $M_{int\text{-}extension}$ = -135 N; Eppinger et al., 1999, Eppinger et al., 2000). The Neck Protection Criterion (N_{km}) was calculated from the sagittal shear force (F_X) and the flexion/extension bending moment (M_Y) measured from the upper neck load cell (Equation 5.3; critical F_{int} and M_{int} intercept values used for normalization: $F_{int\text{-}shear\text{-}anterior}$ = 845 N, $F_{int\text{-}shear\text{-}posterior}$ = 845 N, $M_{int\text{-}extension}$ = 47.5 Nm, and $M_{int\text{-}flexion}$ = 88.1 Nm; Schmitt et al., 2001, Schmitt et al., 2002). Peak values of the three neck injury criteria were then extracted for analysis and compared to proposed injury thresholds (NIC: 15 m^2/s^2, Eichberger et al., 1998; N_{ij} and N_{km} : a normalized value of one, Schmitt et al., 2001, Schmitt et al., 2002, Eppinger et al., 1999). These injury thresholds correspond to different human tolerance levels for the causation of whiplash-related injuries – NIC: long-term whiplash-associated disorders (WAD) levels 1-3 (Bostrom et al., 2000, Bostrom et al., 1996), N_{ij}: 22% risk of abbreviated injury scale (AIS) level 3 (i.e., fracture; Eppinger et al., 1999, Eppinger et al., 2000), and N_{km}: AIS level 1 injury causation (i.e., minor injury; Schmitt et al., 2001, Schmitt et al., 2002).

$$NIC_{max}(t) = \text{maximum}_{\text{first 150 ms}}(a_{rel}(t) \cdot L + (v_{rel}(t))^2) \quad \ldots \quad \text{Equation 5.1}$$

$$N_{ij}(t) = \frac{F_z(t)}{F_{int}} + \frac{M_{yOC}(t)}{M_{int}} \quad \ldots \quad \text{Equation 5.2}$$

$$N_{km}(t) = \frac{|F_x(t)|}{F_{int}} + \frac{|M_{yOC}(t)|}{M_{int}} \quad \ldots \quad \text{Equation 5.3}$$

The repeatability of the ATD on the Experimental seats was assessed for the 8 and 12 km/h speed changes using the Coefficient of Variation (COV), which was calculated as the standard deviation (SD) divided by the mean and expressed as a percentage. The National Highway Traffic Safety Administration (NHTSA) defines a COV of 5% or less as excellent, a COV of 10% or less as acceptable and a COV greater than 10% as poor (Rhule et al., 2005). In **Chapter 3**, the repeatability of the ATD on the Control GMHR seat was determined to be excellent or acceptable for most parameters at the 8 and 12 km/h speed changes, except for head restraint height (d_{height}: COV = 22.2% and 11.3% at 8 and 12 km/h respectively) (**Table 5.2**). The COV of all ATD responses and neck injury criteria were compared to determine if the repeatability was different between the Control and the Experimental seats. Because COV is dependent on the mean and SD of the responses, the expected decreases in mean responses (which form the denominator in the COV calculation) for the Experimental seat may generate larger COV values. A comparison of the SD values between the Control and the Experimental seats would provide an alternate assessment of variability and would help to determine whether the larger COV values for the Experimental seat were likely due to the lower mean responses or due to the greater inherent variability (i.e., SD in the ATD responses. The SD values for all kinematic and kinetic responses as well as neck criteria observed at both the 8 and 12 km/h collision speeds were used in this assessment of variability. the COV and SD were assumed to be independent observations and a Wilcoxon Signed-Rank Test was performed after a Kolmogorov-Smirnov test determined the COV and SD values (for a given collision severity or seat) were not normally

distributed. All tests were performed using predefined functions (`kstest` and `signrank`) in Matlab (R2017A, Mathworks, Natick, MA, USA) at a significance level $\alpha = 0.05$.

To compare ATD responses between the Experimental and existing anti-whiplash seats (GMHR, SAHR and WHIPS), 99th percentile predictive intervals were created around the peak responses on the Experimental and GMHR seats using the maximum variability (COV value) observed from repeated trials at either the 8 or 12 km/h collision severity (Horslen et al., 2015). Ninety-ninth (99th) percentile predictive intervals were not created around the WHIPS and SAHR anti-whiplash seats because no repeated trials were collected for these seats. The COV value was then multiplied by 2.58 (z-score for two-tailed 99th percentile) to estimate the predictive limits. Since the COV values were defined as the maximum standard deviations divided by the mean of the peak ATD responses, these predictive limits were represented as a percentage and then multiplied by the peak responses to create predictive intervals at each collision severity (2 – 12 km/h). Any ATD responses from the single-trial anti-whiplash seats (i.e., WHIPS and SAHR seats) located outside the 99th percentile predictive intervals of the Experimental seat were assumed to be statistically different. Statistical differences between the Experimental and GMHR seats were determined if their respective 99th percentile predictive intervals did not overlap. The 99th percentile predictive limits were used to account for the numerous comparisons between the Experimental and existing anti-whiplash seats for each ATD responses at each collision severity and to provide a conservative estimate of statistical significance.

5.3 **Results**

The combination of the seat hinge rotation and seatback cushion deformation on the Experimental seat generated ATD kinematic and kinetic responses that were different from the other existing anti-whiplash seats. The ATD responses on the WHIPS, SAHR and GMHR seats exhibited positively graded responses to increasing speed change in most kinematic ($a_{X\text{-}head}$, $a_{X\text{-}T1}$, $\omega_{Y\text{-}head}$, θ_{head}, R_X, $d_{penetration\text{-}T1}$, $d_{penetration\text{-}pelvis}$ and $d_{rebound}$) and kinetic (F_X, F_Z and M_Y) responses (**Figures 5.5**, **5.6** and **5.7,** see also **Figures E5.2 – E5.5** in the **Appendix E** and **Chapter 2**). On the Experimental seat, with the exception of $a_{X\text{-}T1}$, $d_{penetration\text{-}T1}$, and $d_{penetration\text{-}pelvis}$ that showed a positively graded response to collision severity, most kinematic and kinetic responses were attenuated to a near constant amplitude within each response across all severities (**Figure 5.5, 56 and 5.7**, see also **Figure E5.1** in the **Appendix E**). The pre-perturbation forward seat hinge rotation ($t_{forward\text{-}onset}$= -90 ms) and the seatback cushion deformation ($t_{perturbation\text{-}onset}$= -200 ms) shifted the head-to-head-restraint contact times to before the onset of collision ($\Delta t_{head\text{-}contact}$ = -19.0 ± 3.9 ms; **Figure 5.6** and **5.7G**). With the head restraint supporting the head before the collision, peak rearward head angle (θ_{head} = 2.2 ± 0.3 deg) and rearward head retraction (R_X = -13.4 ± 3.4 mm) remained constant across all collision severities (**Figure 5.7H** and **5.7I)**.

In comparison to the poor-rated GMHR seats, there was no overlap between the 99th percentile predictive intervals of the kinematic responses in the GMHR and Experimental seats for collision speed changes of 4 km/h or greater. Peak forward head ($a_{X\text{-}head}$) and torso ($a_{X\text{-}T1}$) accelerations were 50 – 77% lower and 34 – 65% lower, respectively, in the Experimental seat

than in the GMHR seat. Peak head angular velocity ($\omega_{Y\text{-}head}$) was similarly 71 – 73% lower in the Experimental seat (**Figure 5.7A – 5.7C**). Head-to-head-restraint contact time occurred 131 – 182 ms earlier to support the head before the collision onset ($\Delta t_{head\text{-}contact}$ = -19.0 ± 3.9 ms) and to limit the displacements of the head and neck (θ_{head}: 83 – 89% lower, R_X: 70 – 82% lower and $d_{rebound}$: 51 – 85% lower, **Figure 5.7G – 5.7I** and **57L**). The kinetic responses on the Experimental seat were significantly lower than the GMHR seat for collision speed changes of 6 km/h or greater (F_X: 71 – 73% lower, F_Z: 77 – 89% lower, and M_Y: 77 – 81% lower) (**Figure 5.7D – 5.7F**).

For collision speeds 4 km/h or greater, the Experimental seat significantly decreased all kinematic responses compared to the good-rated seats (WHIPS and SAHR) by 25 – 89%. The observed reductions in peak kinematic responses were 55 – 78% for $a_{X\text{-}head}$, 29 – 70% for $a_{X\text{-}T1}$, 59 – 75% for $\omega_{Y\text{-}head}$, 78 – 89% for θ_{head}, 31 – 86% for $d_{rebound}$, and 25 – 79% for R_X. The Experimental seat also reduced some ATD kinetic responses compared the good-rated seats for collision speeds 6 km/h and higher (**Figure 5.7E** and **5.7F)**: F_Z was 58 – 84% lower and M_Y was 28 – 74%. However, the M_Y response for Volvo S40 WHIPS and Experimental seats at the 8 and 12 km/h collision severities showed no differences. For the 8 and 12 km/h speed changes, the peak upper neck shear force (F_X) was larger for the Experimental seat (57.8 and 76.1 N, respectively) than for the WHIPS and SAHR seats (WHIPS S40: 28.5 and 8.6 N, WHIPS S60: 1.8 and 2.1 N, and SAHR: 19.4 and 1.7 N, respectively), but was still lower than for the GMHR seat (213.5 and 264.4 N, respectively; **Figure 5.7D**).

Across all seats and collision severities, none of the neck injury criteria (NIC_{max}, N_{ij} and N_{km}) exceeded the proposed injury thresholds. Positively graded responses to increasing collision severity for all three neck injury criteria were observed for all existing anti-whiplash seats, whereas, the responses of the Experimental seat were constant across collision severities (NIC_{max} = 2.79 ± 0.65 m^2/s^2, N_{ij} = 0.041 ± 0.004, and N_{km} = 0.15 ± 0.03; **Figure 5.7M – 5.7O**). With the exception of N_{ij} (GMHR and S40 WHIPS at the 4 km/h severity) and N_{km} (S60 WHIPS at the 8 km/h severity), the three neck injury criteria for the Experimental seat were 9 – 73% lower for collision speeds greater than 2 km/h (NIC_{max}: 9 – 71% lower, N_{ij}: 23 – 70% lower, and N_{km}: 16 – 73% lower).

The repeatability of the BioRID II ATD responses for the GMHR seat have been reported in **Chapter 3** and were excellent or acceptable at both speed changes for most parameters except for head restraint height (d_{height}, COV = 22.2% and 11.3% at 8 and 12 km/h respectively). The COV values from the repeated trials on the Experimental seat were more variable than those previously observed on the GMHR seat. COV values for peak accelerations of the head ($a_{X\text{-}head}$), torso ($a_{X\text{-}T1}$) and sled ($a_{X\text{-}sled}$), and occupant penetration at both the T1 and pelvis ($d_{penetration\text{-}T1}$ and $d_{penetration\text{-}pelvis}$, respectively) responses were considered excellent (COV ≤ 5%); whereas, the neck shear force (F_X), initial backset ($d_{backset}$), forward rebound ($d_{rebound}$), and neck injury criteria N_{ij} and N_{km} were considered acceptable (5% < COV ≤ 10%). All other responses had COV values greater 10% and were considered poor ($\Delta t_{head\text{-}contact}$ = 54.3%, F_Z = 25.6%, M_Y = 13.1%, $\omega_{Y\text{-}head}$ = 13.0%, θ_{head} = 19.9%, R_X = 10.8%, NIC_{max} = 14.8%, and d_{height} = 199.1%). The COV values on the Experimental seat were significantly higher than those on the GMHR seat for the

8 and 12 km/h speed changes (Wilcoxon Signed-Rank Test; 8 km/h: $Z = 3.29$, $p = 0.001$, and 12 km/h: $Z = 3.72$, $p = 0.0002$). The standard deviations (SD) of the Experimental and GMHR seats were not significantly different (Wilcoxon Signed-Rank Test; 8 km/h: $Z = -0.89$, $p = 0.37$, and 12 km/h: $Z = 0.72$, $p = 0.47$). The larger COV values on the Experimental seat with similar SD values to the GMHR seat suggested that the COV values considered poor (> 10%) were more likely due to decreased mean responses (which form the denominator in the COV calculation) than due to increased variability in the ATD responses (i.e. SD values).

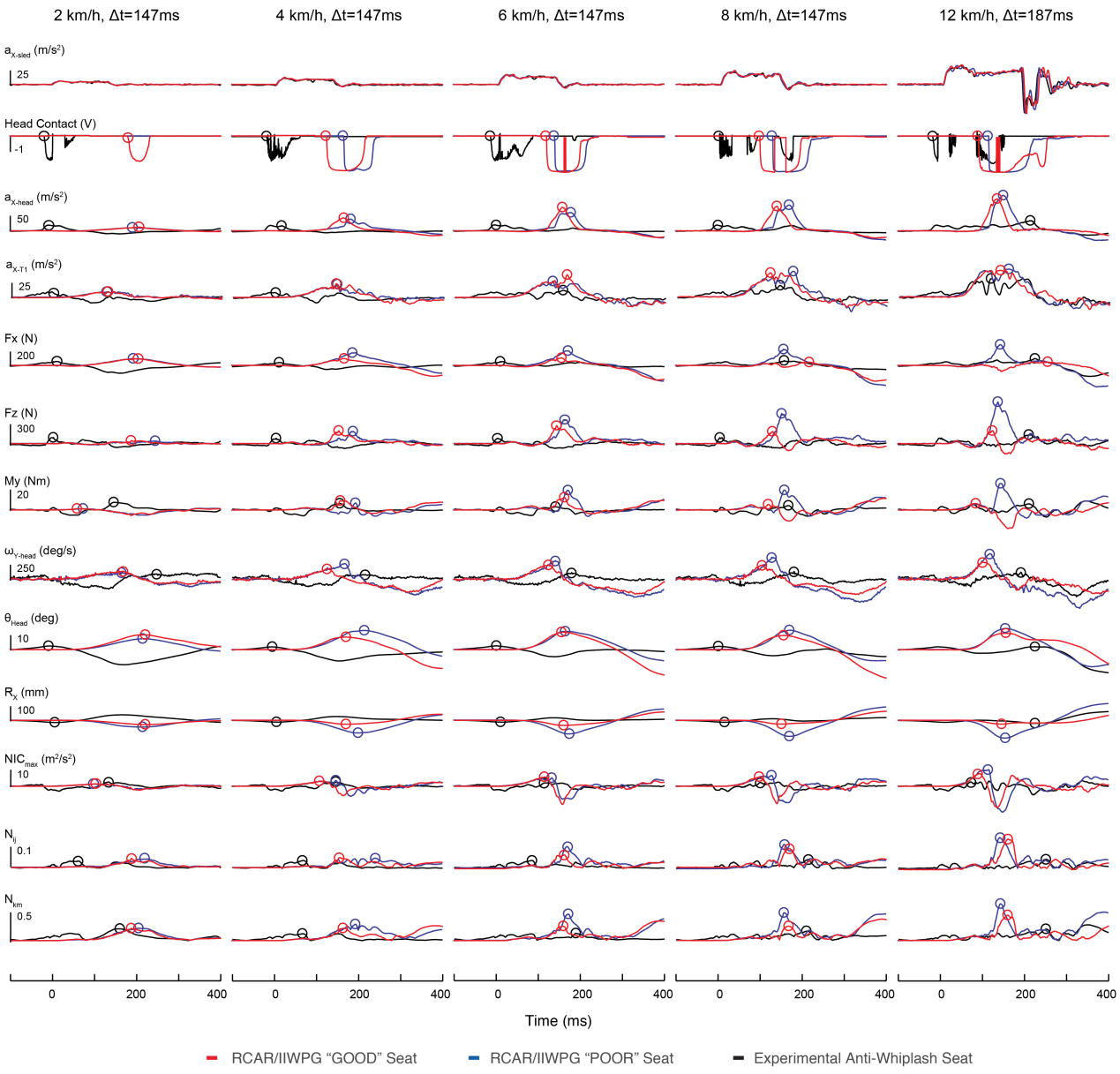

Figure 5.5. Exemplar BioRID II ATD response data comparing the Experimental anti-whiplash seat (black line), a RCAR/IIWPG good-rated (Volvo S40 WHIPS; red line) and a RCAR/IIWPG poor-rated (Pontiac Grand Am GMHR; blue line). Each column represents occupant responses while exposed to various collision severities (Δv of 2, 4, 6 and 8 with a collision pulse duration (Δt) of 147 ms and Δv of 12 km/h with a Δt = 187 ms). Hollow circles represent the onset of head-to-head-restraint contact and peak responses of each ATD response parameter for each trial. Similar plots for all seats are given in the **Appendix E: Figures E5.1 – E5.5**.

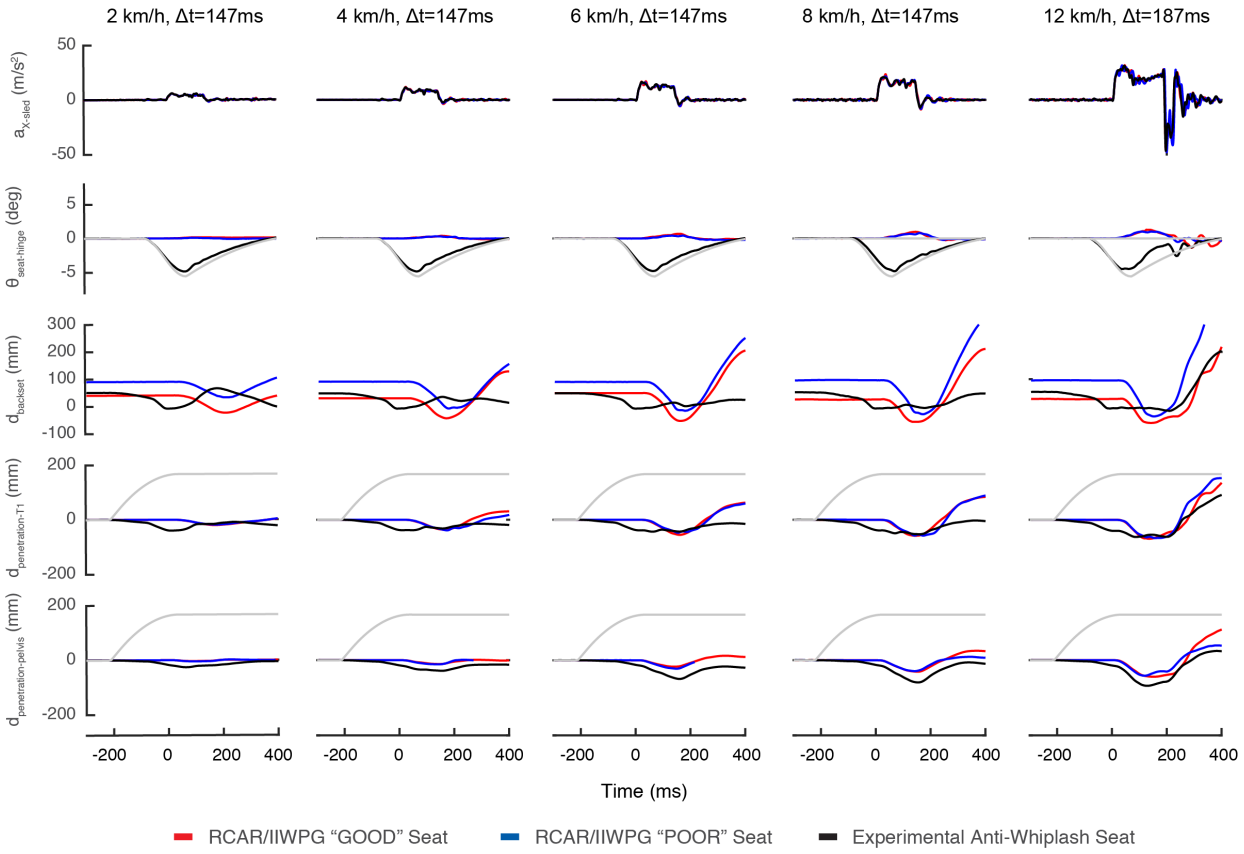

Figure 5.6. Exemplar BioRID II ATD response data comparing the seat hinge rotation, backset and occupant penetration at the T1 and pelvis for the on the Experimental anti-whiplash seat (black line), a RCAR/IIWPG good rated (Volvo S40 WHIPS; red line) and a RCAR/IIWPG poor rated (Pontiac Grand Am GMHR; blue line). Each column represents occupant responses while exposed to various collision severities (Δv of 2, 4, 6 and 8 with a collision pulse duration (Δt) of 147 ms and Δv of 12 km/h with a Δt = 187 ms). The grey lines represent the input seat hinge rotation and seatback motor deformation profiles for the Experimental anti-whiplash seat.

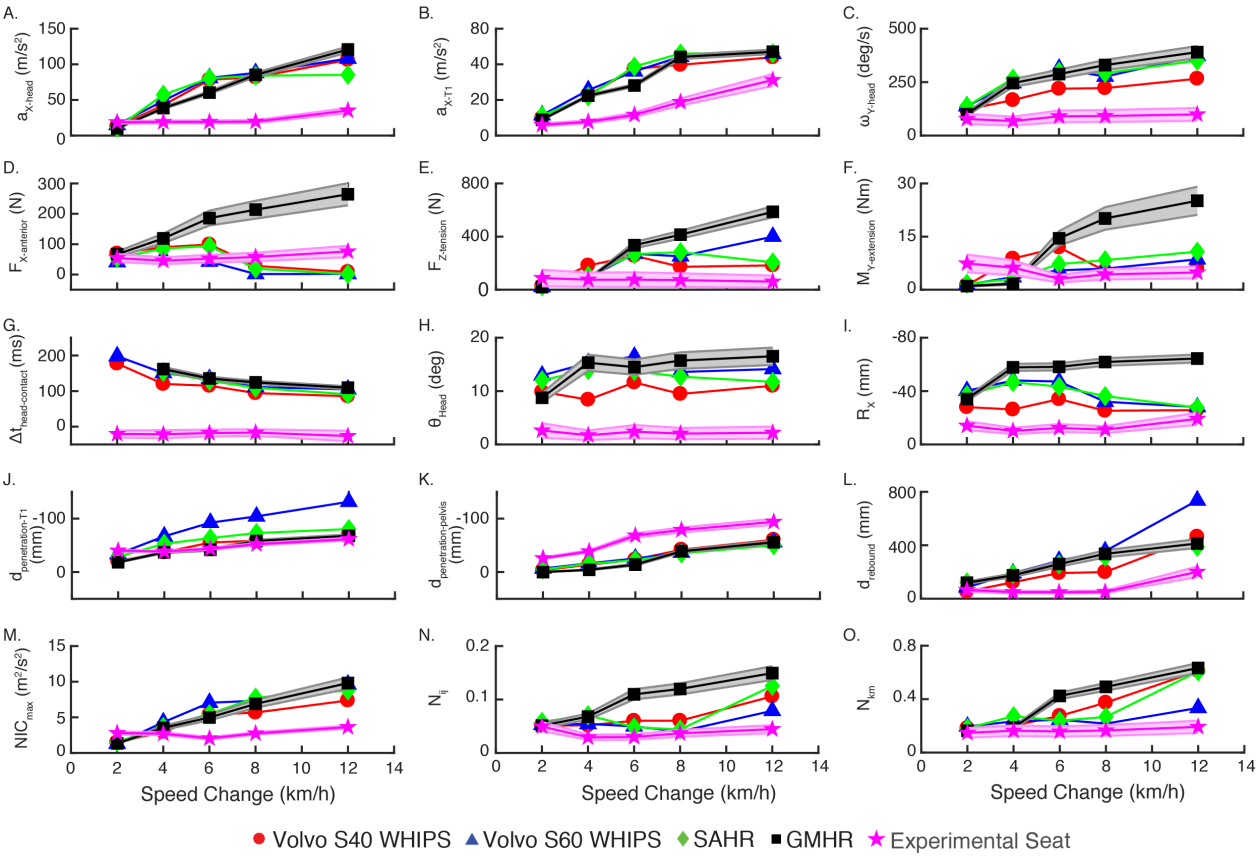

Figure 5.7. Experimental peak kinematic and kinetic responses for the BioRID II ATD seated on the WHIPS, SAHR, GMHR and Experimental seats. For all the graphs, red circles represent the Volvo S40 WHIPS seat, blue triangles represent the Volvo S60 WHIPS seat, green diamonds represent the SAHR seat, black squares represent the GMHR seat and magenta stars represent the Experimental seat. The faded black and magenta bars represent the 99th percentile predictive intervals for the GMHR and Experimental seats, respectively. Y-axis values for panels 6I, 6J and 6K have been inverted for visual purposes to show increasing responses from bottom to top.

Table 5.2. Mean (standard deviation) and Coefficient of Variation (COV) from five repeated perturbations on the GMHR and Experimental seats at Δv = 8 km/h, Δt = 147 ms and Δv = 12 km/h, Δt = 187 ms. The underlined COV values indicate a COV rating of acceptable (5% ≤ COV < 10%), the bolded COV values indicate a COV rating of poor (COV > 10%), and all other values are rated good (COV < 5%).

Automotive Seat	GM Pontiac Grand AM (GMHR)				Experimental Anti-Whiplash Seat			
Δv (km/h)	8 km/h, Δt = 147 ms		12 km/h, Δt = 187 ms		8 km/h, Δt =147 ms		12 km/h, Δt = 187 ms	
Parameter	Mean (SD)	COV (%)	Mean (SD)	COV (%)	Mean (SD)	COV (%)	Mean (SD)	COV (%)
Initial $d_{backset}$ (mm)	94.3 (1.9)	2.0	94.5 (2.6)	2.8	50.4 (1.8)	3.5	51.5 (4.8)	9.3
Initial d_{height} (mm)	-23.8 (5.3)	22.2	-25.0 (2.8)	11.3	5.3 (3.2)	60.4	-1.4 (2.8)	199.1
$a_{X\text{-}sled}$ (m/s^2)	22.8 (1.1)	4.7	31.6 (0.4)	1.2	21.5 (0.5)	2.3	31.6 (0.4)	1.4
$\Delta t_{head\ contact}$ (ms)	124.3 (1.1)	0.9	109.4 (1.6)	1.4	-16.5 (9.0)	54.3	-26.1 (5.7)	5.7
$d_{penetration\text{-}T1}$ (mm)	-58.1 (2.2)	3.8	-67.9 (1.0)	1.5	-52.2 (0.8)	1.5	-61.6 (1.2)	2.0
$d_{penetration\text{-}pelvis}$ (mm)	-38.9 (1.1)	2.9	-55.8 (1.2)	2.2	-78.8 (1.8)	2.3	-94.1 (2.8)	3.0
$a_{X\text{-}head}$ (m/s^2)	85.2 (1.0)	1.1	120.7 (1.7)	1.4	19.5 0.5)	2.8	35.1 (1.4)	4.1
$a_{X\text{-}T1}$ (m/s^2)	44.1 (0.5)	1.0	47.0 (0.3)	0.6	18.8 (0.8)	4.1	31.2 (1.3)	4.1
F_X (N)	213.5 (3.8)	1.8	264.4 (14.1)	5.4	57.8 (5.5)	9.5	76.1 (4.2)	5.5
F_Z (N)	414.4 (9.3)	2.2	586.1 (16.2)	2.8	72.5 (10.0)	13.7	63.5 (17.4)	27.2
M_Y (Nm)	20.1 (1.2)	6.1	25.1 (0.1)	0.2	4.3 (0.5)	10.9	4.9 (0.6)	13.1
$\omega_{Y\text{-}head}$(deg/s)	329.6 (13.5)	4.1	390.2 (11.1)	2.8	91.5 (11.9)	13.0	98.7 (11.6)	11.8
θ_{head} (deg)	15.7 (0.4)	2.3	16.5 (0.6)	3.8	2.0 (0.3)	12.3	2.2 (0.4)	19.9
R_X (mm)	-61.8(1.1)	1.8	-64.4 (2.3)	3.6	-11.1 (1.0)	9.0	-19.2 (2.1)	10.8
$d_{rebound}$ (mm)	335.1 (10.4)	3.5	413.4 (7.7)	1.9	51.3 (2.0)	3.8	201.3 (15.2)	7.5
NIC_{max} (m^2/s^2)	6.9 (0.2)	3.1	9.8 (0.2)	1.7	2.7 (0.4)	14.8	3.6 (0.5)	14.2
N_{ij}	0.12 (0.00)	2.3	0.16 (0.00)	1.5	0.04 (0.00)	9.3	0.05 (0.00)	5.5
N_{km}	0.48 (0.02)	3.4	0.60 (0.02)	2.9	0.15 (0.01)	6.6	0.18 (0.01)	5.8

5.4 **Discussion**

The goal of this study was to evaluate the performance of the Experimental seat against four existing anti-whiplash seats (WHIPS S40, WHIPS S60, SAHR, and GMHR) across a range of speed changes. Existing anti-whiplash seats yielded positively graded ATD responses to increased collision severity while the Experimental anti-whiplash seat evoked nearly constant ATD responses across the tested speed changes (2 to 12 km/h). With the exception of upper neck shear force (F_X), the Experimental seat performed better than existing anti-whiplash seats at reducing ATD kinematics, kinetics, and neck injury criteria for collision severities between 4 and 12 km/h. At the 2km/h speed change, the Experimental seat lowered θ_{head}, R_X, and $\Delta t_{head\text{-}contact}$ in comparison to the existing anti-whiplash seats, but the other ATD responses and neck injury criteria were similar in amplitude across all tested seats. Epidemiological studies have not shown whiplash injury at speed changes as low as 2 km/h (Bartsch et al., 2008, Krafft, 2002, Krafft et al., 2005) and, thus the lack of a difference between the seats at 2km/h collision speed was not considered further. The results of this study showed that combining seat hinge rotation and seatback cushion deformation reduces peak ATD responses and potentially mitigates the risk of whiplash injuries following low-speed, rear-end collisions (Δv = 4 – 12 km/h).

The Experimental seat appeared to achieve its benefits in multiple ways. The pre-impact forward rotation of the seatback and the deformation of the seatback allowed the occupant to pocket into the seatback while rotating the head restraint towards the occupant's head to decrease the backset distance. Head restraint contact occurred before collision onset,

which reduced the relative movement of the head and neck, and attenuated the peak kinematic and kinetic responses. Another benefit of the forward seat hinge rotation was an initial increase in effective stiffness of the seat hinge to resist the rearward deflection of the seatback created by the occupant's inertia. A third benefit of the Experimental seat was that the seat hinge and seatback motors prolonged the ATD-seatback interaction and did not return to their original configurations after the impact. This seat behaviour reduced the energy typically returned to the occupant during the rebound or restitution phase of the occupant-seat interaction. Together these benefits of actively controlling the seat hinge rotation and seatback deformation profiles generated robust decreases in most kinematic and kinetic responses and could potentially reduce the risk of whiplash injuries.

The Experimental seat attenuated all ATD responses and neck injury criteria in comparison to the poor-rated GMHR seat, and most ATD responses (with the exception of upper neck shear force: F_X) and neck injury criteria in comparison to the good-rated WHIPS and SAHR seats. Epidemiological studies have estimated that current anti-whiplash seats (SAHR, WHIPS and GMHR) reduce the risk of whiplash injuries following a rear-end collision by approximately 50% (Jakobsson et al., 2008, Kullgren and Krafft, 2010, Viano and Olsen, 2001), with the good-rated seats exhibiting a further 11 – 15% decline in occupant neck injury risk compared to poor-rated seats (Farmer et al., 2008, Trempel et al., 2016). In addition, no whiplash associated disorders (WAD) symptoms have been reported in field data at collision severities ≤ 4 km/h while a 20% risk of WAD symptoms lasting more than one month has been

observed for 8 km/h collisions (Krafft et al., 2005, Bartsch et al., 2008). Since the Experimental seat reduced most of the occupant responses at 8 km/h and 12 km/h speed change to the levels observed at 2 and 4 km/h, it can be postulated that the Experimental anti-whiplash seat could potentially reduce the overall 20% WAD risk at 8 km/h collisions to near zero. Although these results demonstrated the ability of the anti-whiplash seat to attenuate peak ATD responses (with the exception of F_X) better than current anti-whiplash seats, real-world testing of the interventions built into the Experimental anti-whiplash seat is required to quantify the actual reduction in the risk of whiplash injuries following low-speed, rear-end collisions.

Across all tested seats, the initial head restraint backset was different, with RCAR/IIWPG ratings ranging from good to marginal: good ($d_{backset} \leq 70$ mm): S40 WHIPS, S60 WHIPS and Experimental seat, acceptable ($70 \text{ mm} < d_{backset} \leq 90$ mm): SAHR seat, and marginal/poor ($d_{backset} > 90$ mm): GMHR. In comparison to the good-rated WHIPS seats (S40 WHIPS: $d_{backset}$ = 42.8 mm and d_{height} = -2.3 mm, and S60 WHIPS: $d_{backset}$ = 69.2 mm and d_{height} = -42.2 mm), the Experimental seat ($d_{backset}$ = 50.4 mm and d_{height} = 1.5 mm) decreased most ATD response (with the exception of F_X) by 25 – 89% and neck injury criteria by 9 – 73% for collision speeds 4 km/h or higher despite similar initial head restraint backsets. The decreased ATD responses observed on the Experimental seat may be due to the pre-impact forward rotation of the hinge and seatback deformation to decrease the head-to-head-restraint distance, time-to-head-contact and the relative movement between the head, neck and torso. The head contacted the head restraint 19.0 ± 3.9 ms before collision onset. This factor in isolation could lead to decreased

risk of whiplash injuries. Indeed, the risk of whiplash injury was found to decrease by 10% for every 25 mm decrease in $d_{backset}$, and was the lowest when the $d_{backset}$ = 0 mm (Eriksson, 2005). Thus, decreasing the backset from 50.4 mm to 0 mm prior to collision onset could potentially decrease the risk of neck injury by 20%. Future testing is required to determine the relative contribution of initial head-to-head-restraint contact prior to the collision, the seat hinge rotation, and the seatback cushion deformation on the peak ATD responses to the risk of whiplash injury following rear-end collisions.

All existing anti-whiplash seats generated positively graded responses to increasing speed changes in most ATD responses ($a_{X\text{-}head}$, $a_{X\text{-}T1}$, $\omega_{Y\text{-}head}$, F_X, F_Z, M_Y, θ_{head}, R_X, and $d_{rebound}$) and neck injury criteria (NIC_{max}, N_{ij}, N_{km}). Similar to a previous study (**Chapter 2**), the ATD responses on the good-rated seats (WHIPS and SAHR) attenuated only four peak responses (F_X: 47 - 99% reduction, F_Z: 19 - 68% reduction, M_Y: 18 - 75% reduction, R_X: 19 – 60% reduction) compared to the RCAR/IIWPG poor-rated seat (GMHR). These four variables (F_X, F_Z, M_Y and R_X) attenuated by the WHIPS and SAHR seats had the most overlap with the 99th percentile predictive intervals of the Experimental seat responses. At the 8 and 12 km/h collision speeds, the WHIPS and SAHR seats attenuated the peak F_X responses more than the Experimental seat. The possible activation of the WHIPS and SAHR safety mechanisms at these higher collision severities transitioned the F_X responses from positive to negative peaks, reducing the rearward neck loading and adopting a forward flexion position to reduce the risk of whiplash injuries. The WHIPS and SAHR seats are equipped with dynamic anti-whiplash devices that rely on occupant

loading of the seatback to deform a recliner mechanism that controls seatback translation and rotation (WHIPS) (Jakobsson et al., 2008, Jakobsson et al., 2000) or to move the head restraint upward and forward (SAHR) (Viano and Olsen, 2001). Thus, the WHIPS and SAHR seats may require increased occupant loading of the seatback during higher collision speeds (Δv > 12 km/h) to fully activate their respective safety mechanism and reduce the F_X responses. These results suggest that these seats may have been optimized for higher collision pulses closer to the industry standard RCAR/IIWPG 16 km/h test pulse (Δt = 91 ms) and were not designed to attenuate ATD response during the lower speed changes used in this study ($\Delta v \leq$ 12 km/h). The inability of the WHIPS and SAHR seats to attenuate ATD responses at lower speed changes may explain why existing anti-whiplash seats are currently only 50% effective at reducing the risk of whiplash injury.

The COV values of the BioRID II ATD responses were used to test the repeatability of the ATD on both the GMHR and Experimental seats. Compared to the GMHR seat, the COV values for the Experimental seat were more variable, with 8 of the 18 COV values rated as poor (COV > 10%) at the 8 and 12 km/h speed changes. Although the COV values were higher for the Experimental seat than for the GMHR seat at both the 8 and 12 km/h speed changes, the SD values were at similar magnitudes between seats. Consequently, the larger COV values for the Experimental seat were likely due to lower mean values (which form the denominators in the COV calculation) than due to greater variability (i.e., SD values) in the ATD responses. Thus, we

believe that the Experimental seat had sufficient repeatability to justify the comparisons made to the other anti-whiplash seats in this study.

The collision severities used in this study were less severe than the RCAR/IIWPG standard crash test pulse (16 km/h, Δt = 91 ms) but provided a graded range of collision velocities applicable to some real-world collisions that cause whiplash injury (Krafft et al., 2005, Kullgren et al., 2007). A collision pulse duration of Δt = 147 ms was selected for collision speeds up to 8 km/h because it was similar to the 135 ms observed in prior vehicle-to-vehicle rear-end crashes (Brault et al., 1998). However, a collision pulse duration of Δt = 187 ms was needed to reach a 12 km/h collision speed due to the weight of the Experimental seat (total mass = 191 kg). The Experimental seat has only been tested at collision speeds up to 12 km/h and it remains unclear whether the combined seat hinge rotation and seatback deformation profile can attenuate ATD responses at collision speeds greater than 12 km/h. Future testing of the Experimental anti-whiplash seat is required at the RCAR/IIWPG crash pulse (Δv = 16 km/h, Δt = 91 ms) to compare the effectiveness of actively controlling seat hinge rotation and seatback deformation on the attenuation of ATD responses against existing anti-whiplash seats.

Another limitation of the present study was that the automotive floor geometry relative to the seat base were not properly maintain between seats. The WHIPS and SAHR seats contained electrical motors under the seat pan to adjust fore/aft position and seat pan tilt angle. To mount these seats, the seat base was elevated to allow for clearance under the seat pan and changed the vertical distance between the top of the seat pan and automotive floor

(see **Chapter 2**). However, the relative geometry between the BioRID II ATD's head, torso and pelvis were replicated between the different automotive seats to ensure that the ATD was in a similar initial position and confirmed using IRED marker positions (**Figure 5.1** and **5.3**). Despite the resulting differences in ATD lower limb positions, the similarities observed in T1 accelerations across the four existing anti-whiplash seats in both a previous study and this current study suggested that lower limb/foot position had little influence on peak ATD kinematic and kinetic responses.

The BioRID ATD used for this study represented a 50^{th} percentile male occupant, and further work is needed to evaluate the Experimental seat for male and female occupants of different heights and weights. Although the BioRID ATD was designed to mimic the motion of human occupants, including their active muscle response, further work is needed to evaluate whether the pre-perturbation forward rotation of the seat hinge alters the neck muscle response in humans and whether the BioRID ATD remains a valid surrogate for human occupants under these pre-crash conditions. Further work is also needed on how to affordably and efficiently implement an active seat that behaves like the large, heavy and expensive prototype seat used for this study.

5.5 **Conclusion**

Compared to the current anti-whiplash seats currently on the market (WHIPS, SAHR and GMHR), the Experimental anti-whiplash seat attenuated all peak ATD responses (with the

exception of F_X). The observed peak ATD responses on the Experimental seat remained essentially constant for collision severities ranging from 2 to 12 km/h. For a 12 km/h collision, the peak ATD responses on the Experimental seat were similar or below those observed in current anti-whiplash seats for a 4 km/h collision. The results of this study suggested that the Experimental seat dynamically controlling seat hinge rotation and seatback cushion deformation could potentially reduce the risk of whiplash injury during low-speed, rear-end collisions.

Chapter 6. General Discussion and Conclusion

6.1 Summary of the Research and Discussion

The overall objective of these experiments presented in this dissertation was to design, build and test a novel Experimental anti-whiplash to prevent whiplash injuries following low-speed, rear-end collisions. The key safety features of the anti-whiplash seat were the dynamic control of seat hinge rotation and seatback cushion deformation before and during the collision. A series of four experiments was conducted to determine the performance of the Experimental anti-whiplash seat and to compare its performance to existing anti-whiplash seats. The goal of Experiment 1 (**Chapter 2**) was to gain insight into how current anti-whiplash seats perform during low-speed, rear-end collisions at collision severities lower than the Research Council for Automobile Repairs/International Insurance Whiplash Prevention Group (RCAR/IIWPG) standard 16 km/h crash pulse. The results of Experiment 1 revealed that anti-whiplash seats rated as good according to the RCAR/IIWPG (2 Volvo Whiplash Injury Prevention seats: WHIPS and 1 Saab's Active Head Restraint: SAHR) only attenuated four key ATD responses (upper neck shear and compressive forces, upper neck flexion and extension moment, and rearward retraction) compared to a poor-rated seat (General Motor's High Retention seat: GMHR). The goals of the next two experiments (Experiment 2 and 3) were to determine if the active control of seat hinge rotation or of seatback cushion deformation could attenuate ATD responses during low-speed, rear-end collisions. Active rotation of the seat

hinge and active modulation of the seatback decreased most ATD responses and neck injury criteria compared to a Control seat (**Chapters 3 and 4**). The goals of Experiment 4 were to determine if co-activation of both the seat hinge rotation and seatback deformation safety mechanisms on the Experimental anti-whiplash seat could attenuate further the ATD responses and to compare the performance of the Experimental anti-whiplash seat against existing anti-whiplash seats (GMHR, SAHR and WHIPS). The co-activation of both the seat hinge rotation and seatback deformation safety mechanisms resulted in ATD responses that were not different from those observed when only the seatback deformation mechanism was used. In comparison to existing anti-whiplash seats, the Experimental seat decreased ATD kinematic and kinetic responses by 25 – 99% and decreased neck injury criteria by 9 – 73% for collision speeds of 4 km/h or greater. Through the four experiments included in this dissertation, we accomplished the overall research objective of developing an Experimental anti-whiplash seat that dynamically modified the seat hinge and seatback cushion properties to attenuate occupant kinematic and kinetic responses as well as neck injury criteria during low-speed, rear-end collisions.

The safety features of the Experimental anti-whiplash automotive seat were the use of motors to dynamically control seat hinge rotation and seatback cushion deformation during the whiplash perturbation. By controlling seat hinge rotation and seatback cushion deformation, the anti-whiplash seat was designed to decrease the amplitude of the forces applied by the vehicle to the occupant and to support the head earlier in the collision to minimize the

displacement of the head relative to the torso. The seat hinge profile rotated the seatback forward prior to the collision onset to decrease the head-to-head-restraint distance before actively rotating the seatback rearward as the occupant loaded the seat to attenuate the acceleration experienced by the occupant. In addition to decreasing head restraint backset, the active rotation of the seatback may have increased the effective stiffness of the seat hinge to resist the rearward seatback deflection created by the occupant's inertia as the sled was accelerated forward. The predictive seatback-motor deformation profile introduced slack into the webbing prior to the collision onset to allow deeper occupant penetration into the mid-torso and pelvis regions of the seatback and to reduce the pre-impact backset. After reaching peak rearward rotation, both the seat hinge rotation and seatback deformation profiles stopped in order to attenuate forward rebound of the seatback. This attenuated rebound reduced the acceleration and speed change experienced by the occupant. Consequently, the changes in both the seat hinge rotation and seatback cushion deformation both before and during the collision combined with the termination of the motion at peak hinge angle and cushion displacement served to prolong the ATD-seatback interaction and reduced the energy typically returned to the occupant during the rebound or restitution phases of the occupant-seat interaction.

When comparing the relative benefits of the seat hinge rotation and seatback deformation safety mechanisms at each collision severity, the seat hinge rotation better reduced peak acceleration of the head and torso ($a_{X\text{-}head}$ and $a_{X\text{-}T1}$), whereas the seatback

deformation improved occupant penetration ($d_{penetration\text{-}T1}$ and $d_{penetration\text{-}pelvis}$) and better minimized the relative motion between the head and upper torso to reduce kinetic responses (F_X, F_Z, and M_Y), linear displacements (R_X and $d_{rebound}$), angular rotation and velocity (θ_{head} and $\omega_{Y\text{-}head}$), head-to-head-restraint contact time ($\Delta t_{head\text{-}contact}$), and neck injury criteria (NIC_{max}, N_{ij} and N_{km}) (**Table 6.1**). Both safety mechanisms decreased most ATD responses compared to the Control seat, but the seatback cushion deformation mechanism generated greater reductions (average of -61%) than the seat hinge rotation mechanism (average of -46%) for the ATD responses in the bottom portion of **Table 6.1** (paired t-test, p=0.007).

The combination of both safety mechanisms (**Chapter 5**) typically generated the largest reductions in ATD responses compared to the Control seat (see the bold percentages in **Table 6.1**), although these reductions (average of -73%) were not significantly different from the seatback deformation mechanism alone (paired t-test, p=0.088). The lack of additional benefits from the combined activation of the seat safety mechanisms compared to the isolated activation of the seatback mechanism could suggest that implementing only one of these safety features is sufficient to protect an occupant during a rear-end collision. In terms of the future use of these mechanisms as potential safety devices, the seatback deformation mechanism may be easier to implement as there was only one component (i.e., introducing slack in the seatback cushion support at the mid-torso and pelvis), whereas, the seat hinge rotation mechanism would require two components (i.e., the pre-impact forward rotation of the seat hinge and the subsequent rearward rotation of the seat hinge). Further work is needed to develop a cost-

effective method of achieving this seatback cushion behavior. Further research may also be required to understand why the lack of a reduction in the horizontal acceleration of T1 ($a_{X\text{-}T1}$), a variable that is currently used as a test metric in evaluating the performance of anti-whiplash seats, was the only variable not attenuated by the seatback-deformation mechanism.

Across all experiments presented in this dissertation, differences in initial position of the head restraint relative to the occupant's head potentially confounded the observed ATD kinematic and kinetic responses. The horizontal backset ($d_{backset}$) and vertical height (d_{height}) of the head restraint relative to the head are known to affect the occupant responses and the risk of whiplash injury (Nygren et al., 1985, Siegmund et al., 1999, Stemper et al., 2006, Eichberger et al., 1996, Eriksson, 2005). For example, every 25 mm reduction in $d_{backset}$ reportedly decreases the risk of neck injury by 10% (Eriksson, 2005). The Experimental seat was designed to have a good-rated initial head restraint position and the pre-impact rotation seat hinge and deformation of the seatback further reduced the initial backset distance prior to the collision onset. In **Chapter 3**, the addition of the seat hinge rotation affected the ATD responses more than differences in initial backset between the poor-rated GMHR seat and the Experimental seat. In comparison to good-rated existing anti-whiplash seats (e.g., WHIPS and SAHR; **Chapter 5**), the Experimental seat with co-activation of the seat hinge rotation and seatback deformation decreased all kinematic and most kinetic responses (with the exception of F_X) despite having a similar initial backset. The pre-impact forward rotation of the seat hinge and rearward deformation of the seatback cushion reduced the head-to-head-restraint distance and

caused the time-to-head-contact to occur 26.1 ms before the collision onset (**Table 6.1**, Δv = 12 km/h). Given that approximately 30% of vehicles observed at intersections have marginal- or poor-rated head restraint positions (Romilly et al., 2011), the pre-impact activation of the Experimental anti-whiplash seat would actively change the positions of both the occupant and the head restraint to support the head and neck during the collision and to better protect the occupants of these vehicles.

Table 6.1. Mean (standard deviation) and percent change (%) from Control GMHR seat for the Experimental seat with seat hinge rotation only (**Chapter 3**), seatback deformation only (**Chapter 4**) and the combination of both seat hinge rotation and seatback deformation (**Chapter 5**) during at a Δv = 12 km/h collision speed. Five repeated perturbations were collected of the ATD seated on the GMHR and each test condition of the Experimental seat. The largest beneficial change is shown in bold.

Automotive Seat	GM Pontiac Grand AM (GMHR) Control Seat	Experimental **Chapter 3:** Seat Hinge Rotation		Experimental **Chapter 4:** Seatback Deformation		Experimental **Chapter 5:** Rotation and Deformation	
Δv (km/h)	12 km/h, Δt = 185 ms	12 km/h, Δt = 185 ms		12 km/h, Δt =194 ms		12 km/h, Δt = 187 ms	
Parameter	Mean (SD)	Mean (SD)	Change (%)	Mean (SD)	Change (%)	Mean (SD)	Change (%)
Initial $d_{backset}$ (mm)	94.5 (2.6)	51.5 (4.8)	-45.5	52.0 (7.3)	-45.0	51.5 (4.8)	-45.5
Initial d_{height} (mm)	-25.0 (2.8)	-1.6 (1.2)	-93.6	2.5 (7.1)	-110.0	-1.4 (2.8)	-94.4
$a_{X\text{-}sled}$ (m/s^2)	31.6 (0.4)	30.2 (0.4)	-4.4	30.7 (0.5)	-2.8	31.6 (0.4)	0.0
$\Delta t_{head\ contact}$ (ms)	109.4 (1.6)	82.8 (6.0)	-24.3	51.4 (10.2)	-53.0	-26.1 (5.7)	**-123.9**
$d_{penetration\text{-}T1}$ (mm)	-67.9 (1.0)	-	-	-78.5 (1.7)	15.6	-61.6 (1.2)	**-9.3**
$d_{penetration\text{-}pelvis}$ (mm)	-55.8 (1.2)	-	-	-99.6 (3.8)	**78.5**	-94.1 (2.8)	68.6
$a_{X\text{-}head}$ (m/s^2)	120.7 (1.7)	49.3 (3.1)	-59.1	60.7 (4.6)	-49.7	35.1 (1.4)	**-70.9**
$a_{X\text{-}T1}$ (m/s^2)	47.0 (0.3)	35.7 (1.0)	-24.0	47.1 (1.0)	0.2	31.2 (1.3)	**-33.6**
F_X (N)	264.4 (14.1)	140.7 (5.7)	-46.8	87.8 (22.8)	-66.8	76.1 (4.2)	**-71.2**
F_Z (N)	586.1 (16.2)	267.3 (4.4)	-54.4	134.7 (21.6)	-77.0	63.5 (17.4)	**-89.2**
M_Y (Nm)	25.1 (0.1)	11.9 (0.7)	-52.6	5.9 (1.2)	-76.5	4.9 (0.6)	**-80.5**
$\omega_{Y\text{-}head}$(deg/s)	-390.2 (11.1)	-189.4 (11.5)	-51.5	-147.8 (11.9)	-62.1	-98.7 (11.6)	**-74.7**
θ_{head} (deg)	16.5 (0.6)	8.9 (0.4)	-46.1	5.3 (1.7)	-67.9	2.2 (0.4)	**-86.7**
R_X (mm)	-64.4 (2.3)	-35.8 (1.3)	-44.4	-32.6 (6.7)	-49.4	-19.2 (2.1)	**-70.2**
$d_{rebound}$ (mm)	413.4 (7.7)	267.5 (7.0)	-35.3	126.0 (17.1)	**-69.5**	201.3 (15.2)	-51.3
NIC_{max} (m^2/s^2)	9.8 (0.2)	4.0 (0.4)	-59.2	2.0 (0.9)	**-79.6**	3.6 (0.5)	-63.3
N_{ij}	0.16 (0.00)	0.09 (0.01)	-43.8	0.027 (0.006)	**-83.1**	0.05 (0.00)	-68.8
N_{km}	0.60 (0.02)	0.28 (0.02)	-53.3	0.23 (0.05)	-61.7	0.18 (0.01)	**-70.0**

6.2 **Implications for Whiplash Injury Research**

Current anti-whiplash seats are tested using the RCAR/IIWPG test pulse with a speed change of 16 km/h. Despite 53% of rear-end collisions occurring at collision severities less than 15 km/h (Hell et al., 1998), there is limited research into occupant responses below the 16 km/h standard test pulse. The results of **Chapter 2** revealed positively graded ATD kinematic and kinetic responses to an increasing speed changes from 2 – 14 km/h while seated on existing anti-whiplash seats (e.g., Volvo's WHIPS, Saab's SAHR and General Motor's GMHR). The attenuation of only four key ATD responses (peak upper neck shear and axial forces, flexion/extension moment and rearward retraction) by the good-rated seats in comparison to a poor-rated seat demonstrated the limited low-speed, occupant protection available in the tested seats. Since the exact injury mechanisms underlying whiplash injuries remain unclear, reducing occupant accelerations (head and torso) and/or minimizing the movement of the head relative to the upper torso, although potential targets, may not completely protect occupants against whiplash injuries (Siegmund et al., 2009). Future work is needed to identify the biomechanical factors leading to whiplash injuries to help the development of anti-whiplash automotive seats.

The main difference between the Experimental anti-whiplash seat and existing anti-whiplash seats is that the Experimental seat dynamically changes its properties both before (predictive) and during (reactive) the collision to reduce ATD kinematic and kinetic responses. Current anti-whiplash seats (WHIPS and SAHR) seats are mostly reactive seats that require the inertial mass of an occupant loading the seatback during the whiplash perturbation to activate their respective safety mechanisms. One key predictive factor that

the Experimental seat addressed is the pre-impact reduction of initial backset by dynamically rotating the seatback forward to bring the head restraint towards the ATD's head and/or translating the seatback cushion rearward to bring the ATD's head towards the head restraint prior to the collision onset. Head restraint backset in isolation reportedly decreases the risk of whiplash injury by 10% for every 25 mm decrease in backset, with the lowest injury risk observed when the $d_{backset}$ = 0 mm (Eriksson, 2005). The pre-impact reduction of backset initiated earlier head-to-head-restraint contact time, decreased displacements of the head relative to the upper torso, and reduced most ATD kinematic and kinetic responses to better reduce the risk of whiplash injuries following low-speed, collision. Although the Experimental seat attenuated the ATD responses relative to the Control seat, even when the head restraint backset was similar, it remains unclear whether similar reductions can be achieved by just adjusting the initial backset to zero. Future testing is required to better quantify the relative contributions of initial head-to-head-restraint contact prior to the collision compared to both the seat hinge rotation and the seatback cushion deformation on the peak ATD responses and the risk of whiplash injury following rear-end collisions.

The risk of developing whiplash associated disorders (WAD) symptoms lasting more than a month is approximately 20% following an 8 km/h rear-end collision and no WAD have been reported in field data at collision speeds less than or equal to 4 km/h (Krafft et al., 2005, Bartsch et al., 2008). In contrast to current anti-whiplash seat, the ATD responses on the Experimental anti-whiplash seat were not graded with increasing collision severity but were attenuated to a similar level despite an increase in collision speeds (**Chapter 5**). Thus,

the Experimental anti-whiplash seat, with both seat hinge rotation and seatback cushion deformation, attenuated most ATD responses at the 8 km/h and 12 km/h speed changes to levels observed at a 4 km/h speed change on existing anti-whiplash seats (**Figure 6.1**). Based on these data, the combination of seat hinge rotation and seatback cushion deformation on the Experimental anti-whiplash seat could potentially reduce the overall 20% WAD risk at an 8 km/h collision speed to near zero, i.e. the risk of WAD at 4 km/h collision speed or less. Future experiments at higher collision speeds are required to determine the effectiveness of the Experimental anti-whiplash seat at higher collision speeds and future field tests of a production version of the seat are needed to determine the potential reduction in the risk of whiplash injuries in the field.

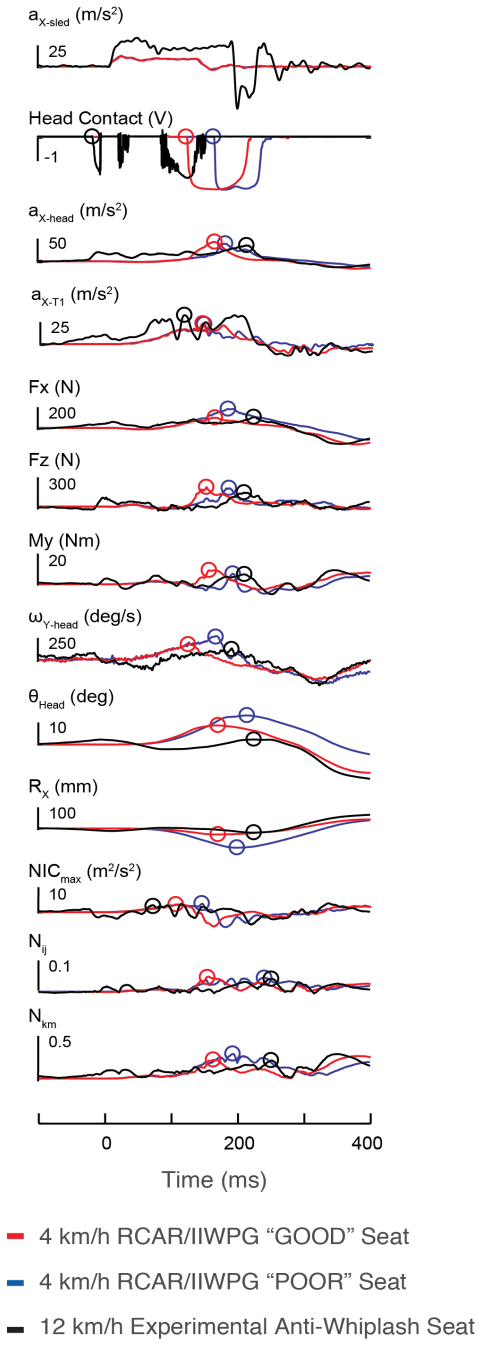

Figure 6.1. Exemplar BioRID II ATD response data comparing the Experimental anti-whiplash seat (black line) with the co-activation of both seat hinge rotation and seatback cushion deformation during a 12 km/h collision (Δt = 187 ms) to a RCAR/IIWPG good-rated seat (Volvo S40 WHIPS; red line) and a RCAR/IIWPG poor-rated seat (Pontiac Grand Am GMHR; blue line) during a 4 km/h collision (Δt = 147 ms). Hollow circles represent the onset of head-to-head-restraint contact and peak responses of each ATD response parameter for each trial.

6.3 General Limitations and Future Directions

All of the experiments conducted in this dissertation utilized a BioRID II anthropomorphic test device (ATD) and a custom linear sled located in a laboratory. The ATD was a useful model throughout the experiments as it allowed the testing of collision severities that might cause injury to human volunteers (Brault et al., 2000). Now that the overall effectiveness of the anti-whiplash seat in the reduction of ATD kinematic and kinetic responses has been established, its effectiveness on human occupants can be tested. For example, human volunteers exhibit a startle response during rear-end collisions that can be modified by a pre-impact stimuli (Mang et al., 2015, Mang et al., 2012). Whether the seat hinge rotation and/or seatback cushion deformation of the Experimental anti-whiplash seat elicits a startle response that can reduce occupant responses remains unknown. In addition, all experiments were conducted on an ATD that represents a 50^{th} percentile male. It remains unclear whether the seat hinge rotation and seatback cushion deformation profiles will also attenuate the responses of male and female occupants with different anthropometric measurements. Further testing should first be done using the 50^{th} percentile female and 95^{th} percentile male ATDs to verify the robustness of the seat hinge rotation and seatback deformation profiles for occupants with different anthropometry. Then, these experiments should be expanded in human volunteers of both sexes with a range of anthropometric characteristics. Initial human experimentations could begin with a speed change of 2.8 km/h (Δv = 0.78 m/s) and a peak acceleration of 2.1g (used previously with human volunteers), although little or no reduction in the ATD responses were observed at these low levels. After these initial tests, higher speed changes could be explored incrementally given the expected

reduction in kinematics and kinetics responses associated with the Experimental anti-whiplash seat.

The GMHR seat was initially selected due to the availability of a finite element model of the GMHR seat developed at UBC using LS-Dyna explicit finite element solver (Livermore Software Technology Corp., Livermore, CA, USA) (Romilly and Skipper, 2005). The GMHR seat was designed with a rigid perimeter frame and a yielding center to promote pocketing of the pelvis to increase occupant retention (Viano, 2003a, Viano and Parenteau, 2015). However, because the GMHR seat received a poor rating by the RCAR/IIWPG seat/head restraint evaluation protocol, any comparisons between the GMHR seat and either the good-rated seats (e.g., WHIPS and SAHR) or the Experimental anti-whiplash seat will potentially be confounded by differences in initial backset distance. The effect of initial backset was addressed in Experiment 2 (**Chapter 3**) and showed that the seat hinge rotation had a larger effect on ATD responses than the differences in initial backset.

All the collision severities used in these experiments were less severe than the industry-standard, RCAR/IIWPG collision test pulse (16 km/h, Δt = 91 ms). The whiplash test sled used in these experiments was designed for human testing and was not designed to generate the RCAR/IIIWPG collision pulse. Also, the weight of the Experimental seat and all the motors added an additional 191 kg to the load carried by the sled and limited its peak acceleration and performance. Further testing at the standard 16 km/h test pulse is required to evaluate the performance of the Experimental anti-whiplash seat according to the dynamic test component of the RCAR/IIWPG seat and head restraint evaluation protocol (Insurance Institute of Highway Safety, 2008b, Insurance Institute of Highway Safety,

2008a). Additional testing at the RCAR/IIWPG collision test pulse will require a redesign of the Experimental anti-whiplash seat to transform the large, heavy and expensive prototype seat used in these experiments into a lightweight, affordable and efficient implementation of the seat. Due to the robustness of the attenuated ATD responses observed in the Experimental anti-whiplash seat, we anticipate that the Experimental anti-whiplash seat will also attenuate ATD kinematic and kinetic responses at higher collision severities (≥ 16 km/h).

The original design and implementation of the Experimental anti-whiplash seat was a flexible system with large motors to allow the testing of a wide range of seat hinge rotation and seatback cushion deformations profiles. The use of the large motors may not be required to generate the small seat hinge rotations (< 4 deg) and seatback cushion deformations (< 10 cm) that was observed to successfully attenuate the ATD responses. Replacing the motors in the final design of the anti-whiplash seat will simplify the seat hinge rotation and seatback deformation mechanisms as well as reduce the overall production cost. Instead of motors, future redesigns may utilize different combinations of deformable structures, springs and dampeners, ratchets, and pyrotechnic components to generate predefined seat hinge rotation and seatback deformation profiles. Final implementation of the anti-whiplash seat will also require interfacing with a radar-based collision-detection system that triggers the early onsets of the seat hinge rotation and the seatback cushion deformation profiles. The final product could be a low-cost solution that could be implemented with existing collision avoidance systems to reduce whiplash injuries.

6.4 **Conclusion**

The experiments presented in this dissertation focused on the development and testing of a novel Experimental anti-whiplash automotive seat to address whiplash injuries and its associated disorders during rear-end collisions. Through a series of experiments, seat hinge rotation and seatback cushion deformation profiles were identified that best attenuated BioRID II ATD kinematic, kinetic and neck injury criteria responses across a range of collision severities (2 – 12 km/h). The Experimental anti-whiplash seat, with the co-activation of the seat hinge rotation and the seatback cushion deformation profiles, attenuated the ATD responses during a 12 km/h speed change to the same response levels observed during a 4 km/h speed change while seated on other existing anti-whiplash seats (GMHR, SAHR and WHIPS). Thus, the results of the experimental work presented in this dissertation confirmed that dynamic control of the seat hinge rotation and seatback cushion deformation during a whiplash collision can attenuate peak occupant responses and could potentially reduce the risk of whiplash injuries following low-speed, rear-end collisions.

Bibliography

ALDMAN, B. An Analytical Approach to the Impact Biomechanics of Head and Neck. 30th Annual AAAM Conference, 1986 Montreal, QC, Canada. 439-454.

ANDERSON, J. S., HSU, A. W. & VASAVADA, A. N. 2005. Morphology, architecture, and biomechanics of human cervical multifidus. *Spine,* 30**,** E86-91.

BARNSLEY, L., LORD, S. & BOGDUK, N. 1994. Whiplash injury. *Pain,* 58**,** 283-307.

BARNSLEY, L., LORD, S. M., WALLIS, B. J. & BOGDUK, N. 1995. The prevalence of chronic cervical zygapophysial joint pain after whiplash. *Spine (Phila Pa 1976),* 20**,** 20-5; discussion 26.

BARTSCH, A. J., GILBERSTON, L. G., PRAKASH, V., MORR, D. R. & WIECHEL, J. F. Minor Crashes and 'Whiplash' in the United States. 52nd Annals of Advances in Automotive Medicine Annual Conference, October 2008 San Diego, California, USA.

BOGDUK, N. & YOGANANDAN, N. 2001. Biomechanics of the cervical spine Part 3: minor injuries. *Clin Biomech (Bristol, Avon),* 16**,** 267-75.

BOSTROM, O., FREDRIKSSON, R., HALAND, Y., JAKOBSSON, L., KRAFFT, M., LOVSUND, P., MUSER, M. H. & SVENSSON, M. Y. 2000. Comparison of car seats in low speed rear-end impacts using the BioRID dummy and the new neck injury criterion (NIC). *Accid Anal Prev,* 32**,** 321-8.

BOSTROM, O., SVENSSON, M., ALDMAN, B., HANSSON, H. A., HALAND, Y., LOVSUND, P., SEEMAN, T., SUNESON, A., SALJO, A. & ORTENGREN, R. A new neck injury criterion candidate based on injury findings in the cervical spine ganglia after experimental neck extension trauma. 1996 International IROCBI Conference on the Biomechanics of Impact, 1996 Dublin, Ireland. 123-136.

BRAULT, J. R., SIEGMUND, G. P. & WHEELER, J. B. 2000. Cervical muscle response during whiplash: evidence of a lengthening muscle contraction. *Clin Biomech,* 15**,** 426-35.

BRAULT, J. R., WHEELER, J. B., SIEGMUND, G. P. & BRAULT, E. J. 1998. Clinical response of human subjects to rear-end automobile collisions. *Arch Phys Med Rehabil,* 79**,** 72-80.

BUITENHUIS, J., DE JONG, P. J., JASPERS, J. P. & GROOTHOFF, J. W. 2009. Work disability after whiplash: a prospective cohort study. *Spine (Phila Pa 1976),* 34**,** 262-7.

CAPPON, H., PHILIPPENS, M. M. & WISMANS, J. A new test method for the assessment of neck injuries in rear-end collisions 16th International Technical Conference on the Enhanced Safety if Vehicles (ESV) 2001 Amsterdam, The Netherlands.

CASSIDY, J. D., CARROLL, L. J., COTE, P., LEMSTRA, M., BERGLUND, A. & NYGREN, A. 2000. Effect of eliminating compensation for pain and suffering on the outcome of insurance claims for whiplash injury. *N Engl J Med,* 342**,** 1179-86.

DAVIDSSON, J. 1999. BioRID II Final Report. Goteborg, Sweden: Chalmers University of Technology.

EICHBERGER, A., GEIGL, B. C., MOSER, A., FACHBACH, B. & STEFFAN, H. 1996. Comparison of Difference Car Seats Regarding Head - Neck Kinematics of Volunteers during Rear End Impact. *1996 International IRCOBI Conference on the Blomechanics of Impacts.* Dublin, Ireland.

EICHBERGER, A., STEFFAN, H., GEIGL, B. C., SVENSSON, M., BOSTROM, O., LEINZINGER, P. E. & DAROK, M. Evaluation of the applicability of the neck injury criterion (NIC) in rear end impacts on the basis of human subject tests. 1998 International IRCOBI Conference on the Biomechanics of Impact, 1998 Goteborg, Sweden. 321-333.

EPPINGER, R., SUN, E., BANDAK, F., HAFFNER, M., KHAEWPONG, N., MALTESE, M., KUPPA, S., NGUYEN, T., TAKHOUNTS, E., TANNOUS, R., ZHANG, A. & SAUL, R. 1999. Development of Improved Injury Criteria for the Assessment of Advanced Automotive Restraint Systems - II.: National Highway Traffic Safety Administration (NHTSA).

EPPINGER, R., SUN, E., KUPPA, S. & SAUL, R. 2000. Supplement: Development of Improved Injury Criteria for the Assessment of Advanced Automotive

Restraint Systems - II. National Highway Traffic Safety Administration (NHTSA).

ERIKSSON, L. 2005. Influence of Head Restraint Position on Long-Term AIS 1 Neck Injury Risk. *International Journal of Crashworthiness,* 10**,** 545-555.

EVANS, R. W. 1992. Some observations on whiplash injuries. *Neurol Clin,* 10**,** 975-97.

EVANS, T. H., MAYER, T. G. & GATCHEL, R. J. 2001. Recurrent disabling work-related spinal disorders after prior injury claims in a chronic low back pain population. *Spine J,* 1**,** 183-9.

FARMER, C. M., WELLS, J. K. & LUND, A. K. 2003. Effects of head restraint and seat redesign on neck injury risk in rear-end crashes. *Traffic Inj Prev,* 4**,** 83-90.

FARMER, C. M., ZUBY, D. S., WELLS, J. K. & HELLINGA, L. A. 2008. Relationship of dynamic seat ratings to real-world neck injury rates. *Traffic Inj Prev,* 9**,** 561-7.

FICE, J. B., BLOUIN, J. S. & SIEGMUND, G. P. Seatback rotational control reduces whiplash injury potential: a preliminary computational study. Injury Biomechanics Research - Proceedngs of the Fourtienth International Workshop, October 28th, 2012 2012 Savanah, GA.

HARDER, S., VEILLEUX, M. & SUISSA, S. 1998. The effect of socio-demographic and crash-related factors on the prognosis of whiplash. *J Clin Epidemiol,* 51**,** 377-84.

HELL, W., LANGWIEDER, K. & WALZ, F. Reported Soft Tissue Neck Injuries After Rear-End Car Collisions. 1998 International IROCBI Conference on the Biomechanics of Impact, 1998 Gothenburg, Sweden 261 - 274.

HOFINGER, M., MAYRHOFER, E., GEIGL, B. C., MOSER, A. & STEFFAN, H. Reduction of neck injuries by improving the occupant interaction with the seat back cushion. 1999 International IRCOBI Conference on Biomechanics of Impact, 1999 Sitges, Spain. 201-212.

HOLM, L. W., CARROLL, L. J., CASSIDY, J. D., HOGG-JOHNSON, S., COTE, P., GUZMAN, J., PELOSO, P., NORDIN, M., HURWITZ, E., VAN DER VELDE, G., CARRAGEE, E. & HALDEMAN, S. 2008. The burden and determinants of neck pain in whiplash-associated disorders after traffic collisions: results of the Bone and Joint Decade 2000-2010 Task Force on Neck Pain and Its Associated Disorders. *Spine,* 33**,** S52-9.

HORSLEN, B. C., DAKIN, C. J., INGLIS, J. T., BLOUIN, J.-S. & CARPENTER, M. G. 2015. Modulation of human vestibular reflexes with increased postural threat. *J Physiol,* 592**,** 3671-85.

ICBC 2000. Annual Report. British Columbia: Insurance Company of British Columbia.

ICBC 2006. Annual Report. British Columbia: Insurance Company of British Columbia.

ICBC 2007. Traffic Collision Statistics: Police-attended Injury and Fatal Collisions. British Columbia: Insurance Company of British Columbia.

INSURANCE INSTITUTE OF HIGHWAY SAFETY 2004. Status Report - Special Issue: Protecting Against Neck Injury in Rear Crashes.

INSURANCE INSTITUTE OF HIGHWAY SAFETY 2008a. A Procedure for Evaluating Motor Vehicle Head Restraints (Issue 3). Ruckersville, VA, USA: Research Council for Automobile Repairs.

INSURANCE INSTITUTE OF HIGHWAY SAFETY 2008b. RCAR-IIWPG Seat/head restraint evaluation protocol (version 3). Arlington, VA, USA: Research Council for Automobile Repairs & International Insurance Whiplash Prevention Group.

IVANCIC, P. C. 2011. Does knowledge of seat design and whiplash injury mechanisms translate to understanding outcomes? *Spine (Phila Pa 1976),* 36**,** S187-93.

JAKOBSSON, L., ISAKSSON-HELLMAN, I. & LINDMAN, M. 2008. WHIPS (Volvo Cars' Whiplash Protection System)—The Development and Real-World Performance. *Traffic Injury Prevention,* 9**,** 600-605.

JAKOBSSON, L., LUNDELL, B., NORIN, H. & ISAKSSON-HELLMAN, I. 2000. WHIPS - Volvo's Whiplash Protection Study. *Accid Anal Prev,* 32**,** 307-19.

KANEOKA, K., ONO, K., INAMI, S. & HAYASHI, K. 1999. Motion analysis of cervical vertebrae during whiplash loading. *Spine,* 24**,** 763-9; discussion 770.

KRAFFT, M. 2002. When do AIS 1 neck injuries result in long-term consequences? Vehicle and human factors. *Traffic Inj Prev,* 3**,** 89-97.

KRAFFT, M., KULLGREN, A., MALM, S. & YDENIUS, A. Influence of crash severity on various whiplash injury symptoms: A study based on real-life rear-end crashes with recorded crash pulses. 19th International Technical Conference on the Enhanced Safety of Vehicles (ESV), 2005 Washington, D.C., USA.

KULLGREN, A. & KRAFFT, M. Gender analysis on whiplash seat effectiveness: results from real-world crashes. 2010 International IRCOBI Conference on the Biomechanics of Impact, 2010 Hanover, Germany. 17-28.

KULLGREN, A., KRAFFT, M., LIE, A. & TINGVALL, C. The Effect of Whiplash Protection Systems in Real- Life Crashes and Their Correlation to Consumer Crash Test Programmes. The 20th International Technical Conference on the Enhanced Safety of Vehicles Conference (ESV), 2007 Lyon, France.

LANGWIEDER, K. & HELL, W. 2002. Proposal of an International Harmonized Dynamic Test Standard for Seal/Head Restraints. . *Traffic Inj Prev,* 3**,** 150-158.

LINDER, A., AVERY, M., KRAFFT, M. & KULLGREN, A. Change of velocity and pulse characteristics in rear impacts - Real world and vehicle tests data. The 18th International Technical Conference on the Enhanced Safety of Vehicles, 2003 Nagoya, Japan. Paper No. 285.

LINDER, A., AVERY, M., KRAFFT, M., KULLGREN, A. & SVENSSON, M. Acceleration pulses and crash severity in low velocity rear impacts – Real world data and barrier test. The 17th International Technical Conference on the Enhanced Safety of Vehicles, 2001 Amsterdam, The Netherlands. Paper No. 216.

LUAN, F., YANG, K. H., DENG, B., BEGEMAN, P. C., TASHMAN, S. & KING, A. I. 2000. Qualitative analysis of neck kinematics during low-speed rear-end impact. *Clin Biomech (Bristol, Avon),* 15**,** 649-57.

LUNDELL, B., JAKOBSSON, L., ALFREDSSON, B., JERNSTROM, C. & ISAKSSON-HELLMAN, I. Guidelines for and the desgin of a car seat concept for improved protection against neck injuries in rear end car impacts. Internation Congress and Exposition, February 23-26, 1998 1998a Detriot, Michigan. Society of Automotive Engineers, Inc.

LUNDELL, B., JAKOBSSON, L., ALFREDSSON, B., LINDSTROM, M. & SIMONSSON, L. The WHIPS seat - A car seat for improved protection against neck injuries in rear end impacts. 16th International Technical Conference on the Enhanced Safety of Vehicles, 1998b Windsor, Ontario, Canada.

MACNAB, I. 1971. The "whiplash syndrome". *Orthop Clin North Am, 2***,** 389-403.

MANG, D. W., SIEGMUND, G. P., BROWN, H. J., GOONETILLEKE, S. C. & BLOUIN, J. S. 2015. Loud preimpact tones reduce the cervical multifidus muscle response during rear-end collisions: a potential method for reducing whiplash injuries. *Spine J,* 15**,** 153-61.

MANG, D. W., SIEGMUND, G. P., INGLIS, T. J. & BLOUIN, J. S. 2012. The startle response during whiplash: a protective or harmful response? *J Appl Physiol,* 113**,** 532-40.

MCCONNELL, W. E., HOWARD, R. P., GUZMAN, H. M., BOMAR, J. B., RADDIN, J. H., BENEDICT, J. V., SMITH, H. L. & HATSELL, C. P. Analysis of human test subject kinematic responses to low velocity rear end impacts (930889). Proceedings of the 37th Stapp Car Crash Conference, 1993 San Antonio, Texas. Society of Automotive Engineers, 21-30.

MCCONNELL, W. E., HOWARD, R. P., VAN POPPEL, J., KRAUSE, R., GUZMAN, H. M., BOMAR, J. B., RADDIN, J. H., BENEDICT, J. V. & HATSELL, C. P. Human head and neck kinematic after low velocity rear-end impacts - Understanding "whiplash" (952724). Proceedings of the 39th Stapp Car Crash Conference, 1995 Coronado, CA. Society of Automotive Engineers, 215-238.

MCGUCKIN, N. & FUCCI, A. 2018. Summary of Travel Trends: 2017 National Household Travel Survey. *In:* FEDERAL HIGHWAY ADMINISTRATION (ed.). Washington, DC, USA: U.S. Department of Transportation.

MOORHOUSE, K., DONNELLY, B., KANG, Y.-S., BOLTE, J. H. & HERRIOTT, R. 2012. Evaluation of the internal and external biofidelity of current rear impact ATDs to response targets developed from moderate-speed rear impacts of PMHS. *Stapp Car Crash J,* 56**,** 171-229.

MORDAKA, J. & GENTLE, C. R. Biomechanical analysis of whiplash injuries: Women are not scaled down men., 2003. 4th European LS-DYNA Users Conference.

NATIONAL HIGHWAY TRAFFIC SAFETY ADMINISTRATION 2014. Traffic Safety Facts 2014: A compilation of motor vehicle crash data from the fatality analysis reporting system and the general estimates system. *In:* ANALYSIS, N. C. F. S. A. (ed.). United States Department of Transportation.

NYGREN, A., GUSTAFSSON, H. & TINGVALL, C. 1985. Effect of different types of headrest in rear-end collisions. *In:* NATIONAL HIGHTWAY TRAFFIC SAFERY ADMINISTRATION (ed.) *Tenth Experimental Safert Vehicle Conference.* Washington, DC.: US Department of Transportation.

ORTENGREN, T., HANSSON, H. A., LOVSUND, P., SVENSSON, M. Y., SUNESON, A. & SALJO, A. 1996. Membrane leakage in spinal ganglion nerve cells induced by experimental whiplash extension motion: a study in pigs. *J Neurotrauma,* 13**,** 171-80.

OTREMSKI, I., MARSH, J. L., WILDE, B. R., MCLARDY SMITH, P. D. & NEWMAN, R. J. 1989. Soft tissue cervical spinal injuries in motor vehicle accidents. *Injury,* 20**,** 349-51.

PEARSON, A. M., IVANCIC, P. C., ITO, S. & PANJABI, M. M. 2004. Facet joint kinematics and injury mechanisms during simulated whiplash. *Spine,* 29**,** 390-7.

QUINLAN, K. P., ANNEST, J. L., MYERS, B., RYAN, G. & HILL, H. 2004. Neck strains and sprains among motor vehicle occupants-United States, 2000. *Accid Anal Prev,* 36**,** 21-7.

RHULE, D., RHULE, H. & DONNELLY, B. 2005. The Process of Evaluation and Documentation of Crash Test Dummies for Part 572 of the Code of Federal Regulations. *The 19th International Technical Conference on the Enhanced Safety of Vehicles (ESV).* Washington, D.C., USA: Paper No. 05-0284.

ROMILLY, D. P., LUK, H., XING, P., WHITE, M. & DESAPRIYA, E. Whiplash Prevention Campaign Initiative: Development of an Observational Protocol for Proper Head Restraint Use. *In:* PROFESSIONALS, C. A. O. R. S., ed. 21st Canadian Multidisciplinary Road Safety Conference, May 8 - 11, 2011 2011 Halifax, Nova Scoitia.

ROMILLY, D. P. & SKIPPER, C. 2005. Seat structural design choices and the effect on occupant injusty potential in rear end collisions. *SAE International Journal of Passenger Cars - Mechanical Systems,* 114**,** 1512-1520.

SAE 1995. Surface Vehicle Recommended Practice. *Instrumentation for impact test - Part 1 - Electronic Instrumentation.* Warendale, PA, USA: Society of Automotive Engineers.

SCHMITT, K.-U., MUSER, M. H. & NIEDERER, P. F. A new injury criterion candidate for rear-end collisions taking into account shear forces and bending moments. 17th Enhanced Safety of Vehicles (ESV) Conference, 2001 Amsterdam, Netherlands.

SCHMITT, K.-U., MUSER, M. H., WALZ, F. H. & NIEDERER, P. F. 2002. Nkm - A proposal for a neck protection criterion for low-speed rear-end impacts. *Traffic Inj Prev,* 3**,** 117-126.

SEKIZUKA, M. Seat Designs for Whiplash Injury Lessening. *In:* NHTSA, ed. 16th International Technical Conference on the Enhansced Safety of Vehicles, May 31st - June 4th, 1998 1998 Windsor, ON, Canada. 1570-78.

SEVERY, D., MATHEWSON, J. & CO, B. 1955. Controlled automovile rear-end collisions, an investigation of related engineering and medical phenomena. *Can Serv Med J.,* 11**,** 727-759.

SIEGMUND, G. P., BAILEY, M. N. & KING, D. J. Characteristics of Specific Automobile Bumpers in Low-Velocity Impacts. Paper #940916. *In:* ENGINEERS., S. O. A., ed. Proceedings of the Thirty Eighth Stapp Car Crash

Conference, February 28 - March 4rd, 1994 1994 Detroit, Michigan, ISA. SAE Technical Paper Series.

SIEGMUND, G. P., BLOUIN, J. S., CARPENTER, M. G., BRAULT, J. R. & INGLIS, J. T. 2008a. Are cervical multifidus muscles active during whiplash and startle? An initial experimental study. *BMC Musculoskeletal Disorders,* 9.

SIEGMUND, G. P., BRAULT, J. R. & WHEELER, J. B. 2000. The relationship between clinical and kinematic responses from human subject testing in rear-end automobile collisions. *Accid Anal Prev,* 32**,** 207-17.

SIEGMUND, G. P., DAVIS, M. B., QUINN, K. P., HINES, E., MYERS, B. S., EJIMA, S., ONO, K., KAMIJI, K., YASUKI, T. & WINKELSTEIN, B. A. 2008b. Head-turned postures increase the risk of cervical facet capsule injury during whiplash. *Spine,* 33**,** 1643-9.

SIEGMUND, G. P., HEINRICHS, B. E., CHIMICH, D. D., DEMARCO, A. L. & BRAULT, J. R. 2005a. The effect of collision pulse properties on seven proposed whiplash injury criteria. *Accid Anal Prev,* 37**,** 275-85.

SIEGMUND, G. P., HEINRICHS, B. E., CHIMICH, D. D. & LAWRENCE, J. 2005b. Variability in vehicle and dummy responses in rear-end collisions. *Traffic Inj Prev,* 6**,** 267-77.

SIEGMUND, G. P., HEINRICHS, B. E. & WHEELER, J. B. 1999. The influence of head restraint and occupant factors on peak head/neck kinematics in low-speed rear-end collisions. *Accid Anal Prev,* 31**,** 393-407.

SIEGMUND, G. P., KING, D. J., LAWRENCE, J. M., WHEELER, J. B., BRAULT, J. R. & SMITH, T. A. Head/neck kinematic response of human subjects in low-speed rear-end collisions (973341). Proceedings of the 41st Stapp Car Crash Conference, 1997 Warrendale, PA. Society of Automotive Engineers, 357-385.

SIEGMUND, G. P., MYERS, B. S., DAVIS, M. B., BOHNET, H. F. & WINKELSTEIN, B. A. 2001. Mechanical evidence of cervical facet capsule injury during whiplash: a cadaveric study using combined shear, compression, and extension loading. *Spine,* 26**,** 2095-101.

SIEGMUND, G. P., WINKELSTEIN, B. A., IVANCIC, P. C., SVENSSON, M. Y. & VASAVADA, A. 2009. The anatomy and biomechanics of acute and chronic whiplash injury. *Traffic Inj Prev,* 10**,** 101-12.

SPITZER, W. O., SKOVRON, M. L., SALMI, L. R., CASSIDY, J. D., DURANCEAU, J., SUISSA, S. & ZEISS, E. 1995. Scientific monograph of the Quebec Task Force on Whiplash-Associated Disorders: redefining "whiplash" and its management. *Spine,* 20**,** 1S-73S.

STEMPER, B. D., YOGANANDAN, N. & PINTAR, F. A. 2006. Effect of head restraint backset on head-neck kinematics in whiplash. *Accid Anal Prev,* 38**,** 317-23.

STERNER, Y. & GERDLE, B. 2004. Acute and chronic whiplash disorders--a review. *J Rehabil Med,* 36**,** 193-209; quiz 210.

STIGSON, H., YDENIUS, A. & KULLGREN, A. 2006. Variation of Crash Severity and Injury Risk Depending on Collision with Different Vehicle Types and Objects. *International Research Council on Bioechanics of Injury* Madrid, Spain.

SUISSA, S., HARDER, S. & VEILLEUX, M. 2001. The relation between initial symptoms and signs and the prognosis of whiplash. *Eur Spine J,* 10**,** 44-9.

SVENSSON, M. Y., ALDMAN, B., LOVSUND, P., HANSSON, H. A., SEEMAN, T., SUNESON, A. & ORTENGREN, T. Pressure effects in the spinal canal during whiplash extension motion - a possible cause of injury to the cervical spinal ganglia. 1993 International IRCOBI Conference on the Biomechanics of Impact, 1993 Eindhoven, Netherlands. 189-200.

SVENSSON, M. Y., BOSTROM, O., DAVIDSSON, J., HANSSON, H. A., HALAND, Y., LOVSUND, P., SUNESON, A. & SALJO, A. 2000. Neck injuries in car collisions--a review covering a possible injury mechanism and the development of a new rear-impact dummy. *Accid Anal Prev,* 32**,** 167-75.

SVENSSON, M. Y., LOVSUND, P., HALAND, Y. & LARSSON, S. 1996. The influence of seat-back and head-restraint properties on the head-neck motion during rear-impact. *Accid Anal Prev,* 28**,** 221-7.

TODMAN, D. H. 2007. Whiplash injuries: A historical review. *The Internet Journal of Neurology,* 8.

TREMPEL, R. E., ZUBY, D. S. & EDWARDS, M. A. 2016. IIHS head restraint ratings and insurance injury claim rates. *Traffic Inj Prev,* 17**,** 590-6.

VASAVADA, A. N., BRAULT, J. R. & SIEGMUND, G. P. 2007. Musculotendon and fascicle strains in anterior and posterior neck muscles during whiplash injury. *Spine,* 32**,** 756-65.

VERSTEEGEN, G. J., KINGMA, J., MEIJLER, W. J. & TEN DUIS, H. J. 2000. Neck sprain after motor vehicle accidents in drivers and passengers. *Eur Spine J,* 9**,** 547-52.

VIANO, D. C. 2002. Head restraint position during normal driving: implications to neck injury risks in rear crashes. *Role of seat in rear crash safety.* Warrendale, PA, USA: Society of Automotive Engineers, Inc.

VIANO, D. C. 2003a. Effectiveness of High-Retention Seats in Preventing Fatality: Initial Results and Trends. *Society of Automotive Engineers,* SAE 2003-01-1351.

VIANO, D. C. 2003b. Influence of seat properties on occupant dynamics in severe rear crashes. *Traffic Inj Prev,* 4**,** 324-36.

VIANO, D. C. 2003c. Seat influences on female neck responses in rear crashes: a reason why women have higher whiplash rates. *Traffic Inj Prev,* 4**,** 228-39.

VIANO, D. C. 2003d. Seat properties affecting neck responses in rear crashes: a reason why whiplash has increased. *Traffic Inj Prev,* 4**,** 214-27.

VIANO, D. C. 2008. Seat design principles to reduce neck injuries in rear impacts. *Traffic Inj Prev,* 9**,** 552-60.

VIANO, D. C. & OLSEN, S. 2001. The effectiveness of active head restraint in preventing whiplash. *J Trauma,* 51**,** 959-69.

VIANO, D. C. & PARENTEAU, C. S. 2015. Update on the effectiveness of high retention seats in preventing fatal injury in rear impacts. *Traffic Inj Prev,* 16**,** 154-8.

WIKLUND, K. & LARSSON, H. 1997. SAAB active head restraint (SAHR) - seat design to reduce the risk of neck injuries in rear impacts. Warrendale, PA, USA.

WINKELSTEIN, B. A. & MYERS, B. S. 2000. Experimental and computational characterization of three-dimensional cervical spine flexibility. *Stapp Car Crash J,* 44**,** 139-58.

WINKELSTEIN, B. A., NIGHTINGALE, R. W., RICHARDSON, W. J. & MYERS, B. S. 2000. The cervical facet capsule and its role in whiplash injury: a biomechanical investigation. *Spine,* 25**,** 1238-46.

WINKELSTEIN, B. A. & SANTOS, D. G. 2008. An intact facet capsular ligament modulates behavioral sensitivity and spinal glial activation produced by cervical facet joint tension. *Spine,* 33**,** 856-62.

ZADOR, P., KRAWCHUK, S. & VOAS, R. 2000. FInal Report - Automotive Collision Avoidance System (ACAS) Program. *In:* ADMINISTRATION, N. H. T. S. (ed.). Kokomo, IN, USA: Delphi-Delco Electronic Systems.

Appendix A: Experimental Anti-Whiplash Seat Design

Proof-of-Concept Seat Hinge Rotation Computation Study

In a preliminary computational study, Fice et al. (2013) modelled the feed-forward dynamic control of seat hinge rotation to quantify the potential reduction in occupant kinematics for the Experimental anti-whiplash seat. A model of a simplified 2002 Pontiac Grand Am seat was combined with a model of a Hybrid III anthropomorphic test device (ATD) in LS-Dyna (LSTC, Livermore, CA, USA) to simulate three rear impact speed changes: Δv = 8km/h, 12km/h and 16 km/h (Fice et al., 2012, Romilly and Skipper, 2005). The seat pan and the seatback were de-coupled in the simulation to allow for feed-forward control of seat hinge rotations. The input seat hinge rotation profiles were parameterized and optimized to find the minimum peak forward resultant acceleration of the first thoracic vertebrae (T1) ($a_{resultant\text{-}T1}$) using LS-OPT (LSTC, Livermore, CA, USA). When compared to a standard unmodified seat, the optimized seat hinge rotational profiles reduced $a_{resultant\text{-}T1}$ of the ATD by 58%, 57%, and 59% for rear impact speed changes of 8km/h, 12 km/h and 16 km/h, respectively (Fice et al., 2012). This preliminary study provided a proof-of-concept for the feed-forward control of the seat hinge rotation to reduce $a_{resultant\text{-}T1}$ responses and, potentially, reduce the risk of whiplash injuries during rear-end collisions. Due to differences in the ATD tested and the simplified model of the automotive seat, the results from this preliminary study did not directly transfer to testing of the Experimental anti-whiplash seat but did provide insight to the design of the experiments.

Experimental Anti-Whiplash Seat

The active Experimental anti-whiplash seat consisted of a modified General Motors High Retention seat (GMHR; front passenger seat from a 2004 Pontiac Grand Am) and several motors to control seat hinge rotation and seatback cushion deformation (total mass = 191 kg, **Figure A1** and **A2**). The seat pan and head restraint of the GMHR seat remained unmodified in this design. The seatback consisted of a rigid aluminum outer frame. Depending on the experiment, the seatback cushion from a GMHR seatback was either rigidly mounted to this outer frame (**Chapter 3** and **Appendix B**) or suspended across the outer frame from side-to-side by 47 mm wide seatbelt straps (see **Figure 4.2**; **Chapter 4** and **5**, and **Appendix C** and **D**). To dynamically control seat hinge rotations (**Chapter 3** and **5**), two large rotational servomotors (AKM52K, Kollmorgen, Waltham, MA, USA) connected to helical right-angle gearheads (VTR014-035, 35:1 gear ratio, Thomson Linear, Radford, VA, USA) were mounted on both sides of the seat hinge. These motors were geared to rotate in unison (one in a positive direction and the other in a negative direction) and had a maximum rated speed of 157 revolutions per minute (RPM) (942 deg/s) with a maximum rated torque of 3.90 Nm. Rotation of the seatback was limited from vertical (0 deg) to 50 deg rearward. Initial seatback angle was set to 27 deg rearward from vertical (Siegmund et al., 2005a).

To dynamically control seatback cushion deformation (**Chapter 4** and **5**), three rotational servomotors (AKM24D, Kollmorgen, Waltham, MA, USA) connected to helical right-angle gearheads (VTR006-008, 8:1 gear ratio, Thomson Linear, Radford, VA, USA) were mounted staggered to both sides of the rigid seatback. The seatback motors were capable of rotating at

speeds of 1000 RPM (6000 deg/s) with a maximum torque of 1.11 Nm. These motors were placed at the top, middle and bottom of the seatback and attached to 47 mm wide seatbelt straps that spanned across the perimeter frame to separately control the seatback cushion deformation at the upper-torso, mid-torso and lower pelvis regions (see **Figure 4.2**). Tightening the webbing would pull the suspended GMHR upper seatback cushion towards the front of the seat (+X direction) and increase the apparent stiffness of the seatback; whereas, loosening the webbing would allow the seatback cushion to translate towards the rear of the seat (-X direction) and allow for deeper occupant penetration into the seatback. For all tests, the upper-torso motor was locked in a stationary position and effectively created a hinge point at the upper back to promote pocketing of the pelvis into the seatback. Rotation of the mid-torso and pelvis seatback motors were physically limited from a taut seatbelt strap position of 0 deg to a spooled out loose webbing position of 200 deg. Initial seatback position was set with the mid-torso spooled out by 22 deg and pelvis motors spooled out by 25 deg to achieve an initial seatback angle of 27 deg.

All 5 motors (2 seat hinge and 3 seatback) were controlled independently by separate digital servo drives (Servostar 600, Kollmorgen, Waltham, MA, USA) connected to two NI UMI 7774 universal motion interface and a NI PXI 7350 motion controller (National Instruments Corporation, Austin, Texas, USA). A custom LabVIEW program (National Instruments Corporation, Austin, Texas, USA) was created to send commands to, monitor the status of and record encoder data directly from these motors.

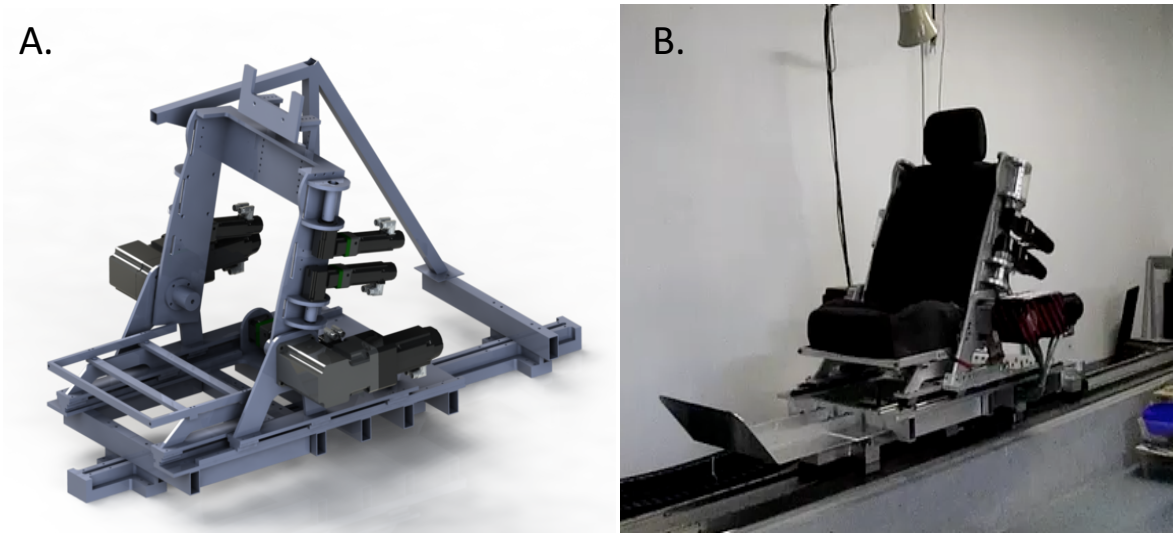

Figure A1. Images of the novel active anti-whiplash automotive seat. A.) preliminary computer aided design (CAD) model and B.) working prototype.

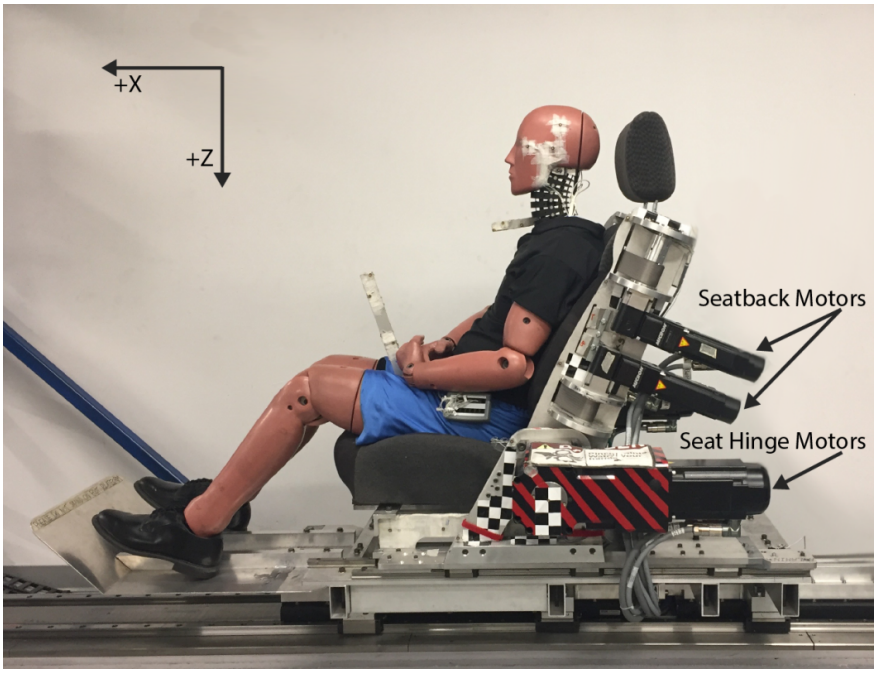

Figure A2. Photograph of the experimental set-up with the BioRID II ATD on the experimental anti-whiplash automotive seat and laboratory reference frame (X, Z). Motors mounted to the seat hinge control seatback hinge rotations; whereas, motors mounted to the seatback control seatback cushion deformations.

Summary

An in-depth literature review revealed a limited number of published studies or research into the development of automotive seats safety devices for injury prevention. Thus, there is a need to understand and determine how different seat hinge rotation or seatback cushion deformation parameters affected occupant responses. Combining parameters such as peak amplitude, initial angular velocity, and onset will create rotation and deformation profiles to define how fast, how far and when either the seat hinge will rotate or the seatback cushion will deform. Other rotation and deformation profile parameters such as profile shape and the pressence of a "pre-perturbation supportive" pulse should also be investigated. These parameters of the seat hinge rotation and seatback deformation will be further investigated in subsequent Appendices to define rotation and deformation profiles to be used throughout experiments presented in this dissertation.

Appendix B: Creating the Seat Hinge Rotation Profile

The goal of this appendix was to develop a seat hinge rotation profile that best reduce whiplash-evoked ATD responses. This appendix summarizes the key steps undertaken to create the active seat hinge rotation profiles used in Experiment 2 (**Chapter 3**). The natural seat hinge response observed from the Control General Motor's High Retention seat (GMHR) during a 12 km/h perturbation was used as a template for the preliminary seat hinge rotation profile (**Figure B1**). This preliminary profile was then modified to only include the retraction phase (onset of seat hinge rotation to peak rearward head angle) and to prevent the seat from rebounding. The timing of the input seat hinge rotation profile was delayed by 20 ms to account for the internal backlash of the motors and gearheads. The resulting input seat hinge rotation profile (**Figure B1**) had a peak rearward angle ($\theta_{rearward\text{-}peak}$) of 5.7 deg, an initial angular velocity ($\omega_{rearward\text{-}int}$) of 8.5 deg/s, and an onset of seat hinge rotation ($t_{rearward\text{-}onset}$) 30 ms after the collision onset. This initial input rotation profile was used as the starting point from which the parameters for a seat hinge rotation profile were isolated and methodically evaluated through a series of five experiments. For all five experiments, a standard GMHR seatback was rigidly mounted to the outer seatback frame to isolate the effects of varying seat hinge rotation on ATD responses during a 12 km/h collision speed with a pulse duration (Δt) of 208 ms. A Control trial on a standard GMHR seat was included to provide baseline ATD responses and to compare against the Experimental profiles.

To quantify the ATD responses, the focus was on nine peak ATD kinematic and kinetic responses ($a_{X\text{-}head}$, $a_{X\text{-}T1}$, $\omega_{Y\text{-}head}$, F_X, F_Z, M_Y, $\theta_{head,}$ R_X and $\Delta t_{head\text{-}contact}$) and three peak neck injury

criteria (NIC, N_{km}, and N_{ij}) responses. Within each response variable, the different profiles were ranked, and then the profile with the lowest averaged rank across all 12 variables was identified as the best profile. A Friedman test determined if there was a significant difference between the average rank of the different profiles (chi-squared value: χ^2, degrees of freedom: df, and the significance level: p). A post-hoc, pair-wise multiple comparison test was then performed on the results of the Friedman test to determine differences between the individual profiles. All tests were performed using predefined functions (`friedman` and `multcompare`) in Matlab using $\alpha = 0.05$.

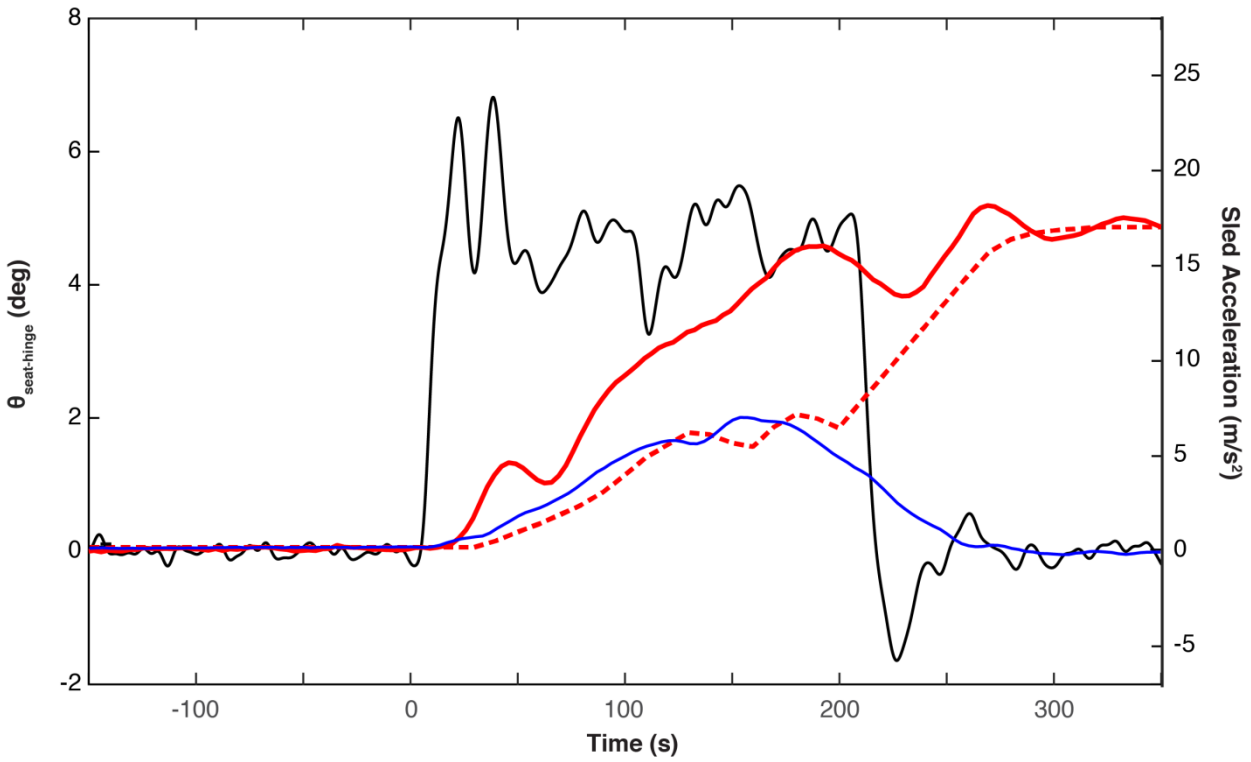

Figure B1. Rearward seat hinge rotations ($\theta_{seat\text{-}hinge}$) for the Control (blue line) and Experimental seat (red solid line) during a 12 km/h collision severity perturbation with a collision pulse duration (Δt) of 208 ms. The dotted red line illustrates the input $\theta_{seat\text{-}hinge}$ profile to the Experimental seat to generate the output $\theta_{seat\text{-}hinge}$ response (solid red line) used as the initial seat hinge rotation profile for Part 1.

Experiment 1: Effects of Individual Seat Hinge Parameters

In this first experiment, the effects of three seat hinge rotation ($\theta_{seat\text{-}hinge}$) parameters (peak angle, initial angular velocity and onset) were isolated and evaluated to determine specific parameters that best reduced ATD responses. Peak rearward angle ($\theta_{rearward\text{-}peak}$), initial angular velocity ($\omega_{rearward\text{-}int}$) and onset ($t_{rearward\text{-}onset}$) of seat hinge rotation defined the maximum rearward angle (negative rotation about the laboratory Y-axis reference frame), the speed at which the seat hinge initially rotated and the timing of when the seat hinge started to rotate, respectively. When varying the effects of one of the seat hinge rotation parameters, the other two rotation parameters remained unchanged at their initial values (**Figure B1**).

Peak Seat Hinge Angle

Peak seat hinge angle was varied from 2.5 to 52 deg from the initial seating position of 27 deg rearward (**Figure B2A** & **B2B**). To achieve these peak angles, the amplitude of the initial seat hinge rotation profile was scaled by 50, 100, 300, 500, 700 and 900% and resulted in $\theta_{rearward\text{-}peak}$ of 2.5, 5.7, 17, 29, 41 and 52 deg. Exemplar experimental data from ATD head and torso acceleration ($a_{X\text{-}head}$ and $a_{X\text{-}T1}$: **Figure B2D** & **B2E**, respectively) and neck injury criteria (NIC: **Figure B2F**) as well as their respective peak ATD response (**Figure B2G – B2I**) showed elevated responses for larger peak seat hinge angle trials. A Friedman test revealed a significant difference between trials (1 Control and 6 Experimental, $\chi^2 = 46.29$, df = 6, $p < 0.001$). The Experimental trial with a $\theta_{rearward\text{-}peak} = 5$ deg had the lowest mean ranked score for all ATD responses and neck injury criteria. This reduction, however, was not significantly different from the Control trial, but was significantly different from larger rearward rotations ($\theta_{rearward\text{-}peak} \geq 29$

deg, $p < 0.001$) (**Figure B2C)**. These results suggested that future implementations and studies do not require large peak rearward rotation of the seatback. Smaller rearward rotation angles prevent the seat from impinging into the cabin space of the rear passengers and lowers the risk of occupants ramping up and ejecting out of the automotive seat. Thus, a peak $\theta_{rearward\text{-}peak}$ of 5.7 deg was selected for subsequent testing in the development of the Experimental anti-whiplash seat.

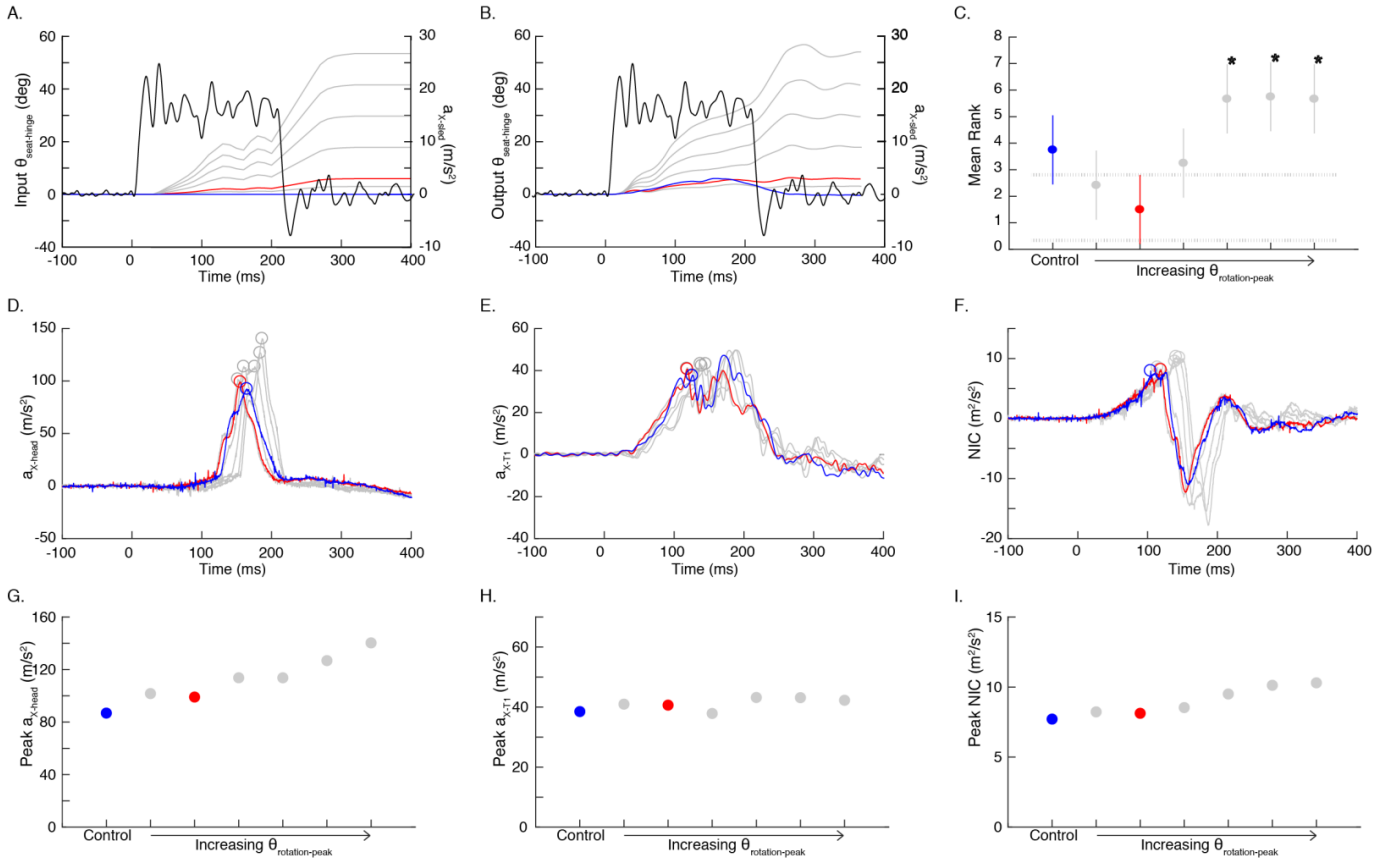

Figure B2. ATD responses to the Control seat (blue lines and markers) and the Experimental seat with various amplitudes of seat hinge rotation ($\theta_{seat\text{-}hinge}$; grey and red lines and markers) during a 12 km/h collision severity (Δt = 208 ms, black lines, right axis, Panels **A** & **B**). The red lines and markers indicate the seat hinge peak angle parameter selected for further testing. Panels (**A**) and (**B**), respectively, show the programmed input and resulting output seat hinge rotations for the Experimental seat with increasing $\theta_{rearward\text{-}peak}$. The results of the post-hoc test (**C**) determined the mean rank of each trial as well as any significant differences (*) between the selected seat hinge rotation parameter trial (red) and the Control or other Experimental trials. Exemplar ATD responses (**D – F**) and their corresponding peak responses (**G-I**) for head and torso accelerations in the X-direction ($a_{X\text{-}head}$ & $a_{X\text{-}T1}$) and neck injury criteria (NIC), respectively.

Initial Seat Hinge Angular Velocity

Initial seat hinge rotation velocity was important because if the rotation was too slow, the ATD would hit the seatback cushion and rebound forward. Conversely if the rotation was too fast, an air gap may form between the seat and the ATD reducing the support provided by the seatback. Initial seat hinge rotation velocities varied from 3.8 to 12.2 deg/s by expanding or contracting the initial seat hinge rotation profile in time. The time-stretched or -shortened rotation profiles resulted in $\omega_{rearward\text{-}int}$ of 3.8, 5.1, 6.2, 8.5, 9.5, and 12.2 deg/s (**Figure B3A** & **B3B**). Exemplar raw data and peak responses of $a_{X\text{-}head}$, $a_{X\text{-}T1}$, and NIC showed lower peak responses with slower initial seat hinge rotation velocities (**Figure B3D – B3I**). The Friedman test revealed a significant difference between all tested trials (1 Control and 6 Experimental, χ^2 = 38.76, df = 6, $p < 0.001$). In comparison to the Control trial, $\omega_{rearward\text{-}int}$ = 3.8 deg/s trial had a lower mean rank across all ATD responses and neck injury criteria ($p = 0.001$, **Figure B3C**). Slower initial seat hinge rotation velocity may be more beneficial as it allows the occupant to penetrate deeper into the seatback to further dissipate the forces and accelerations experienced by the occupant. Thus, an initial angular velocity of 3.8 deg/s was selected for subsequent testing as an effective initial velocity.

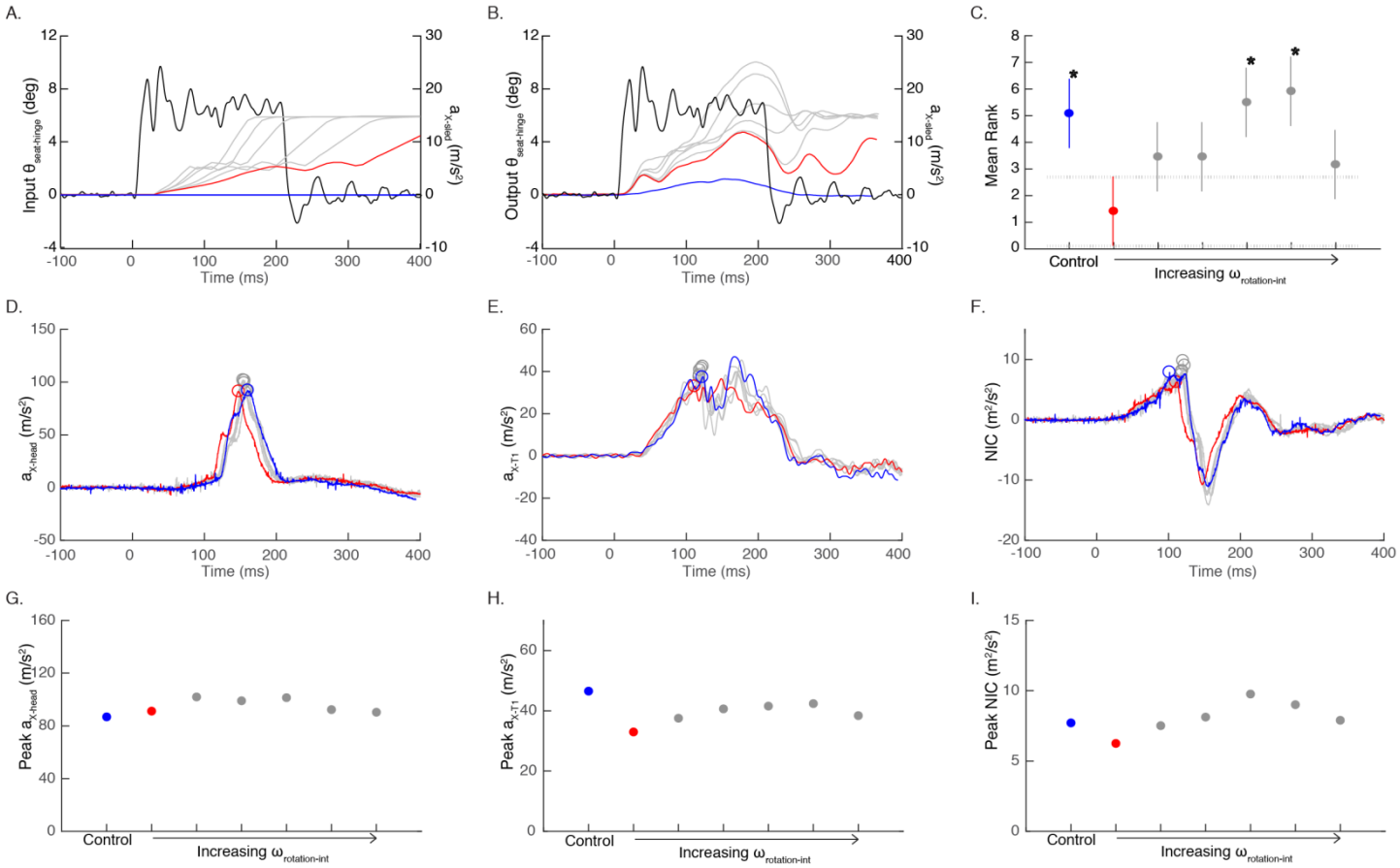

Figure B3. ATD responses to the Control seat (blue lines and markers) and the Experimental seat with various initial velocities of seat hinge rotation ($\theta_{seat\text{-}hinge}$; grey and red lines and markers) during a 12 km/h collision severity (Δt = 208 ms, black lines, right axis, Panels **A** & **B**). The red lines and markers indicate the seat hinge initial angular velocity parameter selected for further testing. Panels (**A**) and (**B**), respectively, show the programmed input and resulting output seat hinge rotations for the Experimental seat with increasing $\omega_{rearward\text{-}int}$. The results of the post-hoc test (**C**) determined the mean rank of each trial as well as any significant differences (*) between the selected seat hinge rotation parameter trial (red) and the Control or other Experimental trials. Exemplar ATD responses (**D – F**) and their corresponding peak responses (**G-I**) for head and torso accelerations in the X-direction ($a_{X\text{-}head}$ & $a_{X\text{-}T1}$) and neck injury criteria (NIC), respectively.

Seat Hinge Rotation Onset

The seat hinge rotation onset determined whether the seat hinge whiplash mitigation system would be a predictive (seat hinge onset before the onset of the whiplash perturbation: $t_{rearward\text{-}onset} < 0$ ms) or a reactive (seat hinge onset after the onset of the whiplash perturbation: $t_{rearward\text{-}onset} > 0$ ms) system. Similar to the effects of initial seat hinge angular velocity, pilot trials showed that $t_{rearward\text{-}onset}$ occurring before the collision onset ($t_{rearward\text{-}onset} < 0$ ms) would create an air gap between the seat and ATD; whereas, a delayed $t_{rearward\text{-}onset}$ ($t_{rearward\text{-}onset} > 80$ ms) would cause the ATD to rebound prematurely away from the seatback. Thus, the $t_{rearward\text{-}onset}$ parameters were tested through a narrow range of onsets between 10 ms to 70 ms after whiplash collision by shifting the initial seat hinge rotation profile ($t_{rearward\text{-}onset}$ = 10, 30, 50 and 70 ms; **Figure B4A** & **B4B**). Exemplar data and peak responses of $a_{X\text{-}head}$, $a_{X\text{-}T1}$, and NIC showed little differences between Control and Experimental trials (**Figure B4D – B4I**. The Friedman test, however, revealed a significant difference between all tested trials (1 Control and 4 Experimental, $\chi^2 = 9.96$, df = 4, p = 0.04), but the post-hoc test showed no differences between any of the trials (p > 0.12) (**Figure B4C**). Consequently, a $t_{rearward\text{-}onset}$ = 30 ms, the original time delay for the unmodified Control GMHR seat, was selected for subsequent experiments.

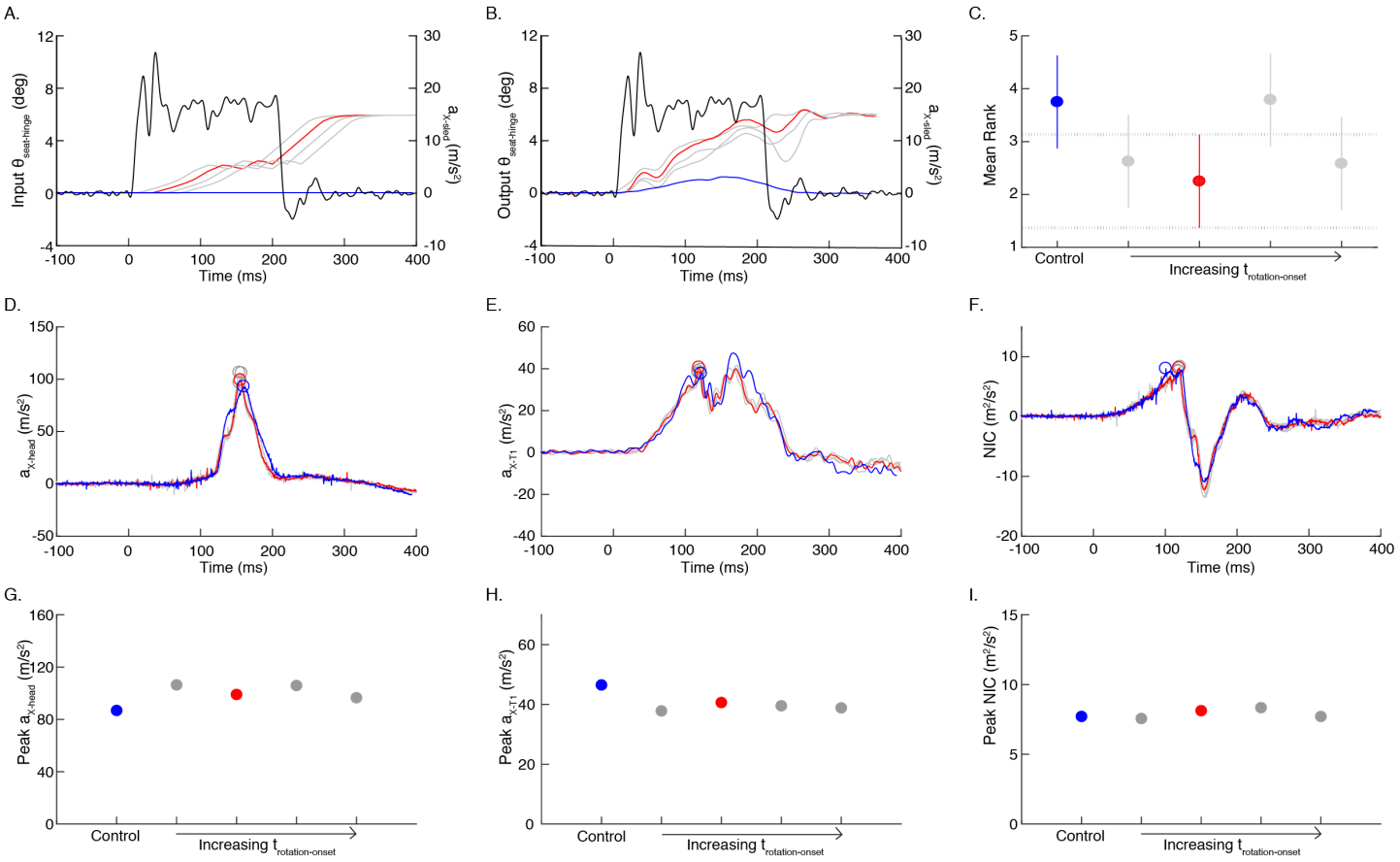

Figure B4. ATD responses to the Control seat (blue lines and markers) and the Experimental seat with various onsets of seat hinge rotation ($\theta_{seat\text{-}hinge}$; grey and red lines and markers) during a 12 km/h collision severity (Δt = 208 ms, black lines, right axis, Panels **A** & **B**). The red lines and markers indicate the seat hinge rotation onset parameter selected for further testing. Panels (**A**) and (**B**), respectively, show the programmed input and resulting output seat hinge rotations for the Experimental seat with increasing $t_{rearward\text{-}onset}$. The results of the post-hoc test (**C**) determined the mean rank of each trial as well as any significant differences (*) between the selected seat hinge rotation parameter trial (red) and the Control or other Experimental trials. Exemplar ATD responses (**D – F**) and their corresponding peak responses (**G-I**) for head and torso accelerations in the X-direction ($a_{X\text{-}head}$ & $a_{X\text{-}T1}$) and neck injury criteria (NIC), respectively.

Experiment 2: Verification of Ideal Seat Hinge Rotation Profile

The goal of Experiment 2 was to verify that the seat hinge rotation profile determined in Experiment 1 ($\theta_{rearward\text{-}peak}$ = 5.7 deg, $\omega_{rearward\text{-}int}$ = 3.8 deg/s, and $t_{rearward\text{-}onset}$ = 30 ms) was a local minimum that best reduced ATD responses. In this experiment, the Control trial (blue lines and markers; **Figure B5**) and the seat hinge rotation profile from Experiment 1 (red lines and markers; **Figure B5**) were compared to 24 additional profile with different combination of seat hinge rotation parameters tested in Experiment 1 ($\theta_{rearward\text{-}peak}$ = 2.4, 5.7, 17, 29, 41 and 52 deg, $\omega_{rearward\text{-}int}$ = 3.8, 5.1, 6.2, 8.5, 9.5, and 12.2 deg/s and $t_{rearward\text{-}onset}$ = 10, 30, 50, and 70 ms; **Figure B5A** & **B5B)**. The Friedman test revealed a significant difference between all tested trials (1 Control and 25 Experimental, χ^2 = 139.67., df = 25, $p < 0.001$). The multiple comparison test further confirmed that the mean rank of the trial with seat hinge rotation profile determined in Experiment 1 (red lines and markers) was ranked significantly lower than the Control and Experimental trials with larger and faster seat hinge rotation profiles (**Figure B5C**). This experiment showed that the current seat hinge rotation profile determined in Experiment 1 best reduced ATD responses following low-speed, rear-end collisions (Δv = 12 km/h, Δt =208 ms).

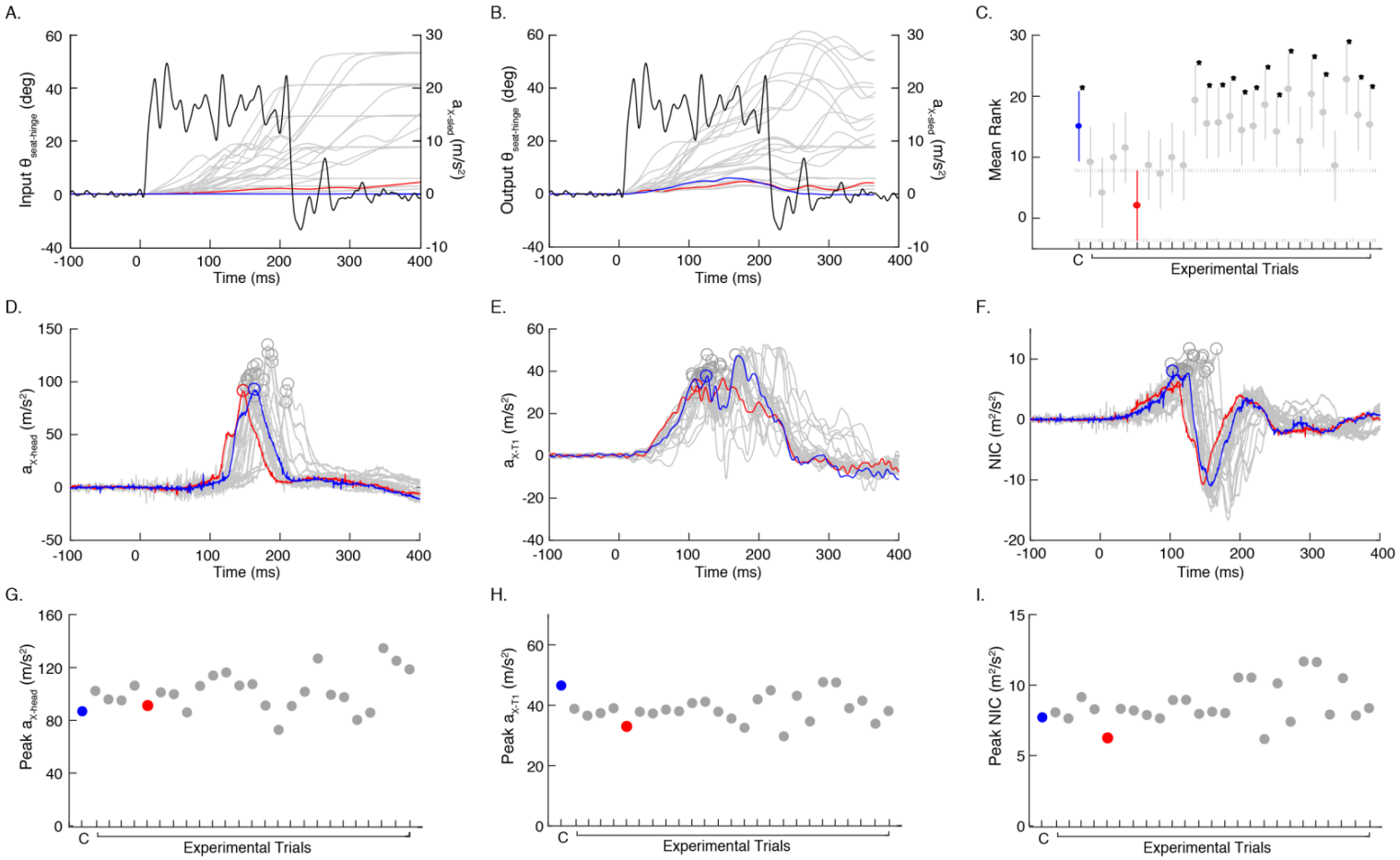

Figure B5. ATD responses to the Control seat (blue lines and markers) and the Experimental seat with various seat hinge rotation profiles ($\theta_{seat\text{-}hinge}$; grey and red lines and markers) during a 12 km/h collision severity (Δt = 208 ms, black lines, right axis, Panels **A** & **B**). The red lines and markers indicate the seat hinge rotation profile selected for further testing. Panels (**A**) and (**B**), respectively, show the programmed input and resulting output seat hinge rotations for all the different Experimental trials. The results of the post-hoc test (**C**) determined the mean rank of each trial as well as any significant differences (*) between the selected seat hinge rotation parameter trial (red) and the Control or other Experimental trials. Exemplar ATD responses (**D – F**) and their corresponding peak responses (**G-I**) for head and torso accelerations in the X-direction ($a_{X\text{-}head}$ & $a_{X\text{-}T1}$) and neck injury criteria (NIC), respectively.

Experiment 3. Effect of Pulse Shape

The seat hinge rotation profile was initially programmed to mimic the retraction phase of the seat hinge rotation observed from an unmodified Control GMHR seat (**Figure B1**). To simplify future implementations of the seatback rotation profile, the shape of the seat hinge rearward rotation profile was converted into a sigmoidal curve while preserving $\theta_{rearward\text{-}peak}$, $\omega_{rearward\text{-}int}$, and $t_{rearward\text{-}onset}$ parameters (**Figure B6**). Twenty-four additional sigmoidal-shaped profiles were then tested and compared to the Control trial (blue lines and markers) as well as the seat hinge rearward rotation profile from previous Experiments 1 & 2 (green lines and markers; $\theta_{rearward\text{-}peak}$ = 5.7 deg, $\omega_{rearward\text{-}int}$ = 3.8 deg/s, and $t_{rearward\text{-}onset}$ = 30 ms) (**Figure B7A** & **B7B**). The Friedman test showed a significant difference between all tested trials (1 Control and 25 Experimental, χ^2 = 217.94., df = 25, $p < 0.001$). However, the post-hoc test showed that the simplified sigmoidal curve of the seat hinge rotation profile from Experiment 1 & 2 (**Figure B6)** was not ranked significantly different from either the Control trial or the previously tested profile in Experiment 1 & 2 **(Figure B7C**). Despite the new sigmoidal profile not reducing overall ATD responses and neck injury criteria as well as the previously test seat hinge rotation profile, the sigmoidal curve would be easier to implement in future implementations of the Experimental anti-whiplash seat. Thus, this new sigmoidal-shaped seat hinge rotation profile was chosen for future experiment.

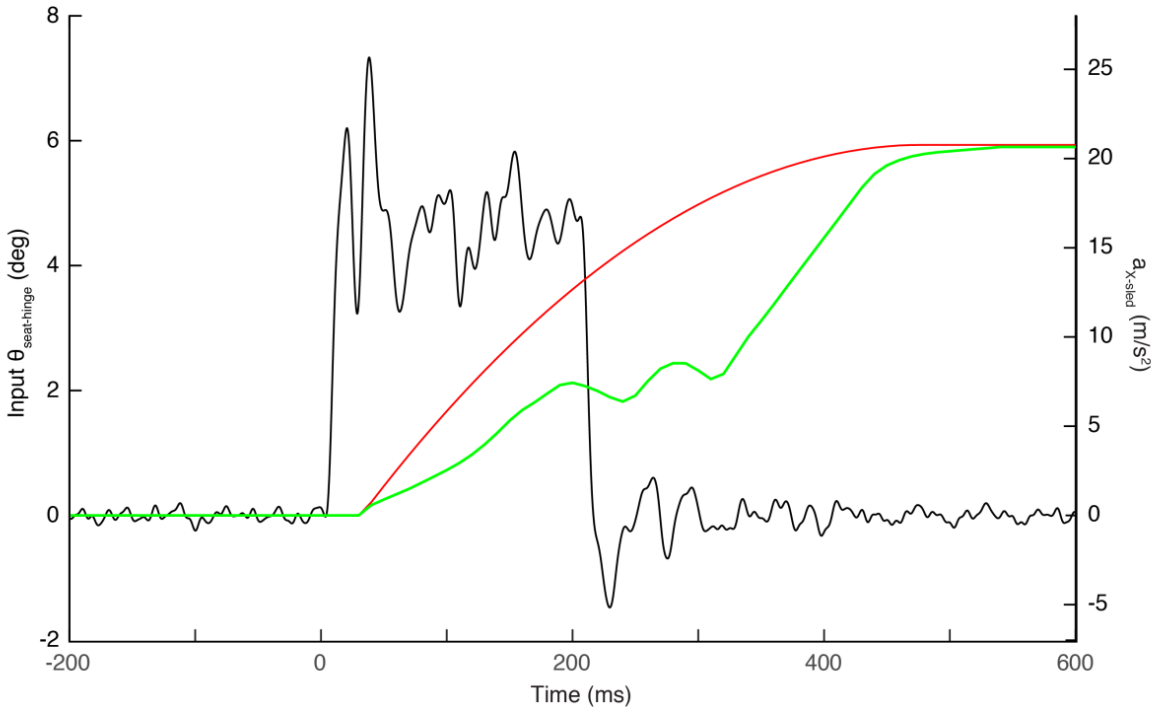

Figure B6. Seat hinge rotation ($\theta_{seat\text{-}hinge}$) input signals for the seat hinge rotation profile determined previously (green line, Experiments 1 & 2) and the new simplified sigmoidal shape curve (red line) during a 12 km/h collision severity (Δt = 208 ms, black lines, right axis).

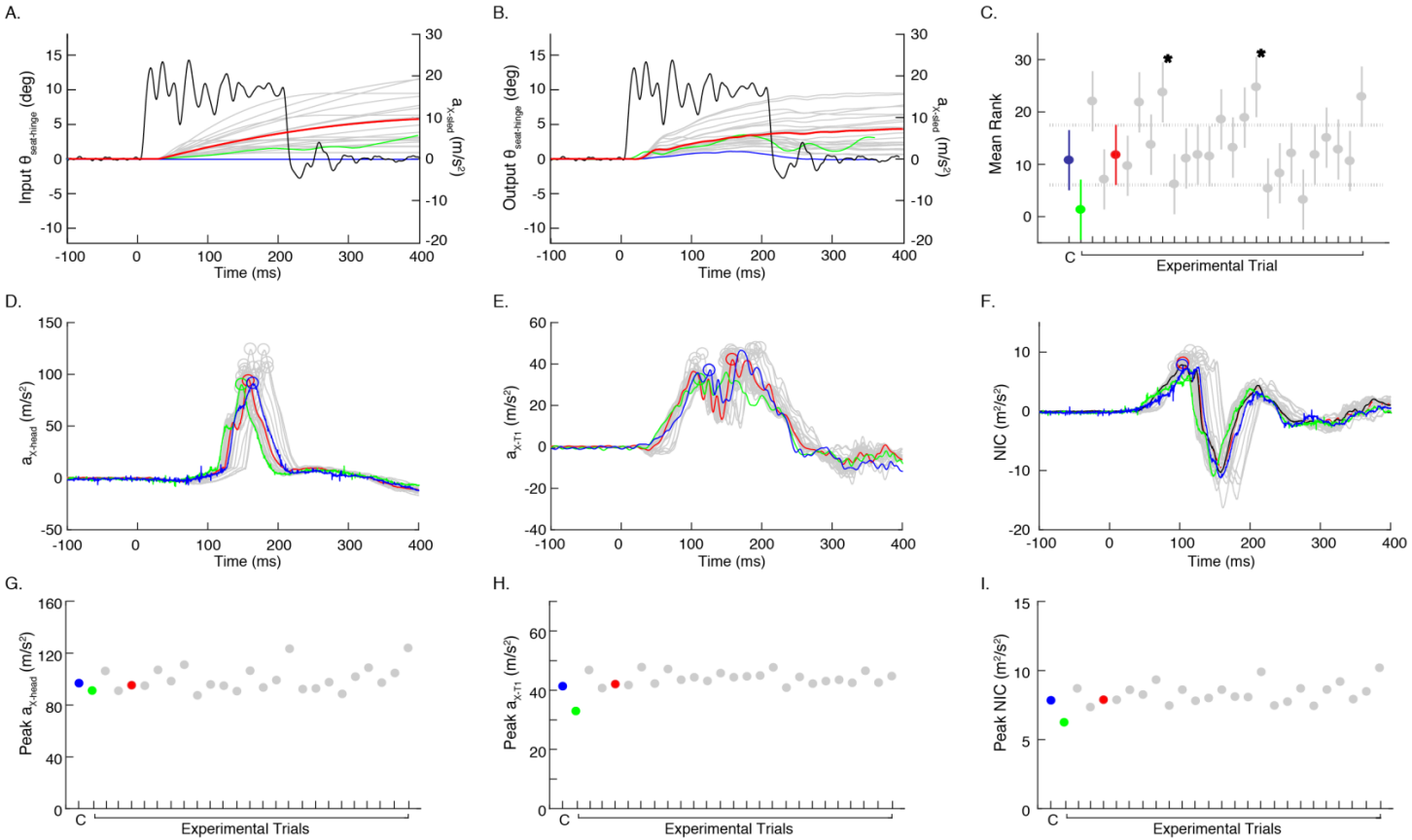

Figure B7. ATD responses to the Control seat (blue lines and markers), the Experimental seat with the seat hinge rotation ($\theta_{seat\text{-}hinge}$) profile determined previously in Experiments 1 & 2 (green lines and markers), and the Experimental seat with various simplified sigmoidal seat hinge rotation profiles (grey and red lines and markers) during a 12 km/h collision severity (Δt = 208 ms, black lines, right axis, Panels **A** & **B**). The red lines and markers indicate the sigmoidal seat hinge rotation profile selected for further testing. Panels (**A**) and (**B**), respectively, show the programmed input and resulting output seat hinge rotations for all the different Experimental trials. The results of the post-hoc test (**C**) determined the mean rank of each trial as well as any significant differences (*) between the selected seat hinge rotation parameter trial (red) and the Control or other Experimental trials. Exemplar ATD responses (**D – F**) and their corresponding peak responses (**G-I**) for head and torso accelerations in the X-direction ($a_{X\text{-}head}$ & $a_{X\text{-}T1}$) and neck injury criteria (NIC), respectively.

Experiment 4: Pre-Perturbation Forward Rotation

To better maintain proper head and neck alignment, we investigated whether dynamically rotating the seat forward towards the occupant (a negative rotation about the Y-axis) prior to the collision would engage the occupant earlier and reduce their responses. The pre-perturbation forward rotation of the seatback was elicited prior to the collision to ensure that the occupant was supported as early as possible. By rotating the seatback forward, the head-to-head-restraint distance would potentially decrease, and the occupant's torso would be better coupled with the seatback throughout the collision. The pre-perturbation rotation onset ($t_{forward\text{-}onset}$) was set at -90 ms prior to the collision. Previous analysis into the biomechanics of rear-end collisions showed that the ATD and the seat remained relatively stationary for the first 60 to 80 ms of the collision following the onset of bumper contact (McConnell et al., 1993, McConnell et al., 1995, Severy et al., 1955). By accounting for the detection and processing time of existing pre-crash avoidance systems (i.e. radar sensors with an operating range of 5 to 200 m, range rate limits of 37 to 70 m/s, and range rate accuracy of 0.25 m/s; Zador et al., 2000)), the Experimental anti-whiplash seat should be able to activate the pre-perturbation rotation at a $t_{forward\text{-}onset}$ = -90 ms prior to onset of the collision.

To determine the effect of the pre-perturbation forward rotation only, the Control trial (blue lines and markers) were compared against the sigmoidal-shaped rearward seat hinge rotation only profile from the previous experiment (green lines and markers) and three peak forward rotation profiles ($\theta_{forward\text{-}peak}$ = -2.9, -4.7, and -8.1 deg, $t_{forward\text{-}onset}$ = -90 ms; **Figure B8A** & **B8B**). During the collision, the Experimental seat was programmed to stop at the maximum

forward angle and was only allowed to return to the normal resting position after the collision. The Friedman test showed a significant difference between all tested trials (1 Control and 4 Experimental, $\chi^2 = 46.2.$, df = 4, $p < 0.001$). Post-hoc analysis revealed that both the -4.7 and -8.1 deg forward pre-perturbation rotations generated ATD responses that were ranked significantly lower than both the Control trial and the rearward only rotation profile (**Figure B8C)**. Thus, a $\theta_{forward\text{-}peak}$ of -4.7 deg would be a beneficial addition to the seat hinge rotation profile as it did not push the ATD too far forward and, yet, reduced peak ATD responses (**Figure B8D – B8I**).

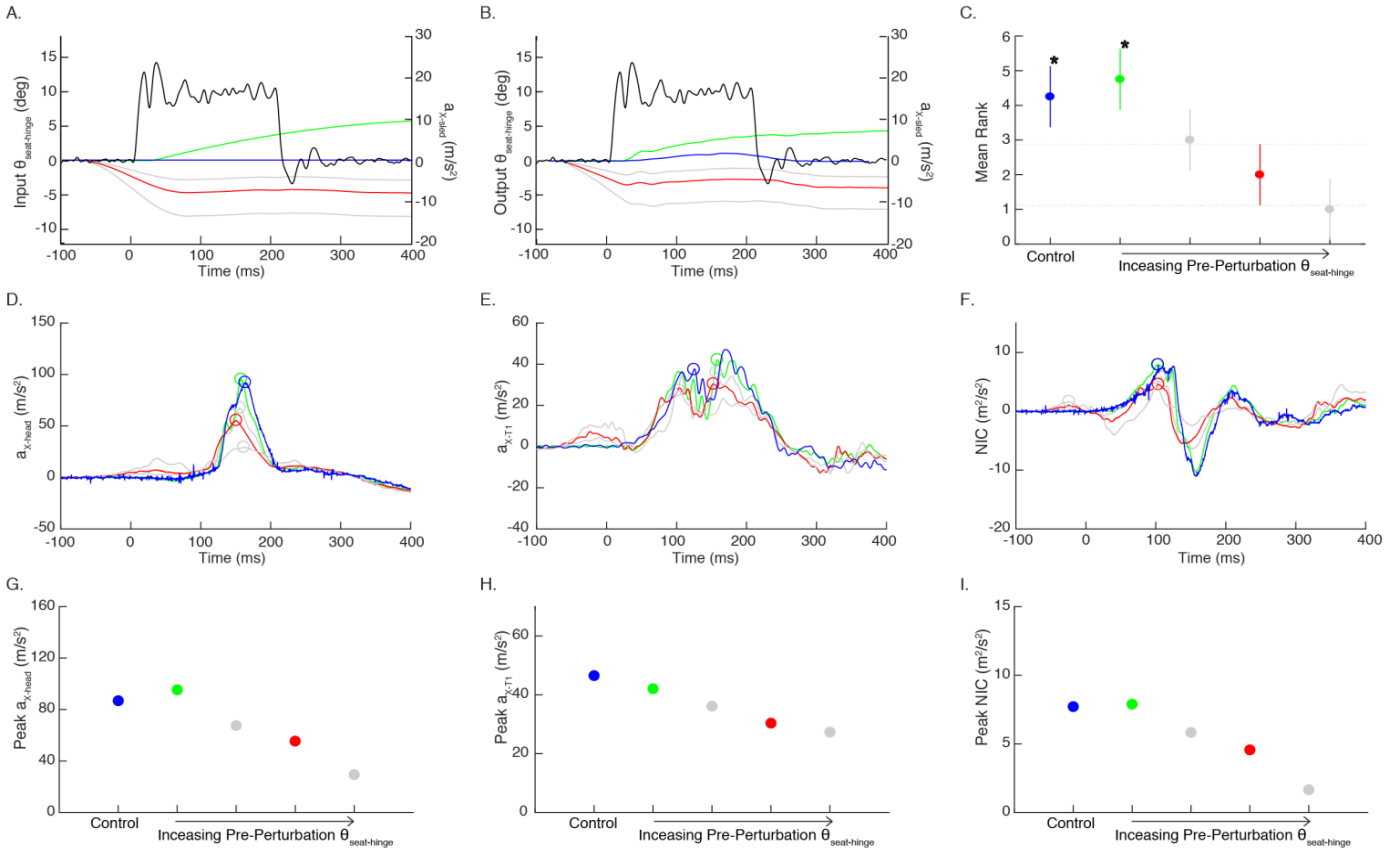

Figure B8. ATD responses to the Control seat (blue lines and markers), the Experimental seat with the sigmoidal rearward rotation profile (green lines and markers, Experiment 3), and the Experimental seat with increasing angles of pre-perturbation only forward seat hinge rotation ($\theta_{seat\text{-}hinge}$; grey and red lines and markers) during a 12 km/h collision severity (Δt = 208 ms, black lines, right axis, Panels **A** & **B**). The red lines and markers indicate the pre-perturbation seat hinge rotation parameter selected for subsequent testing. Panels (**A**) and (**B**), respectively, show the programmed input and resulting output seat hinge rotations for the Experimental seat with increasing forward pre-perturbation $\theta_{seat\text{-}hinge}$ angles. The results of the post-hoc test (**C**) determined the mean rank of each trial as well as any significant difference between the selected seat hinge rotation parameter trial (red) and the Control or other Experimental trials. Exemplar ATD responses (**D – F**) and their corresponding peak responses (**G-I**) for head and torso accelerations in the X-direction ($a_{X\text{-}head}$ & $a_{X\text{-}T1}$) and neck injury criteria (NIC), respectively.

Experiment 5: Final seat hinge profile combination

In this last experiment, the pre-perturbation rotation profile was combined with the sigmoidal rearward rotation profile determined from Experiment 3. Peak forward angles ($\theta_{forward\text{-}peak}$ = -2.9, -4.7, -5.6, -6.5, -7.2 and -8.1 deg, $t_{forward\text{-}onset}$ = -90 ms, **Figure B9A** & **B9B**) combined with the rearward rotation profile were compared to the Control seat (blue lines and markers) and the rearward seat hinge rotation only profile (green lines and markers). In combining the rearward rotation profile with the forward pre-perturbation rotation, the onset of the rearward rotation was delayed by 60 ms to a $t_{rearward\text{-}onset}$ of 90ms after the onset of sled acceleration. The exemplar data and peak responses of $a_{X\text{-}head}$, $a_{X\text{-}T1}$, and NIC showed graded decreasing ATD responses with increase forward pre-perturbation seat hinge angle (**Figure B93D – B9I**). The Friedman test showed a significant difference between all tested trials (1 Control and 7 Experimental, χ^2 = 70.58., df = 7, $p < 0.001$). Post-hoc comparison showed that forward pre-perturbations of -5.6 deg and greater generated ATD responses that were ranked significantly lower than both the Control trial and the rearward only rotation profile (**Figure B9C)**. Rotating the seat forward supported the occupant earlier in the collision and the subsequent rearward rotation further helped to reduce the accelerations and forces applied to the ATD's head and torso. This combined movement of forward and backward seat hinge rotation reduced head and torso accelerations, upper neck forces and moments, head rearward rotation angle and retraction as well as all neck injury criteria between 23% and 48% in comparison to the Control seat. A $\theta_{forward\text{-}peak}$ of -5.6 deg (red lines and markers, **Figure B9**) was selected for further testing because this peak angle was the lowest forward angle to show a significant difference in mean rank from the Control and rearward seat hinge rotation only

trials. This lower peak $\theta_{forward\text{-}peak}$ may also be easier to implement in the future development of the anti-whiplash seat.

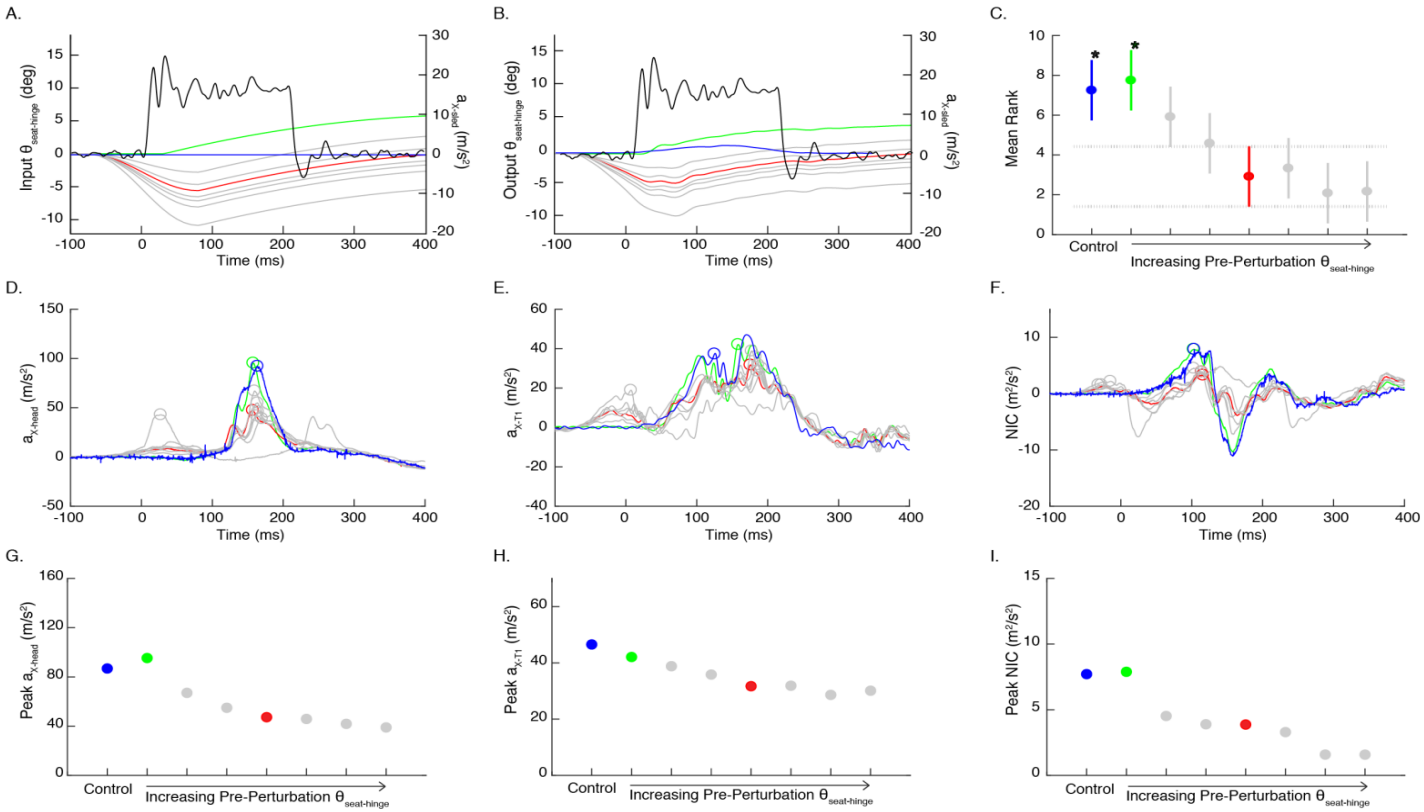

Figure B9. ATD responses to the Control seat (blue lines and markers), the Experimental seat with the sigmoidal rearward rotation profile ($\theta_{seat\text{-}hinge}$; green lines and markers, Experiment 3), and the Experimental seat with a combination of increasing amplitudes of pre-perturbation forward seat hinge angle and the rearward rotation profile (grey and red lines and markers) during a 12 km/h collision severity (Δt = 208 ms, black lines, right axis, Panels **A** & **B**). The red lines and markers indicate the pre-perturbation seat hinge rotation parameter selected for subsequent testing. Panels (**A**) and (**B**), respectively, show the programmed input and resulting output seat hinge rotations for the Experimental seat with increasing forward pre-perturbation $\theta_{seat\text{-}hinge}$ amplitudes. The results of the post-hoc test (**C**) determined the mean rank of each trial as well as any significant difference between the selected seat hinge rotation parameter trial (red) and the Control or other Experimental trials. Exemplar ATD responses (**D – F**) and their corresponding peak responses (**G-I**) for head and torso accelerations in the X-direction ($a_{X\text{-}head}$ & $a_{X\text{-}T1}$) and neck injury criteria (NIC), respectively.

Summary

A seat hinge rotation profile has been defined to investigate the effects of dynamic seat hinge rotation during low-speed, rear-end collisions. This dynamic seat hinge rotation (**Figure B10**, grey line) was programmed to rotate the seatback forward ($t_{forward\text{-}onset}$) -90 ms before the collision to a peak pre-perturbation forward angle ($\theta_{forward\text{-}peak}$) of -5.6 deg and then rotate the seatback rearward to a peak rearward angle ($\theta_{rearward\text{-}peak}$) of 5.7 deg at an initial angular velocity ($\omega_{rearward\text{-}int}$) of 3.8 deg/s occurring 90 ms ($t_{rearward\text{-}onset}$) after the collision onset. The observed output seat hinge rotation (**Figure B10**, red line) resulted in a pre-perturbation $\theta_{forward\text{-}peak}$ of -3.6 deg occurring at a $t_{forward\text{-}onset}$ of -90 ms followed by the rearward seat hinge rotation with a $\theta_{rearward\text{-}peak}$ of 3.6 deg occurring at a $t_{rearward\text{-}onset}$ of 40 ms.

The seat hinge rotation profile includes two components: a 'pre-perturbation' forward rotation followed by a rearward rotation. To determine the individual contribution of each component and the combined effect of the components, the peak responses to the following seat hinge rotation pulses were compared: 1. 'Rearward Rotation Only' (Experiment 3: $\theta_{rearward\text{-}peak}$ = 5.7 deg, $\omega_{rearward\text{-}int}$ = 3.8 deg/s, and $t_{rearward\text{-}onset}$ = 30 ms), 2. 'Pre-Perturbation Rotation Only' (Experiment 4: $\theta_{forward\text{-}peak}$ = -4.7 deg, $t_{forward\text{-}onset}$ = -90 ms), and 3. the 'Combination' of the selected pre-perturbation forward rotation, followed by rearward rotation (Experiment 5; $\theta_{forward\text{-}peak}$ = -5.6 deg, $t_{forward\text{-}onset}$ = -90 ms, $\theta_{rearward\text{-}peak}$ = 5.7 deg, $\omega_{rearward\text{-}int}$ = 3.8 deg/s, and $t_{rearward\text{-}onset}$ = 90 ms). In the 'Pre-Perturbation Rotation Only' condition, the selected $\theta_{rearward\text{-}peak}$ = -5.7 deg amplitude was not tested and, thus, the $\theta_{rearward\text{-}peak}$ = -4.7 deg trial was used in this comparison. All peak responses were normalized to the Control seat to allow for comparison

between seat hinge rotation profiles (**Table B1**). In comparison to the Control trial, the 'Rearward Rotation Only' profile generated 2% - 19% larger peak responses in most ATD responses and only decreased $a_{X\text{-}T1}$, N_{ij}, N_{km}, and $\Delta t_{head\text{-}restraint}$ peak responses by -0.8% to -9.6%. from Control. The 'Pre-Perturbation Rotation Only' and the 'Combination' seat hinge rotation profiles decreased peak responses by 11% to 53% and 23% to 48%, respectively, from the Control trial (**Figure B8** and **Figure B9**). These larger decreases observed from Control seat in trials that included a pre-perturbation forward seat hinge rotation suggested the pre-perturbation rotation may be the key component generating these reduced ATD responses and neck injury criteria responses.

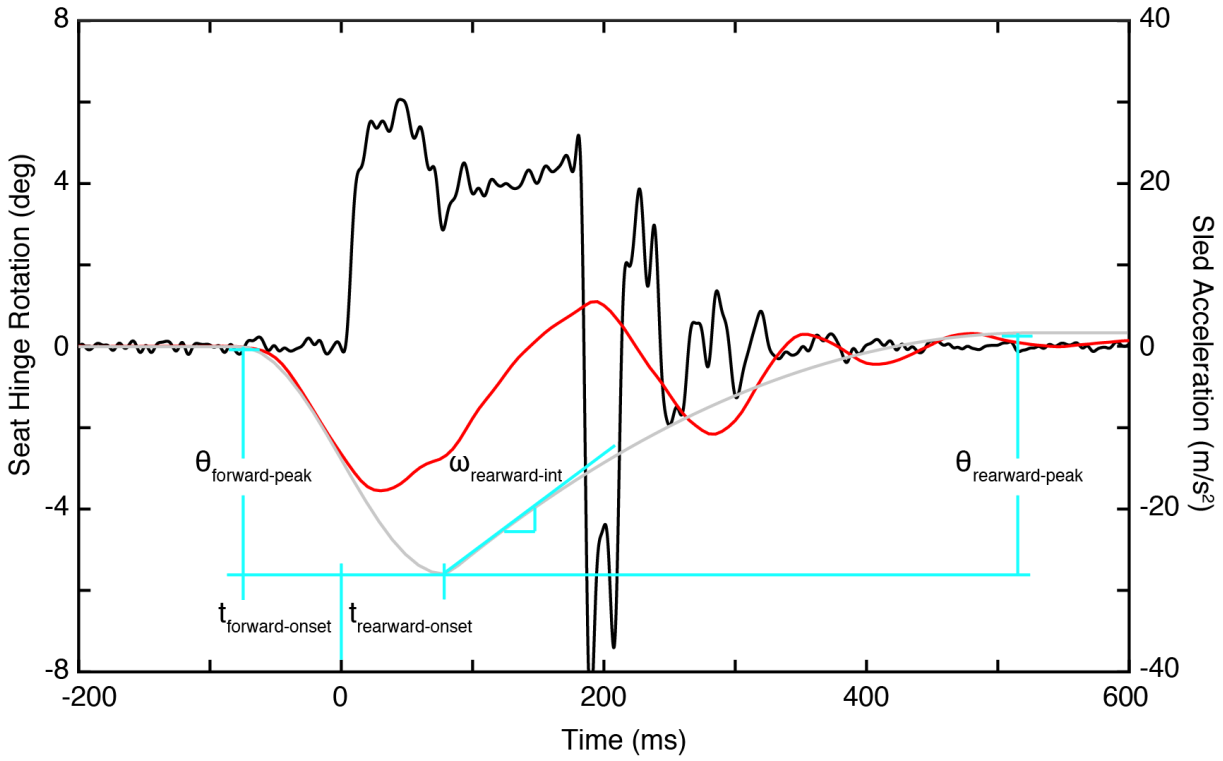

Figure B10. The programed input seat hinge rotation profile (grey line) and the observed output seat hinge rotation (red line) of the anti-whiplash seat during a 12 km/h perturbation (black line, right axis). The cyan lines illustrated measurements of each seat hinge rotation parameter used to define the input rotation profile (onset delay of pre-perturbation forward rotation: $t_{forward\text{-}onset}$, peak pre-perturbation forward angle: $\theta_{forward\text{-}peak}$, peak rearward angle: $\theta_{rearward\text{-}peak}$, initial rearward angular velocity: $\omega_{rearward\text{-}int}$, and onset delay of rearward rotation: $t_{rearward\text{-}onset}$). This figure is a repeat of **Figure 3.2**.

Table B1. Comparing percentage decreases of normalized Experimental conditions from Control seat for 'Rearward Rotation Only', forward 'Pre-Perturbation Rotation Only' and the 'Combination' of the two different rotational components.

Condition	$a_{X\text{-}head}$	$a_{X\text{-}T1}$	F_X	F_Z	M_Y	$\omega_{Y\text{-}head}$	θ_{head}	NIC	N_{ij}	N_{km}	R_X	$\Delta t_{head\text{-}contact}$
Rearward Rotation Only	9.8	-9.6	2.4	18.6	4.7	-5.8	5.8	2.3	-4.3	-4.4	4.2	-0.8
Pre-Perturbation Rotation Only	-36.1	-34.7	-34.4	-45.4	-47.1	44.5	-52.7	-40.8	-46.4	-41.7	-41.7	-10.5
Combination	--43.2	-23.3	-33.3	-35.2	-43.2	45.0	-41.4	-47.8	-29.4	-41.3	-39.3	-33.5

Appendix C: Creating the Seatback Cushion Deformation Profile

The goal of this appendix was to develop a seatback cushion deformation profile that best reduce whiplash-evoked ATD responses. This appendix summarizes a series of three experiments undertaken to create the active seatback cushion deformation profiles used in Experiment 3 (**Chapters 4**). In all three experiments, the ATD was seated in the Experimental anti-whiplash seat and exposed to a series of perturbations with a collision severity of 12 km/h (Δt = 195 ms). Rigid metal braces were installed between the seatback and the base of the sled to prevent the seatback from rotating and to isolate only the effects of seatback cushion deformation (**Figure C1**). For these experiments, a standard GMHR seatback was suspended across the rigid seatback by seatbelt straps attached to the three seatback motors (upper-torso, mid-torso and pelvis). For all tests, the upper-torso motor was locked in a stationary position and effectively created a hinge point at the upper back to promote pocketing of the pelvis into the seatback.

A motion capture system (Optotrak Certus, Northern Digital, Waterloo, ON, Canada) was used to estimate the deformation of the seatback cushion during the perturbation because slack in the straps induced by the two lower seatback motors did not correspond with the physical penetration of the occupant. Maximum rearward penetration of the ATD T1 ($d_{penetration\text{-}T1}$) and pelvis ($d_{penetration\text{-}pelvis}$) were defined as the horizontal displacement (along the global X-axis, **Figure C1**) of the T1 vertebra and pelvis infrared light emitting diode (IRED) markers relative to the seatback. Rearward displacement deeper into the seatback was defined

as negative values and forward rebound away from the seat was defined as positive values. The initial position of the ATD was set as $d_{penetration\text{-}T1}$ = 0 mm and $d_{penetration\text{-}pelvis}$ = 0 mm.

A sigmoidal-shaped profile was used as a template for the seatback motors. The input seatback cushion deformation profile rotated the seatback motors and gear head combination to a peak angle ($\theta_{deformation\text{-}peak}$) of 56 deg with an initial angular velocity ($\omega_{deformation\text{-}int}$) of 228 deg/s. Preliminary experiments showed little effect of seatback cushion deformation on ATD responses when the seatback motors onset time ($t_{deformation\text{-}onset}$) occurred 30 ms after the collision onset. However, decreased ATD responses were observed when $t_{deformation\text{-}onset}$ was shifted to -130 ms before the collision onset. The initial seatback cushion deformation profile to the motors ($\theta_{deformation\text{-}peak}$ = 56 deg, $\omega_{deformation\text{-}int}$ = 228 deg/s, $t_{deformation\text{-}onset}$ = -130ms) generated occupant penetration into the seatback of $d_{penetration\text{-}T1}$ = -78 mm, and $d_{penetration\text{-}pelvis}$ = -75 mm. This rotation profile was used as the starting point from which the parameters for a seatback cushion deformation profile were isolated and evaluated through a series of three experiments. In addition to the Control GMHR seat used in **Appendix B**, a No Motion condition which consisted of the Experimental seat with rigid metal braces and the seat hinge and seatback motors locked in their initial position was also tested.

Nine peak kinematic and kinetic ($a_{X\text{-}head}$, $a_{X\text{-}T1}$, $\omega_{Y\text{-}head}$, F_X, F_Z, M_Y, $\theta_{head,}$ R_X and $\Delta t_{head\text{-}contact}$) and three peak neck injury criteria (NIC, N_{km}, and N_{ij}) responses were selected to quantify the ATD responses. Within each response variable, the different profiles were ranked, and then the profile with the lowest averaged rank across all 12 variables was identified as the best profile. A Friedman test determined if there was a significant difference between the average rank of the

different profiles (chi-squared value: χ^2, degrees of freedom: df, and the significance level: p). A post-hoc, pair-wise multiple comparison test was then performed on the results of the Friedman test to determine differences between individual profiles. All tests were performed using predefined functions (`friedman` and `multcompare`) in Matlab using $\alpha = 0.05$.

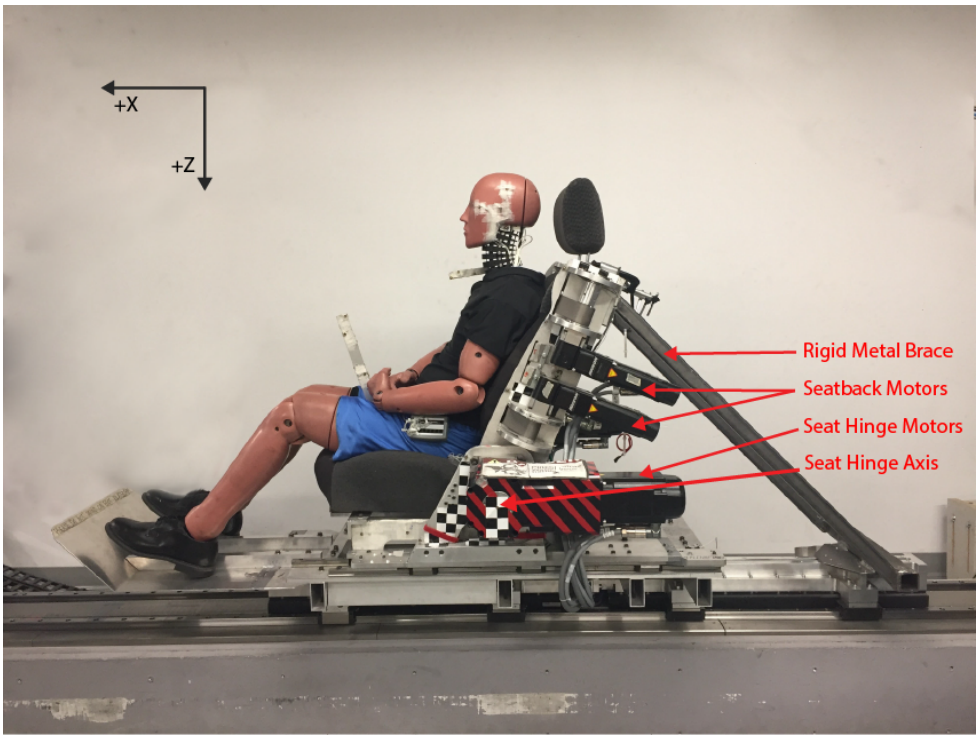

Figure C1. Photograph of the experimental set-up with the BioRID II ATD on the Experimental anti-whiplash automotive seat and rigid metal braces to prevent seat hinge rotation. The global laboratory reference frame is illustrated with positive X-axis forward and positive Z-axis downwards. The seat hinge and seatback motors on the left side of the Experimental seat are labelled. Additional seat hinge and seatback motors are located on the right side of the seat (not labelled). The seat hinge motors are not used in this current appendix. This figure is a repeat of **Figure 4.1**.

Experiment 1: Effects of Individual Seatback Parameters

The effects of three seatback motor rotation parameters (peak amplitude, initial angular velocity and onset) were evaluated to determine specific parameters that best reduced ATD responses. Each parameter of the initial profile was sequentially varied to determine its effect on the ATD responses. In these experiments, the seatback motor rotation parameters defined the characteristics of a motor pulley that controlled the deformation of the seatback cushion. Thus, a motion capture system (Optotrak Certus, Northern Digital, Waterloo, ON, Canada) was used to estimate the deformation of the seatback cushion during the perturbation because the rotation of the seatback motors did not correspond with the physical penetration of the occupant. However, these seatback motor rotation parameters were used to define the seatback deformation profile because they were manipulated to provide a repeatable profile.

Peak Seatback Motor Angle

The first parameter varied was peak angle of the seatback motors from 28 to 168 deg from the initial resting position (mid-torso motor: 22 deg and pelvis motor: 25 deg, where 0 deg is defined as a taut seatbelt) (**Figure C2A**). To achieve these peak rotations, the amplitude of the initial seatback motor profile was scaled by 50, 100, 150, 200, 250 and 300% and resulted in $\theta_{deformation\text{-}peak}$ of 28, 56, 84, 112, 140 and 168 deg. Increasing $\theta_{deformation\text{-}peak}$ led to increased peak $d_{penetration\text{-}pelvis}$ and had little effect on peak $d_{penetration\text{-}T1}$. Exemplar ATD head acceleration ($a_{X\text{-}head}$) and neck injury criteria (NIC) data showed decreasing peak responses with increased $\theta_{deformation\text{-}peak}$; whereas, peak T1 acceleration ($a_{X\text{-}T1}$) remained similar across all test conditions (**Figure C3)**. A Friedman test showed a significant difference between all tested trials (1 Control

seat, 1 No Motion and 6 Experimental conditions, $\chi^2 = 53.43$, df = 7, $p < 0.001$). The profile with a $\theta_{deformation\text{-}peak}$ = 168 deg, which generated occupant penetration at T1 ($d_{penetration\text{-}T1}$) of -81.6 mm and at the pelvis ($d_{penetration\text{-}pelvis}$) of -93.7 mm, received the lowest mean rank score for all ATD responses and neck injury criteria (**Figure C2C** & **C2D**). Post-hoc comparisons showed that this ranked score was significantly lower than the Control seat, the No Motion condition and $\theta_{deformation\text{-}peak} \leq 84$ deg profiles (multiple $p \leq 0.024$) (**Figure C2B)**. These results suggested that larger $\theta_{deformation\text{-}peak}$ better reduced occupant responses despite similar $a_{X\text{-}T1}$ levels across all conditions. Deeper penetration of the occupant into the seatback may delay the onset of torso acceleration and decrease the head-to-head-restraint distance to better support the head and neck during the collision. Subsequent experiments to determine the seatback motor deformation profile will be conducted at the largest tested seatback motor angle of $\theta_{deformation\text{-}peak}$ = 168 deg.

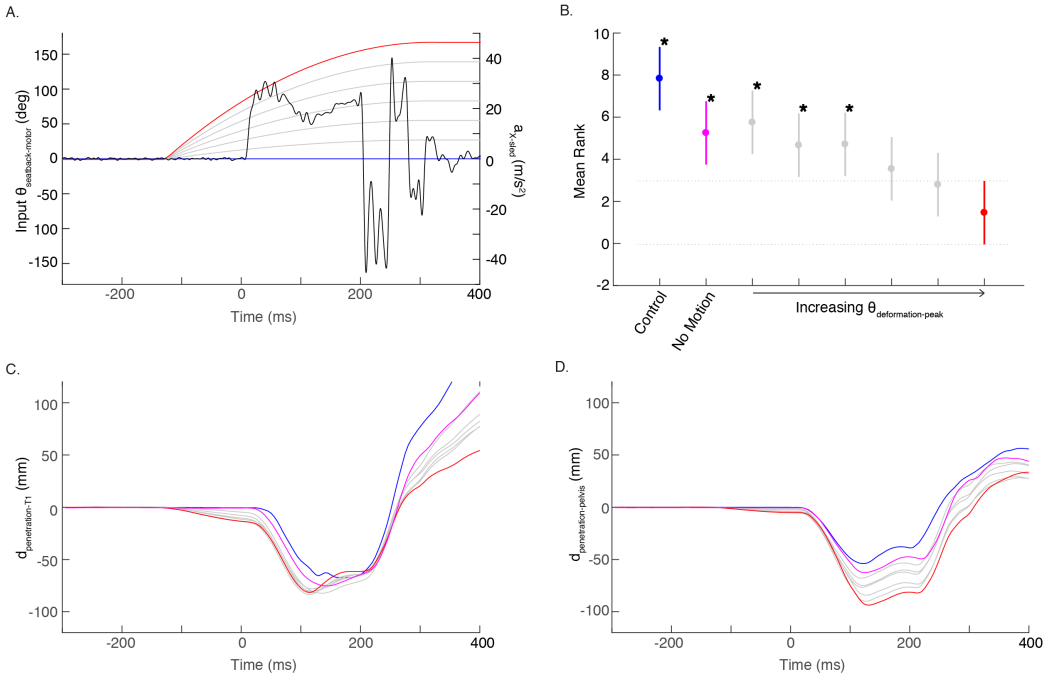

Figure C2. Seatback motor profiles and ATD responses to the Control seat (blue lines and markers), the No Motion condition (magenta lines and markers) and the Experimental seat with various peak angles of seatback motor rotations ($\theta_{deformation\text{-}peak}$; grey and red lines and markers) during a 12 km/h collision severity (Δt = 195 ms, black lines, Panel A, right axis). The red lines and markers indicate the seatback motor parameter ($\theta_{deformation\text{-}peak}$ = 168 deg) selected for further testing. Panel **A** shows the programmed input seatback motor rotation for the Experimental seat with increasing $\theta_{deformation\text{-}peak}$. The results of the post-hoc test (**B**) determined the mean rank of each trial as well as any significant differences (*) between the selected seatback motor parameter trial (red) and the Control, the No Motion or other Experimental trials. Panels **C** and **D** show the resulting seatback deformation at the T1 spinal level and at the pelvis ($d_{penetration\text{-}T1}$ and $d_{penetration\text{-}pelvis}$, respectively).

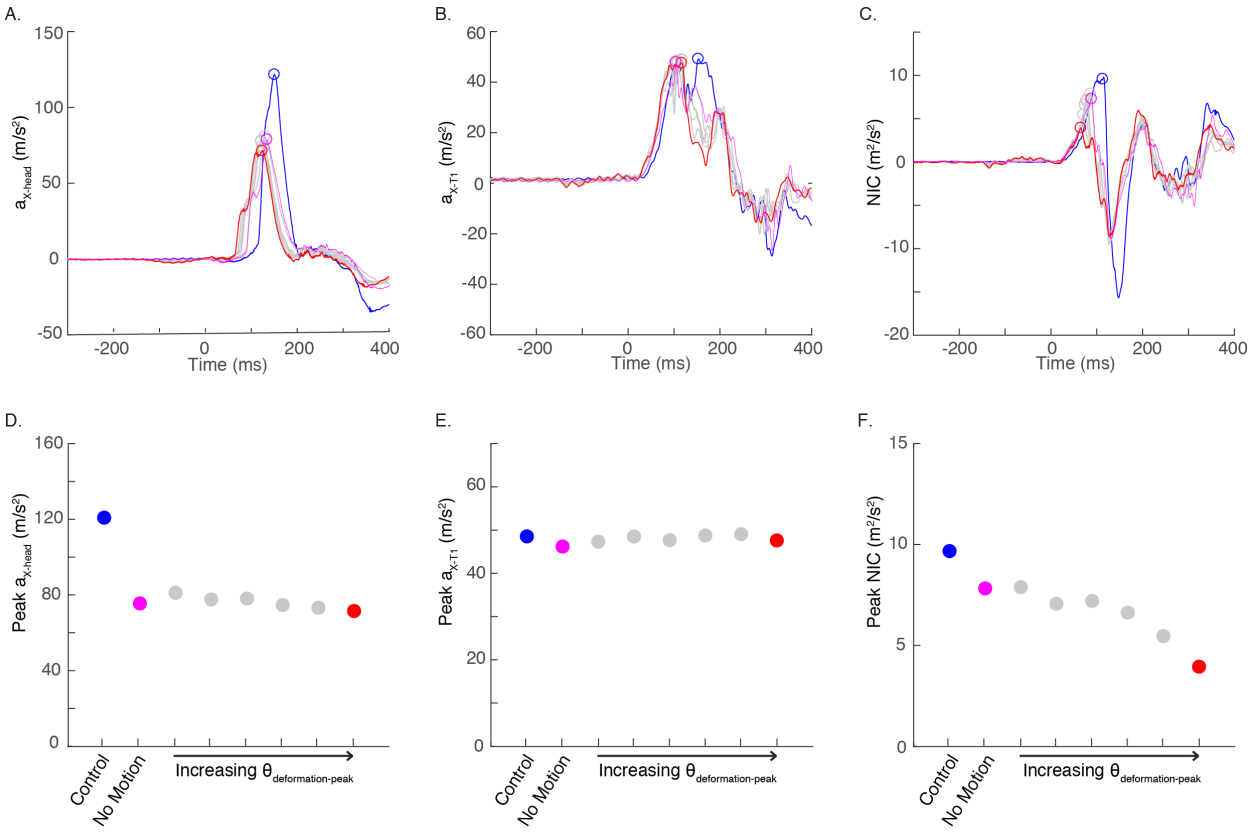

Figure C3. Exemplar ATD responses for the Control seat (blue lines and markers), the No Motion condition (magenta lines and markers), and the Experimental seat with various peak angles of the seatback motors ($\theta_{deformation\text{-}peak}$; grey and red lines and markers) during a 12 km/h collision severity (Δt = 195 ms). Calibrated responses (**A – C**) and their corresponding peak responses (**D – F**) for head and torso accelerations in the X-direction ($a_{X\text{-}head}$ & $a_{X\text{-}T1}$) and neck injury criteria (NIC), respectively. The red lines and markers indicate the seatback motor parameter ($\theta_{deformation\text{-}peak}$ = 168 deg) selected for further testing.

Initial Seatback Motor Angular Velocity

Initial seatback motor angular velocity controlled the rate at which the motors unspooled the seatbelt webbing to allow occupant penetration into the seatback. The initial angular velocities varied from 268 to 1201 deg/s and were created by expanding or contracting the initial seatback motor rotational profiles in time. The resulting profiles consisted of $\theta_{deformation\text{-}peak}$ = 168 deg, $t_{deformation\text{-}onset}$ = -130 ms, and $\omega_{deformation\text{-}int}$ of 268, 351, 683, 826, 980, and 1201 deg/s (**Figure C4A**). Exemplar peak ATD head and T1 acceleration responses ($a_{X\text{-}head}$ and $a_{X\text{-}T1}$: **Figure C5A** & **C5B**) did not vary with the different profiles, but peak neck injury criteria (NIC: **Figure C5C**) decreased with increased $\omega_{deformation\text{-}int}$. The Friedman test revealed a significant difference between all tested trials (1 Control, 1 No Motion condition, and 6 Experimental, χ^2 = 60.07, df = 7, $p < 0.001$). Post-hoc comparisons showed that the Experimental trial with $\omega_{deformation\text{-}int}$ = 980 deg/s had the lowest mean rank score and ranked lower than the Control seat, the No Motion condition and profiles with $\omega_{deformation\text{-}int} \leq 351$ deg/s ($p \leq 0.014$, **Figure C4B**). The Experimental trial with $\omega_{deformation\text{-}int}$ = 980 deg/s resulted in peak penetration of -83.2 mm at T1 ($d_{penetration\text{-}T1}$) and of -99.8 mm at the pelvis ($d_{penetration\text{-}pelvis}$). Subsequent experiments to determine the seatback motor deformation profile will be conducted with an $\omega_{deformation\text{-}int}$ = 980 deg/s to the $\theta_{deformation\text{-}peak}$ = 168 deg.

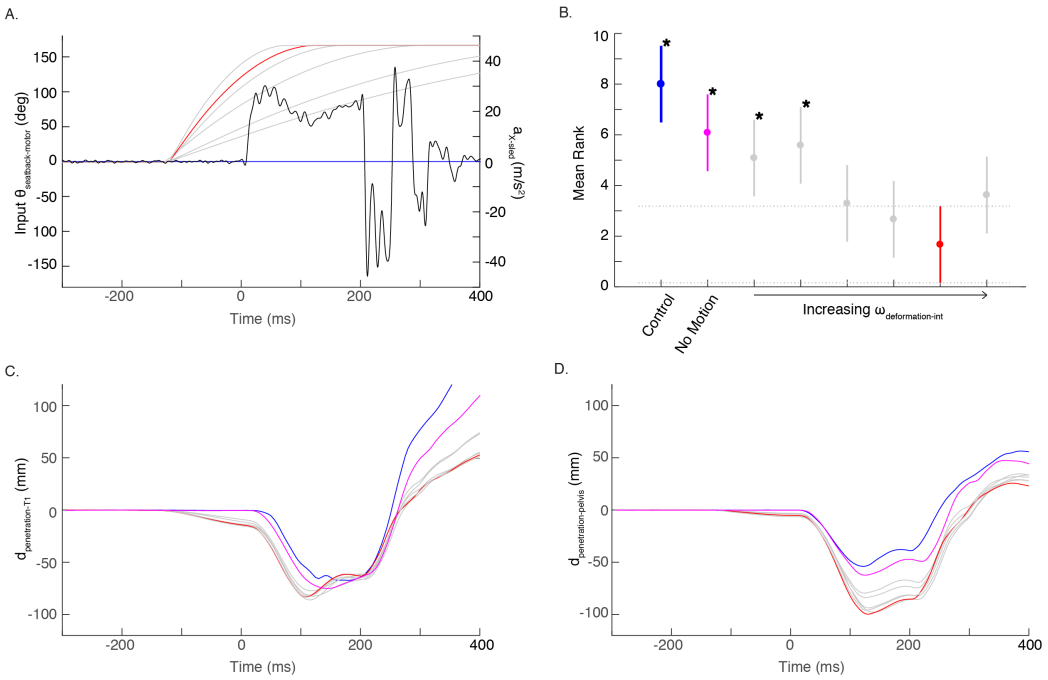

Figure C4. Seatback motor profiles and ATD responses to the Control seat (blue lines and markers), the No Motion condition (magenta lines and markers), and the Experimental seat with various initial angular velocities of the seatback motors ($\omega_{deformation\text{-}int}$; grey and red lines and markers) during a 12 km/h collision severity (Δt = 195 ms, black lines, Panel A, right axis). The red lines and markers indicate the initial angular velocity parameter ($\omega_{deformation\text{-}int}$ = 980 deg/s) of the seatback motors selected for further testing. Panel **A** shows the programmed input of the seatback motors for the Experimental seat with increasing $\omega_{deformation\text{-}int}$. The results of the post-hoc test (**B**) determined the mean rank of each trial as well as any significant differences (*) between the selected seatback motor parameter trial (red) and the Control seat, the No Motion condition or other Experimental trials. Panels **C** and **D** show the resulting seatback deformation at the T1 spinal level and at the pelvis ($d_{penetration\text{-}T1}$ and $d_{penetration\text{-}pelvis}$, respectively).

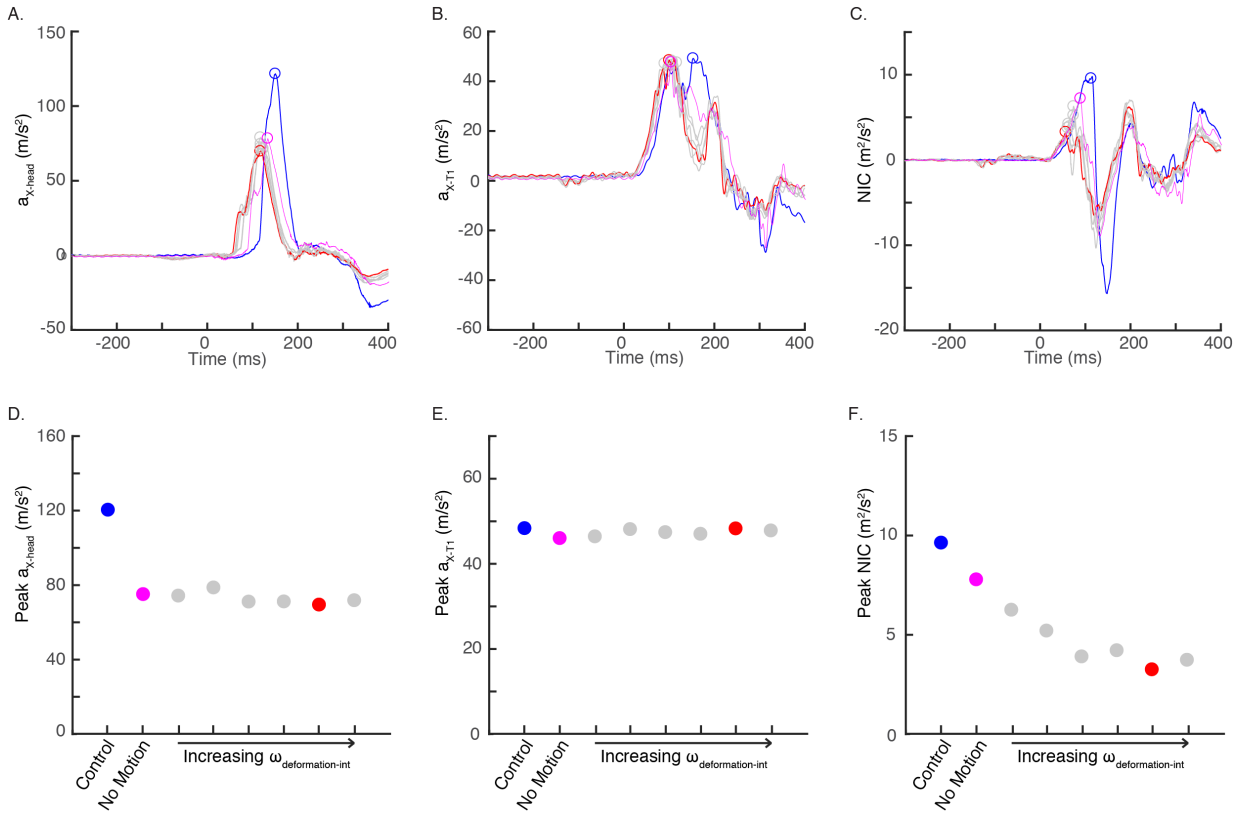

Figure C5. Exemplar ATD responses for the Control seat (blue lines and markers), the No Motion condition (magenta lines and markers), and the Experimental seat with various initial angular velocity of the seatback motor ($\omega_{deformation\text{-}int}$; grey and red lines and markers) during a 12 km/h collision severity (Δt = 195 ms). Calibrated responses (**A – C**) and their corresponding peak responses (**D – F**) for head and torso accelerations in the X-direction ($a_{X\text{-}head}$ & $a_{X\text{-}T1}$) and neck injury criteria (NIC), respectively. The red lines and markers indicate the initial seatback motor rotation velocity parameter ($\omega_{deformation\text{-}int}$ = 980 deg/s) selected for further testing.

Seatback Cushion Deformation Onset

The seatback cushion deformation onset ($t_{deformation\text{-}onset}$) defined when the seatback motors start to unspool. In this experiment, $t_{deformation\text{-}onset}$ was varied between -250 ms before to 200 ms after the collision onset ($t_{deformation\text{-}onset}$ = -250, -200, -150, -130, -100, -50, 0, 50, 100, 150 or 200 ms) (**Figure C6A**). For $t_{deformation\text{-}onset}$ = -200 ms or earlier, the $a_{X\text{-}head}$ and NIC showed lower peak responses than both the Control seat and the No Motion condition (**Figure C7D** & **C7F**); whereas peak $a_{X\text{-}T1}$ responses were similar across all trials (**Figure C7E**). The Friedman test revealed a significant difference between trials (1 Control seat, 1 No Motion condition, and 11 Experimental conditions, χ^2 = 89.18, df = 12, $p < 0.001$). Post-hoc comparisons showed that $t_{deformation\text{-}onset}$ of -250 and -200 ms were ranked significantly lower than the Control seat and the No Motion condition as well as $t_{deformation\text{-}onset}$ = 100 and 200 ms trials ($p \leq 0.016$, **Figure C6B**). For the profile with $t_{deformation\text{-}onset}$ = -200 ms, the ATD reached a peak penetration of -80.1 mm at T1 ($d_{penetration\text{-}T1}$) and -99.4 mm at the pelvis ($d_{penetration\text{-}pelvis}$) (**Figure C6C** & **C6D**). The combination of existing pre-crash avoidance systems as well as the time for the acceleration pulse to propagate through the vehicle to the seat would be sufficient to activate the deformation of the seatback -200 ms prior to the onset of the collision (McConnell et al., 1993, McConnell et al., 1995, Severy et al., 1955, Zador et al., 2000). Thus, a $t_{deformation\text{-}onset}$ = -200 ms was selected for subsequent experiments with the seatback motor deformation pulse.

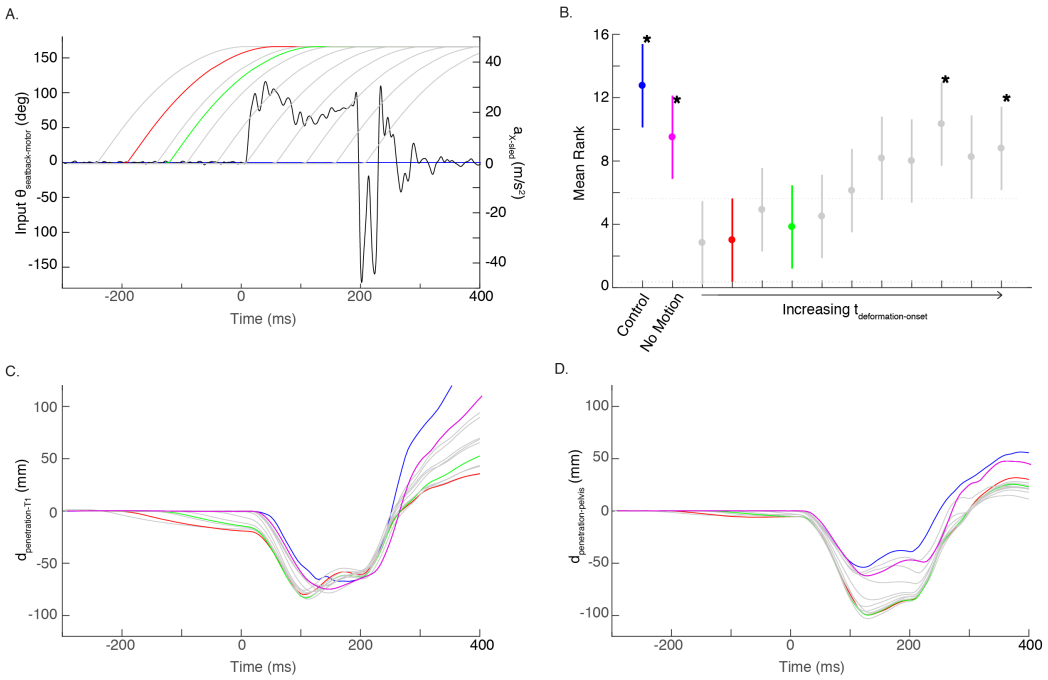

Figure C6. Seatback motor profiles and ATD responses to the Control seat (blue lines and markers), the No Motion condition (magenta lines and markers), and the Experimental seat with various onsets of the seatback motor rotation ($t_{deformation\text{-}onset}$; grey, green, and red lines and markers) during a 12 km/h collision severity (Δt = 195 ms, black lines, Panel A, right axis). The green lines and markers indicate the initial seatback motor onset used in the previous two experiments ($t_{deformation\text{-}onset}$ = -130 ms) and the red lines and markers indicate the seatback motor onset parameter ($t_{deformation\text{-}onset}$ = -200 ms) selected for further testing. Panel **A** shows the programmed input of the seatback motors for the Experimental seat with increasing $t_{deformation\text{-}onset}$. The results of the post-hoc test (**B**) determined the mean rank of each trial as well as any significant differences (*) between the selected seatback motor parameter trial (red) and the Control seat, the No Motion condition or other Experimental trials. Panels **C** and **D** show the resulting seatback deformation at the T1 spinal level and at the pelvis ($d_{penetration\text{-}T1}$ and $d_{penetration\text{-}pelvis}$, respectively).

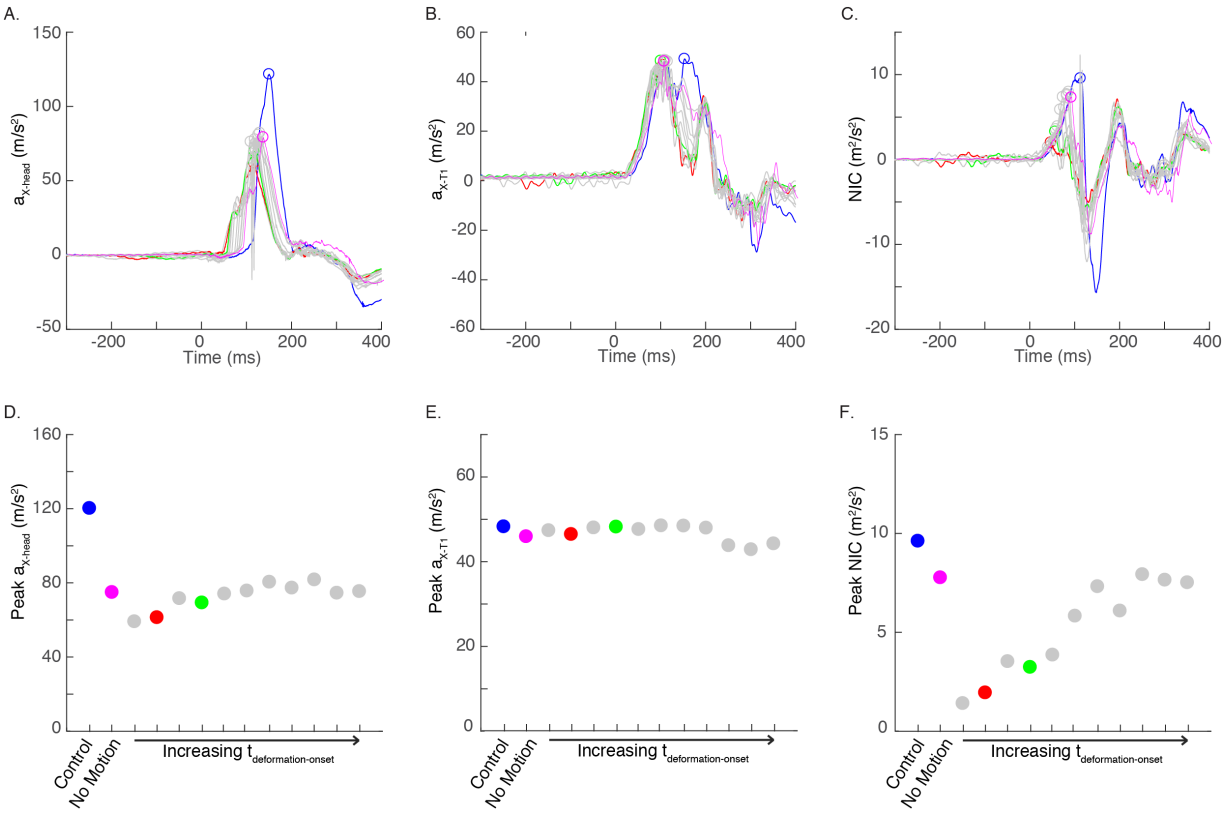

Figure C7. Exemplar ATD responses for the Control seat (blue lines and markers), the No Motion condition (magenta lines and markers), and the Experimental seat with various onsets of the seatback motor rotation ($t_{deformation\text{-}onset}$; grey, green, and red lines and markers) during a 12 km/h collision severity (Δt = 195 ms). Calibrated responses (**A – C**) and their corresponding peak responses (**D – F**) for head and torso accelerations in the X-direction ($a_{X\text{-}head}$ & $a_{X\text{-}T1}$) and neck injury criteria (NIC), respectively. The green lines and markers indicate the initial seatback motor onset used in the previous two experiments ($t_{deformation\text{-}onset}$ = -130 ms) and the red lines and markers indicate the seatback motor onset parameter ($t_{deformation\text{-}onset}$ = -200 ms) selected for further testing.

Experiment 2: Verification of Ideal Seatback Deformation Profile

The goal of Experiment 2 was to verify that the seatback deformation profile determined in Experiment 1 ($\theta_{deformation\text{-}peak}$ = 168 deg, $\omega_{deformation\text{-}int}$ = 980 deg/s, and $t_{deformation\text{-}onset}$ = -200 ms) was a local minimum that best reduced ATD responses. In this experiment, the Control seat (blue lines and markers), the No Motion condition (magenta lines and markers), and the seatback deformation profile from Experiment 1 (red lines and markers) were compared against 12 additional profiles with different combinations of seatback motor parameters. The $t_{deformation\text{-}onset}$ parameter was kept constant at -200 ms, but $\theta_{deformation\text{-}peak}$ and $\omega_{deformation\text{-}int}$ were varied ($\theta_{deformation\text{-}peak}$ = 56, 112 and 168 deg and $\omega_{deformation\text{-}int}$ = 176, 683, 980 and 1485 deg/s; **Figure C8A)**. The Friedman test revealed a significant difference between all tested trials (1 Control, 1 No Motion and 12 Experimental, $\chi^2 = 100.59$, df = 13, $p < 0.001$). Post-hoc comparisons showed that the mean rank of the trial with seatback motor deformation profile determined in Experiment 1 (red plot; $d_{penetration\text{-}T1}$ = -84.3 mm & $d_{penetration\text{-}pelvis}$ = -96.8 mm) was ranked third lowest and was ranked significantly lower than the Control seat, the No Motion condition, and two other Experimental trials (**Figure C8B**). The other two Experimental conditions that ranked lower than the seatback motor profile both had $\theta_{deformation\text{-}peak}$ = 168 deg with different $\omega_{deformation\text{-}int}$ = 683 and 1485 deg/s, but these conditions were not significantly different from the selected seatback profile condition. These results suggest that the $\theta_{deformation\text{-}peak}$ parameter may have a larger influence on the reduction of ATD responses than the $\omega_{deformation\text{-}int}$ parameter. This experiment showed that the current seatback motor deformation profile determined in Experiment 1 is a potentially effective solution to reducing ATD responses following low-speed, rear-end collisions (Δv = 12 km/h, Δt =195 ms).

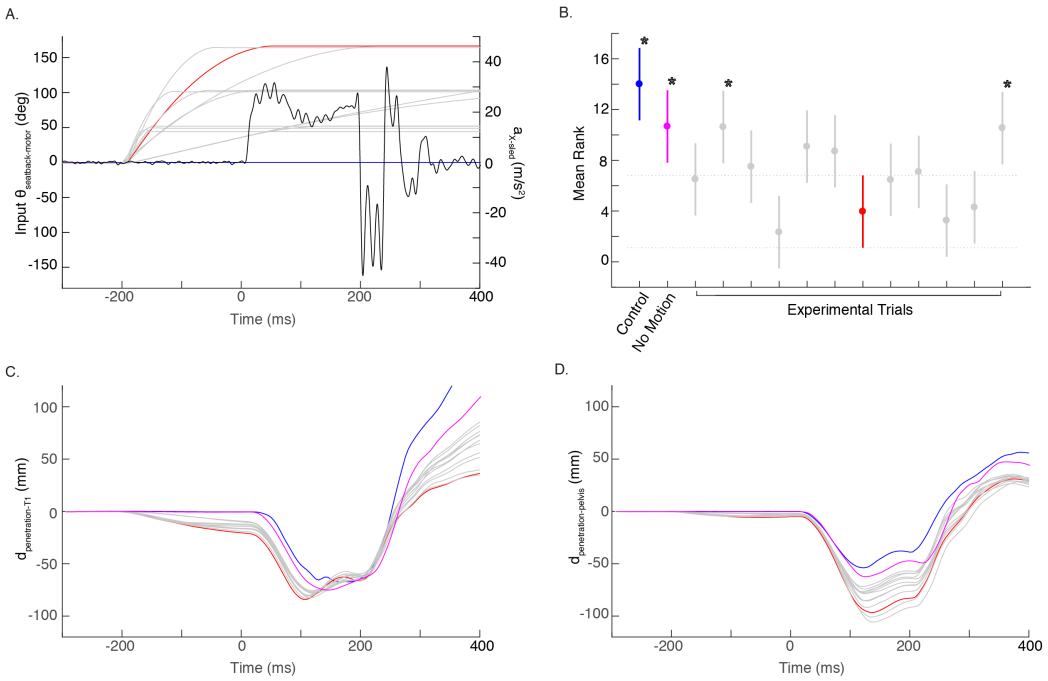

Figure C8. Seatback motor profiles and ATD responses to the Control seat (blue lines and markers), the No Motion condition (magenta lines and markers), and the Experimental seat with various combinations of $\theta_{deformation\text{-}peak}$ and $\omega_{deformation\text{-}int}$ parameters at a constant $t_{deformation\text{-}onset}$ = -200 ms (grey and red lines and markers) during a 12 km/h collision severity (Δt = 195 ms, black lines, Panel A, right axis). The red lines and markers indicate the seatback motor profile ($\theta_{deformation\text{-}peak}$ = 168 deg, $\omega_{deformation\text{-}int}$ = 980 deg/s, and $t_{deformation\text{-}onset}$ = -200 ms) determined from Experiment 1 and selected for further testing. The results of the post-hoc test (**B**) determined the mean rank of each trial as well as any significant differences (*) between the selected seatback motor parameter trial (red) and the Control, the No Motion or other Experimental trials. Panels **C** and **D** show the resulting seatback deformation at the T1 spinal level and at the pelvis ($d_{penetration\text{-}T1}$ and $d_{penetration\text{-}pelvis}$, respectively).

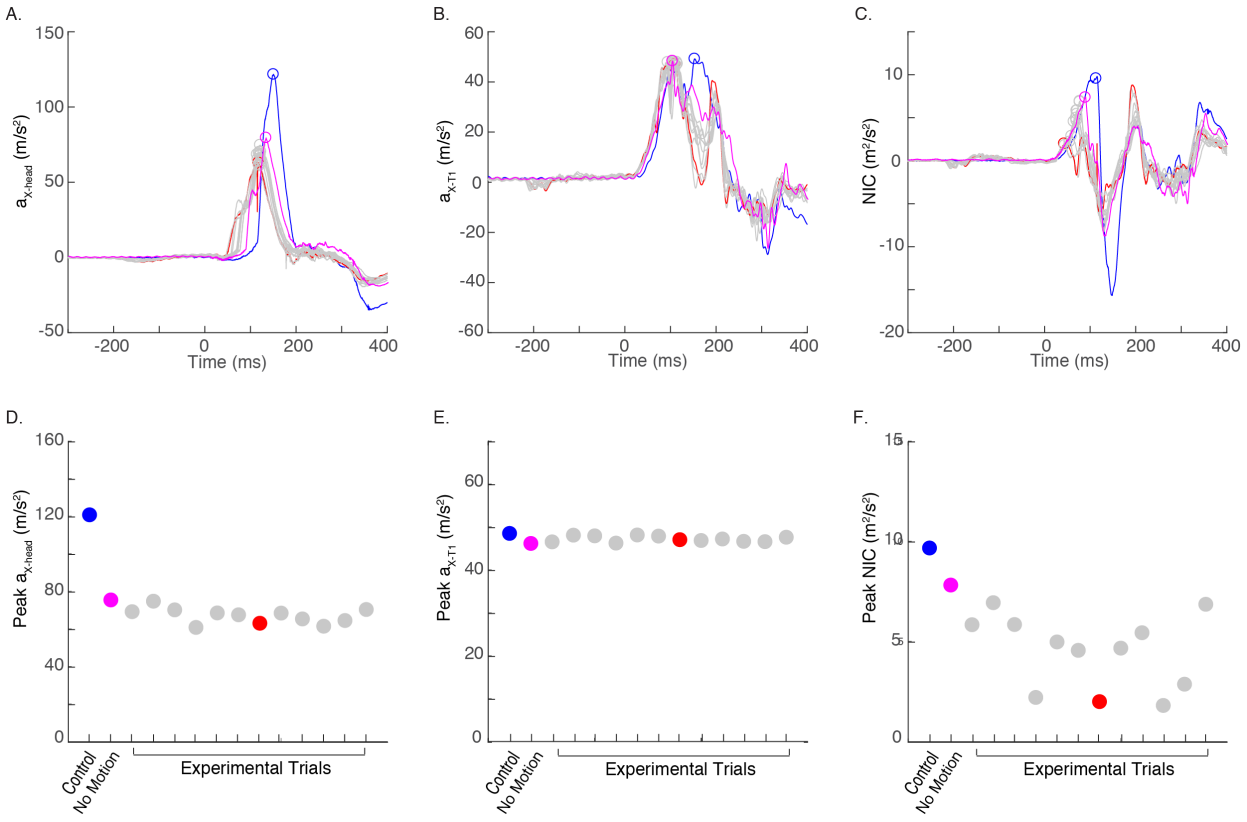

Figure C9. Exemplar ATD responses for the Control seat (blue lines and markers), the No Motion condition (magenta lines and markers), and the Experimental seat with various combinations of $\theta_{deformation\text{-}peak}$ and $\omega_{deformation\text{-}int}$ parameters at a constant $t_{deformation\text{-}onset}$ = -200 ms (grey and red lines and markers) during a 12 km/h collision severity (Δt = 195 ms). Calibrated responses (**A – C**) and their corresponding peak responses (**D – F**) for head and torso accelerations in the X-direction ($a_{X\text{-}head}$ & $a_{X\text{-}T1}$) and neck injury criteria (NIC), respectively. The red lines and markers indicate the seatback motor profile ($\theta_{deformation\text{-}peak}$ = 168 deg, $\omega_{deformation\text{-}int}$ = 980 deg/s, and $t_{deformation\text{-}onset}$ = -200 ms) determined from Experiment 1 and selected for further testing.

Experiment 3: Forward Pre-Perturbation Seatback Deformation

The results from the seat hinge rotation experiments suggested that the addition of a forward pre-perturbation rotation of the seatback can significantly reduce ATD responses during the whiplash perturbation (see **Appendix B: Experiment 4**). Thus, we investigated whether a forward (positive X-direction) deformation of the seatback toward the occupant prior to the perturbation would further reduce ATD responses. A forward pre-perturbation seatback deformation was added to the seatback motor deformation profile determined in Experiment 2. Nine different combinations of peak forward deformation amplitudes ($\theta_{deformation\text{-}forward}$ = -9.1, -15.8, and -21.4 deg) and onsets ($t_{deformation\text{-}forward}$ = -700, -500 and -300 ms, **Figure C10A**) were tested. These nine Experimental conditions were then compared to the Control seat (blue lines and markers), the No Motion condition (magenta lines and markers) and the 'rearward only seatback' deformation profile (red lines and markers). None of the profiles generated markedly lower ATD peak $a_{X\text{-}head}$ and NIC responses than the rearward-only seatback deformation profile (**Figure C11**). The Friedman test revealed a significant difference between all trials (1 Control, 1 No Motion and 10 Experimental, χ^2 = 72.25., df = 11, $p < 0.001$). Post-hoc comparisons showed that only two pre-perturbation conditions and the rearward-only seatback deformation profile were ranked significantly lower than both the Control seat and the No Motion condition ($p \leq 0.037$, **Figure C10B)**. The mean rank of these three lowest conditions were not significantly different from each other. Given that the addition of the pre-perturbation seatback deformation did not significantly further reduce ATD responses, a pre-perturbation component of the seatback deformation was excluded from the final seatback deformation profile.

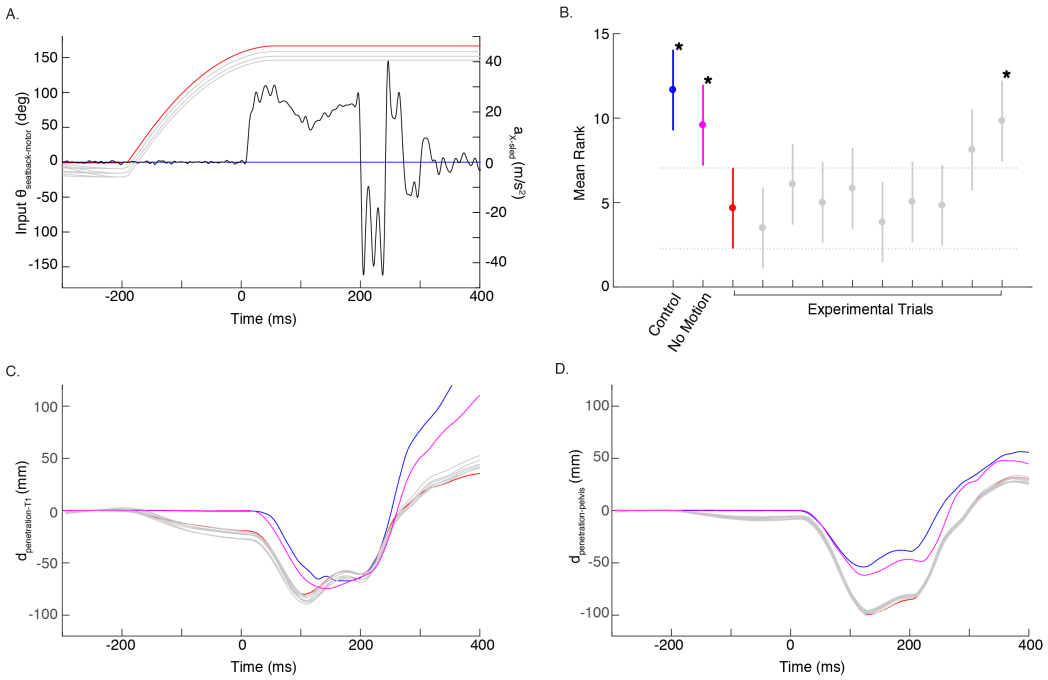

Figure C10. Seatback motor profiles and ATD responses to the Control seat (blue lines and markers), the No Motion condition (magenta lines and markers), and the Experimental seat with either different combinations of pre-perturbation forward seatback deformation pulses parameters ($\theta_{deformation\text{-}forward}$ and $t_{deformation\text{-}forward,}$ grey lines and markers) or without a pre-perturbation (red lines and markers) during a 12 km/h collision severity (Δt = 195 ms, black lines, Panel A, right axis). The red lines and markers indicate the seatback motor profile ($\theta_{deformation\text{-}peak}$ = 168 deg, $\omega_{deformation\text{-}int}$ = 980 deg/s, and $t_{deformation\text{-}onset}$ = -200 ms) determined from Experiment 1 & 2 and selected for further testing. The results of the post-hoc test (**B**) determined the mean rank of each trial as well as any significant differences (*) between the selected seatback motor parameter trial (red) and the Control seat, the No Motion condition or other Experimental trials. Panels **C** and **D** show the resulting seatback deformation at the T1 spinal level and at the pelvis ($d_{penetration\text{-}T1}$ and $d_{penetration\text{-}pelvis}$, respectively).

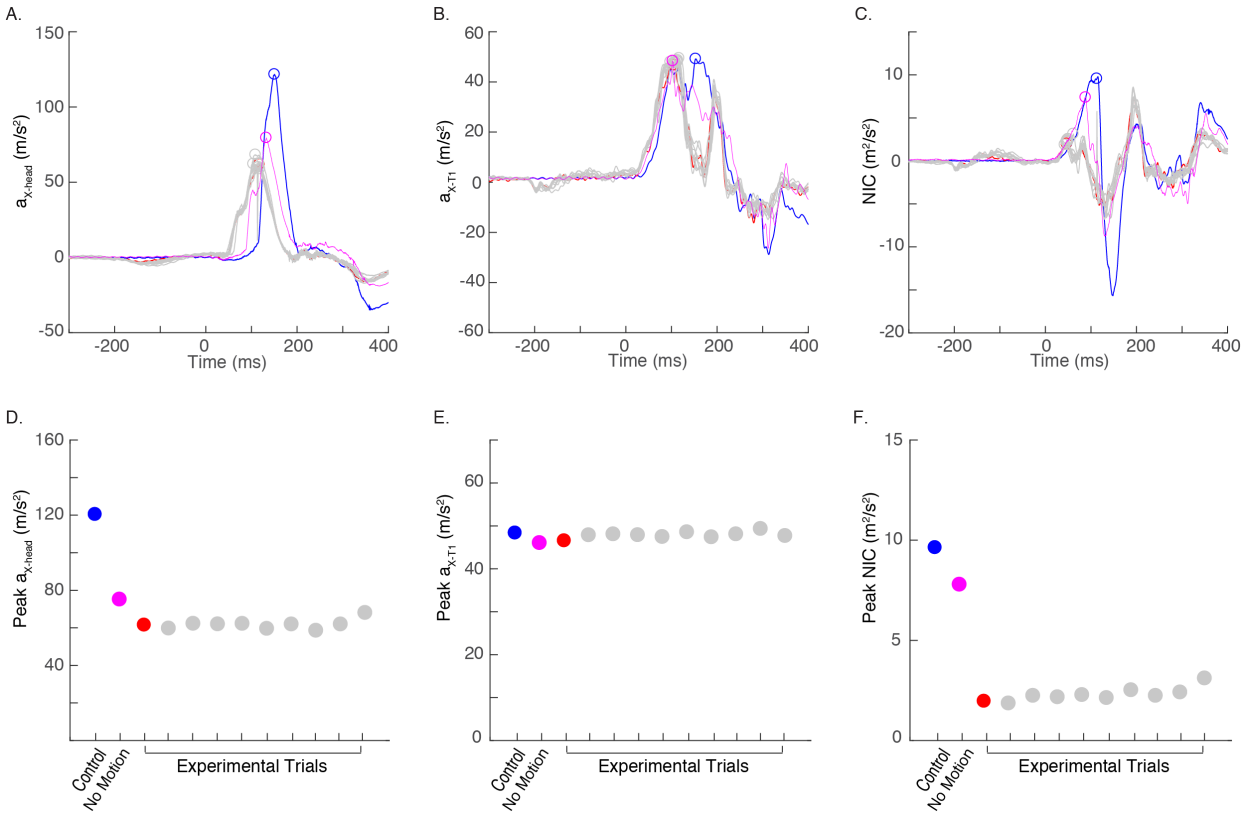

Figure C11. Exemplar ATD responses to the Control seat (blue lines and markers), the No Motion condition (magenta lines and markers), and the Experimental seat with either different combinations of pre-perturbation forward seatback deformation pulses parameters ($\theta_{deformation\text{-}forward}$ and $t_{deformation\text{-}forward}$, grey lines and markers) or without a pre-perturbation (red lines and markers) during a 12 km/h collision severity (Δt = 195 ms). Calibrated responses (**A – C**) and their corresponding peak responses (**D – F**) for head and torso accelerations in the X-direction ($a_{X\text{-}head}$ & $a_{X\text{-}T1}$) and neck injury criteria (NIC), respectively. The red lines and markers indicate the seatback motor profile ($\theta_{deformation\text{-}peak}$ = 168 deg, $\omega_{deformation\text{-}int}$ = 980 deg/s, and $t_{deformation\text{-}onset}$ = -200 ms) determined from Experiment 1 & 2 and selected for further testing.

Summary

A seatback motor deformation profile has been defined to investigate the effects of seatback cushion deformation on ATD responses to low-speed, rear-end collisions. The dynamic seatback motor deformation profile (**Figure C12**, grey line) was programmed to rotate the seatback motors ($t_{deformation\text{-}onset}$) -200 ms before the collision onset to a peak seatback motor angle ($\theta_{deformation\text{-}peak}$) of 168 deg at an initial angular velocity ($\omega_{deformation\text{-}int}$) of 980 deg/s. The resulting ATD penetration into the seatback was -84.3 mm at T1 ($d_{penetration\text{-}T1}$, green line) and -96.8 mm at the pelvis ($d_{penetration\text{-}pelvis}$, blue line) (**Figure C12**). With the exception of linear forward acceleration of the T1 vertebrae ($a_{X\text{-}T1}$), the dynamic seatback cushion deformation decreased the other eight peak kinematic and kinetic responses ($a_{X\text{-}head}$, $\omega_{Y\text{-}head}$, F_X, F_Z, M_Y, $\theta_{head,}$ R_X and $\Delta t_{head\text{-}contact}$) and three peak neck injury criteria (NIC, N_{km}, and N_{ij}) from the Control trial.

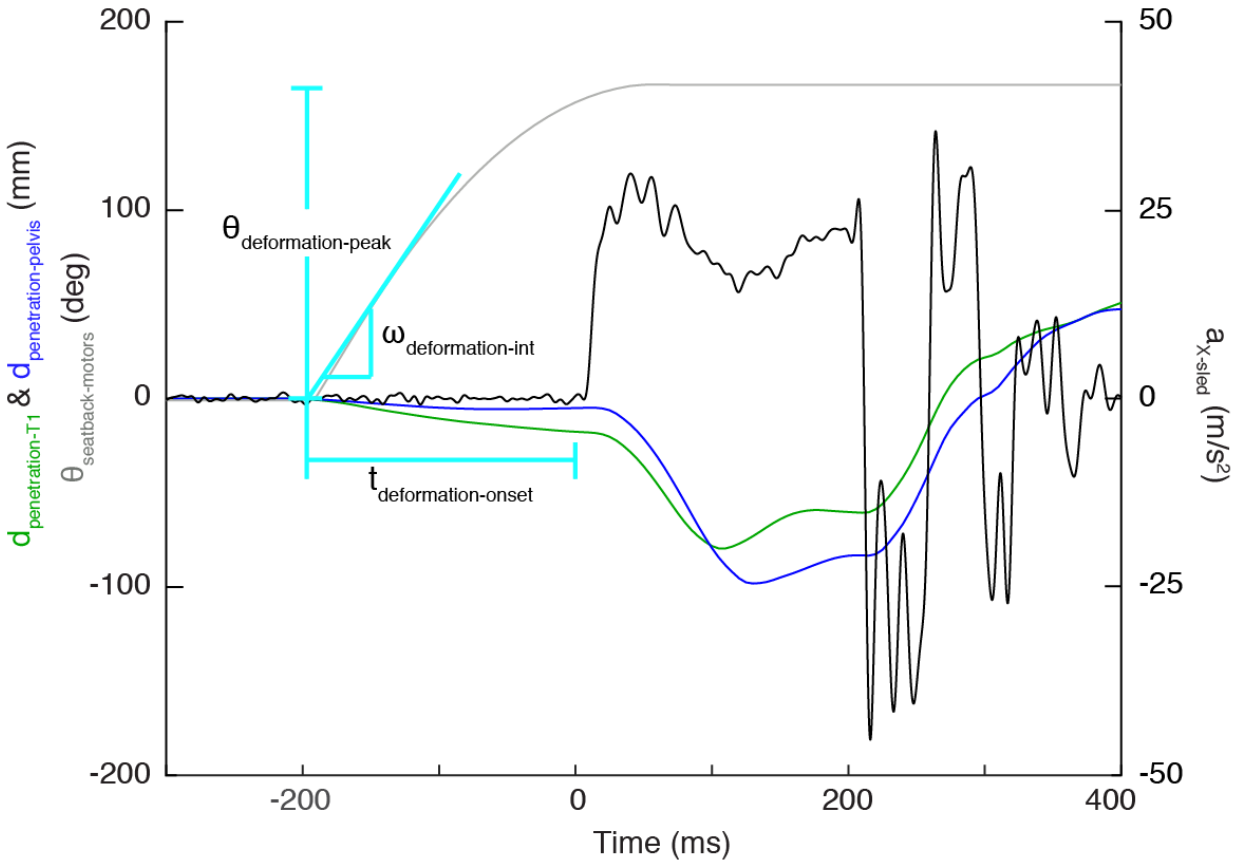

Figure C12. Horizontal seatback cushion deformation of the T1 vertebra and pelvis ($d_{penetration\text{-}T1}$, green line & $d_{penetration\text{-}pelvis}$, blue line) in response to the seatback motor rotation ($\theta_{seatback\text{-}motor}$, grey line) with $\theta_{deformation\text{-}peak}$ = 168 deg, $\omega_{deformation\text{-}int}$ = 980 deg/s, and $t_{deformation\text{-}onset}$ = -200 (deformation profile parameters, cyan lines) during a 12 km/h collision severity ($a_{X\text{-}sled}$, Δt = 195 ms, black line, right axis).

Appendix D: Combining the Seat Hinge Rotation and the Seatback Cushion Deformation Profiles

In this appendix, the combined effects of the seat hinge rotation and the seatback cushion deformation profiles identified in **Appendix B** and **C** were evaluated through a series of three experiments varying the relative onset of the seat hinge and seatback deformation profiles. An ATD seated on the Experimental anti-whiplash seat was exposed to a series of perturbations with a collision severity of 12 km/h (Δt = 187 ms) (**Figure D1**). An Optotrak 3-D motion capturing system was used to quantify the seatback deformation induced by the rotations of the seatback motors. Maximum rearward penetration of the ATD T1 ($d_{penetration\text{-}T1}$) and pelvis ($d_{penetration\text{-}pelvis}$) were defined as the horizontal displacement (along the global X-axis, see **Figure A4** in **Appendix A**) of the T1 vertebra and pelvis infrared light emitting diode (IRED) markers relative to the seatback. Rearward displacement deeper into the seatback was defined as negative values and forward rebound away from the seat was defined as positive values. The initial position of the ATD was set as $d_{penetration\text{-}T1}$ = 0 mm and $d_{penetration\text{-}pelvis}$ = 0 mm.

The dynamic seat hinge rotation profile (**Figure D1A**, grey line) was programmed to rotate the seatback forward commencing at 90 ms ($t_{forward\text{-}onset}$) before the collision onset by 5.6 deg ($\theta_{forward\text{-}peak}$) at an angular velocity of -33.4 deg/s ($\omega_{forward\text{-}int}$) and to then rotate the seatback rearward by 5.7 deg ($\theta_{rearward\text{-}peak}$) at an angular velocity ($\omega_{rearward\text{-}int}$) of 24.0 deg/s beginning 70 ms ($t_{rearward\text{-}onset}$) after collision onset. The observed output seat hinge rotation (**Figure 5.2A**, red line) resulted in a forward rotation of 4.6 deg followed by a rearward seat hinge rotation of 3.8 deg. The seatback motor deformation profile was programmed to unspool the webbing from

the two lower seatback motors beginning 200 ms ($t_{deformation\text{-}onset}$) before the collision onset to a peak angle ($\theta_{rearward\text{-}peak}$) of 168 deg (angular velocity $\omega_{deformation\text{-}int}$ = 980 deg/s). The resulting ATD penetration into the seatback was -61.6 mm at T1 ($d_{penetration\text{-}T1}$, green line) and -94.1 mm at the pelvis ($d_{penetration\text{-}pelvis}$, blue line) (**Figure D1B**). These profiles were used as the relative timing between the seat hinge rotation ($t_{rotation\text{-}onset}$) and seatback deformation ($t_{deformation\text{-}onset}$) profiles were manipulated through a series of three experiments varying: 1) $t_{rotation\text{-}onset}$ 2) $t_{deformation\text{-}onset}$, and 3) both $t_{rotation\text{-}onset}$ and $t_{deformation\text{-}onset}$. For comparison, the ATD was exposed to the same collision (12 km/h; Δt = 187 ms) while seated on the Control GMHR seat and on the Experimental seat but with the hinge and seatback motors locked in their initial position (No Motion condition).

To quantify the ATD responses, nine peak kinematic and kinetic ($a_{X\text{-}head}$, $a_{X\text{-}T1}$, $\omega_{Y\text{-}head}$, F_X, F_Z, M_Y, $\theta_{head,}$ R_X and $\Delta t_{head\text{-}contact}$) and three peak neck injury criteria (NIC, N_{km}, and N_{ij}) responses were selected for analysis. Within each response variable, the different profiles were ranked, and then the profile with the lowest averaged rank across all 12 variables was identified as the best profile. A Friedman test determined if there was a significant difference between the average rank of the different profiles (chi-squared value: χ^2, degrees of freedom: df, and the significance level: p). A post-hoc, pair-wise multiple comparison test was then performed on the results of the Friedman test to determine differences between individual profiles. All tests were performed using predefined functions (`friedman` and `multcompare`) in Matlab using α = 0.05.

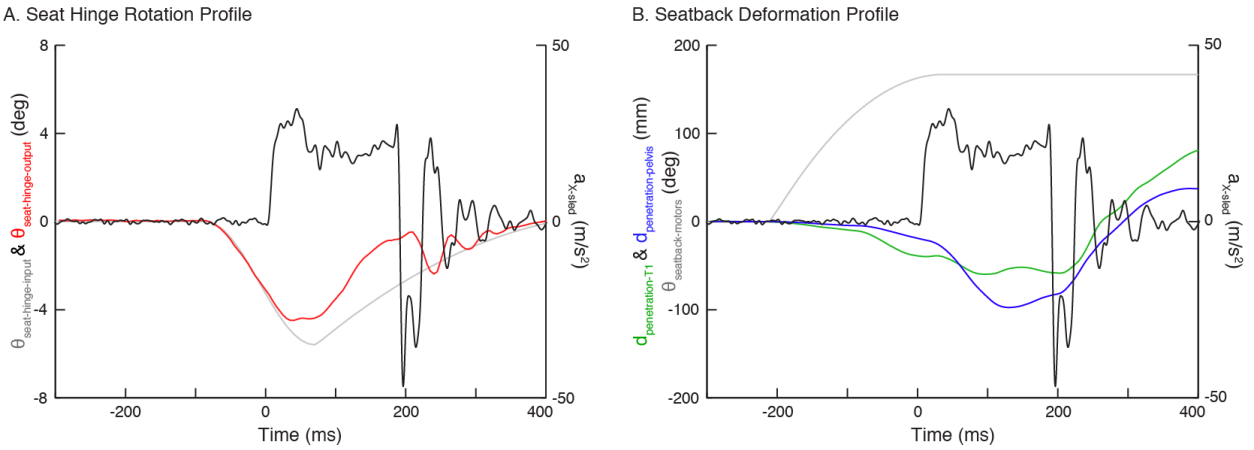

Figure D1. Programmed inputs and resulting outputs for A.) seat hinge rotation and B.) seatback cushion deformation profiles during a 12 km/h collision (Δt = 187 ms; black line). Grey lines represent input rotation ($\theta_{seat\text{-}hinge}$) and deformation ($\theta_{seatback\text{-}motors}$) profiles to seat hinge and seatback motors, respectively. Seat hinge rotation ($\theta_{seat\text{-}hinge\text{-}output}$: red line) as well as rearward penetration of ATD T1 ($d_{penetration\text{-}T1}$: green line) and pelvis ($d_{penetration\text{-}pelvis}$: blue line) into the seatback indicate resulting outputs to their respective input profiles.

Experiment 1: Varying Onset of Seat Hinge Rotation

In this first experiment, the effects of shifting the seat hinge rotation onset from -170 to -10 ms ($t_{rotation\text{-}onset}$ = -170, -150, -130, -110, -90, -70, -50, -30 and -10 ms) relative to the seatback deformation ($t_{deformation\text{-}onset}$ = -200ms) were tested (**Figure D2A**). Exemplar ATD head acceleration ($a_{X\text{-}head}$) data showed lower peak responses for $t_{rotation\text{-}onset}$ between -110 to -50 ms from the Control seat and the No Motion condition, whereas, peak T1 acceleration ($a_{X\text{-}T1}$) decreased only $t_{rotation\text{-}onset}$ = -90ms (**Figure D3)**. A Friedman test confirmed these observations, showing a significant difference between all tested trials (1 Control, 1 No Motion and 9 Experimental, χ^2 = 88.61, df = 10, $p < 0.001$). Post-hoc comparison showed that $t_{rotation\text{-}onset}$ of -90 and -70 ms were ranked significantly lower than the Control seat and the No Motion condition as well as $t_{rotation\text{-}onset}$ = -170, -150 and -10 ms trials (multiple $p \leq 0.044$; **Figure D2C**).

Since there was no significant difference between $t_{rotation\text{-}onset}$ = -90 and -70 ms trials, a $t_{rotation\text{-}onset}$ = -90 ms was selected for subsequent experimental testing. Overall, these results suggested that $t_{rotation\text{-}onset}$ had a significant effect on peak ATD responses and the selected pulse timing (-90 ms) was a local minimum. The profile with a $t_{rotation\text{-}onset}$ = -90 ms and a $t_{deformation\text{-}onset}$ = -200 ms generated occupant penetrations of $d_{penetration\text{-}T1}$ = -61.6 mm and $d_{penetration\text{-}pelvis}$ = -94.1mm (**Figure D2E** and **D2F**).

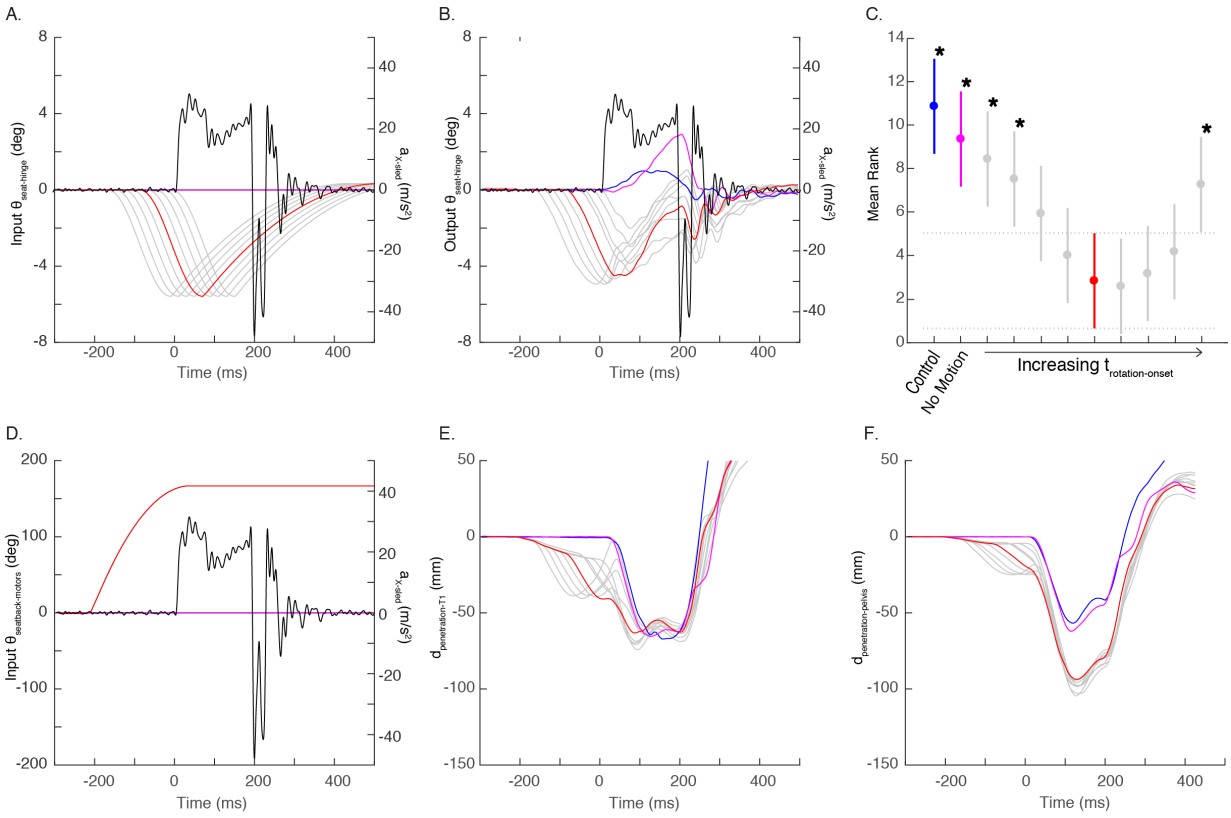

Figure D2. Seat hinge and seatback motor profiles as well as ATD responses to the Control seat (blue lines and markers), the No Motion condition (magenta lines and markers) and the Experimental seat with various seat hinge motor onsets at a constant seatback motor onset ($t_{rotation\text{-}onset}$ & $t_{deformation\text{-}onset}$ = -200 ms; grey and red lines and markers) during a 12 km/h collision severity (Δt = 187 ms, black lines, right axis). The red lines and markers indicate the seat hinge onset ($t_{rotation\text{-}onset}$ = -90 ms) selected for further testing. Panels **A** and **B** show the programmed input and output seat hinge rotation profiles. Panel **D** shows the programmed input seatback motor profiles with resulting seatback deformation at the T1 spinal level ($d_{penetration\text{-}T1}$) and at the pelvis ($d_{penetration\text{-}pelvis}$) in Panels **E** and **F**, respectively. The results of the post-hoc test (**C**) determined the mean rank of each trial as well as any significant differences (*) between the selected seatback motor parameter trial (red) and the Control, No Motion or other experimental trials.

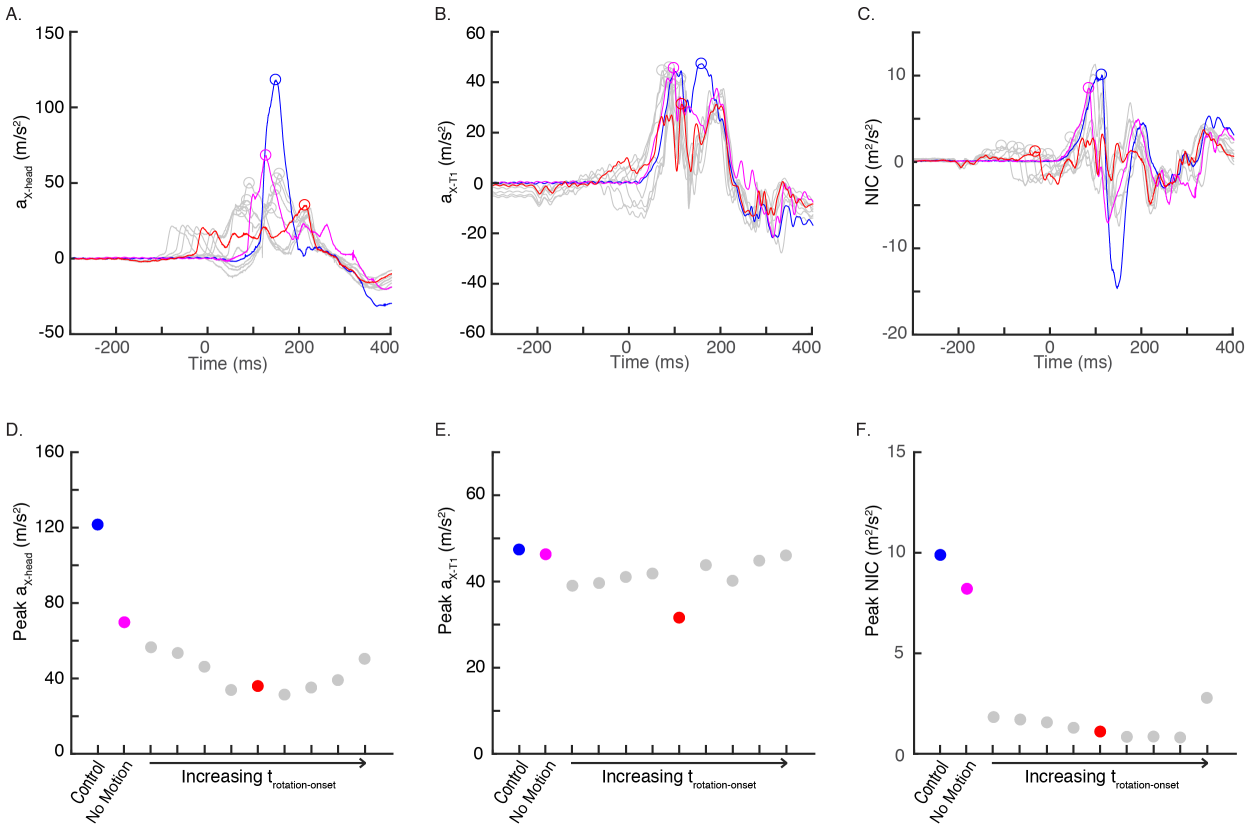

Figure D3. Exemplar ATD responses for the Control seat (blue lines and markers), the No Motion condition (magenta lines and markers), and the Experimental seat with various seat hinge motor onsets and a constant seatback motor onset ($t_{rotation\text{-}onset}$ & $t_{deformation\text{-}onset}$ = -200 ms; grey and red lines and markers) during a 12 km/h collision severity (Δt = 187 ms). Calibrated responses (**A – C**) and their corresponding peak responses (**D – F**) for head and torso accelerations in the X-direction ($a_{X\text{-}head}$ & $a_{X\text{-}T1}$) and neck injury criteria (NIC), respectively. The red lines and markers indicate the seatback motor parameter ($t_{rotation\text{-}onset}$ = -90 ms) selected for further testing.

Experiment 2: Varying Onset of Seatback Deformation

In this experiment, the seatback deformation onset was shifted from -280 to -120 ms ($t_{deformation\text{-}onset}$ = -280, -260, -240, -220, -200, -180, -160, -140 and -120 ms) before the collision relative to a fixed seat hinge rotation onset ($t_{rotation\text{-}onset}$ = -90 ms) to determine the influence of varying seatback deformation onset (**Figure D4D**). Exemplar ATD responses ($a_{X\text{-}head}$, $a_{X\text{-}T1}$, and NIC) for the Experimental trials were lower than the Control seat and the No Motion condition but remained similar across all Experimental trials despite varying $t_{deformation\text{-}onset}$ (**Figure D5**). A Friedman test showed a significant difference between all tested trials (1 Control, 1 No Motion and 9 Experimental, χ^2 = 62.82, df = 10, $p < 0.001$). Post-hoc comparison confirmed all Experimental conditions were significantly lower than the Control seat and the No Motion condition ($p \leq 0.044$, **Figure D4C**) but no significant differences between Experimental conditions were observed. Thus, the seatback $t_{deformation\text{-}onset}$ at -200 ms was selected for future testing (**Figure D4C**). These results suggested that changes to $t_{deformation\text{-}onset}$ between the range of -280 to -120 ms before the collision onset had little effect on peak ATD responses between trials. The selected onsets for seat hinge rotation ($t_{rotation\text{-}onset}$ = -90 ms) and seatback deformation ($t_{deformation\text{-}onset}$ = -200 ms) were the same from Experiment 1 and generated occupant penetration at T1 ($d_{penetration\text{-}T1}$) of -61.6 mm and at the pelvis ($d_{penetration\text{-}pelvis}$) of -94.1mm (**Figure D4E** and **D4F**).

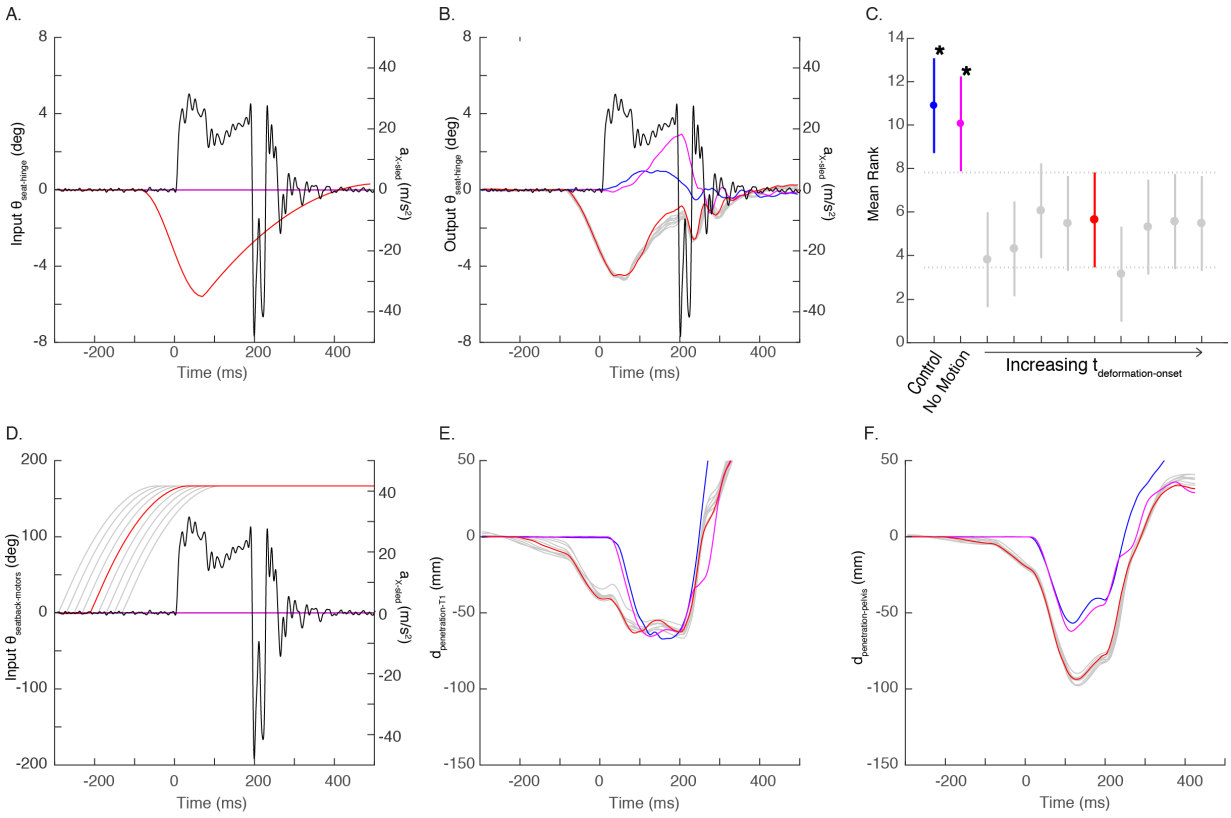

Figure D4. Seat hinge and seatback motor profiles as well as ATD responses to the Control seat (blue lines and markers), the No Motion condition (magenta lines and markers) and the Experimental seat with various seatback motor onsets at a constant seat hinge motor onset ($t_{deformation\text{-}onset}$ & $t_{rotation\text{-}onset}$ = -90 ms; grey and red lines and markers) during a 12 km/h collision severity (Δt = 187 ms, black lines, right axis). The red lines and markers indicate the seat hinge onset ($t_{deformation\text{-}onset}$ = -200 ms) selected for further testing. Panels **A** and **B** show the programmed input and output seat hinge rotation profiles. Panel **D** shows the programmed input seatback motor profiles with resulting seatback deformation at the T1 spinal level ($d_{penetration\text{-}T1}$) and at the pelvis ($d_{penetration\text{-}pelvis}$) in Panels **E** and **F**, respectively. The results of the post-hoc test (**C**) determined the mean rank of each trial as well as any significant differences (*) between the selected seatback motor parameter trial (red) and the Control, No Motion or other Experimental trials.

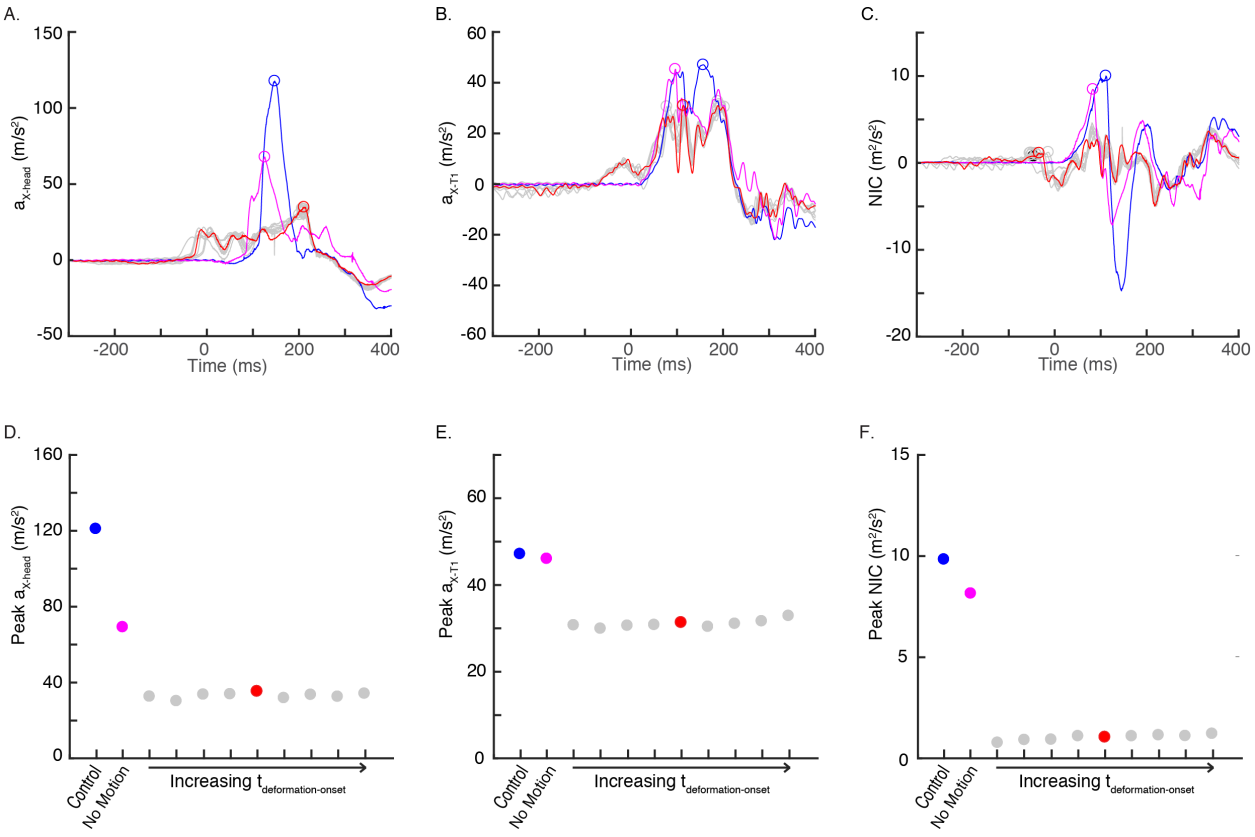

Figure D5. Exemplar ATD responses for the Control seat (blue lines and markers), the No Motion condition (magenta lines and markers), and the Experimental seat with various seatback motor onsets and a constant seat hinge motor onset ($t_{deformation\text{-}onset}$ & $t_{rotation\text{-}onset}$ = -90 ms; grey and red lines and markers) during a 12 km/h collision severity (Δt = 187 ms). Calibrated responses (**A – C**) and their corresponding peak responses (**D – F**) for head and torso accelerations in the X-direction ($a_{X\text{-}head}$ & $a_{X\text{-}T1}$) and neck injury criteria (NIC), respectively. The red lines and markers indicate the seatback motor parameter ($t_{deformation\text{-}onset}$ = -200 ms) selected for further testing.

Experiment 3: Varying both Seat Hinge Rotation and Seatback Deformation Onsets

The results from the previous two experiments confirmed that a combined seat hinge rotation ($t_{rotation\text{-}onset}$ = -90ms) and seatback deformation ($t_{deformation\text{-}onset}$ = -200ms) could reduce ATD responses following a rear-end collision. In this experiment, the relative timing between the two profiles (Δt_{onset} = 110 ms) was preserved and the timing of both the seat hinge rotation and the seatback deformation onsets were shifted in unison. The tested $t_{rotation\text{-}onset}$ and $t_{deformation\text{-}onset}$ were identical to the onset values used in the previous two experiments ($t_{rotation\text{-}onset}$ = -170, -150, -130, -110, -90, -70, -50, -30 and -10 ms; $t_{deformation\text{-}onset}$ = -280, -260, -240, -220, -200, -180, -160, -140, and -120 ms; **Figure D6A** and **D6D**). Hence, the earliest seat hinge and seatback onsets were $t_{rotation\text{-}onset}$ = -170 ms and $t_{deformation\text{-}onset}$ = -280 ms, while the latest onsets were $t_{rotation\text{-}onset}$ = -10 ms and $t_{deformation\text{-}onset}$ = -120 ms. Exemplar ATD responses ($a_{X\text{-}head}$, $a_{X\text{-}T1}$, and NIC, **Figure D7**) showed similar peak responses to just changing $t_{rotation\text{-}onset}$ in Experiment 1. ATD head acceleration ($a_{X\text{-}head}$) showed lower peak responses for $t_{rotation\text{-}onset}$ between -110 to -70 ms and $t_{deformation\text{-}onset}$ between -220 to -180 ms from the Control and the No Motion conditions, whereas peak T1 acceleration ($a_{X\text{-}T1}$) decreased only for the $t_{rotation\text{-}onset}$ = -90 ms and $t_{deformation\text{-}onset}$ = -200 ms condition. Neck injury criterion (NIC) decreased compared to the Control seat and the No Motion condition in all experimental trials. The Friedman test revealed a significant difference between trials (1 Control, 1 No Motion, and 9 Experimental, $\chi^2 = 82.26$, df = 10, $p < 0.001$). Post-hoc comparisons revealed that $t_{rotation\text{-}onset}$ = -90 ms and $t_{deformation\text{-}onset}$ = -200 ms was ranked significantly lower than the Control seat and the No Motion condition as well as two conditions with $t_{rotation\text{-}onset} \leq$ - 150 ms and $t_{deformation\text{-}onset} \leq$ -260 ms ($p \leq 0.036$, **Figure D6C**). The similarities in the results of this experiment and Experiment 1 further suggested that

changing seat hinge $t_{rotation\text{-}onset}$ had a greater effect on peak ATD responses than changing seatback $t_{deformation\text{-}onset}$. Despite showing the second lowest rank, the $t_{rotation\text{-}onset}$ = -90 ms and $t_{deformation\text{-}onset}$ = -200 ms profile timing was selected for future experiments because 1) it decreased peak T1 acceleration ($a_{X\text{-}T1}$) and 2) an onset of 200 ms prior to the collision was reasoned to be the upper limit possible for impending impact detection and subsequent active deformation of the automotive seat.

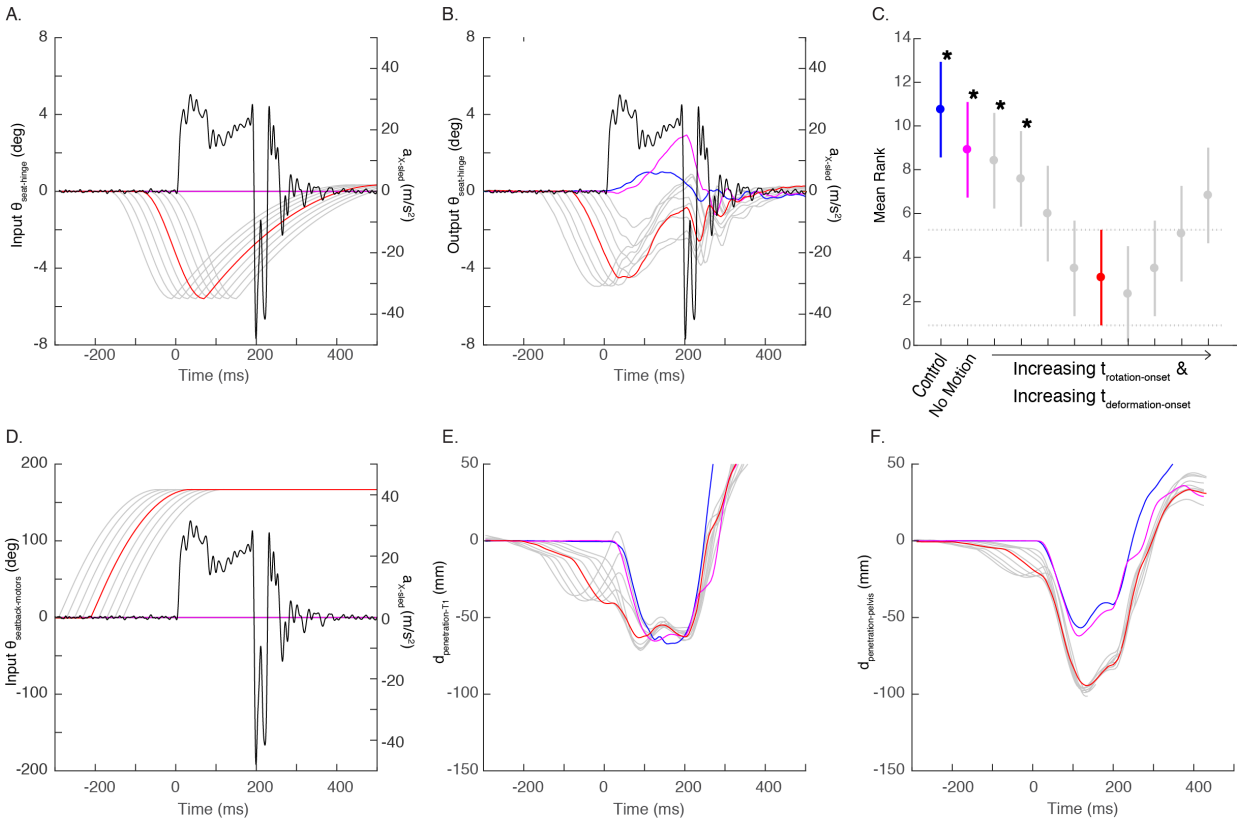

Figure D6. Seat hinge and seatback motor profiles as well as ATD responses to the Control seat (blue lines and markers), the No Motion condition (magenta lines and markers) and the Experimental seat with shifted seat hinge and seatback motor onsets ($t_{rotation\text{-}onset}$ & $t_{deformation\text{-}onset}$; grey and red lines and markers) during a 12 km/h collision severity (Δt = 187 ms, black lines, right axis). The red lines and markers indicate the seat hinge onset ($t_{rotation\text{-}onset}$ = -90 ms and $t_{deformation\text{-}onset}$ = -200 ms) selected for further testing. Panels **A** and **B** show the programmed input and output seat hinge rotation profiles. Panel **D** shows the programmed input seatback motor profiles with resulting seatback deformation at the T1 spinal level ($d_{penetration\text{-}T1}$) and at the pelvis ($d_{penetration\text{-}pelvis}$) in Panels **E** and **F**, respectively. The results of the post-hoc test (**C**) determined the mean rank of each trial as well as any significant differences (*) between the selected seatback motor parameter trial (red) and the Control, No Motion or other experimental trials.

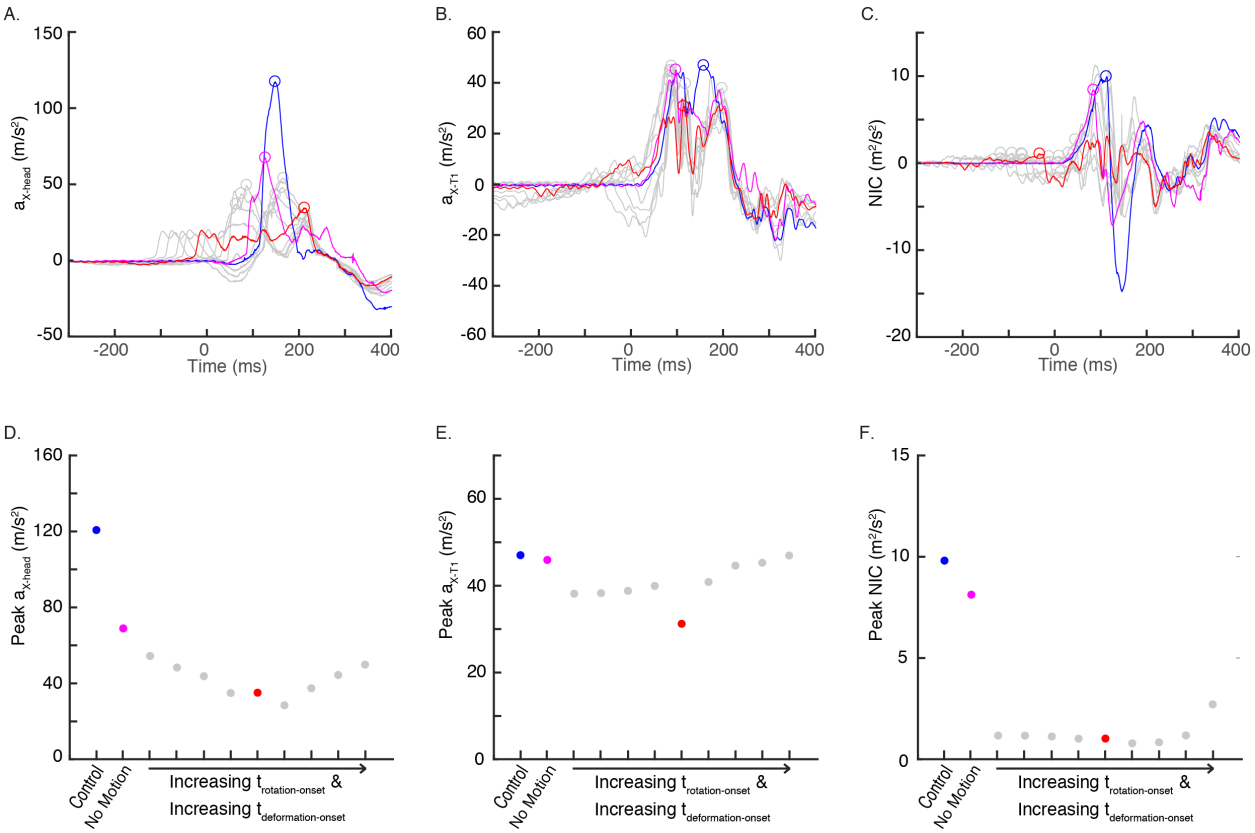

Figure D7. Exemplar ATD responses for the Control seat (blue lines and markers), the No Motion condition (magenta lines and markers), and the Experimental seat with shifted seat hinge and seatback motors onsets ($t_{rotation\text{-}onset}$ & $t_{deformation\text{-}onset}$; grey and red lines and markers) during a 12 km/h collision severity (Δt = 187 ms). Calibrated responses (**A – C**) and their corresponding peak responses (**D – F**) for head and torso accelerations in the X-direction ($a_{X\text{-}head}$ & $a_{X\text{-}T1}$) and neck injury criteria (NIC), respectively. The red lines and markers indicate the seat hinge and seatback motor parameters ($t_{rotation\text{-}onset}$ = -90 ms and $t_{deformation\text{-}onset}$ = -200 ms) selected for further testing.

Summary

The onsets for the seat hinge rotation ($t_{rotation\text{-}onset}$ = -90ms) and the seatback deformation ($t_{deformation\text{-}onset}$ = -200ms) profiles have been optimally combined into one dynamic movement on the Experimental anti-whiplash seat. This optimal solution was a direct combination of the seat hinge rotation profile determined in **Appendix B** and the seatback deformation profile determined in **Appendix C** (**Figure D1**). Between the Control seat and the No Motion (seat hinge and seatback motors held in initial position, but the seatback was not rigidly braced against the sled) condition, the No Motion decreased seven of the nine peak responses and all three peak neck injury criteria by -17% to -58%. Only peak linear forward acceleration of the T1 vertebra ($a_{X\text{-}T1}$) and time-to-head-restraint contact ($\Delta t_{head\text{-}contact}$) remained the same as the Control seat. In comparison to the Control seat, the combined seat hinge rotation and seatback deformation profile reduced all nine peak kinematic and kinetic responses ($a_{X\text{-}head}$: -71%, $a_{X\text{-}T1}$: -34%, F_X: -71%, F_Z: -89%, M_Y: -81%, $\omega_{Y\text{-}head}$: -75%, θ_{head}: -87%, R_X: -70% and $\Delta t_{head\text{-}contact}$: -136 ms) and three peak neck injury criteria (NIC: -90%, N_{km}: -70%, and N_{ij}: -70%). Thus, the combined seat hinge rotation and seatback deformation profile may be a potentially effective solution to reducing ATD responses following low-speed, rear-end collisions.

Appendix E: Supplementary Material

Supplementary Material for Chapter 2

Table E2.1. Mean (Standard Deviation) and Coefficient of Variation (COV) from five repeated whiplash-like perturbation at a Δv = 4, 8 and 12 km/h with a Δt = 141 ms on the 2004 GM Pontiac Grand AM GMHR seat.

Automotive Seat	GM Pontiac Grand AM (GMHR)					
Δv (km/h)	4 km/h, Δt = 141 ms		8 km/h, Δt = 141 ms		12 km/h, Δt = 141 ms	
Parameter	Mean (SD)	COV (%)	Mean (SD)	COV (%)	Mean (SD)	COV (%)
$a_{X\text{-}sled}$ (m/s^2)	11.0 (0.7)	6.2*	20.5 (0.2)	0.8	28.6 (0.1)	0.4
$\Delta t_{head\text{-}contact}$ (ms)	159.6 (1.7)	1.1	122.8 (2.7)	1.3	108.9 (1.5)	1.4*
$a_{X\text{-}head}$ (m/s^2)	37.7 (0.4)	0.9	86.0 (1.6)	1.9*	130.4 (1.4)	1.1
$a_{X\text{-}T1}$ (m/s^2)	22.0 (1.2)	5.3*	42.1 (0.7)	1.6	51.3 (0.5)	1.0
F_X (N)	113.3 (4.6)	4.0	222.9 (18.1)	8.1*	220.9 (17.5)	7.9
F_Z (N)	85.4 (3.8)	4.5	562.5 (35.2)	6.3*	684.7 (39.5)	5.8
M_Y (Nm)	1.6 (0.2)	**11.2***	13.6 (0.6)	4.2	14.0 (0.6)	4.2
$\omega_{Y\text{-}head}$(deg/s)	238.6 (21.8)	9.2*	315.9 (11.6)	3.7	433.1 (12.7)	2.9
$\omega_{Y\text{-}T1}$ (deg/s)	160.1 (13.4)	8.4*	305.1 (16.6)	5.4	443.0 (20.6)	4.7
θ_{head} (deg)	14.4 (0.3)	2.4	15.2 (0.9)	5.7*	17.4 (0.5)	2.8
R_X (mm)	-48.3 (0.8)	1.7	-51.0 (2.8)	5.5*	-54.9 (1.7)	3.0
NIC (m^2/s^2)	3.5 (0.2)	6.9*	8.1 (0.4)	4.3	11.0 (0.3)	3.1
N_{ij}	0.05 (0.00)	4.3	0.13 (0.01)	5.3	0.14 (0.01)	5.4*
N_{km}	0.25 (0.01)	2.5	0.42 (0.03)	6.7*	0.42 (0.03)	6.4

Notes: The underlined COV values indicate a COV rating of acceptable (5% ≤ COV < 10%), the **bolded** COV values indicate a COV rating of poor (COV > 10%), and all other values are rated good (COV < 5%). * indicates the maximum COV value for each experimental ATD parameter.

Table E2.2. Mean (standard deviation) and Coefficient of Variation (COV) from five repeated whiplash-like perturbation at a Δv = 8 km/h with a Δt = 141 ms for the 2005 Saab 9.3 SAHR, 2005 Volvo S40 WHIPS and 2004 Volvo S60 WHIPS seats.

Parameter	Mean (SD)	COV (%)	Mean (SD)	COV (%)	Mean (SD)	COV (%)
Automotive Seat	Saab 9.3 SAHR		Volvo S40 WHIPS		Volvo S60 WHIPS	
Δv (km/h)	8 km/h, Δt = 141 ms		8 km/h, Δt = 141 ms		8 km/h, Δt = 141 ms	
$a_{X\text{-}sled}$ (m/s^2)	19.9 (0.1)	0.6	20.4 (0.2)	1.0	20.3 (0.1)	0.3
$\Delta t_{head\text{-}contact}$ (ms)	95.1 (1.1)	1.2	96.7 (2.2)	2.3	104.5 (3.8)	3.6
$a_{X\text{-}head}$ (m/s^2)	68.4 (1.6)	2.4	87.2 (3.4)	3.9	87.9 (6.1)	7.0
$a_{X\text{-}T1}$ (m/s^2)	42.5 (0.7)	5.3	44.6 (1.1)	2.5	46.5 (0.7)	1.5
F_X (N)	16.5 (1.8)	11.1	38.1 (6.1)	15.9	2.2 (1.0)	44.1
F_Z (N)	155.1 (13.6)	8.8	170.6 (19.9)	11.7	241.5 (37.6)	15.6
M_Y (Nm)	5.8 (0.0)	0.8	4.5 (0.4)	9.8	5.0 (0.4)	7.5
$\omega_{Y\text{-}head}$(deg/s)	251.1 (9.3)	3.7	220.9 (22.9)	10.4	266.3 (21.5)	8.1
$\omega_{Y\text{-}T1}$ (deg/s)	264.3 (23.4)	8.8	262.8 (15.8)	6.0	292.9 (26.0)	8.9
θ_{head} (deg)	11.1 (0.2)	2.1	10.6 (0.6)	5.3	12.4 (0.6)	5.2
R_X (mm)	-25.7 (1.9)	7.6	-28.1 (2.2)	7.9	-20.9 (2.3)	10.9
NIC (m^2/s^2)	5.4 (0.2)	4.1	5.7 (0.4)	6.1	6.2 (0.4)	5.6
N_{ij}	0.15 (0.01)	9.3	0.09 (0.01)	8.5	0.05 (0.00)	8.2
N_{km}	0.48 (0.03)	6.7	0.23 (0.02)	10.0	0.16 (0.01)	5.9

Notes: The underlined COV values indicate a COV rating of acceptable (5% ≤ COV < 10%), the **bolded** COV values indicate a COV rating of poor (COV > 10%), and all other values are rated good (COV < 5%).

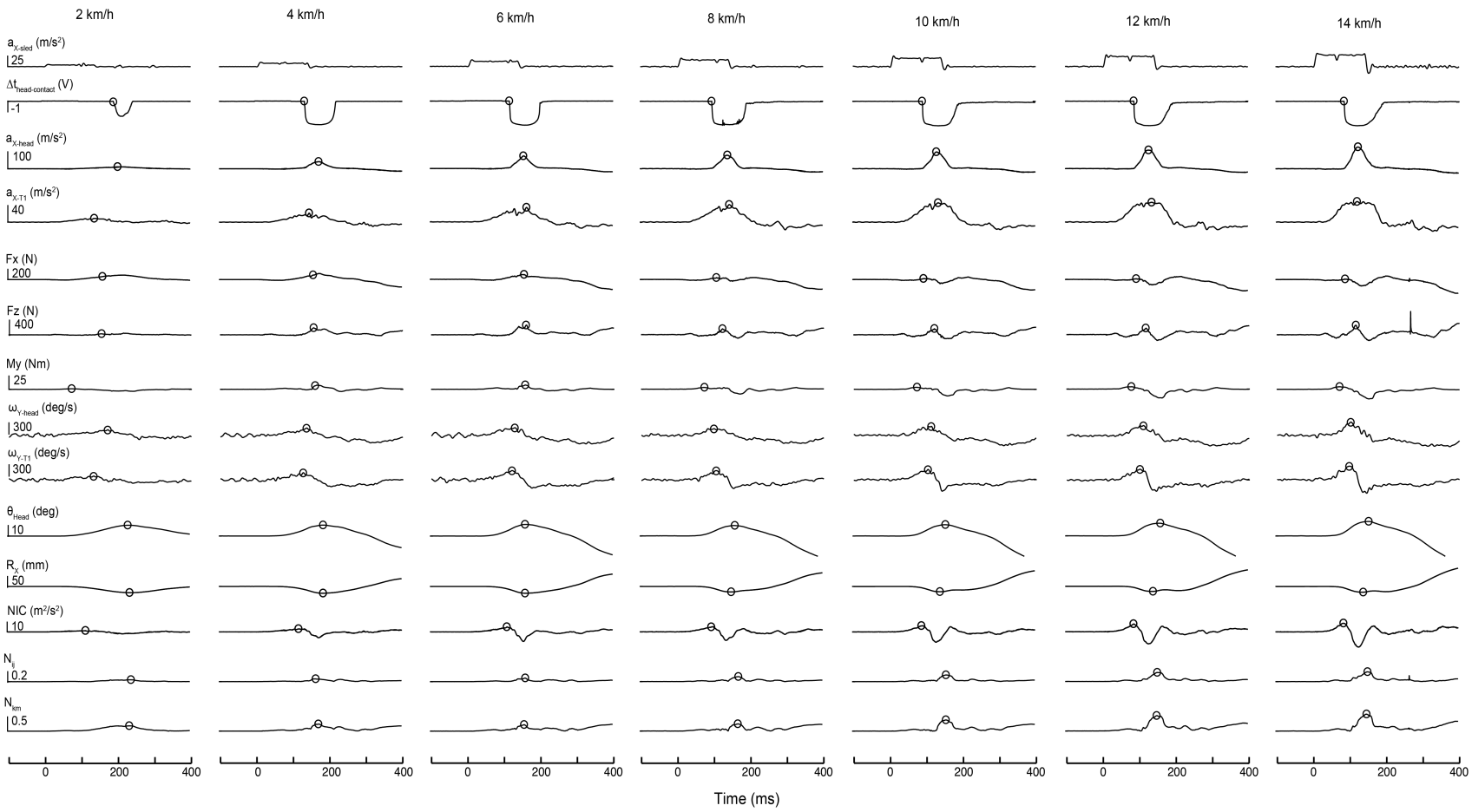

Figure E2.1. Experimental data for the BioRID II ATD seated on a 2005 Volvo S40 WHIPS seat. Each column represents occupant responses while exposed to various collision severities (Δv = 2, 4, 6, 8, 10, 12 and 14 km/h with a collision pulse duration (Δt) of 141 ms). Hollow circles represent the onset of head-to-head-restraint contact and peak responses of each ATD response parameter for each trial.

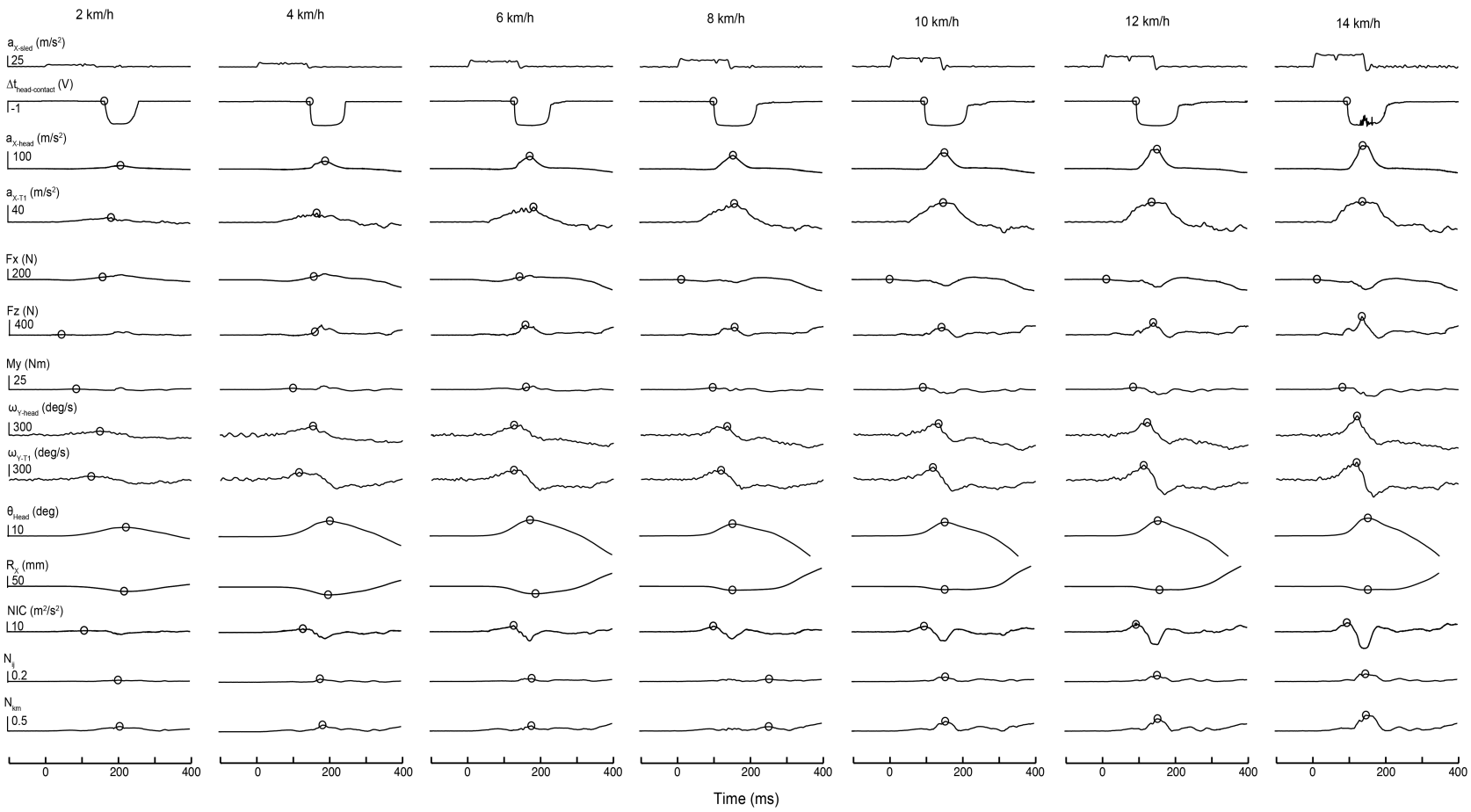

Figure E2.2. Experimental data for the BioRID II ATD seated on a 2004 Volvo S60 WHIPS seat. Each column represents occupant responses while exposed to various collision severities (Δv = 2, 4, 6, 8, 10, 12 and 14 km/h with a collision pulse duration (Δt) of 141 ms). Hollow circles represent the onset of head-to-head-restraint contact and peak responses of each ATD response parameter for each trial.

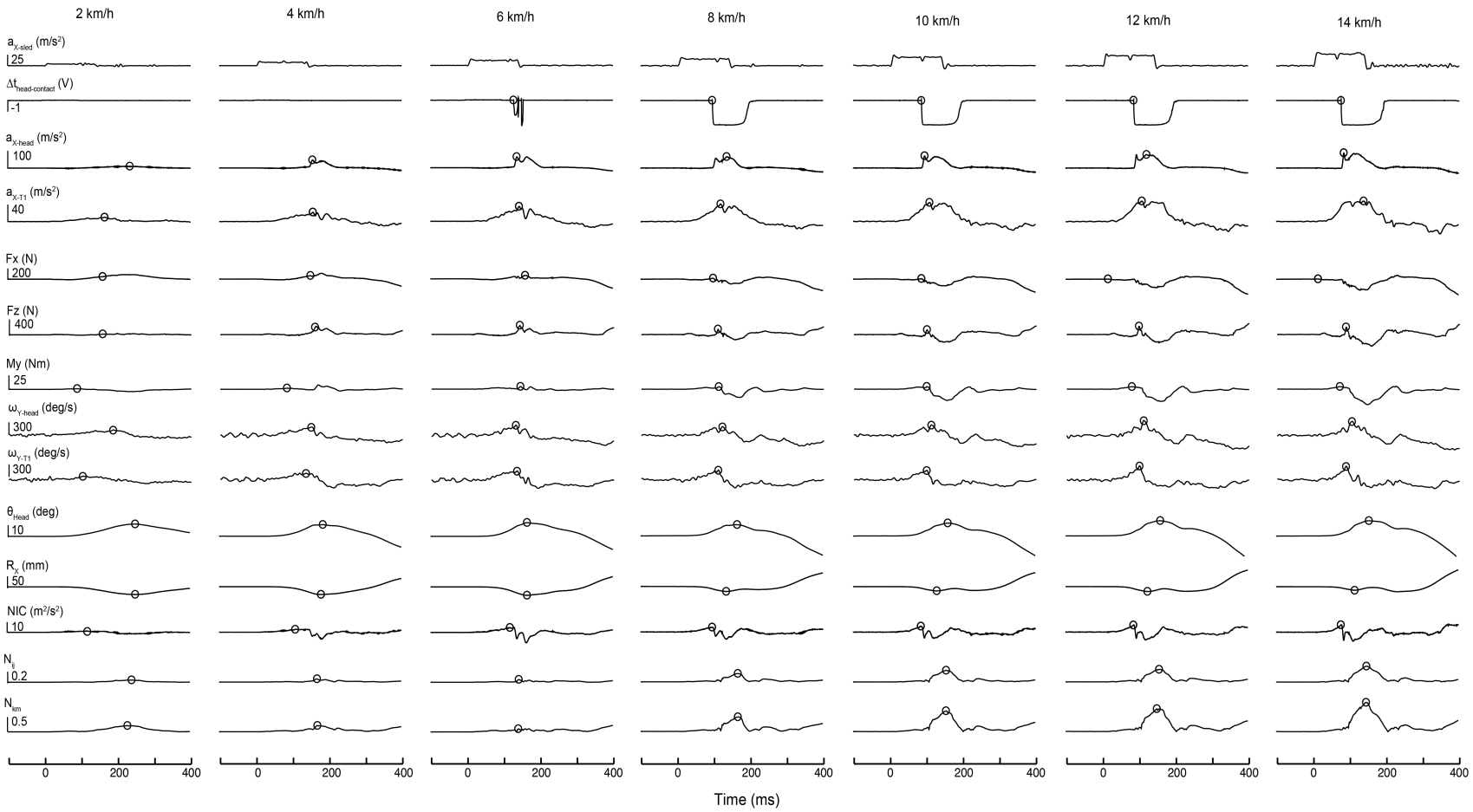

Figure E2.3. Experimental data for the BioRID II ATD seated on a 2005 Saab 9.3 SAHR seat. Each column represents occupant responses while exposed to various collision severities (Δv = 2, 4, 6, 8, 10, 12 and 14 km/h with a collision pulse duration (Δt) of 141 ms). Hollow circles represent the onset of head-to-head-restraint contact and peak responses of each ATD response parameter for each trial.

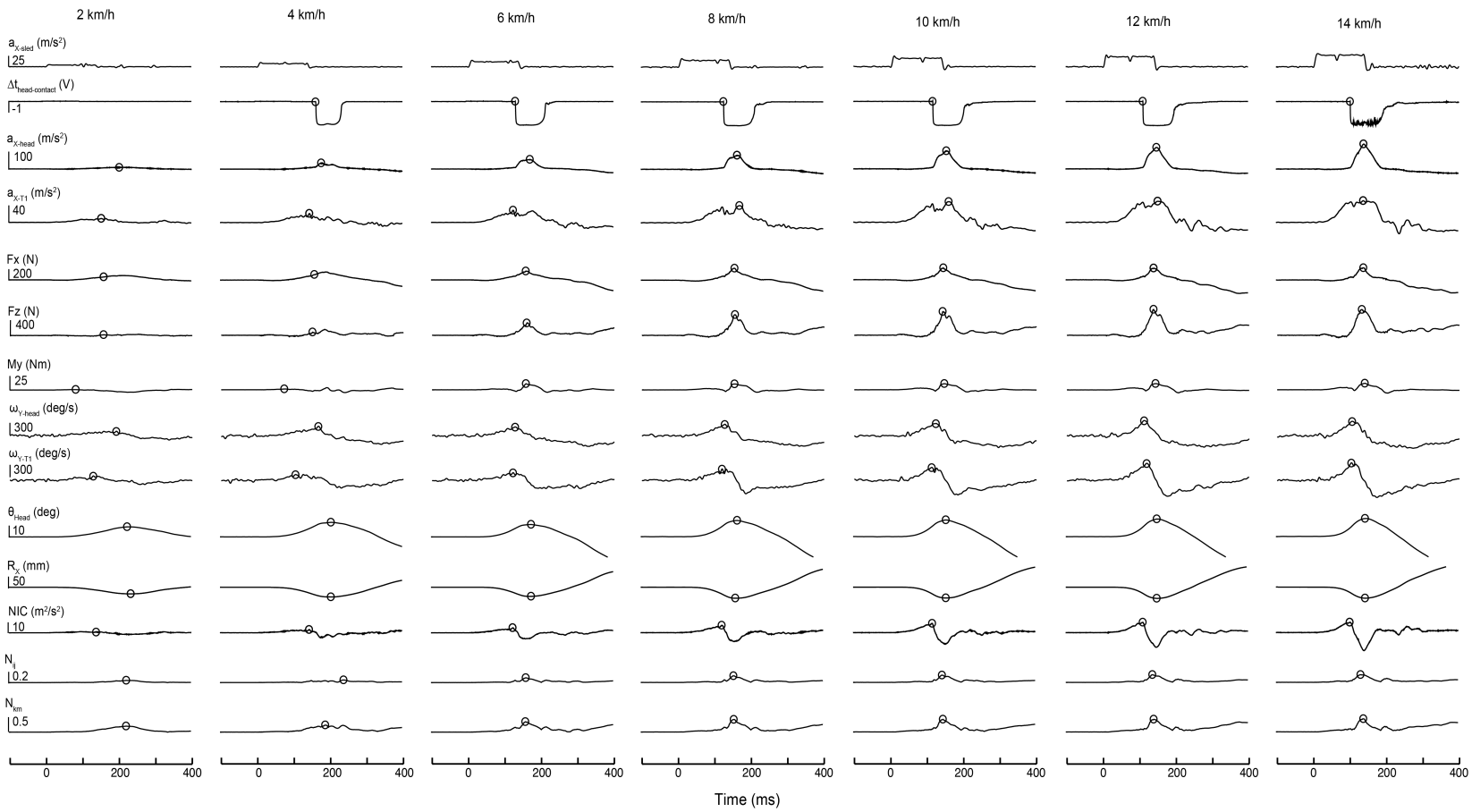

Figure E2.4. Experimental data for the BioRID II ATD seated on a 2004 Pontiac Grand Am GMHR seat. Each column represents occupant responses while exposed to various collision severities (Δv = 2, 4, 6, 8, 10, 12 and 14 km/h with a collision pulse duration (Δt) of 141 ms). Hollow circles represent the onset of head-to-head-restraint contact and peak responses of each ATD response parameter for each trial.

Supplementary Material for Chapter 5

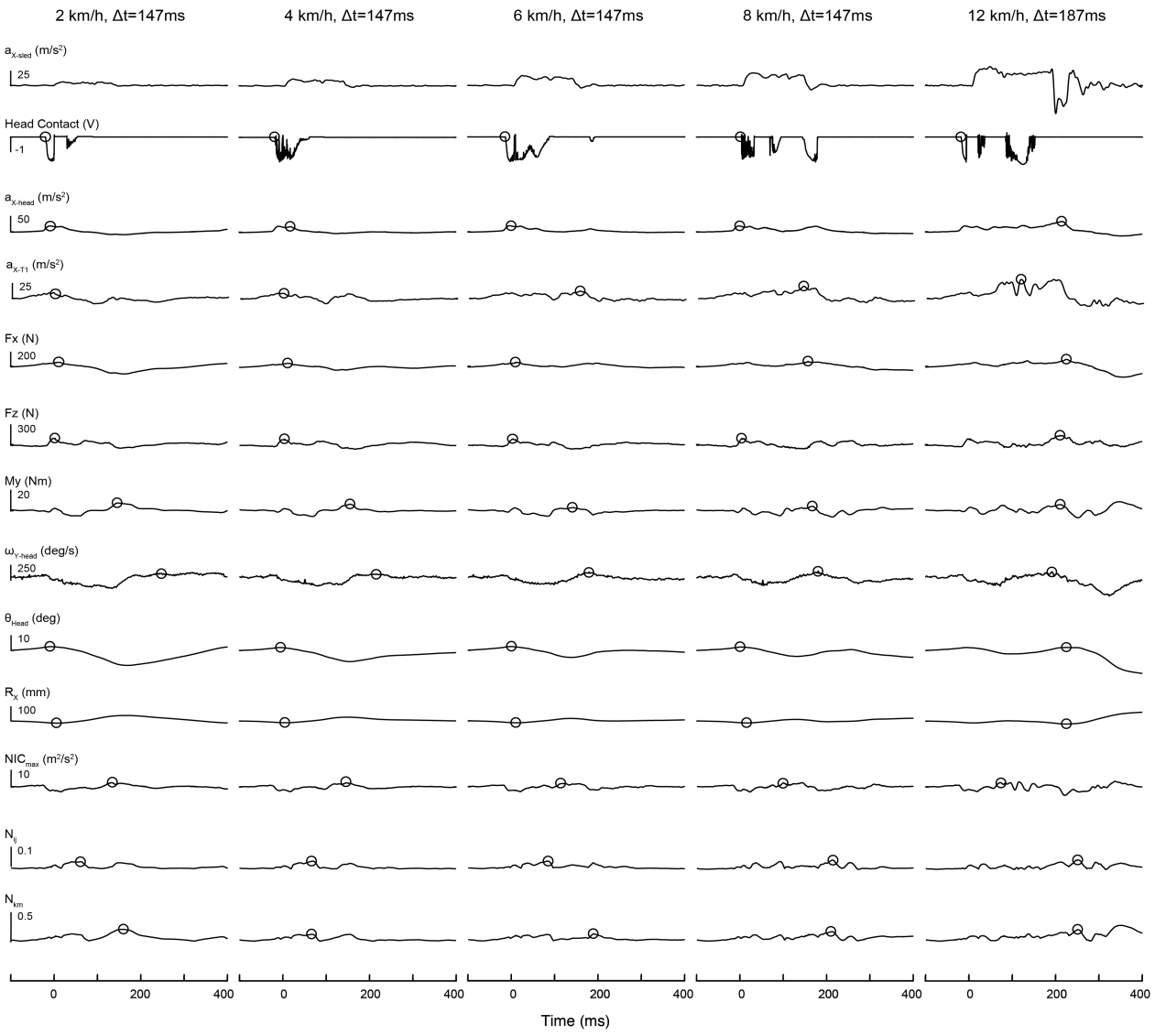

Figure E5.1. Experimental data for the BioRID II ATD seated on the Experimental seat utilizing both seat hinge rotation and seatback cushion deformation safety mechanisms. Each column represents occupant responses while exposed to various collision severities (Δv = 2, 4, 6 and 8 km/h, Δt = 147 ms and Δv = 12 km/h, Δt = 187 ms). Hollow circles represent the onset of head-to-head-restraint contact and peak responses of each ATD response parameter for each trial. Whiplash perturbation onset occurred at t = 0 ms.

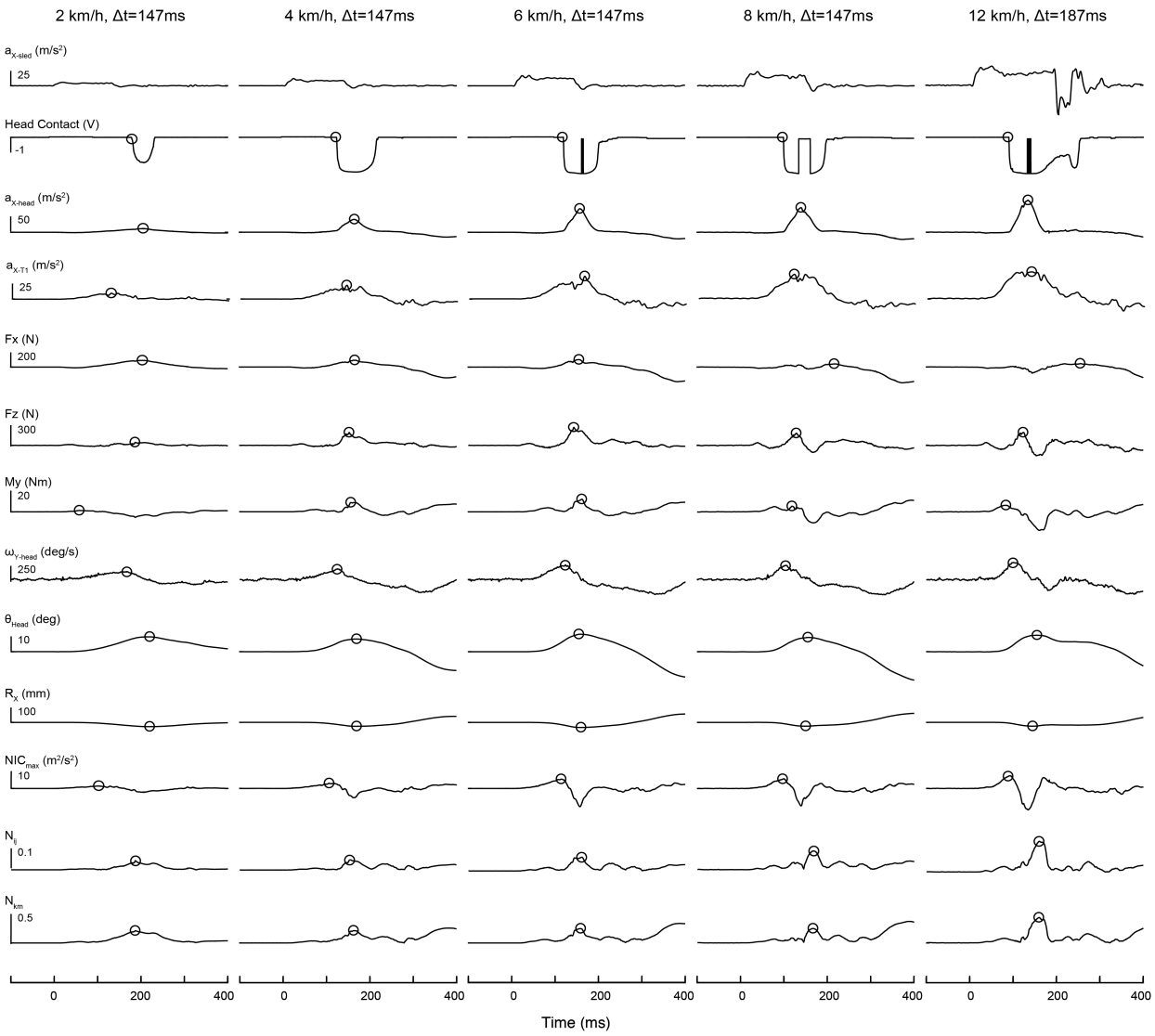

Figure E5.2. Experimental data for the BioRID II ATD seated on a 2005 Volvo S40 WHIPS seat. Each column represents occupant responses while exposed to various collision severities (Δv = 2, 4, 6 and 8 km/h, Δt = 147 ms and Δv = 12 km/h, Δt = 187 ms). Hollow circles represent the onset of head-to-head-restraint contact and peak responses of each ATD response parameter for each trial. Whiplash perturbation onset occurred at t = 0 ms.

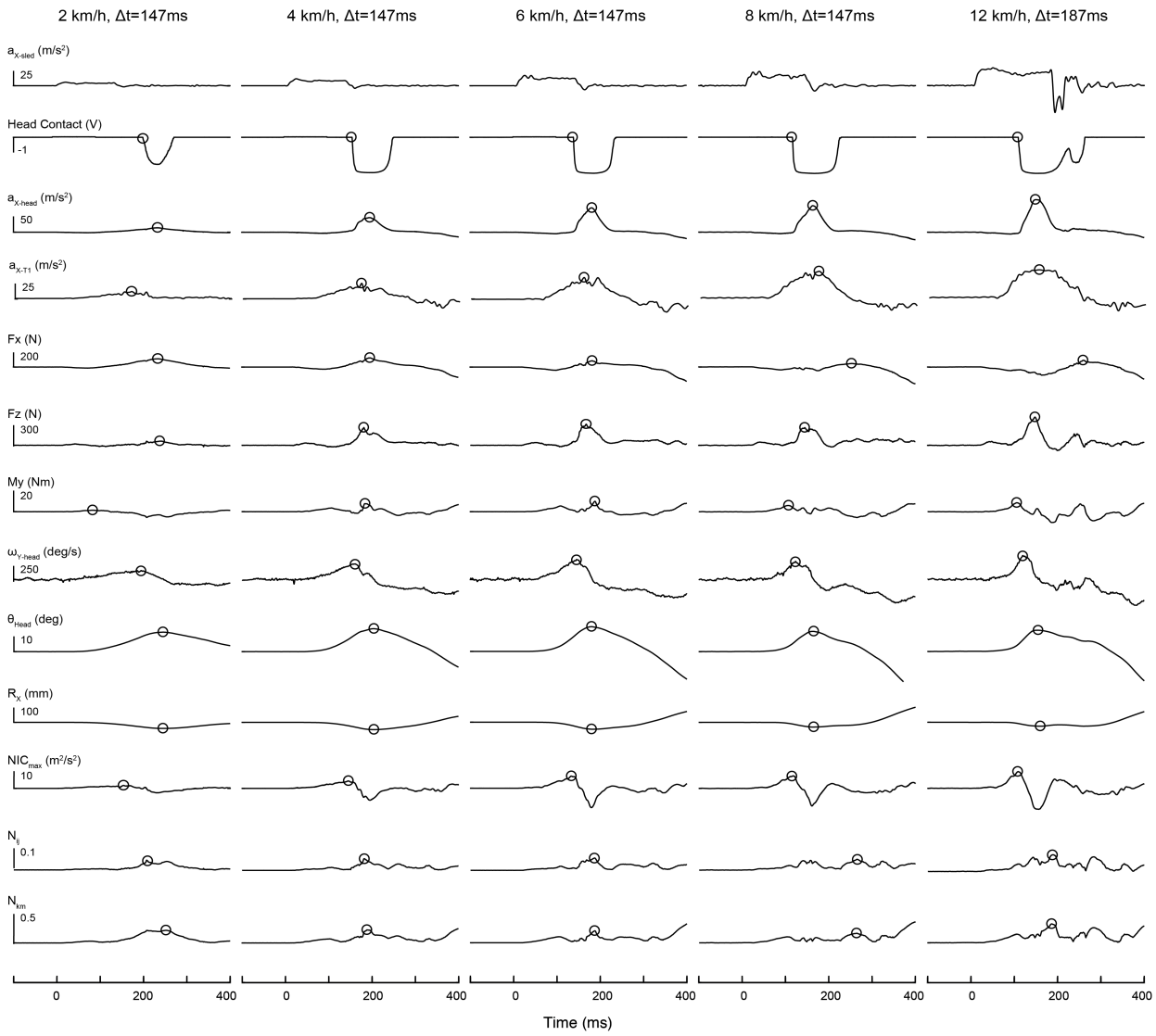

Figure E5.3. Experimental data for the BioRID II ATD seated on a 2004 Volvo S60 WHIPS seat. Each column represents occupant responses while exposed to various collision severities (Δv = 2, 4, 6 and 8 km/h, Δt = 147 ms and Δv = 12 km/h, Δt = 187 ms). Hollow circles represent the onset of head-to-head-restraint contact and peak responses of each ATD response parameter for each trial. Whiplash perturbation onset occurred at t = 0 ms.

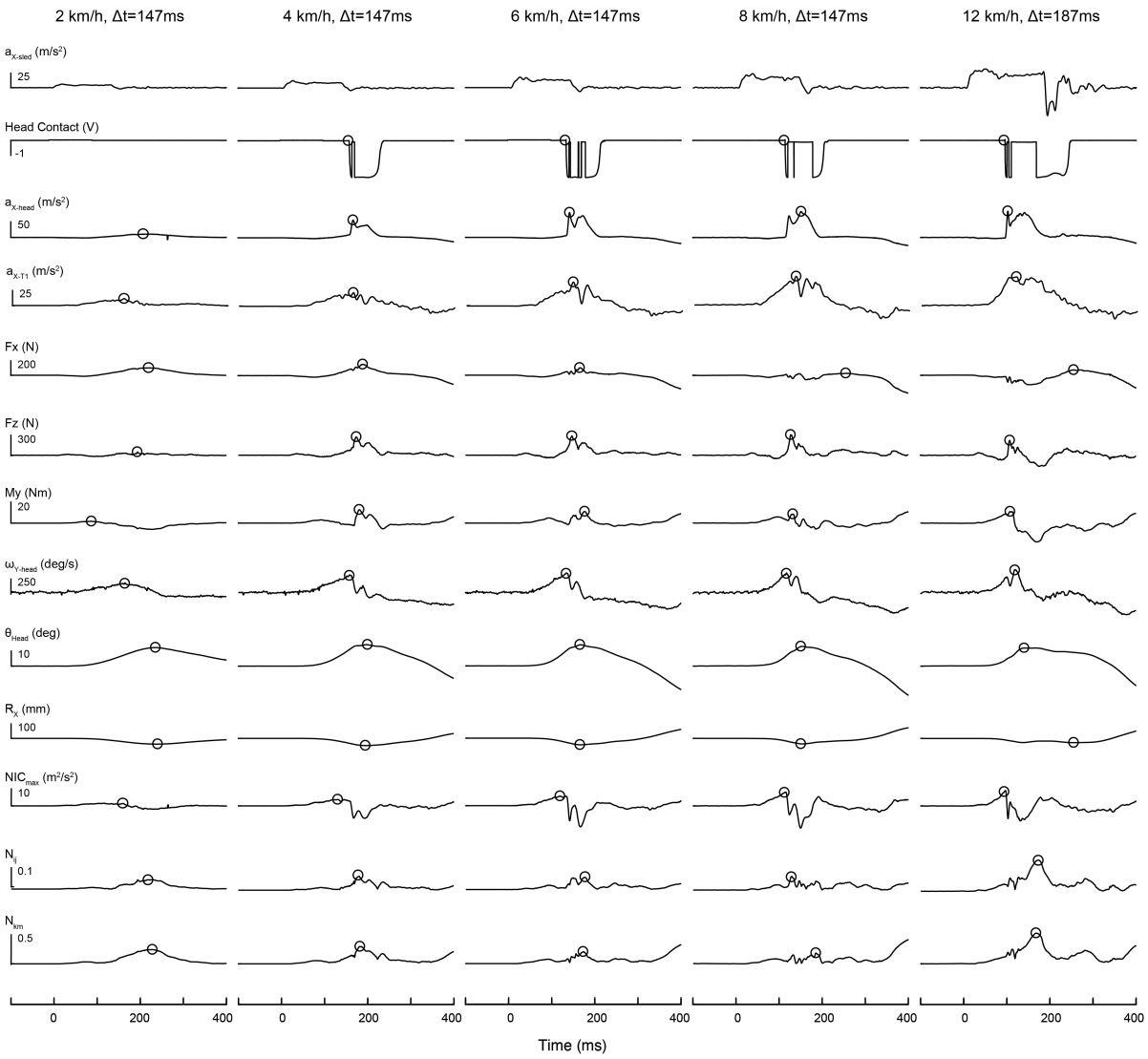

Figure E5.4. Experimental data for the BioRID II ATD seated on a 2005 Saab 9.3 SAHR seat. Each column represents occupant responses while exposed to various collision severities (Δv = 2, 4, 6 and 8 km/h, Δt = 147 ms and Δv = 12 km/h, Δt = 187 ms). Hollow circles represent the onset of head-to-head-restraint contact and peak responses of each ATD response parameter for each trial. Whiplash perturbation onset occurred at t = 0 ms.

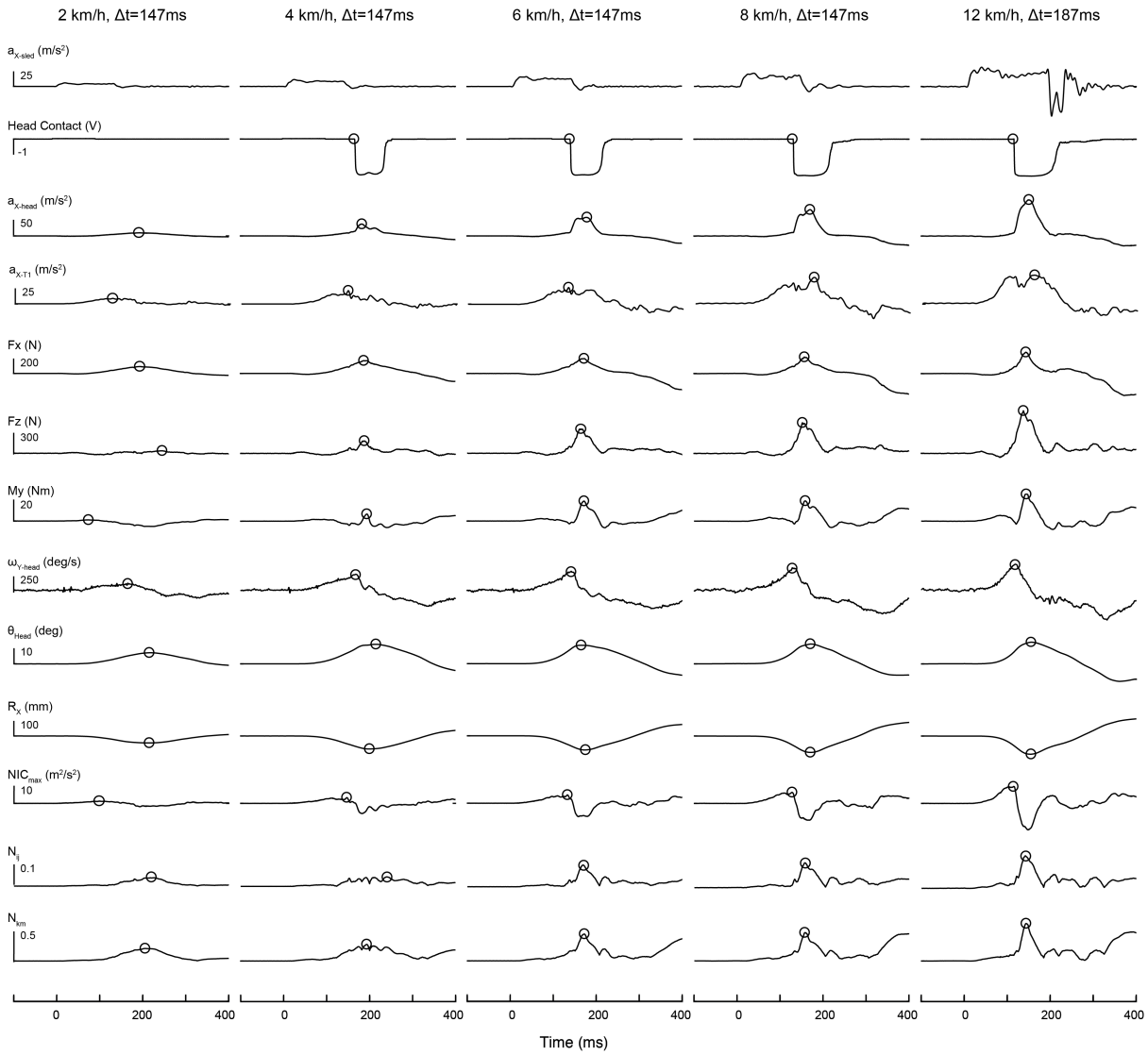

Figure E5.5. Experimental data for the BioRID II ATD seated on a 2004 Pontiac Grand Am GMHR seat. Each column represents occupant responses while exposed to various collision severities (Δv = 2, 4, 6 and 8 km/h with a collision pulse duration (Δt) = 147 ms and Δv = 12 km/h with a Δt = 187 ms). Hollow circles represent the onset of head-to-head-restraint contact and peak responses of each ATD response parameter for each trial. Whiplash perturbation onset occurred at t = 0 ms.